"STUDY OF BIOMEDICAL APPLICATIONS OF SURFACE FUNCTIONALIZED GOLD NANOPARTICLES-NUCLEIC ACID CONJUGATE"

SUBMITTED BY

MISS. TEJASWINI PRUTHVIRAJ PATIL

M.Sc.

UNDER THE GUIDANCE OF

DR. ARPITA PANDEY-TIWARI

M.Sc. Ph.D.

For the Degree of

Doctor of Philosophy

2024

"STUDY OF BIOMEDICAL APPLICATIONS OF SURFACE FUNCTIONALIZED GOLD NANOPARTICLES-NUCLEIC ACID CONJUGATE"

A THESIS SUBMITTED TO

D. Y. PATIL EDUCATION SOCIETY,
(DEEMED TO BE UNIVERSITY), KOLHAPUR

FOR THE DEGREE OF

DOCTOR OF PHILOSOPHY

IN

MICROBIOLOGY

UNDER THE FACULTY OF

INTERDISCIPLINARY STUDIES

SUBMITTED BY

MISS. TEJASWINI PRUTHVIRAJ PATIL

M.Sc.

UNDER THE GUIDANCE OF

DR. ARPITA PANDEY-TIWARI

M.Sc. Ph.D.

CENTRE FOR INTERDISCIPLINARY RESEARCH

D. Y. PATIL EDUCATION SOCIETY,

(DEEMED TO BE UNIVERSITY),

KOLHAPUR – 416 006 [M.S.] INDIA

2024

DECLARATION

I hereby declare that the thesis entitled, **"Study of Biomedical Applications of Surface Functionalized Gold Nanoparticles-Nucleic Acid Conjugate"** submitted here for the degree of **Doctor of Philosophy** in **Microbiology,** under the faculty of **Centre for Interdisciplinary Research (CIR), D. Y. Patil education Society (Deemed to be University), Kolhapur** is completed and written by me has not previously formed the basis for the degree or Diploma or other similar title of this or any other University or examining body.

Date:

Place: Kolhapur

Research Student

Miss. Tejaswini Pruthviraj Patil
Centre for Interdisciplinary Research,
D. Y. Patil Education Society,
(Deemed to be University),
Kolhapur- 416 006

CERTIFICATE

This is to certify that the thesis entitled **"Study of Biomedical Applications of Surface Functionalized Gold Nanoparticles-Nucleic Acid Conjugate"**, which is being submitted here for the award of the degree of **Doctor of Philosophy** in **Microbiology** under the faculty of **Centre for Interdisciplinary Research (CIR), D. Y. Patil Education Society, (Deemed to be University), Kolhapur** is the result of original Research work completed by **Miss. Tejaswini Pruthviraj Patil** under my supervision and guidance and to the best of my knowledge and belief the work bound in this thesis has not formed earlier the basis for the award of any degree or similar title of this or any other university or examining body.

Date:

Place: Kolhapur

Research Guide

Dr. Arpita Pandey-Tiwari
Associate Professor
Department of Medical Biotechnology
and Stem Cell & Regenerative Medicine,
Centre for Interdisciplinary Research,
D. Y. Patil Education Society,
(Deemed to be University),
Kolhapur – 416 006

Forwarded Through,

Prof. Meghnad G. Joshi
HOD
Department of Medical Biotechnology
and Stem Cell & Regenerative Medicine,
Centre for Interdisciplinary Research,
D. Y. Patil Education Society,
(Deemed to be University),
Kolhapur – 416 006

Prof. C. D. Lokhande
Dean and Research Director
Centre for Interdisciplinary Research,
D. Y. Patil Education Society,
(Deemed to be University),
Kolhapur – 416 006

ACKNOWLEDGEMENTS

Shivani Patil, Pranoti Kamble, and Vishakha Parkhe for helping with my experiments, and providing the friendly environment in laboratory. I thank all the teaching and non-teaching staff of CIR for their cooperation.

I would like to express my deep sense of gratitude to my parents, **Mr. Pruthviraj Patil** and **Mrs. Lata Patil** for their love, support, patience, encouragement, and belief in me. I am thankful to my elder sister **Mrs. Priyanka Kadam** and her husband **Mr. Suhas Kadam** for their support. I thank to my younger brother, **Omkar Patil** to cheer me up throughout this journey. My loving thanks to my nephew, **Ridhant Kadam,** my stressbuster, for giving me happy vibes. I extend my thanks to my all Rajaramiyan friends, the extended family of mine; for their encouragement and trust. I would like to offer my special thanks to my new family, my husband **Mr. Sanket Kesarkar** and my mother-in-law **Ms. Sujata Kesarkar** for their support and understanding.

Finally, one and all, I am thankful to all who make this journey possible and memorable.

- *Tejaswini Patil*

LIST OF PUBLICATIONS

Patent (Published): (1)

1. **A Method for Detection of Viral/Bacterial Nucleic Acid using Gold Nanoparticles.**
   (Application Number : 202321003114)

Copyrights (Granted): (3)

1. **Colorimetric Detection of Nucleic Acid by Gold Nanoparticles (AuNPs),**
   Dr. Arpita Pandey Tiwari, **Miss Tejaswini Pruthviraj Patil.**
   Registration No. L-144215/2024.

2. **Covalent Interactions between Gold nanoparticles (AuNPs) and Nucleic acid,**
   Dr. Arpita Pandey Tiwari, **Miss Tejaswini Pruthviraj Patil.**
   Registration No. L-147677/2024.

3. **Electrochemical Detection of SARS-CoV-2 RNA by Poly-L-Lysine functionalized Gold Nanoparticles (PLL-AuNPs),**
   Dr. Arpita Pandey Tiwari, **Miss Tejaswini Pruthviraj Patil.**
   Registration No. L-157364/2024

Papers: (11)

1. **T. Patil**, A. Vibhute, S. Patil, T. Dongale, A. P. Tiwari, **Green synthesis of gold nanoparticles via *Capsicum annum* fruit extract: Characterization, antiangiogenic, antioxidant and anti-inflammatory activities.** *Applied Surface Science Advances*, 13, (2023), 100372. doi: 10.1016/j.apsadv.2023.100372. **(I.F. 7.5)**

2. **T. Patil**, V. Khot, A. Pandey-Tiwari, **Single-step antibiotic-mediated synthesis of kanamycin-conjugated gold nanoparticles for broad-spectrum antibacterial applications.** *Letters in Applied Microbiology*, 75(4), (2022), 913-923. doi:10.1111/lam.13764. **(I.F. 2.4)**

3. **T. Patil**, R. Gambhir, A. Vibhute, A. P. Tiwari, **Gold Nanoparticles: Synthesis Methods, Functionalization and Biological Applications.** *Journal of Cluster Science*, 4, (2022), 1-21. doi: 10.1007/s10876-022-02287-6. **(I.F. 2.8)**

4. **T. Patil,** S. S. Rohiwal, A. P. Tiwari, **Stem Cells: Therapeutic implications in chemotherapy and radiotherapy resistance in Cancer Therapy.** *Current Stem Cell Research & Therapy*, (2022). doi:0.2174/1574888x17666221003125208. **(I.F. 2.7)**

5. **T. Patil,** V. Parkhe, S. Kundale, R. Kamat, T. Dongale, R. Patil, A. P. Tiwari. **Antisense oligonucleotide conjugated gold nanoconstructs-based electrochemical biosensor for detection of SARS-CoV-2**. *Applied Surface Science Advances*, 22, (2024), 100618. doi: 10.1016/j.apsadv.2024.100618. **(I.F. 7.5)**

6. **T. Patil**, A. K. Parthasarathy, D. Malavekar, J. Kim, A. P. Tiwari. **Optical Biosensing of SARS-CoV-2 RNA Based on Positively Charged Poly-l-Lysine Functionalized Gold Nanoparticles.** *Journal of Cluster Science,* 35, (2024), 2525-38. doi: 10.1007/s10876-024-02678-x. **(I.F. 2.8)**

7. A. Vibhute, **T. Patil**, R. Gambhir, A. P. Tiwari, **Fluorescent carbon quantum dots: Synthesis methods, functionalization and biomedical applications.** *Applied Surface Science Advances*, 11, (2022), 100311. doi: 10.1016/j.apsadv.2022.100311. **(I.F. 7.5).**

8. A. Vibhute, **T. Patil**, D. Malavekar, S. Patil, S. Lee, A. P. Tiwari, **Green synthesis of fluorescent carbon dots from *Annona squamosa* leaves: optical and structural properties with bactericidal, anti-inflammatory, anti-angiogenesis applications.** *Journal of Fluorescence*, (2023), 1-11. doi: 10.1007/s10895-023-03159-6. **(I.F. 2.7)**

9. V. Parkhe, **T. Patil**, A. P. Tiwari, **Biowaste-mediated green synthesis of gold nanoparticles using *Solanum tuberosum* peel extract for antibacterial, antioxidant, and photocatalytic applications**. *Nanotechnology for Environmental Engineering*, (2023), 1-5. doi: 10.1007/s41204-023-00342-9.

10. R. Jadhav, **T. Patil,** A. P. Tiwari, **Trends in sensing of creatinine by electrochemical and optical biosensors**. *Applied Surface Science Advances*, (2024), 100567. doi: 10.1016/j.apsadv.2023.100567. **(I.F. 7.5)**

11. A. Vibhute, **T. Patil,** A. P. Pandey-Tiwari. **Bio-Conjugated Carbon Quantum Dots for Intracellular Uptake and Bioimaging Applications**. *Journal of Fluorescence*, (2025), 1-11. doi: 10.1007/s10895-024-04103-y. **(I.F. 2.7)**

Book chapter: (1)

1. R. Gambhir, A. Vibhute, **T. Patil**, A. P. Tiwari. **Surface-Functionalized Iron Oxide (Fe3O4) Nanoparticles for Biomedical Applications.** *InChemically Deposited Metal Chalcogenide-based Carbon Composites for Versatile Applications,* 2023, (pp. 411-432). Cham: Springer International Publishing.

Conferences/seminars/workshops attended/papers presented (3 workshop, 4 conferences, 1 hands on training):

1. One-day workshop on **"Development of Scientific Instrumentation"** organised by Stem Cell and Regenerative Medicine (SCRM), D. Y. Patil Education Society, Kolhapur on 17th December, 2021.

2. Presented poster in **"Dyanshodh 2022"** organised by Centre for Interdisciplinary Research (CIR), D. Y. Patil Education Society (Deemed to be University), Kolhapur, Maharashtra, India on 28th February, 2022.

3. Participated and hands on training programme on **"Bio Atomic Force Microscopy (Bio-AFM)"** organised by Shivaji University, Kolhapur on 4-5th January, 2022.

4. Attended International conference on **"Emerging and Re-emerging Infections (ICERI) 2022"** on 8th April, 2022.

5. Attended workshop on **"Protein Purification Techniques and Polyclonal Antibody Development"** on 21-22nd April, 2022.

6. Presented poster in International Workshop on **"Recent Trends in Functional Nanomaterials for Technological Applications"** organized by Center for Nanoscience and Nanotechnology, Amity University, Mumbai and ICON Labs, Navi Mumbai, India on 2-3rd August, 2022.

7. Presented poster in RUSA sponsored, International Conference on **"Emerging Trends in Applied Microbiology and Food Science (ETAMFS)"** organized by Department of Microbiology and Food Processing and Packaging, Yashwantrao Chavan Institute of Science, Satara, Maharashtra, India on 2-3rd December, 2022.

8. Presented poster in International conference on **"Biology Beyond Boundaries (BBB)"** organised by Department of Biotechnology, Savitribai Phule Pune University, Pune, Maharashtra, India on 29-31st January, 2024.

9. Oral presentation in International conference on **"Nanotechnology Addressing the Convergence of Materials Science, Biotechnology, and Medical Science (IC-NACMBM-2024)"** organised by D. Y. Patil Education Society (Deemed to be University), Kolhapur, Maharashtra, India on 12-14th February, 2024.

10. Presented poster in **"Dyanshodh 2024"** organised by Centre for Interdisciplinary Research (CIR), D. Y. Patil Education Society (Deemed to be University), Kolhapur, Maharashtra, India on 28th February, 2024.

LIST OF ABBREVIATIONS

Au^{3+}	Gold ions	HIV-1	Human immunodeficiency virus-1
ASO	Antisense oligonucleotides	HPLC	High-performance liquid chromatography
AuNPs	Gold nanoparticles	HNO_3	Nitric acid
AuNPs-NA	Gold nanoparticles-nucleic acid conjugates	*K2A*	K2 associated protein A gene
BSL-2	Biosafety laboratory-2	LOD	Limit of detection
CPE	Constant phase element	M	Molar
CPS	Capsular polysaccharides	MB	Methylene blue
-COOH	Carboxyl group	mg/mL	Milligram per millilitre
COVID-19	Corona virus disease 2019	MIC	Minimum inhibitory concentration
CTAB	Cetyltrimethylammonium bromide	min	Minute
CV	Cyclic voltammetry	miRNAs	Micro ribonucleic acid
DFA	Direct fluorescent antibody	mM	Millimolar
DLS	Dynamic light scattering	mV	Millivolt
DNA	Deoxyribonucleic acid	NABH	National Accreditation Board for Hospital & Healthcare Providers
DPV	Differential pulse voltammetry	NaCl	Sodium chloride
dsDNA	Double-stranded deoxyribonucleic acid	NaOH	Sodium hydroxide
E. coli	*Escherichia coli*	ng/mL	Nanogram per millilitre
EDS/EDAX	Energy-dispersive X-ray spectroscopy	$-NH_2$	Amine group
EIS	Electrochemical impedance spectroscopy	nm	Nanometre
ELISA	Enzyme linked immune-sorbent assay	nM	Nanomolar
EMSA	Electrophoretic mobility shift assay	-OH	Hydroxyl group
Exo III	Exonuclease III	PAA	Polyacrylic acid
fM	Femtometre	PBS	Phosphate buffer saline
FT-IR	Fourier transform infrared spectroscopy	PCR	Polymerase chain reaction
GCE	Glassy carbon electrode	PEG	Polyethylene glycol
h	Hour	PEI	Polyethyleneimine
$HAuCl_4$	Chloroauric acid	PLL	Poly-L-Lysine
HCl	Hydrochloric acid	PLL-AuNPs	Poly-L-Lysine functionalized gold nanoparticles

PLL-AuNPs-NA	Poly-L-Lysine functionalized gold nanoparticles-antisense oligonucleotide conjugate	SPR	Surface plasmon resonance
pM	Picomolar	ssDNA	Single stranded deoxyribonucleic acid
PVA	Polyvinyl alcohol	SWV	Square wave voltammetry
PVP	Polyvinyl pyrrolidone	TAE	Tris Acetate EDTA
qRT-PCR	Quantitative reverse transcription polymerase chain reaction	TEM	Transmission electron microscopy
Rct	Charge transfer resistance	UTI	Urinary tract infection
RdRp	RNA-dependent RNA polymerase gene	UV-Vis	Ultraviolet visible
RNA	Ribonucleic acid	XRD	X-ray diffraction analysis
rpm	Rotation per minute	µL	Microlitre
Rs	Solution resistance	µm	Micrometre
RT-PCR	Reverse transcription polymerase chain reaction	µg/mL	Microgram per millilitre
S. aureus	*Staphylococcus aureus*	µM	Micromolar
SARS-CoV-2	Severe acute respiratory syndrome corona virus 2	µA	Microampere
siRNA	Small interfering ribose nucleic acid	σ	Standard deviation
-SH	Thiol group	ζ potential	Zeta potential

INDEX

LIST OF FIGURES

LIST OF TABLES

Chapter I

Introduction and review of literature

1.1   Introduction:

The use of nanoscale items in a variety of applications is made possible by nanotechnology. Richard P. Feynman at first articulated the idea of nanotechnology in 1959 [1]. The physicochemical properties of a substance changes drastically when it reaches to nanosize in comparison to its bulk component. The size of material varies depending on the applications in industries [2]. For significant precision, sensitivity, efficiency, and high-speed measurement, contemporary nanotechnology methods have successfully supplanted traditional biomedical techniques in recent years. Gold nanoparticles (AuNPs) are one of the most investigated nanoparticles for biomedical applications among all other nanoparticles due to their favorable physicochemical characteristics such as, simple synthesis, ease of surface modification, colloidal stability, non-toxicity, biocompatibility, size tunability, optical properties, and large surface to volume ratio as shown in **figure 1.1**. Properties of AuNPs are dependent on their size and form, however bulk gold has different characteristics from nanoscale particles [3].
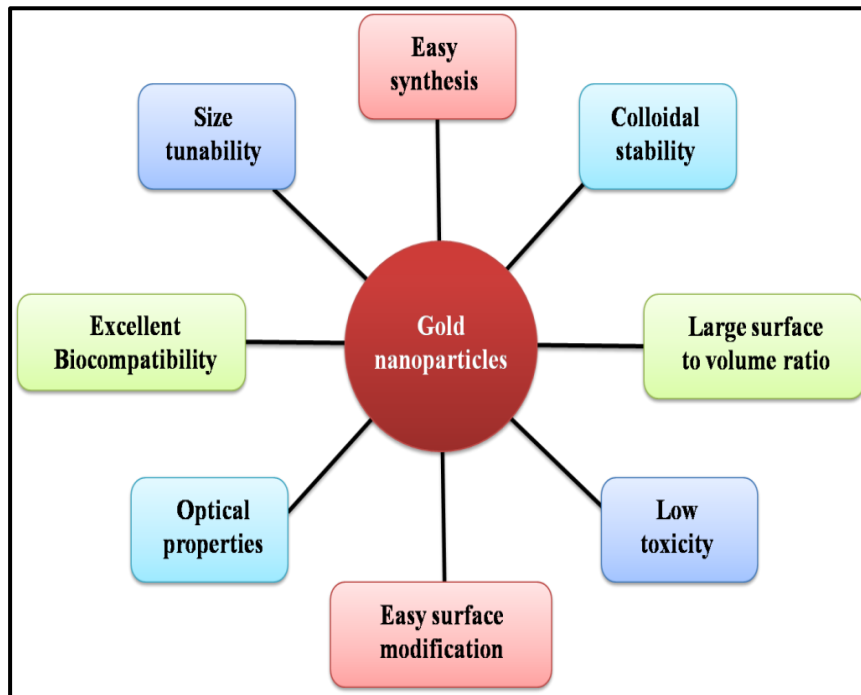
Figure 1.1: Unique characteristics of gold nanoparticles (AuNPs) [4]

Colloidal stability of AuNPs can be defined by the ability of the AuNPs to remain suspended in a solution and the interactions between the nanoparticles. AuNPs can be synthesized in different sizes by varying the ratio of reducing agent and precursor. Smaller size of AuNPs displays large surface to volume ratio that exhibit potential of AuNPs as drug and gene carrier. Optical properties of gold nanoparticles depend on particle size and shape which is displayed by observing change in color. The colloidal gold nanoparticles suspension appears wine red for particle size less than 100 nm or blue for larger particles.

The optical and electrochemical characteristics of gold nanoparticles are greatly influenced by their surface chemistry, size, shape, and interparticle distance. Particle size variation is influenced by synthesis-related factors such as, precursor concentration, temperature, ratio of reducing agent to precursor, and pH. Another important physical characteristic of AuNPs that affected by different sizes of AuNPs is Surface Plasmon Resonance (SPR). The SPR is defined as, collective oscillation of electrons in metal nanoparticles that are excited by incident of light [5, 6]. The high surface energy of gold causes the AuNPs to frequently precipitate in liquids. Various functionalizing agents such as, polymers that reduce the surface energy of gold, are used to modify the surface of AuNPs, preventing self-assembly and stabilizing the nanoparticles. The ability of gold nanoparticles to be used in biomedical applications depends on their surface chemistry. Surface characteristics play a crucial role in biomedical applications, as they determine the efficiency with which functionalizing chemicals are loaded onto nanoparticles. The biomolecules, like proteins, are readily adsorbed on the surface because of their strong surface affinity. In some cases, the reducing agent of gold precursor for synthesis of AuNPs also serves as a stabilizing agent. For instance, the antibiotic serves as both reducing and a capping agent in antibiotic-conjugated AuNPs [7].

Due to their low toxicity, biocompatibility, and colloidal stability, the functionalized AuNPs are utilized extensively in biomedical applications, including biosensing, anticancer therapy, hyperthermia, drug and gene delivery, and bioimaging [8]. The AuNPs are produced using various synthetic procedures and surface functionalized with various compounds including biomolecules such as, nucleic acid and proteins for different biomedical applications.

1.2   Synthesis of gold nanoparticles (AuNPs):

AuNPs can be synthesized by variety of approaches. These methods are primarily grouped as "top-down" and "bottom-up" methods. In the top-down method, matter is taken out of bulk material through a subtractive process in order to produce the desired, self-assembled nanoscale objects whereas, the bottom-up approach uses assembly of tiny atoms or reducing ions [9]. The top-down technique is rarely used due to the uncontrolled size distribution and the significant energy requirements needed to maintain the high pressure and temperature conditions for synthesis. The chemical and biological approaches are two of the most popular bottom-up methods. Although the chemical processes are simple and commonly used for synthesis, most reducing agents involved are harsh and toxic chemicals. However, biological techniques are safe for the environment because they do not require harmful chemicals and are environmentally friendly [10]. In contrast to biological approaches, which use the same reducing and functionalizing agents, chemical methods offer a wide range of functionalization options for nanoparticles. Chemical synthesis techniques offer control over particle size, whereas biological techniques produce big particles [11].

The chemical method is widely used approach for synthesis of AuNPs that involve reduction of gold ions (Au^{3+}) by reducing agent to get AuNPs (Au^0). The AuNPs synthesis is completed in two steps; 1) reduction by reducing agent (sodium borohydride, sulfites, sodium citrate, sugars, hydrogen peroxide, polymers, and acetylene), 2) stabilization by stabilizing agents (dendrimers, nitrogen/sulfur (thiolates)/oxygen-based ligands, and cetyltrimethylammonium bromide (CTAB)) [12]. The chemical synthesis methods are divided into different types such as, Turkevich reduction method, Brust method, seeded growth method, and miscellaneous method. Among these methods, the Turkevich reduction method is most commonly used for synthesis of AuNPs. In 1951, Turkevich described a chemical reduction method for synthesis of AuNPs with spherical shape and 10-30 nm size range [13]. The basic principle of Turkevich method involves reduction of gold precursor ($HAuCl_4$) by different reducing agents like, trisodium citrate, amino acid, ascorbic acid, and different polymers. The Turkevich method was further modified by Frens in 1973, to generate AuNPs within range of 10 to 150 nm using

reducing agent in different concentration ratios. A higher citrate concentration results in smaller AuNPs, whereas a lower concentration causes small particles to aggregate into larger ones. Variation in synthesis parameters (pH, temperature, precursor concentration, and reaction time) affects the size of AuNPs.

1.3 Functionalization of gold nanoparticles (AuNPs):

Following synthesis, functionalization of AuNPs is a crucial step that can increase the usefulness of AuNPs in numerous ways. AuNPs are functionalized to increase their stability and suitability for application in aqueous and physiological conditions [14]. Various chemicals and biomolecules can be used to modify AuNPs. They can interact with substances that contain sulphur such as, thiols, disulfides, and amino acids. Surface modification of AuNPs is accomplished using alkane thiols. Functionalization of AuNPs with antibodies is possible through -COOH functional group present in antibody structure [15]. Coating the surface of AuNPs with polymers such as, polyvinyl pyrrolidone (PVP), polyacrylic acid (PAA), and polyvinyl alcohol (PVA) is another approach that facilitate functionalization with antibodies. Interactions between AuNPs and proteins in the biosystem can influence sensing results, so the functionalization of AuNPs is employed to prevent unwanted interactions with proteins. For instance, functionalization using PEG (polyethylene glycol) prevents the unintended interaction of protein and AuNPs [16].

Water-soluble polymers like PEG can be used to modify materials, and PEG-modified AuNPs are created using either electrostatic interactions or thiol group linkage. The stability of AuNPs is also influenced by the molecular weight and chain length of polymers. The PEG functionalization, or PEGylation as it is more commonly known, increases the effectiveness of AuNPs in the physiological environment. PEG functionalized AuNPs were reported to be used in numerous biomedical applications, including sensing, bioimaging research, and drug delivery [17].

Nanoparticles functionalized with biomolecules, such as DNA, hold great potential for a wide range of biomedical applications. The functionalization of AuNPs depends on the specific characteristics of both the nanoparticles and the DNA

molecules [18]. AuNPs can be functionalized with various biomolecules, including nucleic acids (DNA, RNA), proteins, peptides, and antibiotics, making them versatile carriers for different applications. Functionalization is achieved through the incorporation of thiol groups, peptides, amino acids, and electrostatic interactions. This addition provides the surface that is required for biomolecules to bind with the surface of AuNPs. Various methods, including gel electrophoresis, plasmon absorption, quartz crystal microbalance (QCM), light scatter, and high-performance liquid chromatography (HPLC) are used to characterize the AuNPs and biomolecule conjugates. These biomolecule conjugates have particular functions and could be used in molecular therapy for a number of illnesses [19].

When AuNPs are functionalized with antibiotics, they become more effective against pathogenic and resistant bacteria and reduce the minimum inhibitory concentration (MIC) range of antibiotics in comparison to antibiotics alone. Variety of antibiotics, including kanamycin, amoxicillin, tetracycline, colistin, and ampicillin has been used for functionalization of AuNPs. The AuNPs are also modified with medicinal molecules such as, anticancer drugs, for use in drug delivery systems. According to reports, glutathione-modified AuNPs were utilized for the intracellular drug delivery [20]. The functionalization of AuNPs with biomolecules such as, nucleic acids, proteins (antibiotics), and peptides improve the detection and treatment of diseases. Additionally, functionalization with biomolecules reduces the interaction between nanoparticles and the immune system. Because AuNPs are capable of imaging and sensing, antibody-modified AuNPs are used for efficient immunosensing applications. Pathogen detection from the samples is carried out using specific oligonucleotide functionalized AuNPs [21]. Functionalization not only increases the efficiency of AuNPs for drug transport, bio-imaging, and therapeutic capacities but also enhances the potential for future functionalization and sensing capabilities. Thus, the functionalization of AuNPs with various compounds enhances stability of AuNPs and is discovered to be quite advantageous.

1.4   Interactions between nucleic acid and gold nanoparticles (AuNPs):

The study of structural biology depends on the interactions of DNA with ligands, whether they be lengthy DNA chains with hundreds of base pairs or small

oligonucleotides. Its biological activity can frequently be influenced by the speed of those formed complex, in addition to the thermodynamic characteristics of DNA-ligand complexes. In contrast, gold nanoparticles are well known for their exceptional biocompatibility with biomolecules and are notable for their structural, electronic, catalytic, and optical properties. In order to control and modulate these interactions, as well as to open up new research areas in the fields of nanomedicine, analytical chemistry, and biology, a better understanding of how DNA interacts with nanoparticles acting as small ligands is essential.

For gene delivery, it is essential to evaluate how well a nucleic acid binds to the respective nanoparticle. The broad search for diverse gene carriers has led to the emergence of complexes formed between nucleic acids and nonviral nanocarriers, which hold promise as efficient alternatives to the mostly viral-based gene delivery vehicles [22]. It has been reported that the biomolecules like DNA [23, 24] and proteins [25] are adsorbed on surface of AuNPs by either covalent or non-covalent interactions.

1.4.1   Covalent interactions between gold nanoparticles and Nucleic acid:

Very few reports are available for interactions between nucleic acid and AuNPs. The study of interaction is crucial for biological applications, as nitrogenous bases of nucleic acid strongly influence the nucleic acid adsorption on gold surface. Thus, the type and degree of nucleic acid interaction with gold surface actually depends on the sequence of nitrogenous bases (Adenine, Guanine, Cytosine and Thymine) present in nucleic acid. The binding ability of nitrogenous bases to surface of AuNPs is ranked as A>G>C>T [26, 27].

The interaction between sulphur and gold (S-Au) is a strong metal ligand interaction that allows binding of chemical and biological molecules on surface of AuNPs. According to energy decomposition study, as compare to copper (Cu) and silver (Ag), gold (Au) shows stronger covalent interactions with sulphur [28]. It has been reported that, nucleic acid can attach to AuNPs via covalent interactions for various biomedical applications including gene silencing and bioimaging where, the modifications does not interfere with biological activity [29, 30]. Mirkin *et. al.* [31] in

1996, first time reported the binding of nucleic acid to gold nanoparticles via covalent interactions that widely exploited the DNA and AuNPs interaction. Oligonucleotides, a small DNA sequence of nucleotides, attached to AuNPs surface and get protection against nuclear degradation by nucleases. Thiol groups in the 5' or 3' positions of DNA suggest the potential for the development of a covalent link with the surface of the AuNPs, which could improve the colloidal stability and functionalize the target AuNPs. **Figure 1.2** shows the covalent binding of nucleic acid sequences to surface of AuNPs by thiol group and involvement of nucleotide in interactions. The interaction between sulphur and gold is a strong metal ligand interaction (S-Au covalent interaction) that allows binding of chemical and biological molecules on surface of AuNPs. Thus, thiolated nucleic acid sequences interact with AuNPs surface via strong covalent interactions. Beside this, the nucleotides (Adenine, Thymine, Cytosine and guanine) are also involved in interactions with surface of AuNPs through amine (-NH$_2$) and hydroxyl group (-OH) present in their structure [32].
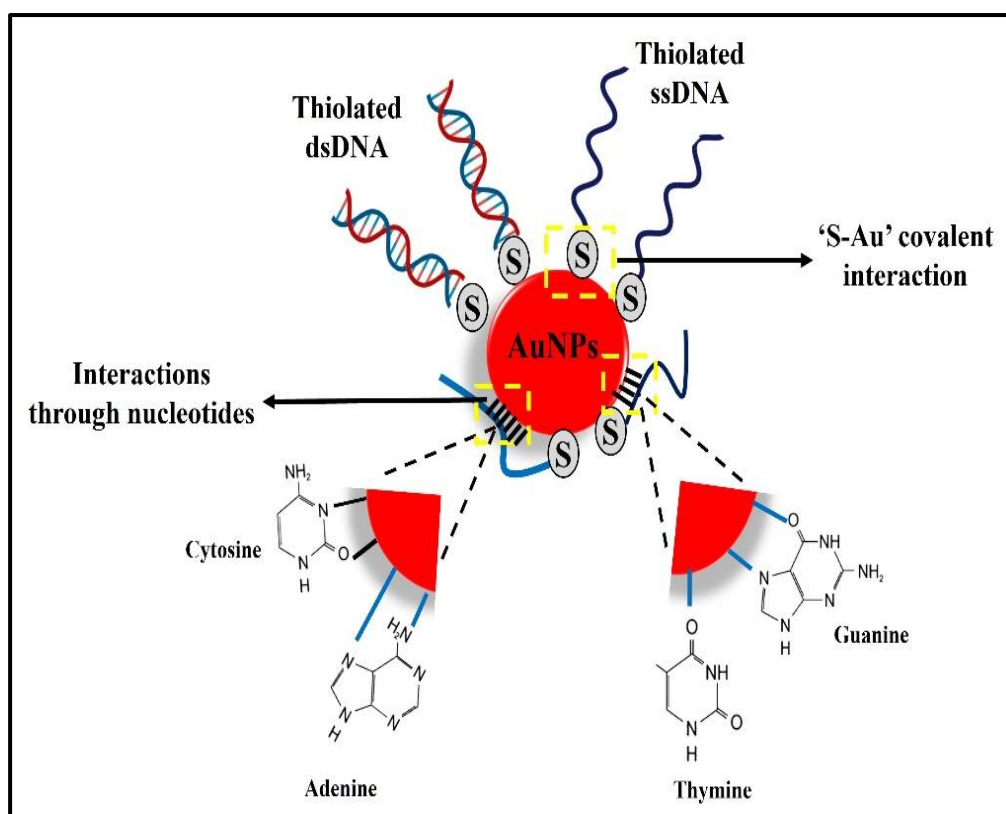
Figure 1.2: Covalent interactions between nucleic acid and gold nanoparticles (AuNPs)

1.4.2   Non-covalent interactions between gold nanoparticles and Nucleic acid:

The non-covalent interactions for nucleic acid conjugation provides a better alternative for covalent interactions. Unmodified nucleic acid (DNA for gene therapy and RNA for gene silencing) can be delivered using supramolecular conjugates. These systems offer a variety of possibilities for vehicle design, including layer-by-layer-fabricated AuNPs, amino acid or polymer functionalized AuNPs, and mixed-monolayer-protected AuNPs. The cationic polymers such as, chitosan, Poly-L-Lysine (PLL), polyethyleneimine (PEI), cationic lipids, and cysteine are used for AuNPs synthesis with surface positive charge. These synthesized positively charged AuNPs shows stability without aggregation in presence of biological conditions [33].

The cationic AuNPs acts as better partner for binding of nucleic acid due to the strong negative charge of nucleic acid. The negatively charged nucleic acid binds with positively charged AuNPs via non-covalent (electrostatic) interactions. Here, the nucleic acid binds to AuNPs by bending over AuNPs so DNA gets protection against nuclear degradation by nucleases [28]. The non-covalent interactions between nucleic acid and AuNPs are the type of either electrostatic, hydrophobic or Van der Waals interactions by involvement of phosphate groups, and amino groups of nitrogenous bases. Non-covalent interactions of nucleic acid and AuNPs are reported for showing higher resistance against nuclear degradation and provides effective desorption in synthetic biological media [34].

Chitosan, PEI, amino acids (cysteine) and biopolymer like Poly-L-Lysine (PLL) offer variable molecules that can be used to modify AuNPs functionality. Studies on the interaction between double-stranded DNA (dsDNA) and AuNPs functionalized with cationic amino acids revealed that side chains with higher cationic character were more effective binders than hydrophobic analogues [35]. AuNPs are modified with amino acids and polypeptides to produce biologically inspired characteristics. The first-generation lysine-dendron-functionalized AuNPs and the high charge density of lysine allow for compact complexes with plasmid DNA. By using this technique, monodispersed PLL-AuNPs nanoparticles with a strong plasmid DNA binding ability are produced [30]. Thus, cationic polymer acts as an effective carrier for nucleic acid binding that utilized for biosensing application.

1.5   Biomedical applications of gold nanoparticles (AuNPs):

AuNPs with different functionalization have biomedical applications in biosensing, drug delivery, cancer treatment, anticancer, and antibacterial activity. In **figure 1.3**, the various biomedical applications of AuNPs and potential mechanisms are described.
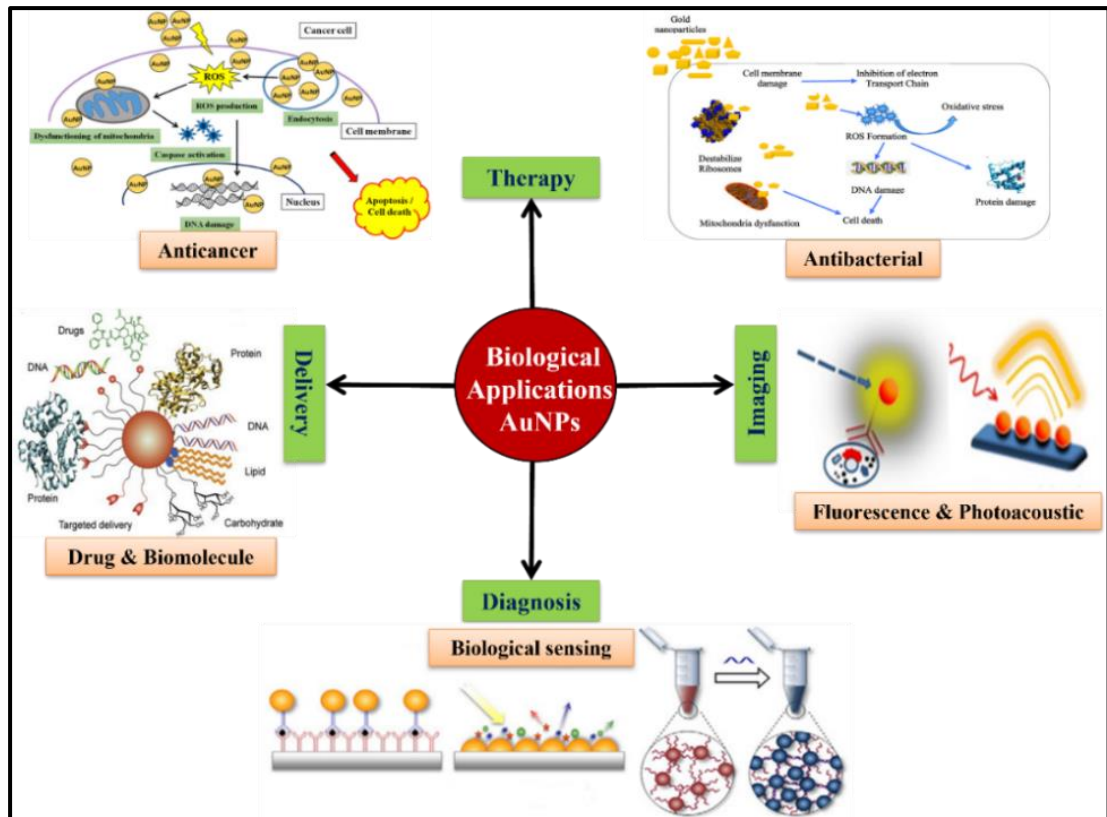
Figure 1.3: Mechanism of different biomedical applications of gold nanoparticles (AuNPs) regarding therapy, imaging, diagnosis, and delivery [4]

In cancer therapy, AuNPs are employed for gene delivery. Nucleic acids are utilised to silence oncogenes, control the cell cycle, and repair damaged genes. For entry inside the cells and protection against nuclear degradation by nucleases, DNA needs a carrier. AuNPs demonstrate excellent transfection capabilities owing to their biocompatibility and low toxicity. Thus, nucleic acid is conjugated with AuNPs for gene delivery into cancer cells [36]. To silence genes without compromising biological activity, oligonucleotides are covalently coupled to gold nanoparticles. Here, mRNA and RNA interference (RNAi) are employed to create a double-stranded

hybrid that inhibited the expression of an oncogene. Small interfering RNAs (siRNAs) and microRNAs (miRNAs) are transfected with AuNPs to silence certain genes [37].

The conjugation between thiolated nucleic acid and AuNPs demonstrates greater affinity for complementary strand than the linear one and quick cellular absorption. Functionalized AuNPs have been used to transport nucleic acids via non-covalent contact. RNA molecules and plasmid DNA can transfer through functionalized AuNPs with quaternary ammonium, poly-ethylenimine (PEI), amino acids, and biopolymer like Poly-L-Lysine (PLL). Positively charged AuNPs are the superior alternative for negatively charged nucleic acids. Like the chromatin structure, positively charged spherical AuNPs attach to negatively charged nucleic acids non-covalently, protecting them from nuclease destruction. These non-covalent interactions show how the nucleic acid to AuNPs ratio, surface charge, and hydrophobic nature of the conjugate influence gene delivery [32].
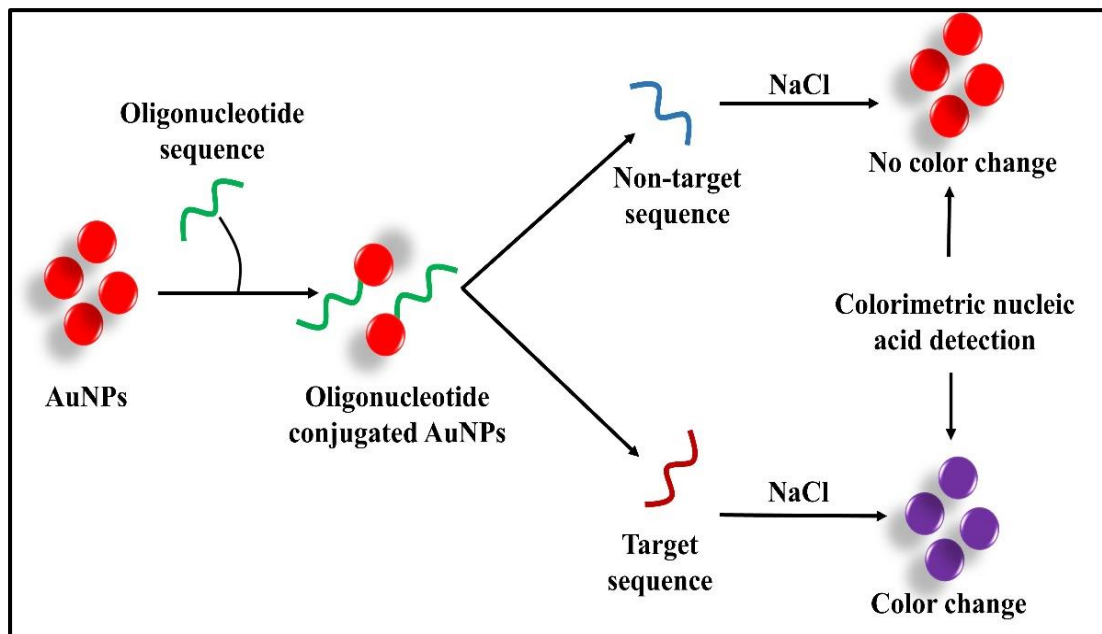
Figure 1.4: Schematic presentation for colorimetric detection of target by oligonucleotide conjugated gold nanoparticles (AuNPs)

AuNPs are highly effective in both optical and electrochemical biosensing applications due to their physicochemical properties [38]. The biosensors are made by assembling AuNPs with certain biomolecules such as, nucleic acid sequences

(oligonucleotides) or antibodies. The particular nucleic acid sequences are either coupled to functionalized or non-functionalized AuNPs. Pathogens can be found using this method in clinical, food, or water samples, even at concentrations as low as pg/mL. The complementary pathogenic DNA sequences in the oligonucleotides are composed of 20–30 nucleotides [39]. Standard AuNPs tend to agglomerate when exposed to salt unless they are stabilised by a nucleic acid. When these nanocomplexes are combined with target and non-target samples, the target sample exhibits a change in color (from wine-red to violet) as a result of complementary strand interactions that lead to AuNPs aggregation, as seen in **figure 1.4**. Similar to this, AuNPs are also utilised in electrochemical biosensing, a quick, easy, and accurate method for detecting biomolecules. Between electroactive biological organisms and electrodes, AuNPs can transport electrons [40]. The oxidation and reduction of analytes, which are catalysed by the bioreceptor unit, are part of the enzyme biosensing process. In order to transmit the electrons needed for the redox reaction from the redox centre of enzyme to the electrode, AuNPs operate as an electron shuttle [41]. Electrochemical biosensors can detect target molecule even at fM concentration from the mixture showing high sensitivity towards analyte.

1.6   Literature survey on biomedical applications of gold nanoparticles nucleic acid (AuNPs-NA) conjugate:

DNA conjugation with AuNPs is achieved by either covalent or non-covalent interactions. The reported study mentions the use of oligonucleotides for synthesis of AuNPs-nucleic acid conjugate. The thiolated and non-specific interactions of oligonucleotide with AuNPs have been utilized for development of colorimetric and electrochemical pathogen detection system [42, 43], detection of defective DNA [44], and gene delivery [45]. Through oligonucleotide modification, the characteristics of AuNPs can be modified. Interesting characteristics of nanoconjugate includes, high internalization in a wide range of cells and no toxicity [46]. Rapid and precise point-of-care diagnostic methods are essential in tailored medicine. Nucleic acid-based detection is crucial for the detection of diseases caused by genetic abnormalities, viral/bacterial infections. Conventional techniques like RT-PCR, while highly accurate and sensitive, are not ideal for routine diagnosis due to their time-consuming nature, the need for expensive equipment, and the requirement for skilled personnel to

operate them. Thus, there is need to develop novel, rapid, easy to handle detection system for sensitive diagnosis of diseases [47]. AuNPs and oligonucleotides conjugation is achieved by incubating the oligonucleotides with AuNPs. Though the preparation may have slight change depending on use of linkers. Use of thiol or dithiol for preparation of stronger nanoconjugate require few hours to 24 hours. Modified AuNPs can be used as sensors for range of biomarkers or pathogenic nucleic acid, with their electrical and optical features being utilized for a practical, simple, and quick detection [48]. The various applications of AuNPs-nucleic acid conjugates are listed in **table 1.1**. AuNPs were functionalized with different polymers such as, PEI, PEG, chitosan, and Diosmin and conjugated with thiolated nucleic acid (mRNA, DNA, siRNA). These conjugates were utilized for pathogen detection, gene silencing, and gene delivery.

Table 1.1: Different biomedical applications of gold nanoparticles-nucleic acid (AuNPs-NA) conjugates

Sr. No.	AuNPs/ Functionalized AuNPs	Type of nucleic acid entity	Biomedical application	Ref
1.	PEI- AuNPs	Oligonucleotide	Pathogen detection	[49]
2.	PEG- AuNPs	mRNA	Gene delivery for immune-modulatory treatment	[50]
3.	AuNPs	Thiolated DNAi	Silencing of Bcl-2 oncogene in cancer cell line	[51]
4.	AuNPs	DNA	Colorimetric assay of helicase activity	[52]
5.	AuNPs	DNA	mRNA detection	[53]
6.	Chitosan, PEG	siRNA	Increase *c-MYC* silencing in breast cancer cells	[45]
7.	AuNPs	siRNA	Regulate tumour necrotic factor α (TNFα) gene expression in inflammatory diseases	[54]
8.	AuNPs	Histidine tagged DNA aptamer	Elimination of intracellular *S. Typhimurium* cells *in-vitro* and *in-vivo*.	[55]
9.	Diosmin- AuNPs	Calf thymus DNA	Rational drug designing at molecular level	[56]

10.	AuNPs	ssDNA probe	Detection of foodborne bacteria	[57]
11.	AuNPs	Oligonucleotides	*Salmonella* spp detection from food sample	[21]
12.	AuNPs	Antisense oligonucleotides	Electrochemical biosensing of SARS-CoV-2 RNA	[58]

1.6.1 Literature survey on colorimetric detection of nucleic acid by gold nanoparticles-nucleic acid (AuNPs-NA) conjugate:

Surface Plasmon Resonance (SPR) characteristics of AuNPs were dependent on the morphological characteristics of the nanoparticles. The surface plasmon resonance (SPR) of gold nanoparticles (AuNPs) is an optical property that involves the oscillation of electrons in the conduction band when exposed to light of a specific wavelength. This oscillation results in a shift in the frequency, leading to a visible color change in the gold nanoparticles, which can be observed with the naked eye. The color change is caused by variations in both the light frequency and the size of the nanoparticles [59]. Various colorimetric biosensors for biomolecule detection and immunobiosensors have been developed using this unique property of AuNPs. AuNPs in a variety of shapes, including nanorods, nanospheres, nanoshells, and nanostars, have been investigated for their optical characteristics and potential use in biosensing. The SPR of AuNPs increases the sensitivity of sensors for the detection of nucleic acid, proteins, and enzymes.

The AuNPs are conjugated with biomolecules for biosensor preparation. When these nanocomplexes are combined with target and non-target samples, the target sample exhibits a color change (from wine-red to blue) as a result of complementary interactions that lead to AuNPs aggregation. The 2,2,6,6-tetramethylpiperidin-1-piperidinyloxy (TEMPO)-oxidized cellulose nanocrystal (TEMPO-CNC) functionalized AuNPs were utilized in the investigation to detect unamplified pathogenic DNA of methicillin-resistant *Staphylococcus aureus* [60].

AuNPs are conjugated with oligonucleotides by two methods for nucleic acid detection: (i) by the adsorption of nucleic acid on AuNPs or through the reaction of thiol group hybridized nucleic acid; and (ii) through the use of cationic gold

nanoparticles that conjugated to the anionic nucleic acid to prevent aggregation. Colorimetric detection of Hepatitis C RNA was carried out by using gold nanoparticles and antisense oligonucleotide conjugates with 100 IU/mL detection limit within 30 min of time period [61]. The colorimetric detection approach of AuNPs was used by many researchers for the detection of different pathogens from different sources such as, food, water, and clinical samples that are listed in following **table 1.2**. AuNPs conjugated with DNA are reported for the detection of different bacteria and viruses from food, urine, and serum samples.

Table 1.2: Colorimetric detection of pathogens by gold nanoparticles-nucleic acid (AuNPs-NA) conjugates

Sr. No.	Name of pathogen	Functionalized AuNPs	Aptamer	LOD	Ref
1.	*Salmonella spp*	AuNPs	Thiol modified oligonucleotides	<10 CFU/mL	[21]
2.	Methicillin-resistant *Staphylococcus aureus*	TEMPO-CNC-AuNPs	DNA	20 fM	[60]
3.	*E. coli O157*	AuNPs	DNA	10^3 CFU/mL	[62]
4.	*Klebsiella pneumoniae*	AuNPs	DNA	3.4×10^3 CFU/mL	[63]
5.	*Helicobacter pylori*	AuNPs	DNA probe	0.5 nM	[64]
6.	*Salmonella*	AuNPs	DNA	nucleic acids from 10^7 bacteria	[65]
7.	*Mycobacterium avium subspecies paratuberculosis*	AuNPs	Thiol-modified oligonucleotide	103 ng	[66]
8.	*Pseudomonas aeruginosa*	AuNPs	Aptamers	10^8 to 10^5 CFU mL^{-1}	[67]
9.	*Salmonella* enteric serovar typhimurium	AuNPs	Bifunctional oligonucleotide probes	10 CFU/mL	[68]

10.	*S. aureus*	AuNPs	Peptide nucleic acid	10^6 cells	[69]
11.	*Listeria monocytogenes*	Biosynthesized flower-shaped AuNPs	ssDNA	100.4 ng	[70]
12.	SARS-CoV-2	AuNPs	oligonucleotides	$\geq$103 - 104 viral RNA copies/μL	[71]
13.	SARS-CoV-2	Cys-AuNPs	DNA	0.12 nM	[72]
14.	Bovine viral diarrhea virus	AuNPs	Charge neutral peptide nucleic acid	10.48 ng	[73]
15.	HIV-1	AuNPs	Oligonucleotides (5'UTR)	1.5 pM	[74]
16.	Dengue	Dextrin-AuNPs	DNA	1.2×10^4 pfu/mL	[75]
17.	Hepatitis E	AuNPs	DNA	10 pM	[76]
18.	Hepatitis C	AuNPs	DNA	4.57 IU/μL	[77]
19.	SARS-CoV-2, Influenza B, MERS	Sialic acid-AuNPs	-	0.1 μM	[78]

1.6.2 Literature survey on electrochemical detection of nucleic acid by gold nanoparticles-nucleic acid (AuNPs-NA) conjugate:

Another use for AuNPs in the biosensing field is the electrochemical biosensor. For quick, simple, and accurate detection of biomolecules, electrochemical biosensors are used. Gold nanoparticles have the capacity to transport electrons between electrodes and electroactive biological entities [79]. In the enzyme biosensing process, the function of bioreceptor unit is to catalyse the oxidation and reduction of analytes. AuNPs function as an electron shuttle, transporting the required electrons for the redox reaction to the electrode as they approach the redox center of an enzyme [41].

Table 1.3: Electrochemical detection of pathogens by gold nanoparticles-nucleic acid (AuNPs-NA) conjugates

Target	Probe	Modified electrode	Hybridization indicator	Analysis period	Method	LOD	Ref
SARS-CoV-2 RNA	Functionalized amine group with DNA probe	Interdigitated platinum/titanium electrodes	-	2 h	Capacitance measurement	10 nM	[80]
Klebsiella pneumoniae carbapenemase	Thiolated DNA	AuNPs/Gr/GCE	Methylene blue	1.5 h	DPV	2×10^{-13} mol/L	[81]
Helicobacter pylori	Thiolated DNA	GO/AuNPs/GCE	Oracet blue	3.41h	DPV	27.0 pM	[82]
SARS-CoV-2 RNA	Thiolated DNA	AuNTs/SPCE	Azure A	1.5 h	DPV	22.2 fM	[44]
SARS-CoV-2 RNA	Thiolated DNA	Au/G-PLA	-	1.5 h	CV and EIS	0.30 μmol	[83]
SARS-CoV-2 RNA	Oligonucleotides (51 Nt length)	AuNPs/WO3-SCPE with 4ATP monolayer	-	10 min	CV and EIS	298 fM	[84]
Hepatitis C RNA	Thiolated DNA	Cu$_2$O/AuNPs/NG/FTO	-	2.5 h	DPV	1×10^{-15} M	[85]
SARS-CoV-2 (ORF1ab)	Thiolated DNA	AuNs/AuSPE	MB-CDs	1.5 h	DPV	2.2 aM	[86]

According to the study, L-cysteine in bodily fluids and an anti-HIV medication in serum and urine samples could both be found using AuNPs-based electrochemical biosensors. The response time of these electro-biosensors, which can detect µM/L, is only a few seconds. According to reports, HPV was sensitively detected using electrochemical DNA biosensors. An electrochemical impedimetric biosensor based on AuNPs can also be used to detect the breast cancer tumor marker MUC1. In this case, MUC1 aptamer-functionalized AuNPs were employed, with cDNA serving as a linker to bind and amplify the signal. According to the study, even at concentrations as low as 0.1 nM, aptamer-conjugated AuNPs are capable of sensitively detecting MUC1 [87]. All of these AuNPs sensing applications are applied not only in bioanalytical research but also, in other fields of study. Any desired size and shape of nanoparticles can be produced using a particular synthesis method, and these various AuNPs sizes exhibited various optical, catalytic, and electrical behaviours. Various examples of electrochemical biosensing using AuNPs-NA conjugates were listed in **table 1.3**.

According to available literature survey, only few publications are known for synthesis of cationic gold nanoparticles and their interactions with nucleic acid for biosensing and transfection applications. Thus, the purpose of this proposed work is to synthesize cationic gold nanoparticles using one pot synthesis approach. These cationic nanoparticles interact with nucleic acid to form gold nanoparticles-nucleic acid (AuNPs-NA) conjugate without any surface modification by simple incubation procedure. These AuNPs-NA conjugates are then utilized for biomedical application like biosensing. The proposed method is simple, low cost, and applicable for viral/bacterial nucleic acid detection without need of any complex instrumentation.

1.7   Orientation and purpose of thesis:

Metal nanoparticles have been used for a variety of biomedical applications because they possess beneficial properties. Gold nanoparticles is one of the widely used metal nanoparticles for different biomedical applications like, biosensing, gene delivery, drug delivery, antibacterial and antiviral activity, heavy metal detection and anticancer activity. Gold nanoparticles have unique physico-chemical characteristics like, easy synthesis, high surface to volume ratio, easy functionalization, non-toxicity,

biocompatibility, and size tunability. These characteristics make them an excellent contender for biomedical applications, including biosensing. The researchers have worked on various strategies for improving the interactions of AuNPs with nucleic acid. Biosensing can be improved by conjugating nucleic acid with AuNPs with respect to specificity, sensitivity, cost effectiveness, and simplicity. An effective colorimetric and electrochemical detection ability of gold nanoparticles possibly increases its application in biosensing. The surface functionalization of AuNPs and their interaction with nucleic acid are the important factors in conjugate formation for biomedical applications. Polymer coating of AuNPs contributes to stability and the cationic nature of polymer provides efficient binding with anionic genetic material that helps in biomedical applications. Cationic polymer coating gold nanoparticles can act as a suitable carrier for nucleic acid in different applications. However, there is need to find out efficiency of cationic polymer functionalized AuNPs as a suitable candidate for nucleic acid binding and to be used in biosensing and transfection study.

It is reported that, nucleic acid is a promising therapeutic approach in different diseases such as, cancer, genetic disorders, and diabetes. Nucleic acid-based biosensors are also developed due to their specificity and sensitivity. Nucleic acids need a carrier or vector to protect them from nucleases that can degrade the genetic material. Nanomaterials are used as a vector due to their unique characteristics. The use of metal nanoparticles in gene delivery as a non-viral vector is well documented. Among different metal nanoparticles, gold nanoparticles are gaining attention to be used as gene carrier for different biomedical applications including diagnosis and treatment. Negatively charged gold nanoparticles are conjugated with nucleic acid probe via covalent interactions such as, disulphide (S-S) bonding. This will need thiol (-SH) modification of either nucleic acid probe or AuNPs surface. The gold nanoparticles are first synthesized with chemical reduction method and then modified with different chemical agents. The nanoparticles also need salt aging process for their stability. This overall process is time consuming and tedious that also increase the overall cost of the method. Beside this, the use of positively charged gold nanoparticles minimizes the need of surface modification of nanoparticles as well as nucleic acid. They can easily interact with negatively charged nucleic acid through

electrostatic interactions. Also, salt aging process is not required for stabilization of the nanoparticles.

Data suggests the use of gold nanoparticles in optical detection of pathogenic nucleic acid for diagnosis of disease without use of any complex instrumentation. AuNPs are widely used for detection of pathogen and to prepare point of care devices. For DNA biosensor, negatively charged AuNPs are used for either colorimetric or electrochemical detection but, the positively charged AuNPs are rarely explored. The negatively charged AuNPs were conjugated with nucleic acid through thiol modification. This will require functionalization of AuNPs with different chemical agents as well as modified nucleic acid probe, that eventually increases the cost of the process. Despite the fact that AuNPs are utilized as non-viral gene carriers, there are still some issues that need to be resolved. These challenges contain, easy synthesis of AuNPs, choice of functional group that acts as both reducing and functionalizing agent, cytotoxicity of AuNPs, sensitivity for colorimetric as well as electrochemical detection, and increasing their transfection ability.

The work is focused on PLL functionalized gold nanoparticles (PLL-AuNPs) synthesis by one pot synthesis method and its conjugation with nucleic acid for biomedical applications. The synthesized material offers exclusive properties like, high surface to volume ratio, crystal structure, and positive surface charge. The biopolymer Poly-L-Lysine itself acts as reducing and functionalizing agent, thus there is no need of any other functionalizing agent. Thus, functionalization is carried out in further steps of synthesis using PLL. The prepared PLL-AuNPs are then conjugated with DNA probe under optimized conditions. These conjugates are utilized for different biomedical applications such as, viral and bacterial nucleic acid detection. The pathogen detection is carried out in terms of optical and electrochemical analysis. Finally, the conclusions are drawn based on the evaluation of the conjugate formed between PLL-AuNPs and nucleic acids, which is assessed for its stability, binding efficiency, and functional performance in the intended application.

The physico-chemical and biological properties of synthesized material is studied by different characterization techniques. Nanoparticles preparation is visibly confirmed by observing color transition from pale yellow to wine-red and then conjugate preparation from wine-red to purple. After this, the nanoparticles and

nanocomplexes are preliminary characterized by UV-Vis absorption spectrum. The crystalline nature of PLL-AuNPs is studied by X-ray diffraction (XRD) technique. Fourier Transform Infrared Spectroscopy (FTIR) is used to examine the presence of functional groups. Transmission electron microscopy (TEM) is used to examine the shape and dimensions of nanomaterial. For the purpose of analyzing the elemental composition of PLL-AuNPs, the Energy-Dispersive X-ray Spectroscopy (EDAX) method is applied. Surface charge present on PLL-AuNPs and their conjugate is studied by zeta potential analysis. The hydrodynamic size of PLL-AuNPs and its conjugate is studied by Litesizer 500. The formation of conjugation between PLL-AuNPs and nucleic acid is confirmed by band shift assay. The optical detection of pathogen using PLL-AuNPs nucleic acid conjugate is analyzed by naked eye as well as confirmed by UV-Vis absorption study. The electrochemical detection was studied by observing Cyclic Voltammetry (CV), Square Wave Voltammetry (SWV), Differential Pulse Voltammetry (DPV), and Electrochemical Impedance Spectroscopy (EIS) by using three electrode system.

1.8   References:

[1] Feynman RP. There's plenty of room at the bottom. Resonance. 2011;16(9):890-905.

[2] Morais MG, Martins VG, Steffens D, Pranke P, da Costa JA. Biological applications of nanobiotechnology. Journal of nanoscience and nanotechnology. 2014;14(1):1007-17.

[3] Elahi N, Kamali M, Baghersad MH. Recent biomedical applications of gold nanoparticles: A review. Talanta. 2018;184(1):537-56.

[4] Patil T, Gambhir R, Vibhute A, Tiwari AP. Gold nanoparticles: Synthesis methods, functionalization and biological applications. Journal of Cluster Science. 2023;34(2):705-25.

[5] Yeh YC, Creran B, Rotello VM. Gold nanoparticles: preparation, properties, and applications in bionanotechnology. Nanoscale. 2012;4(6):1871-80.

[6] Amendola V, Pilot R, Frasconi M, Maragò OM, Iatì MA. Surface plasmon resonance in gold nanoparticles: a review. Journal of Physics: Condensed Matter. 2017;29(20):203002-50.

[7] Patil T, Khot V, Pandey-Tiwari A. Single-step antibiotic-mediated synthesis of kanamycin-conjugated gold nanoparticles for broad-spectrum antibacterial applications. Letters in Applied Microbiology. 2022;75(4):913-23.

[8] Shah M, Badwaik VD, Dakshinamurthy R. Biological applications of gold nanoparticles. Journal of Nanoscience and Nanotechnology. 2014;14(1):344-62.

[9] Mehravani B, Ribeiro AI, Zille A. Gold nanoparticles synthesis and antimicrobial effect on fibrous materials. Nanomaterials. 2021;11(5):1067-104.

[10] Hammami I, Alabdallah NM. Gold nanoparticles: Synthesis properties and applications. Journal of king Saud university-science. 2021;33(7):101560-70.

[11] Ahmed S, Ikram S. Biosynthesis of gold nanoparticles: a green approach. Journal of Photochemistry and Photobiology B: Biology. 2016;161(1):141-53.

[12] Herizchi R, Abbasi E, Milani M, Akbarzadeh A. Current methods for synthesis of gold nanoparticles. Artificial cells, nanomedicine, and biotechnology. 2016;44(2):596-602.

[13] Dong J, Carpinone PL, Pyrgiotakis G, Demokritou P, Moudgil BM. Synthesis of precision gold nanoparticles using Turkevich method. KONA Powder and Particle Journal. 2020;37(1):224-32.

[14] Alex S, Tiwari A. Functionalized gold nanoparticles: synthesis, properties and applications—a review. Journal of nanoscience and nanotechnology. 2015;15(3):1869-94.

[15] Mahato K, Nagpal S, Shah MA, Srivastava A, Maurya PK, Roy S, Jaiswal A, Singh R, Chandra P. Gold nanoparticle surface engineering strategies and their applications in biomedicine and diagnostics. 3 Biotech. 2019;9(1):1-9.

[16] Suk JS, Xu Q, Kim N, Hanes J, Ensign LM. PEGylation as a strategy for improving nanoparticle-based drug and gene delivery. Advanced drug delivery reviews. 2016;99(1):28-51.

[17] Anniebell S, Gopinath SC. Polymer conjugated gold nanoparticles in biomedical applications. Current medicinal chemistry. 2018;25(12):1433-45.

[18] Tiwari AP, Ghosh SJ, Pawar SH. Biomedical applications based on magnetic nanoparticles: DNA interactions. Analytical Methods. 2015;7(24):10109-20.

[19] Lee JW, Choi SR, Heo JH. Simultaneous stabilization and functionalization of gold nanoparticles via biomolecule conjugation: Progress and perspectives. ACS Applied Materials & Interfaces. 2021;13(36):42311-28.

[20] Amina SJ, Guo B. A review on the synthesis and functionalization of gold nanoparticles as a drug delivery vehicle. International journal of nanomedicine. 2020;15(1):9823-57.

[21] Quintela IA, de Los Reyes BG, Lin CS, Wu VC. Simultaneous colorimetric detection of a variety of *Salmonella spp.* in food and environmental samples by optical biosensing using oligonucleotide-gold nanoparticles. Frontiers in microbiology. 2019;10(1):1138-50.

[22] Singh M. Assessing nucleic acid: Cationic nanoparticle interaction for gene delivery. Bio-Carrier Vectors: Methods and Protocols. 2021;2211(1):43-55.

[23] Gorbunova EA, Epanchintseva AV, Pyshnyi DV, Pyshnaya IA. Noncovalent Adsorption of Single-Stranded and Double-Stranded DNA on the Surface of Gold Nanoparticles. Applied Sciences. 2023;13(12):7324-46.

[24] Epanchintseva A, Vorobjev P, Pyshnyi D, Pyshnaya I. Fast and strong adsorption of native oligonucleotides on citrate-coated gold nanoparticles. Langmuir. 2018;34(1):164-72.

[25] Fleischer CC, Payne CK. Nanoparticle–cell interactions: molecular structure of the protein corona and cellular outcomes. Accounts of chemical research. 2014;47(8):2651-59.

[26] Farkhari N, Abbasian S, Moshaii A, Nikkhah M. Mechanism of adsorption of single and double stranded DNA on gold and silver nanoparticles: investigating some important parameters in bio-sensing applications. Colloids and Surfaces B: Biointerfaces. 2016;148(1):657-64.

[27] Liu B, Liu J. Methods for preparing DNA-functionalized gold nanoparticles, a key reagent of bioanalytical chemistry. Analytical methods. 2017;9(18):2633-43.

[28] Ding Y, Jiang Z, Saha K, Kim CS, Kim ST, Landis RF, Rotello VM. Gold nanoparticles for nucleic acid delivery. Molecular therapy. 2014;22(6):1075-83.

[29] Yañez-Aulestia A, Gupta NK, Hernández M, Osorio-Toribio G, Sánchez-González E, Guzmán-Vargas A, Rivera JL, Ibarra IA, Lima E. Gold nanoparticles: Current and upcoming biomedical applications in sensing, drug, and gene delivery. Chemical Communications. 2022;58(78):10886-95.

[30] Bahadur KC R, Thapa B, Bhattarai N. Gold nanoparticle-based gene delivery: promises and challenges. Nanotechnology Reviews. 2014;3(3):269-80.

[31] Mirkin CA, Letsinger RL, Mucic RC, Storhoff JJ. A DNA-based method for rationally assembling nanoparticles into macroscopic materials. InSpherical Nucleic Acids. 1st edition, Jenny Stanford publishing, 2020;3-11.
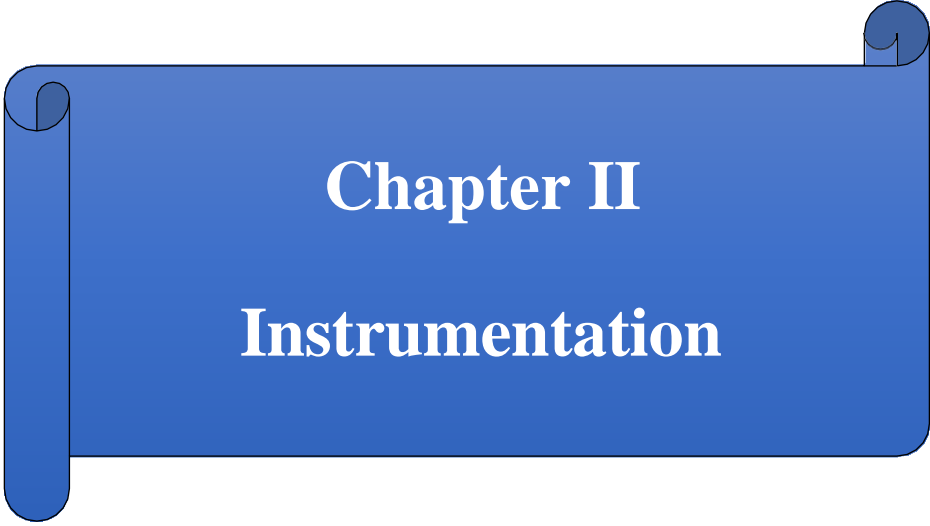
[32] Carnerero JM, Jimenez-Ruiz A, Castillo PM, Prado-Gotor R. Covalent and Non-Covalent DNA–Gold-Nanoparticle Interactions: New Avenues of Research. ChemPhysChem. 2017;18(1):17-33.

[33] Lazarus GG, Singh M. Cationic modified gold nanoparticles show enhanced gene delivery in vitro. Nanotechnology Reviews. 2016;5(5):425-34.

[34] Epanchintseva A, Dolodoev A, Grigor'eva A, Chelobanov B, Pyshnyi D, Ryabchikova E, Pyshnaya I. Non-covalent binding of nucleic acids with gold nanoparticles provides their stability and effective desorption in environment mimicking biological media. Nanotechnology. 2018;29(35):355601-20.

[35] Ghosh PS, Han G, Erdogan B, Rosado O, Krovi SA, Rotello VM. Nanoparticles Featuring Amino Acid-functionalized Side Chains as DNA Receptors. Chemical Biology & Drug Design. 2007;70(1):13-18.

[36] Graczyk A, Pawlowska R, Jedrzejczyk D, Chworos A. Gold nanoparticles in conjunction with nucleic acids as a modern molecular system for cellular delivery. Molecules. 2020;25(1):204-30.

[37] Ekin A, Karatas OF, Culha M, Ozen M. Designing a gold nanoparticle-based nanocarrier for microRNA transfection into the prostate and breast cancer cells. The journal of gene medicine. 2014;16(11-12):331-35.

[38] Verma MS, Rogowski JL, Jones L, Gu FX. Colorimetric biosensing of pathogens using gold nanoparticles. Biotechnology advances. 2015;33(6):666-80.

[39] Amirjani A, Rahbarimehr E. Recent advances in functionalization of plasmonic nanostructures for optical sensing. Microchimica Acta. 2021;188(1):1-17.

[40] Rasheed PA, Sandhyarani N. Electrochemical DNA sensors based on the use of gold nanoparticles: a review on recent developments. Microchimica Acta. 2017;184(1):981-1000.

[41] Hutter E, Maysinger D. Gold-nanoparticle-based biosensors for detection of enzyme activity. Trends in pharmacological sciences. 2013;34(9):497-507.

[42] Ahmadi S, Kamaladini H, Haddadi F, Sharifmoghadam MR. Thiol-capped gold nanoparticle biosensors for rapid and sensitive visual colorimetric detection of *Klebsiella pneumoniae*. Journal of Fluorescence. 2018;28(1):987-98.

[43] Del Caño R, García-Mendiola T, García-Nieto D, Álvaro R, Luna M, Iniesta HA, Coloma R, Diaz CR, Milán-Rois P, Castellanos M, Abreu M. Amplification-free detection of SARS-CoV-2 using gold nanotriangles functionalized with oligonucleotides. Microchimica Acta. 2022;189(4):171-83.

[44] Trantakis IA, Bolisetty S, Mezzenga R, Sturla SJ. Reversible aggregation of DNA-decorated gold nanoparticles controlled by molecular recognition. Langmuir. 2013;29(34):10824-30.

[45] Daniels AN, Singh M. Sterically stabilized siRNA: gold nanocomplexes enhance c-MYC silencing in a breast cancer cell model. Nanomedicine. 2019;14(11):1387-401.

[46] Mioc A, Mioc M, Ghiulai R, Voicu M, Racoviceanu R, Trandafirescu C, Dehelean C, Coricovac D, Soica C. Gold nanoparticles as targeted delivery systems and theranostic agents in cancer therapy. Current Medicinal Chemistry. 2019;26(35):6493-513.

[47] Coutinho C, Somoza Á. MicroRNA sensors based on gold nanoparticles. Analytical and bioanalytical chemistry. 2019;411(1):1807-24.

[48] Milan-Rois P, Rodriguez-Diaz C, Castellanos M, Somoza A. Conjugation of Nucleic Acids and Drugs to Gold Nanoparticles. InAntisense RNA Design, Delivery, and Analysis. 1st edition, Springer publishing, 2022;103-16.

[49] Jamdagni P, Khatri P, Rana JS. Nanoparticles based DNA conjugates for detection of pathogenic microorganisms. International Nano Letters. 2016;6(3):139-46.

[50] Ke X, Shelton L, Hu Y, Zhu Y, Chow E, Tang H, Santos JL, Mao HQ. Surface-Functionalized PEGylated Nanoparticles Deliver Messenger RNA to Pulmonary Immune Cells. ACS Applied Materials & Interfaces. 2020;12(32):35835-44.

[51] Karimi S, Fouani MH, Moshaii A, Nikkhah M, Hosseinkhani S, Sheikhnejad R. Development of Dual Functional Nucleic Acid Delivery Nanosystem for DNA Induced Silencing of Bcl-2 Oncogene. International Journal of Nanomedicine. 2020;15(1):1693-708.

[52] Deka J, Mojumdar A, Parisse P, Onesti S, Casalis L. DNA-conjugated gold nanoparticles based colorimetric assay to assess helicase activity: a novel route to screen potential helicase inhibitors. Scientific reports. 2017;7(1):44358-67.

[53] Moros M, Kyriazi ME, El-Sagheer AH, Brown T, Tortiglione C, Kanaras AG. DNA-coated gold nanoparticles for the detection of mRNA in live *Hydra vulgaris* animals. ACS applied materials & interfaces. 2018;11(15):13905-11.

[54] Hosseinzadeh L, Nemati H, Nemati N, Sadeghi M. Spherical gold nanoparticles: Small interfering RNA delivery in regulation of the tumor necrosis factor-alpha gene expression. Journal of Interferon & Cytokine Research. 2020;40(10):490-96.

[55] Yeom JH, Lee B, Kim D, Lee JK, Kim S, Bae J, Park Y, Lee K. Gold nanoparticle-DNA aptamer conjugate-assisted delivery of antimicrobial peptide effectively eliminates intracellular *Salmonella* enterica serovar Typhimurium. Biomaterials. 2016;104(1):43-51.

[56] Thomas RK, Sukumaran S, Prasanth S, Sudarsanakumar C. Revealing the interaction strategy of Diosmin functionalized gold nanoparticles with ctDNA: Multi-spectroscopic, calorimetric and thermodynamic approach. Journal of Luminescence. 2019;205(1):265-76.

[57] Zheng F, Wang P, Du Q, Chen Y, Liu N. Simultaneous and ultrasensitive detection of foodborne bacteria by gold nanoparticles-amplified microcantilever array biosensor. Frontiers in chemistry. 2019;7(1):232-44.

[58] Alafeef M, Dighe K, Moitra P, Pan D. Rapid, ultrasensitive, and quantitative detection of SARS-CoV-2 using antisense oligonucleotides directed electrochemical biosensor chip. ACS nano. 2020;14(12):17028-45.

[59] Sarfraz N, Khan I. Plasmonic gold nanoparticles (AuNPs): properties, synthesis and their advanced energy, environmental and biomedical applications. Chemistry–An Asian Journal. 2021;16(7):720-42.

[60] Ganguly K, Patel DK, Dutta SD, Lim KT. TEMPO-cellulose nanocrystal-capped gold nanoparticles for colorimetric detection of pathogenic DNA. ACS omega. 2021;6(19):12424-31.

[61] Mohammed AS, Balapure A, Khaja MN, Ganesan R, Dutta JR. Naked-eye colorimetric detection of HCV RNA mediated by a 5′ UTR-targeted antisense oligonucleotide and plasmonic gold nanoparticles. Analyst. 2021;146(5):1569-78.

[62] Dester E, Kao K, Alocilja EC. Detection of unamplified *E. coli O157* DNA extracted from large food samples using a gold nanoparticle colorimetric biosensor. Biosensors. 2022;12(5):274-88.

[63] Deb A, Gogoi M, Mandal TK, Sinha S, Pattader PS. Specific Instantaneous Detection of Klebsiella pneumoniae for UTI Diagnosis with a Plasmonic Gold Nanoparticle Conjugated Aptasensor. ACS Applied Bio Materials. 2023;6(8):3309-18.

[64] Shahrashoob M, Mohsenifar A, Tabatabaei M, Rahmani-Cherati T, Mobaraki M, Mota A, Shojaei TR. Detection of *Helicobacter pylori* genome with an optical biosensor based on hybridization of urease gene with a gold nanoparticles-labeled probe. Journal of Applied Spectroscopy. 2016;83(1):322-29.

[65] Liu CC, Yeung CY, Chen PH, Yeh MK, Hou SY. *Salmonella* detection using 16S ribosomal DNA/RNA probe-gold nanoparticles and lateral flow immunoassay. Food chemistry. 2013;141(3):2526-32.

[66] Ganareal TA, Balbin MM, Monserate JJ, Salazar JR, Mingala CN. Gold nanoparticle-based probes for the colorimetric detection of Mycobacterium avium subspecies paratuberculosis DNA. Biochemical and Biophysical Research Communications. 2018;496(3):988-97.

[67] Schmitz FR, Cesca K, Valério A, de Oliveira D, Hotza D. Colorimetric detection of *Pseudomonas aeruginosa* by aptamer-functionalized gold nanoparticles. Applied Microbiology and Biotechnology. 2023;107(1):71-80.

[68] Xu Z, Bi X, Huang Y, Che Z, Chen X, Fu M, Tian H, Yang S. Sensitive colorimetric detection of *Salmonella* enteric serovar typhimurium based on a gold nanoparticle conjugated bifunctional oligonucleotide probe and aptamer. Journal of Food Safety. 2018;38(5):12482-89.

[69] Ananda Chitra M. Rapid detection of staphylococcus aureus genomic DNA using peptide nucleic acid and gold nanoparticles. Proceedings of the National Academy of Sciences, India Section B: Biological Sciences. 2018;88(1):803-11.

[70] Du J, Singh H, Dong WJ, Bai YH, Yi TH. Colorimetric detection of Listeria monocytogenes using one-pot biosynthesized flower-shaped gold nanoparticles. Sensors and Actuators B: Chemical. 2018;265(1):285-92.

[71] Díaz CR, Lafuente-Gómez N, Coutinho C, Pardo D, Alarcón-Iniesta H, López-Valls M, Coloma R, Milán-Rois P, Domenech M, Abreu M, Cantón R. Development of colorimetric sensors based on gold nanoparticles for SARS-CoV-2 RdRp, E and S genes detection. Talanta. 2022;243(1):123393-403.

[72] Jamaluddin ND, Ibrahim N, Yusof NY, Goh CT, Tan LL. Optical reflectometric measurement of SARS-CoV-2 (COVID-19) RNA based on cationic cysteamine-capped gold nanoparticles. Optics & Laser Technology. 2023;157(1):108763-72.

[73] Askaravi M, Rezatofighi SE, Rastegarzadeh S, Seifi Abad Shapouri MR. Development of a new method based on unmodified gold nanoparticles and peptide nucleic acids for detecting bovine viral diarrhea virus-RNA. AMB Express. 2017;7(1):1-9.

[74] Karami A, Hasani M. A palindromic-based strategy for colorimetric detection of HIV-1 nucleic acid: Single-component assembly of gold nanoparticle-core spherical nucleic acids. Analytica Chimica Acta. 2020;1102(1):119-29.

[75] Yrad FM, Castañares JM, Alocilja EC. Visual detection of dengue-1 RNA using gold nanoparticle-based lateral flow biosensor. Diagnostics. 2019;9(3):74-88.

[76] Ngamdee T, Yin LS, Vongpunsawad S, Poovorawan Y, Surareungchai W, Lertanantawong B. Target Induced-DNA strand displacement reaction using gold nanoparticle labeling for hepatitis E virus detection. Analytica chimica acta. 2020;1134(1):10-17.

[77] Shawky SM, Awad AM, Allam W, Alkordi MH, El-Khamisy SF. Gold aggregating gold: a novel nanoparticle biosensor approach for the direct quantification of hepatitis C virus RNA in clinical samples. Biosensors and Bioelectronics. 2017;92(1):349-56.

[78] Alfassam HA, Nassar MS, Almusaynid MM, Khalifah BA, Alshahrani AS, Almughem FA, Alshehri AA, Alawad MO, Massadeh S, Alaamery M, Aldeailej IM. Development of a colorimetric tool for SARS-CoV-2 and other respiratory viruses detection using sialic acid fabricated gold nanoparticles. Pharmaceutics. 2021;13(4):502-513.

[79] Xiao T, Huang J, Wang D, Meng T, Yang X. Au and Au-Based nanomaterials: Synthesis and recent progress in electrochemical sensor applications. Talanta. 2020;206(1):120210-62.

[80] Hwang C, Park N, Kim ES, Kim M, Kim SD, Park S, Kim NY, Kim JH. Ultra-fast and recyclable DNA biosensor for point-of-care detection of SARS-CoV-2 (COVID-19). Biosensors and Bioelectronics. 2021;185(1):113177-83.

[81] Pan HZ, Yu HW, Wang N, Zhang Z, Wan GC, Liu H, Guan X, Chang D. Electrochemical DNA biosensor based on a glassy carbon electrode modified with gold nanoparticles and graphene for sensitive determination of Klebsiella pneumoniae carbapenemase. Journal of biotechnology. 2015;214(1):133-38.

[82] Hajihosseini S, Nasirizadeh N, Hejazi MS, Yaghmaei P. A sensitive DNA biosensor fabricated from gold nanoparticles and graphene oxide on a glassy carbon electrode. Materials Science and Engineering: C. 2016;61(1):506-15.

[83] Silva LR, Stefano JS, Orzari LO, Brazaca LC, Carrilho E, Marcolino-Junior LH, Bergamini MF, Munoz RA, Janegitz BC. Electrochemical biosensor for SARS-CoV-2 cDNA detection using AuNPs-modified 3D-printed graphene electrodes. Biosensors. 2022;12(8):622-42.

[84] Hussein HA, Hanora A, Solyman SM, Hassan RY. Designing and fabrication of electrochemical nano-biosensor for the fast detection of SARS-CoV-2-RNA. Scientific Reports. 2023;13(1):5139-50.

[85] Roohizadeh A, Ghaffarinejad A, Salahandish R, Omidinia E. Label-free RNA-based electrochemical nanobiosensor for detection of Hepatitis C. Current Research in Biotechnology. 2020;2(1):187-92.

[86] Pina-Coronado C, Martínez-Sobrino Á, Gutiérrez-Gálvez L, Del Caño R, Martínez-Periñán E, García-Nieto D, Rodríguez-Peña M, Luna M, Milán-Rois P, Castellanos M, Abreu M. Methylene Blue functionalized carbon nanodots combined with different shape gold nanostructures for sensitive and selective SARS-CoV-2 sensing. Sensors and Actuators B: Chemical. 2022;369(1):132217-29.

[87] Versiani AF, Andrade LM, Martins EM, Scalzo S, Geraldo JM, Chaves CR, Ferreira DC, Ladeira M, Guatimosim S, Ladeira LO, Da Fonseca FG. Gold nanoparticles and their applications in biomedicine. Future Virology. 2016;11(4):293-309.

Chapter II

Instrumentation

2.1   Introduction

Nanoparticles are synthesized by different methods such as, chemical, biological and physical methods. After successful synthesis the physicochemical properties of nanoparticle was studied by various techniques. These physicochemical properties include surface morphology, size, shape, surface charge, chemical composition, and crystalline nature. The characterization study confirmed the formation of nanoparticles. The characterization methods were also used to check the surface modifications of nanoparticles. Thus, gold nanoparticles (AuNPs) and their surface functionalization were analysed by different characterization techniques. This chapter explains the complete specification about the principle and working of the instruments used for the characterization.

2.2   UV-Visible (UV-Vis) Spectroscopy:

Spectroscopy is the measurement and analysis of electromagnetic radiation that occurs when molecules, atoms, or ions in a sample change from one energy state to another. In UV-Vis spectroscopy, a type of absorption spectroscopy, a molecule absorbs light in the ultra-violet range (200-400 nm), which excite electrons from their ground state to a higher energy state. Different substances absorbed different wavelength of light. UV-Vis spectroscopy can be used to analyse different substances by observing the specific wavelength corresponding to maximum absorbance.

2.2.1   Working principle:

The basic principle of UV-Vis spectroscopy is depends on the measurement of light absorption by the particles. The UV-Vis spectroscopy is based on the absorption of ultraviolet or visible light by chemical compounds, which results in unique spectra. The interaction between light and matter is the basis of spectroscopy. When a substance absorbs light via excitation and de-excitation procedures, a spectrum is produced [1].

The electrons existing in materials experience stimulation when UV radiation is absorbed by it. Due to this, they move quickly from their ground state (an energy state with a relatively low quantity of energy) to excited state (an energy state with a

comparatively big amount of energy). It is crucial to remember that the energy difference between an electron's ground state and excited state and the amount of ultraviolet or visible radiation that it may absorb are always equal [2].

Interaction of gold nanoparticles with the light is dependent on their environment, size, and shape. A coordinated oscillation of electron charge that is in resonance with the frequency of visible light is produced when free electrons interact with the fluctuating electric fields of a light beam passing close to a colloidal nanoparticle. These oscillations are referred to as surface plasmons. The Surface Plasmon Resonance (SPR) phenomenon causes light in the blue-green region to be absorbed and red light to be reflected in the case of tiny, monodisperse gold nanoparticles that are around 30 nm in size [3].

The wavelength of surface plasmon resonance-related absorption shifts towards higher wavelength as particle size increases. As a result, solution turns to light blue or purple due to the absorption of red light and the reflection of blue light. The nanoparticles appear transparent or translucent because they reflect the majority of visible wavelengths. As particle size increases towards the bulk limit, surface plasmon resonance wavelengths shift towards the infrared region of the spectrum. The surface plasmon resonance of the nanoparticles can be altered by altering their size or structure, producing particles with tailored optical properties for a variety of uses.

Figure 2.1: UV-Visible (UV-Vis) spectrometer

2.2.2 Working of instrument:

One of the most straightforward and effective optical techniques for examining the optical and electrical characteristics of nanomaterials is electronic absorption, often known as UV-visible spectroscopy. **Figure 2.1** shows UV-Vis spectrometer instrument named as Nanodrop, Multisky Scan. The main parts of the UV-Vis spectroscopy instrument are, light source, monochromator, light detector, sample or reference cell, and recording devices [4] (**figure 2.2**). Tungsten filament and hydrogen-deuterium lamps are the most popular and suitable light sources since they emit light throughout the whole UV-Vis spectrum. Tungsten filament lights release a lot of red radiations, and more precisely, radiations at a wavelength of 375 nm, while the intensity of Hydrogen-Deuterium lamps is below this wavelength. The intensity of light generated through light source is then measured by light detector by keeping the sample in between the light source and detector. The intensity of the transmitted light shown as a function of light wavelength will produce a spectrum of the sample absorption. If the sample absorbs light at certain wavelength, then it will result in a reduction in the amount of light transmitted. Mostly the spectrometer uses the wavelength range from 200-800 nm. Finally, the recording devices stores the data and produces spectrum of the tested compound. The concentration of tested sample should not be too high as it results in saturated absorption and distorted spectrum. Also, the sample should be clear containing of agglomeration [5].
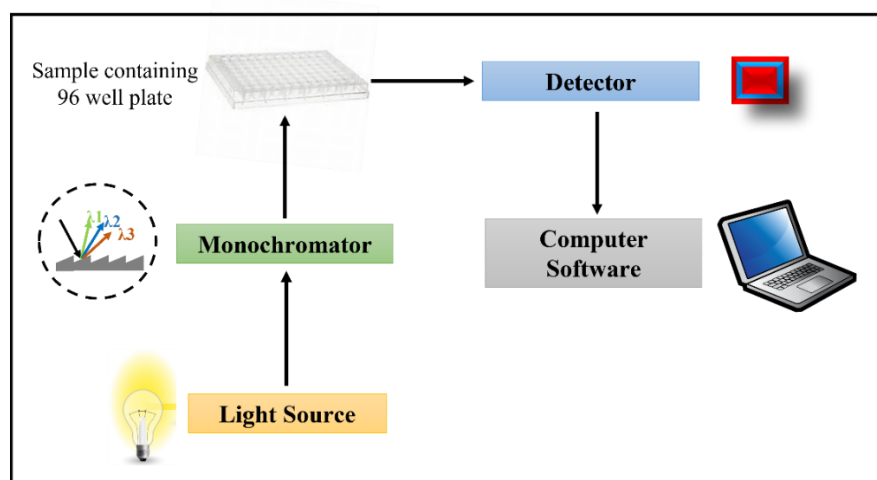
Figure 2.2: Schematic representation of parts and working of UV-Vis Spectroscopy

2.3   X-Ray Diffraction (XRD) Analysis:

XRD is widely used characterization technique that known for its significance to identify the crystalline structure of different materials. It also gives information of unit cell dimensions. XRD analysis can help to determine average crystalline size and calculation of lattice strain [6].
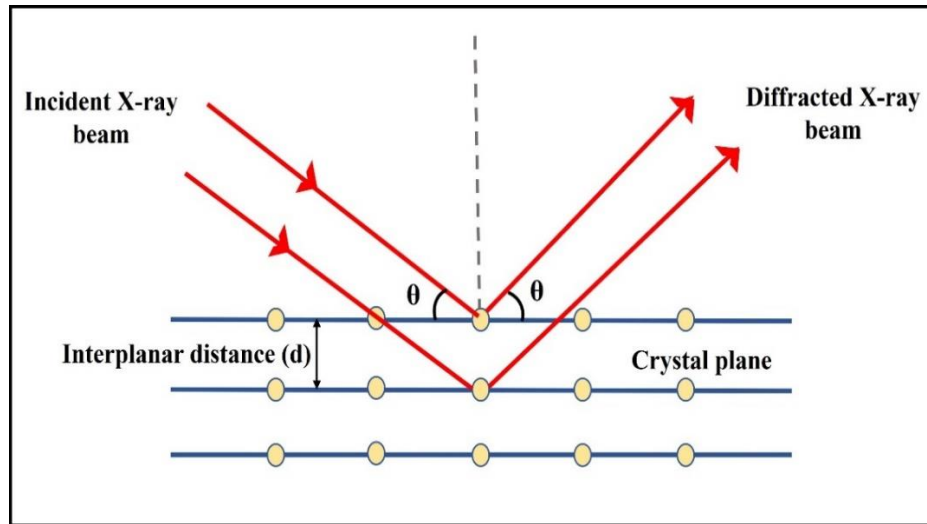
Figure 2.3: Bragg's diffraction

2.3.1   Working principle:

XRD is a technique that is frequently used to examine crystalline structure and atomic spacing. Monochromatic X-rays from a crystalline sample are used as the basis for the XRD analysis. The cathode ray tube produces the X-rays, which are subsequently filtered to produce monochromatic radiation, concentrated, and directed onto the sample. This interaction of incident rays and sample is responsible to produce both constructive and destructive interference as the interatomic distance (d) in materials is on the order of few Angstrom (A°) which corresponds to wavelength of X-rays. The constructive and destructive interferences are produced when the conditions satisfy Bragg's law **(figure 2.3)**. The Bragg's equation is as presented in **equation 2.1** [7],

Equation 2.1: $n\lambda = 2d\sin\theta$

Where, n = order of diffraction θ = Bragg's angle

d = interplanar distance λ = Wavelength

The wavelength of electromagnetic radiation, diffraction angle, and lattice spacing in crystalline samples are all associated with Bragg's equation. The obtained diffracted X-rays are detected and then allow to process and counted. The samples are scanned through range of 2θ angle to attain diffraction directions of lattice due to orientation of materials. The obtained diffraction peaks are converted to d-spacing that helps to identify minerals as different materials have their unique d-spacing. These d-spacing are compared with standard reference patterns [7].

Figure 2.4: X-ray Diffraction instrument

2.3.2   Working of instrument:

Figure 2.4 shows the photograph of XRD instrument. The XRD instrument consist three major elements as, 1) An X-ray tube, 2) A Sample/specimen holder and 3) An X-ray detector. In detail, X-rays are generated in cathode ray tube that made up of cathode, monochromator and target material enclosed in glass or ceramic container at vacuum. X-rays are generated due to heating of a filament (tungsten filament) that results in electrons production. Due to the application of high voltage and the electron bombardment of the target materials, these created electrons are propelled towards the sample or target material. When electrons have enough energy to emit the target material's inner shell electrons, characteristic X-ray spectra are created. The outer electrons jump into inner shell to compensate energy difference by emitting the radiation which is a characteristic of target materials. The most frequent ones in these spectra are K_α and K_β. Part of K_α is made up of $K_{\alpha1}$ and $K_{\alpha2}$. $K_{1\alpha}$ is twice as intense as

K$_{\alpha2}$, with a somewhat shorter wavelength. The target material (Cu, Fe, Mo, Cr) is characterised by the precise wavelengths. For the purpose of diffraction, monochromatic X-rays must be created through filtering utilising foils or crystal monochromators. A weighted average of K1 and K2 is used because their wavelengths are comparable. The most popular target material for single-crystal diffraction is copper, which has a CuK radiation of 1.5418. These collimated X-rays are meant to hit the sample. The intensity of the reflected X-rays is determined when the sample and detector are rotated. The Bragg Equation's criteria are met when the sample's geometry for incident X-rays results in constructive interference and an intensity peak. The detector that captures and processes this X-ray radiation. A count rate is created from the signal and is then output to a device like a printer or computer monitor. The X-ray detector rotates at an angle of 2° and is mounted on an arm to gather diffracted X-rays. The sample rotates at an angle of 2° in the direction of the collimated X-ray beam as a result of the X-ray diffractometer's geometry. In the X-ray scan, information is acquired for typical powder patterns at predetermined angles ranging from 2° to 5° to 70°.

The crystal structure of sample is determined by three methods (a) Laue method, (b) Rotating crystal, and (c) powder method. The X-ray diffraction was first carried out by M. von Laue. The Laue method is the earliest method that used for determination of crystal structure in which, continuous X-ray spectrum is utilized with fixed angle of incidence (θ). The method is known to give faster diffraction as compare to other methods. As a result, it is evident to notice dynamic crystallographic processes. Rotating crystal method have fixed angle of incidence (θ) and variable wavelength (d). Here, the monochromatic X-rays are fall onto sample that rotate with constant angular velocity. Easy analysis of crystal structure can be achieved with powder method where, wavelength (λ) is fixed and variable angle of incidence. The XRD analysis was critically used for determination of average crystalline size of nanomaterials using Scherrer formula as **equation 2.2** [8],

Equation 2.2: $D = \frac{0.9\lambda}{\beta cos\theta}$

Where, D = Crystalline size $\qquad$ β = full width at half maximum (FWHM)

$\qquad$ λ = X-ray wavelength $\qquad$ θ = diffraction or Bragg's angle

2.4   **Fourier transform infrared spectroscopy (FTIR):**

Fourier transform infrared spectroscopy (FTIR) technique is widely used spectroscopic technique for identification of functional groups of organic and inorganic materials [9]. The analysis of FTIR is non-destructive analysis. In order to cause vibrational and rotational excitation of individual atoms within a molecule, lower energy IR radiation (10000-100 cm $^{-1}$) are used. The absorption patterns for a particular species will be distinct, allowing for their identification, as a result of the variety of symmetry of atomic groups and their variations in atomic weights and electronic structures. Different IR regions are used to explore various vibrational modes such as, near-IR (12800-4000 cm^{-1}), mid-IR (4000-200 cm^{-1}), and the far-IR (200-10 cm^{-1}). The FTIR spectroscopy can be used for identification of unknown sample, quality of sample and number of components present in a mixture. The spectroscopy often referred as structural chemical fingerprints of materials.
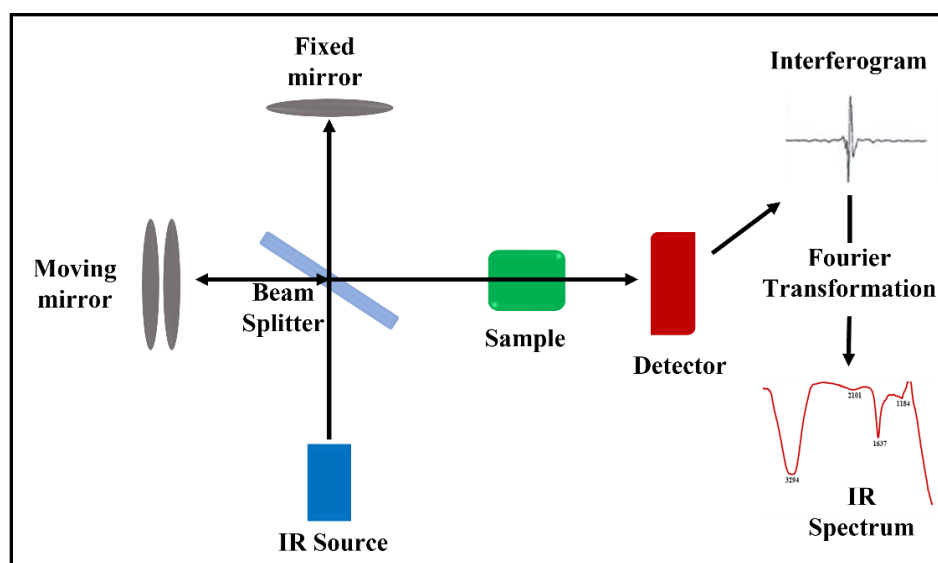
Figure 2.5: Schematic presentation of FTIR working

2.4.1   **Working principle:**

Vibration of molecular bond are occurred at fixed frequencies that dependant on bond type and elemental composition of bonding. These vibrational frequencies are corresponding to excited and ground state by radiation. The bonds get excited state of energy after absorption of light energy at fixed frequency. The energy of the

light should always be larger than or equal to the energy difference between the first excited state and the ground state for any given transition between two states. The identification of vibrating complexes in various materials and the characterization of structural changes in solids are done by vibrational techniques. In IR spectroscopy, a sample is exposed to IR radiations, some of which are absorbed by the sample and some of which pass through. The characteristics of chemical bonds that are visible in a spectrum are the wavelength that is absorbed through the bond. By showing molecule absorption and transmission, the resulting spectrum acts as a molecular fingerprint of the substance [10]. **Figure 2.5** shows the schematic presentation of FTIR instrument with interferogram and IR spectrum.

2.4.2   Working of instrument:

Figure 2.6 shows photograph of FTIR instrument. FTIR analysis includes study of infrared light interaction with matter. Interaction between infrared light and matter results in stretching and bending of chemical bonds. Due to this, there is absorption of infrared radiation by functional group in specific wave number. A normal FTIR spectrometer contains an IR source, Sample section, interferometer, and detector. The IR radiation source in FTIR is either silicon carbide rod, carbon arcs, nichrome wire loop or Nernst glowers. This radiation beam presented controlled amount of energy to the sample by aperture. When beam enters in interferometer then Spectral encoding takes place. After this the interferogram signal exit the interferogram. According to the type of analysis being done, the beam enters the sample compartment where, depending on the sample, it is either transmitted through or reflected through the surface. The sample-specific energy frequencies that are absorbed at this point are those that are specific to the sample. Finally, the beam reaches the detector for the last measurement. The detectors being utilised are specifically created to measure the unique interferogram signal. The sample to be analysed in FTIR is must be thin for easy passing of IR radiation. Thus, small amount of sample is sufficient for FTIR analysis. Upon IR radiation, few radiations are absorbed by the sample whereas, remaining are transmitted. A graph of infrared light absorption with the frequency (wavenumber) on the horizontal axis and the substance (vertical axis) on the vertical axis is known as the IR spectrum. The plotting data then compared with reference spectrum for analysis of bonding. The two unique molecular

structures do not similar yield infrared spectrum. FTIR spectroscopy is utilized for various analysis such as, identification of unknown substances, nature of bond present between two substances, quality of material and functional groups involved in nanoparticles synthesis and functionalization [11].

Figure 2.6: Fourier transform infrared spectroscopy (FTIR) instrument

2.5   Transmission electron microscopy (TEM):

Transmission electron microscopy (TEM) is an analytical microscopic technique that used to visualize smallest structure of a material. In TEM, the image is formed by transmitting beam of electron through specimen. TEM can disclose the atomic structure and size of a nanomaterial by magnifying its structure up to 50 million times.

2.5.1   Working principle:

The TEM uses beam of electrons instead of light like light microscope. Thus, TEM operates on the similar basic principle like light microscope. The only major change between this is the light microscope uses light rays to generate image whereas, in TEM electron beams are focused on specimen to generate an image. The wavelength of electrons is much smaller than that of long wavelength of light. In light microscope, the resolution is increased with decrease in the wavelength of light while,

in case of TEM, the resolution increases with increasing the wavelength of electrons transmission. The electrons have 0.005 nm wavelength that is 1,00,000X smaller than light. As a result, the best resolution possible for TEM images is several orders of magnitude higher and superior to the light microscope's resolution by a factor of roughly 1000. It may make the tiniest and most minute interior characteristics of a substance visible.
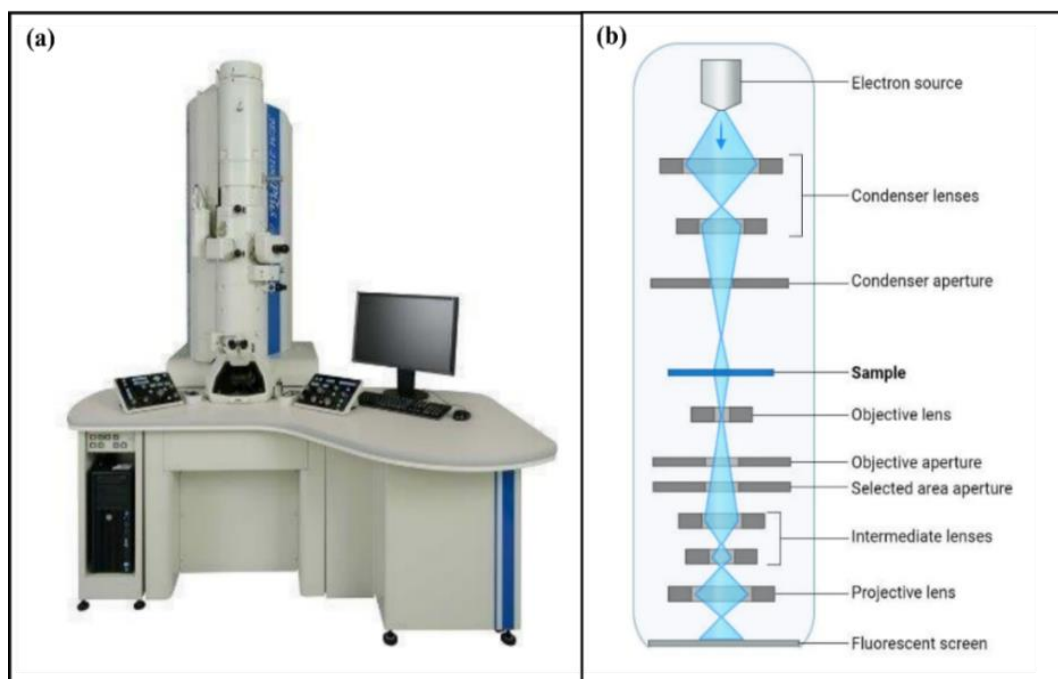
Figure 2.7: (a) Transmission electron microscopy (TEM) and (b) Schematic presentation of TEM instrument working

2.5.2 Working of instrument:

The high-resolution power provide in TEM makes the operating mechanism possible, enabling a wide range of applications, **figure 2.7(a)** shows the photograph of TEM instrument. TEM consist of following parts as, Electron Gun, condenser lens, objective lens, projector lens, condenser aperture, objective aperture, screen and sample holder as shown in **figure 2.7(b).**

Electron gun is the basic part of TEM which act as source of electrons. These electrons are produced by cathode (heated V-shaped tungsten filament). The tungsten filament is covered by a control grid, sometimes known as a Wehnelt cylinder, with a

central hole that is columnar to the tube. The cathode is either above or below the cylindrical column hole. The cathode and control grid have negative potential with disk shaped anode which have axial end. The monochromatic electrons are emitted from the cathode. Here, the cathode filament is heated as positive electrical potential is given to an anode that results in production of an electron stream. The positive potential forces the electrons down whereas, negative potential repels them towards the optical axis. All electrons are collected in the space known as space charge between filament tip and cap. These electrons which are closet to anode then leave the gun area via tiny hole (about 1 mm) in Wehnelt cap towards down the column to be used for imaging.

The specimen is efficiently focused to produce a clearly defined image by the columnar aperture (hole), which is a thin disc of metal through which electrons are transmitted from the cathode to the anode at high voltage and constant energy. The condenser lenses focus the stream of electron to small and coherent beam. There are two condenser lens presents in TEM to focus on specimen. Both lenses are involved to create an image; one lens has strong magnification creating smaller image of specimen while other lens directed it towards objectives. The objective lens focuses the transmitted electrons from sample into image. The objective aperture improves the contrast by preventing diffraction of high-angle electrons. Short focal length objective produces an intermediate image that transmitted to projector lens for magnification. The projector lenses are utilized to increase the beam on phosphor screen and it is of two types, intermediate lens and projector lens. Both the lenses allow greater magnification of the image. Phosphor screen is made up of zinc sulphide (10-100 µm) used for direct observation by the operator. TEM consists of digital camera that records the images. TEM is supplied with vacuum system that enables the straight movement of electrons towards image. Vacuum system helps to prevent bombardment of electrons on air molecules that disturb their movement and focus ability. It is made up of guage and pump. Power supply and valves. The monochromatic image produced here is either grey or black and white that captured by digital camera and viewed on computer screen.

Working of TEM have sequential process that starts with production of electrons by electron gun via heating of tungsten filament. These electrons then focus

on specimen by condenser lenses. The column tube of condenser lens involved in formation of vacuum that consents electrons to generate a clear image. When electrons reach the specimen, they get scattered and focused on magnetic lenses to form large clear image. Electrons scattering is depended on nature of specimen; for dense specimen more electrons get scattered to form a dark image as less electrons reach the screen for visual detection whereas, thin specimen appears as brighter image.

Specimen preparation for TEM imaging is a crucial step for better visualization and appearance of clear image. As described above more electrons are scattered on thick specimen that results in poor visualization. Thus, for TEM imaging the specimen should be thin of about 5-100 nm with 0.025-0.1 nm diameter. For nanoparticles visualization by TEM, copper grid with various support films is used. The carbon black, colloidal gold (Au) solution, thin holey carbon was used as support film. The larger atomic weight nano-particles were simulated by the Au, whereas the lower atomic weight nano-particles were imitated by the carbon black. There are two methods for dispersion of carbon black and Au on TEM grid; one is manual dropping of 10 µL solution on grid that prepared by dispersing solid into methanol and allow to air dry. Second method involves use of ASP-1000 Automated Specimen Processor by Microscopy Innovation. TEM grids were put in mPrep/g capsules and connected to the ASP-1000's reagent lines. Initially, the loaded capsules were filled with the suspension liquid, and the grids were left to dry. After loading, some grids had up to 3-5 min methanol rinses. In the mPrep capsules, the grids were allowed to dry. On a Tecnai F20, evaluation of the grids from both sample methods was finished at low and high magnification. ImageJ was used to calculate the grid's percent coverage and percent agglomeration. The degree of aggregation and interference from the negative support film were two additional criteria assessed. Frequently, complete grid coverage was achieved by automating a single 10 µL loading and loading without rinsing. Less material was on the grid with fewer agglomerations of particles, after the automated loading and rinsing. Single particle imaging is made possible by automation, which requires less initial volume and less agglomeration when combined with controlled rinses [12,13].

2.6   Energy Dispersive X-ray spectroscopy (EDAX, EDS, EDAXS):

The EDAX is analytical technique that used to analyse elemental composition or chemical characterization of material. This technique also called as, energy dispersive X-ray microanalysis (EDAXMA) or energy dispersive X-ray analysis (EDAXA). It gives result in both qualitative and quantitative way for elemental composition of material. This method depends on characteristic X-ray generation for identification of elemental composition of tested sample. The core principle that every element has a unique atomic structure, allowing for a different set of peaks on its electromagnetic emission spectrum, is largely responsible for its capacity to characterise materials.

2.6.1   Working principle:

Most peaks generated in EDAX are obtained by X-ray produced by characteristic fluorescence radiation. The principle of EDAX depends on high energy beam focusing on sample. When X-rays that are high energetic beam focuses on the sample, it can emit characteristic X-ray radiation. The quantity of energy of X-ray radiation from sample can be estimated by energy dispersive spectrometer. The particular fluorescence radiation in energy dispersive study is determined by the energy sorting of proton. The amount of each element present in the sample determines the intensity of each radiation. Each atom produces fluorescence rays and has a unique discrete energy level [9]. X-rays are converted into voltage signals via a detector, which feed a pulse processor, which measures the signals and sends them to a data analyzer for analysis and display. The atoms in the sample include either electron shells bound to the nucleus or ground state (unexcited) electrons at specific energy levels. An electron from an inner shell may be excited by an incident beam, causing it to burst free of its shell and leave a hole where there was a previous electron. An electron from a shell with higher energy can occupy this hole. An X-ray is produced as a result of the difference in energies between the higher and lower energy shells. Energy-dispersive X-ray analysis is a technique that allows for the quantitative assessment of the energy and quantity of these X-rays. Since the energy of these X-rays is a distinguishing characteristic of the energy difference between two shells and the atomic structure of the discharging element. An electron from a higher-

energy shell may fill this hole. An X-ray is produced as a result of the difference between the energies of the higher- and lower-energy shells. The energy of these X-rays can be used by EDAX to determine an object's elemental composition because it is a typical property of the energy difference between two shells and atomic structure of the discharging element [14, 15].

2.6.2   Working of instrument:

The EDAX instrument consist of four parts as, electron beam source, X-ray detector, pulse processor and analyzer. The EDAX is connected with Scanning Electron Microscopy (SEM) thus, it uses same electron gun as an electron source. To avoid the trade-off between the need for high resolution and the effectiveness of X-ray production, the energy of the electron beam must be carefully chosen. Two crystal spectrometers are used to find the produced X-rays. The EDAX detector measures the X-ray counts (the quantity of emitted X-rays) in relation to the X-ray energy. Detector is a silicon drifted by lithium and it is a solid-state device. A charge pulse is produced as X-rays hit the surface of detector. The detector consists of collimator assembly, electron trap, window, crystal, Field Effect transistor (FET) and cryostat. X-rays are pass through collimator towards detector that ensure passing of X-rays being excited by beam of electrons that get detected. Electron trap ensures entry of X-rays into detector and has permanent magnets for strong deflection of passing electrons. Each incident X-ray builds up charge on the feedback capacitor during operation, creating abrupt voltage steps. The step size of this voltage is inversely proportional to the incident X-ray's energy. To prevent preamplifier saturation, the build-up charge must be periodically restored. Cryostat is a self-enclosed vacuum system with liquid nitrogen. In a cryostat, the crystal and FET are positioned on a cold finger to minimise noise through cooling. Pulse processor is a part of EDAX which is a charge sensitive preamplifier that convert the charge pulse to voltage pulse. Analyser sort the pulses by voltage into signals. By monitoring the voltage of the charge pulses, it is possible to determine the energy of X-rays. Then, this energy is used for data processing and display. Intensity vs. voltage histogram is used to display the data in this case. EDAX examined the elemental composition of material by both qualitative as well as quantitative way [16].

2.7   Zeta (ζ) potential:

The surface charge of nanoparticles in colloidal solution is determined by zeta (ζ) potential analysis. Zeta potential is measured in millivolts (mV). The electric potential present on double layer of nanoparticles is called as ζ potential that ranges in between +100 to -100 mV. It is the key indicator for determination of colloidal stability of nanoparticles. The ζ potential within the range of +30 to -30 mV indicated the high degree stability of nanoparticles. Nanoparticles with lower ζ potential leads to aggregation because of particle-particle attraction (Van-der-Wall forces). The ζ potential typically used for determination of successful surface modification of nanoparticles during preparation of nanocomplexes with different functionalizing material or biomacromolecule [17].

2.7.1   Working principle:

The ζ potential is measured by microelectrophoresis method. This method involves passing a voltage across two electrodes located at either end of a cell containing the particle dispersion. Charged particles are drawn to the electrode with the opposing charge. The formation of a net charge at the particle surface affects the distribution of ions in the interfacial region, increasing the concentration of counter ions having a charge opposite to that of the particle close to the surface. This means that each particle is surrounded by an electrical double layer. The liquid layer that envelops the particle is composed of an inner zone (Stern layer) where the ions are tightly connected and an outer region (diffuse) where they are less securely bonded. The ions and particles come together to form a stable entity at a fictitious border within the diffuse layer. When a particle travels because of gravity, ions within the border move the particle. The ions stay with the bulk dispersant beyond the barrier. At this border (surface of hydrodynamic shear), the zeta potential is present.

2.7.2   Working of instrument:

The **figure 2.8** represents photograph of Litesizer 500 instrument used for analysis of zeta potential. The ζ Potential can be examined in a variety of methods. The most popular method is referred to as Laser Doppler Electrophoresis that employed in Microtrac particle analyzers method. The ζ potential analyzers for the

measurement of zeta potential employ the same power spectrum technique as those used to detect nanoparticles and are based on Dynamic Light Scattering (DLS) technology.

Figure 2.8: Litesizer 500 for determination of zeta (ζ) potential and Dynamic Light Scattering (DLS) measurement

Figure 2.9 shows the schematic presentation of Litesizer 500 for determination of ζ potential. Laser beam is used as source of light to illuminate particles of sample. This light source is divided to supply incident as well as reference beam where, reference beam is modulated to satisfy Doppler effect conditions. Since the applied electric fields rapidly vary, electroosmosis is prevented from occurring when the laser-enhanced detection signals are detected in backscatter, as in the size measurement. In order to measure the mobility of the particles in an electric field, an optical probe is employed, and an electrode is used to detect the polarity of the particle charge. Cationic (positive) and anionic (negative) particles are drawn to the optical probe and electrode, respectively, in the sample cell. In order to do the analysis, it is necessary to ascertain the mobility of charged particles in an alternating electric field. Every particle travelling through the measuring volume will affect the intensity of light in the cell when an applied electric field is working in the cell. The frequency of this intensity change is inversely related to the particle speed. A detector will transmit this data to a computerised signal processor. Following the transmission of the data to a computer, software creates a frequency spectrum from which the electrophoretic mobility is determined. Specific range of scattered light is maintained for definite determination of ζ potential. Samples with low concentration or small

particle size unable to produce measurable scattering intensity whereas, high concentrated sample or aggregated particles produces higher scattering intensity. In these cases, the attenuator will automatically work to maintain the scattering intensity. In case of low concentrated sample, attenuator increases light while for high concentrated or aggregated sample the light intensity is reduced. This will help to measure proper ζ potential of desirable sample [18].
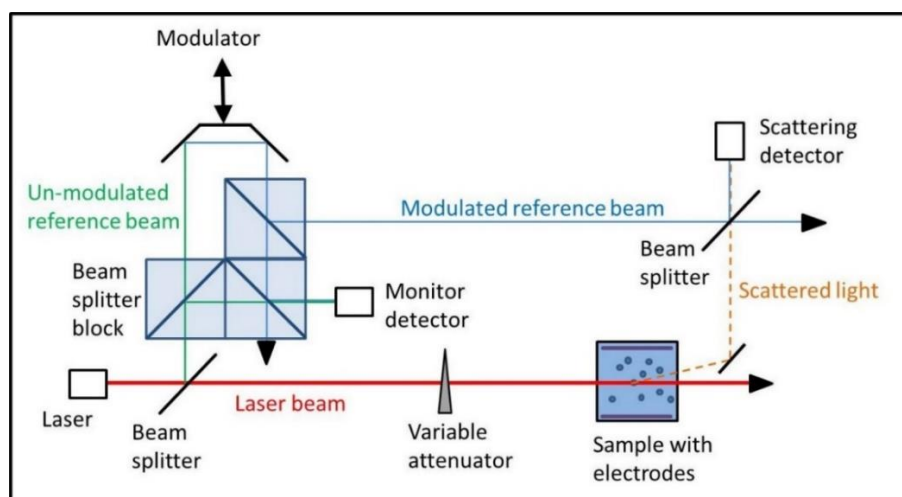
Figure 2.9: Schematic presentation of Litesizer 500 instrument for zeta (ζ) potential analysis [19]

2.8   Dynamic Light Scattering (DLS):

A crucial method for determining the size of suspended particle is Dynamic Light Scattering (DLS). DLS is used in various field such as, chemistry, physics, nanotechnology, material sciences and biochemistry for determination of particle size and size distribution. DLS measures the hydrodynamic diameter of the nanoparticles.

2.8.1   Working principle:

The basic principle behind DLS is the Brownian motion of distributed particles. In a liquid, particles are scattered and flow randomly in all directions. The fundamental idea behind Brownian motion is that solvent molecules and particles constantly collide. Particle movement is brought about by the energy that is transmitted during these collisions. Smaller particles are more affected since the energy transmission is more or less constant. Hence, the smaller particles travel faster

than larger particles. Sedimentation of particles lead to cause inaccurate result as there is no random movement of particles. Thus, sedimentation increases the size of particles whereas, smaller particles show less scattering of light that unable to measure sufficient signal. Therefore, the measurement is dependent on Brownian motion where dispersion of particle is required for scattering of light.

2.8.2 Working of instrument:

The DLS is measured by Litesizer 500 instrument **(figure 2.8)**. The basic set up of DLS instrument consist of laser light source, detector, sample holding cuvette and amplifier. **Figure 2.10** represents schematic presentation for DLS analysis by using Litesizer 500 instrument. Sample placed in cuvette is targeted by single frequency laser. Particles present in the sample dispersed the laser light in all directions.

Turbidity of sample affect the measurement as the processor unable to process the turbid sample due to large number of photons. Thus, in order to receive an adequate yet manageable signal at the detector, the laser light is attenuated. Litesizer 500 is modern DLS instrument that include three detection angles for determination of size of particles. Side scattering (90°) or back scattering (175°) are preferable depending on turbidity of material. It is possible to observe aggregation using a forward angle of 15° [20].
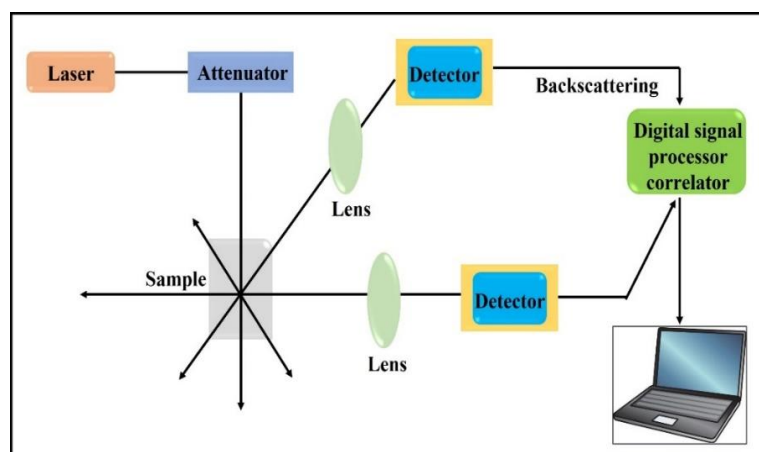
Figure 2.10: Schematic presentation of Litesizer 500 instrument for Dynamic Light Scattering analysis

As previously mentioned, the particle size of the sample is predicated on the movement of the particles rather than being directly measured. The phrase "hydrodynamic diameter" describes the size of spherical, smooth particles that diffuse at the same rate as the sample's particles. When comparing the outcomes of DLS measurements with those of other methods that take into account various physical characteristics of the sample, it is important to keep this in mind. The polydispersity index (PDI) provides the broadness of the particle size distribution. The cumulant approach is also used to determine the polydispersity index. If the percentage falls below 10%, the sample is monodispersed and all of the detected particles are roughly the same size [21].

2.9 References:

[1] Akash MS, Rehman K. Ultraviolet-visible (UV-VIS) spectroscopy. Essentials of pharmaceutical analysis. Limited edition, Springer publishing, 2020:29-56.

[2] https://www.technologynetworks.com/analysis/articles/uv-vis-spectroscopy-principle-strengths-and-limitations-and-applications-349865

[3] Ashraf R, Amna T, Sheikh FA. Unique Properties of the Gold Nanoparticles: Synthesis, Functionalization and Applications. Application of Nanotechnology in Biomedical Sciences. 1st edition, Springer publishing, 2020:75-98.

[4] Kafle BP. Theory and instrumentation of absorption spectroscopy. Chemical Analysis and Material Characterization by Spectrophotometry. 4th edition, Elsevier publishing, 2020:17-38.

[5] https://www.indiastudychannel.com/resources/146681-Principle-working-and-applications-of-UV-spectroscopy.aspx

[6] Cervellino A, Frison R, Masciocchi N, Guagliardi A. X-ray powder diffraction characterization of nanomaterials. X-ray and neutron techniques for nanomaterials characterization. 2016;5(1):545-608.

[7] Lamas DG, de Oliveira Neto M, Kellermann G, Craievich AF. X-ray Diffraction and Scattering by Nanomaterials. Nanocharacterization techniques. 1st edition, William Andrew publishing, 2017:111-182.

[8] Holder CF, Schaak RE. Tutorial on powder X-ray diffraction for characterizing nanoscale materials. Acs Nano. 2019;13(7):7359-65.

[9] Guerrero-Pérez MO, Patience GS. Experimental methods in chemical engineering: Fourier transform infrared spectroscopy—FTIR. The Canadian Journal of Chemical Engineering. 2020;98(1):25-33.

[10] https://www.findlight.net/blog/ftir-principles-applications/

[11] Dutta A. Fourier transform infrared spectroscopy. Spectroscopic methods for nanomaterials characterization. 2017:2(1):73-92.

[12] https://microbenotes.com/transmission-electron-microscope-tem/

[13] Vierrether O, TerBush J, Wisner C. Nano-Particle TEM Sample Preparation Primer. Microscopy and Microanalysis. 2016;22(S3):1914-15.

[14] Mishra RK, Zachariah AK, Thomas S. Energy-dispersive X-ray spectroscopy techniques for nanomaterial. InMicroscopy methods in nanomaterials characterization 1st edition, Elsevier publishing, 2017;383-405.

[15] Hodoroaba VD. Energy-dispersive X-ray spectroscopy (EDS). Characterization of Nanoparticles. 1st edition, Elsevier publishing, 2020;397-417.

[16] Scimeca M, Bischetti S, Lamsira HK, Bonfiglio R, Bonanno E. Energy Dispersive X-ray (EDAX) microanalysis: A powerful tool in biomedical research and diagnosis. European journal of histochemistry: EJH. 2018;62(1):2841-50.

[17] Bhattacharjee S. DLS and zeta potential–what they are and what they are not?. Journal of controlled release. 2016;235(1):337-51.

[18]   https://www.microtrac.com/products/zeta-potential/

[19]   https://wiki.anton-paar.com/ca-en/zeta-potential/

[20]   Falke S, Betzel C. Dynamic light scattering (DLS) principles, perspectives, applications to biological samples. Radiation in bioanalysis: Spectroscopic techniques and theoretical methods. 1st edition, Springer publishing, 2019:173-92.

[21]   https://wiki.anton-paar.com/en/the-principles-of-dynamic-light-scattering/

Chapter III

Synthesis and characterization of gold nanoparticles (AuNPs) and Poly-L-Lysine functionalized gold nanoparticles (PLL-AuNPs)

3.1   Introduction:

Gold nanoparticles (AuNPs) are the most extensively studied nanostructure among the many metal nanoparticles because of their special physiological characteristics, including their ease of synthesis, ease of surface modification, biocompatibility, non-toxicity, high surface-to-volume ratio, and size tunability [1]. Therefore, AuNPs are applicable in varieties of biomedical applications like, biosensing, gene delivery, drug delivery and antibacterial as well as anticancer activities. Gold has been used medicinally from ancient time whereas, the modern advances in nanotechnology have increased its application in the biomedical field [2]. The physical and electronic properties of AuNPs are dependent on their size and shapes. Also, the size and shape are responsible to color diversity of AuNPs solution from violet to dark wine-red where, gold precursor solution appears in yellow color [3]. The size and shape dependent optical and electronic properties of AuNPs are the result of Surface Plasmon Resonance (SPR) phenomenon; SPR is a plasmon oscillation in metal nanocrystals. AuNPs also show easy surface modification or functionalization with different chemicals as well as biomolecules. Attachment of biomolecules such as, nucleic acid, antibodies, and proteins on surface of AuNPs, makes them suitable candidate for specific drug or gene delivery applications [4].

Gold nanoparticles (AuNPs) are generated through different techniques such as, bottom up and top-down approach. Due to unpredictable size distribution and the massive energy required to maintain high pressure and temperature conditions for synthesis, the top-down method is unconventional [5]. Therefore, bottom-up approach is most commonly used by researchers. This includes three common approaches such as, physical, chemical and biological approaches. Among these approaches, the chemical reduction method is simple and easy to handle thus, routinely used for synthesis of AuNPs. The chemical reduction method was developed by Turkevich in 1951 that produces AuNPs of size range 10-20 nm [6] and further improved in 1973 by Frens [7]. The size of AuNPs can be controlled by the ratio of reducing agent to precursor solution [8]. The chemical reduction method involves use of chemical reducing agent that reduces gold salt (Au^{3+}) to gold (Au^0). Same reducing agent

sometimes act as both reducing as well as capping agent [9]. It is based on successive reaction between the reducing agent and precursor with heating and continued stirring conditions [10].

Optical properties of AuNPs are applicable in biosensing field. Moitra *et. al.* [11] detected SARS-CoV-2 RNA by combining gold nanoparticles with thiolated antisense oligonucleotides (ASO). This needs thiol modified oligonucleotides for its conjugation with AuNPs. The positively charged AuNPs were developed by functionalization of AuNPs with functionalizing agent such as, cetyltrimethylammonium bromide (CTAB), cysteamine, and different cationic biopolymer (Poly-L-Lysine) for various biomedical applications. Jamaluddin *et. al.* [12] reported the use of cysteamine capped AuNPs for viral RNA detection through optical reflectometry approach. PLL functionalized AuNPs were reported previously for gene transfection study which were synthesized by combining with a negatively charged nucleic acid via electrostatic interactions [13]. The positively charged AuNPs were employed in detection of pathogen from clinical samples as well as from water and food sample for colorimetric biosensor [14].

The proposed chapter presents the synthesis of AuNPs and Poly-L-Lysine functionalizing AuNPs (PLL-AuNPs) along with their physiochemical characterization. The biopolymer Poly-L-Lysine (PLL) is used as reducing as well as functionalizing agent. The highly cationic nature of PLL provides surface positive charge to synthesized AuNPs. The method completes in single step and single pot thus, named as one pot synthesis method which is easy to handle and requires minimum chemicals. The chapter also contains comparison of AuNPs and PLL-AuNPs depending on the physiochemical characterization.

3.2   Experimental details:

3.2.1   Materials:

All of the reagents utilized in this research were of analytical quality and applied directly. Trisodium citrate (Himedia), (0.01%) Poly-L-Lysine solution, and

gold tetrachloroaurate solution (Sigma Aldrich, Saint Louis, MO) were purchased and used as required.

3.2.2   Synthesis of gold nanoparticles (AuNPs):

The gold nanoparticles were generated using the Turkevich chemical reduction procedure using trisodium citrate as a reducing agent. The 1 mM precursor $HAuCl_4$ solution was prepared in distilled water and heated on magnetic stirrer upto boiling point with continue stirring at 350 rpm. The reducing agent trisodium citrate is then rapidly added into heated precursor solution and continue the stirring upto color change from pale yellow to wine-red. The reaction was completed with color change within 5-6 min where, the gold ions (Au^{3+}) were reduced to Au^0 by reducing agent trisodium citrate. The produced nanoparticle solution was then cooled to room temperature and centrifuged for 20 min at 7500 rpm to obtain pellet. By repeating the centrifugation step, the resulting pellet was washed three times with distilled water. The obtained pellet was then resuspended in distilled water and stored in refrigerator upto further use. For synthesis of AuNPs, the nucleation of gold takes place by the reducing agent. The color change from pale yellow to wine-red indicated reduction of gold salt (Au^{3+}) to gold (Au^0).

3.2.3   Mechanism of gold nanoparticles (AuNPs) formation:

In this reduction method, the heated gold precursor $HAuCl_4$ reacts with trisodium citrate solution. Herein, the citrate ions act as reducing agent (**figure 3.1**). The formation of AuNPs is a multistep process. The Au^{3+} salt gets reduced to Au by reducing agent following the Au nucleus formation as shown in **figure 3.1(a)**. Upon addition of citrate to gold precursor solution, the pH of the solution changes and convert the gold complex equilibrium towards more hydrolysed form with formation of oxidation product of citrate, dicarboxy acetone. After this, there is reduction of auric salt to aurous salt and Au^0. Finally, the AuNPs are formed by assembling aurous salt on Au^0 atom **(figure 3.1b)** [16].

Small part of trisodium citrate reduces the Au^{3+} to Au^0 while the remaining part takes place in stabilization of gold nanoparticles. The size of gold nanoparticles

depends on the ratio of trisodium citrate to precursor $HAuCl_4$ solution. The high concentration of citrate results in development of small sized particles whereas, the concentration more than 4.5:1 shows increase in particle size. The high concentration of citrate rapidly stabilizes AuNPs of smaller size [10]. pH of the solution also affects the ionization of citrate that influences particle size distribution and colloidal stability. The uniform sized nanoparticles were obtained at neutral or near neutral pH [16, 17].
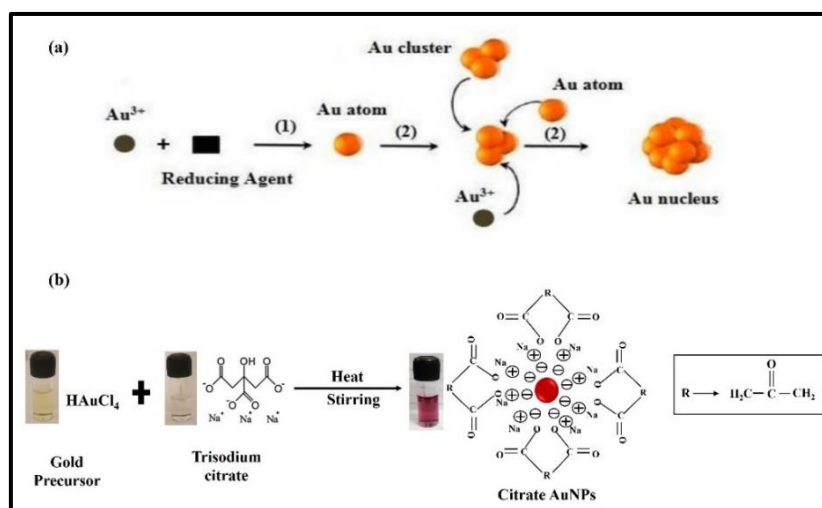
Figure 3.1: (a) Nucleation process for gold nanoparticles (AuNPs) synthesis and (b) presentation of AuNPs synthesis by citrate using chemical reduction method [16]

3.2.4 Synthesis of Poly-L-Lysine functionalized gold nanoparticles (PLL-AuNPs):

The synthesis of PLL-AuNPs was accomplished by one-step synthesis method where Poly-L-Lysine (PLL) itself acts as a reducing as well as stabilizing agent. The synthesis of PLL-AuNPs requires a 0.01% Poly-L-Lysine solution as reducing agent and chloroauric acid ($HAuCl_4$) as a precursor. The synthesis reaction was carried out in pure distilled water. The 1 mM precursor solution ($HAuCl_4$) was heated on magnetic stirrer up to 80°C and 0.01% PLL solution was then rapidly added in heated precursor solution with continue stirring. The reaction was continued to observe color transition from pale yellow to wine-red. The color change indicates formation of AuNPs. To achieve successful synthesis of PLL-AuNPs, reaction parameters such as, pH, concentration of precursor, reaction time, and temperature were varied in a range

of 2-10, 0.5-4 mM, 50-80°C, and 1-10 min, respectively. Every optimization experiment used UV-Vis spectra between 200 and 800 nm to monitor the process. The PLL-AuNPs were then synthesized for further experiments by using the optimized conditions. The solution was then cooled to room temperature, and the produced nanoparticles are centrifuged at 13000 rpm for 15 min at room temperature after being washed three times with distilled water. For later use, the produced nanoparticles were suspended in distilled water and kept at 4°C. The synthesis of PLL-AuNPs through one pot synthesis method is schematically presented in **figure 3.2.**
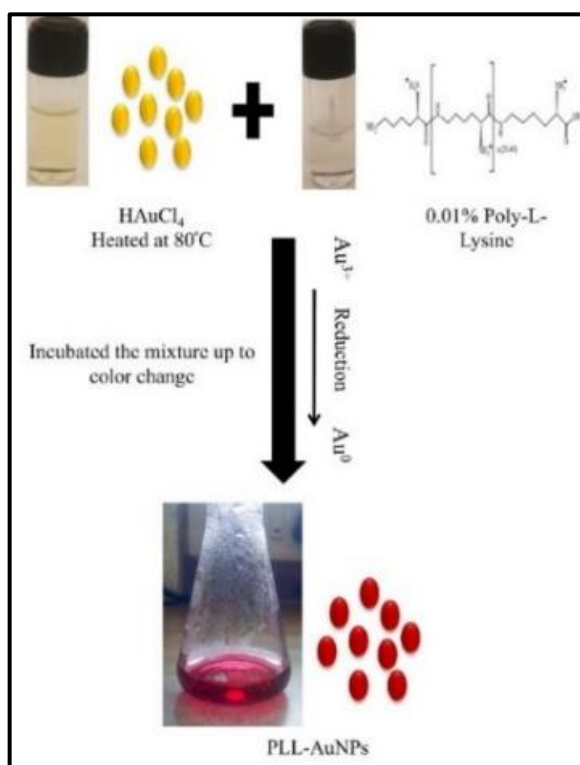
Figure 3.2: Schematic presentation of synthesis of Poly-L-Lysine functionalized gold nanoparticles (PLL-AuNPs) through one pot synthesis method

3.2.5 Mechanism of Poly-L-Lysine functionalized gold nanoparticles (PLL-AuNPs) formation:

Traditionally, AuNPs were synthesized by reduction method and functionalized with various materials by different techniques. One pot synthesis method comprises single step for synthesis of PLL-AuNPs where, PLL itself acts as reducing as well as stabilizing agent. Poly-L-Lysine is a highly cationic biopolymer

that made up of basic amino acid, Lysine. PLL serves as reducing agent as it contains hydroxyl (-OH) and amino (-NH$_2$) group in its structure as a functional group [18]. The inclusion of an amine (-NH$_2$) group in the PLL structure may be the reason of the reduction of the gold salt. Further, in same synthesis condition PLL is responsible for stabilization of gold nanoparticles with surface positive charge. The synthesis proceeds with color transition from pale yellow to wine-red that indicates formation of gold nanoparticles. Basically, gold nanoparticles interact with each other through Van-der-Walls forces; here positive charge is present on AuNPs surface that results in electrostatic repulsion of positively charged AuNPs that avoiding aggregation [12]. Poly-L-Lysine reduced gold salt (Au^{3+}) to gold (Au^0) and also further stabilized the synthesized PLL-AuNPs.

3.2.6 Characterization of gold nanoparticles and Poly-L-Lysine functionalized gold nanoparticles (AuNPs and PLL-AuNPs):

Gold nanoparticle formation was first visually validated by observing the color change from pale yellow to wine-red, and then by measuring the UV-Vis spectrum in the 200-800 nm region. X-ray Diffraction (XRD) (Rigaku 600 miniflex) analysis was used to determine the crystalline nature of the synthesized nanoparticles. The functional groups were analyzed with the help of Fourier transform infrared (FTIR) spectrum. Transmission electron microscopy (TEM) was used to study size and morphology of synthesized gold nanoparticles. Surface charge and hydrodynamic size of nanoparticles were determined by zeta (ζ) potential analyzer and Dynamic Light Scattering (DLS), respectively. The chemical composition of AuNPs was analyzed with the help of Energy Dispersive X-Ray analysis (EDAX).

3.3 Results and discussion:

3.3.1 Characterization of gold nanoparticles (AuNPs):

- **UV-Vis spectroscopy:**

After visual confirmation of the synthesis of the gold nanoparticles, the Surface Plasmon Resonance (SPR) dependent preliminary characterization of the AuNPs was carried out using UV-Vis spectroscopy. As shown in **figure 3.3(a-b),** the

synthesized AuNPs exhibit an absorbance peak at 532 nm, while the gold precursor solution shows a peak at 217 nm. The obtained result of UV-Vis spectroscopy was accompanying with previous data where, the AuNPs synthesized through citrate showed absorbance peak at 525 nm [19] whereas, the biologically synthesized AuNPs by *Physalis minima* and *Capsicum annum* fruit extract showed UV-Vis absorbance peak at 546 nm and 540 nm respectively [20, 21]. Hydroxyl group (-OH) of citrate acts as an electron donor for reduction of gold salt (Au^{3+}) and a capping agent that improve stability of AuNPs [9].
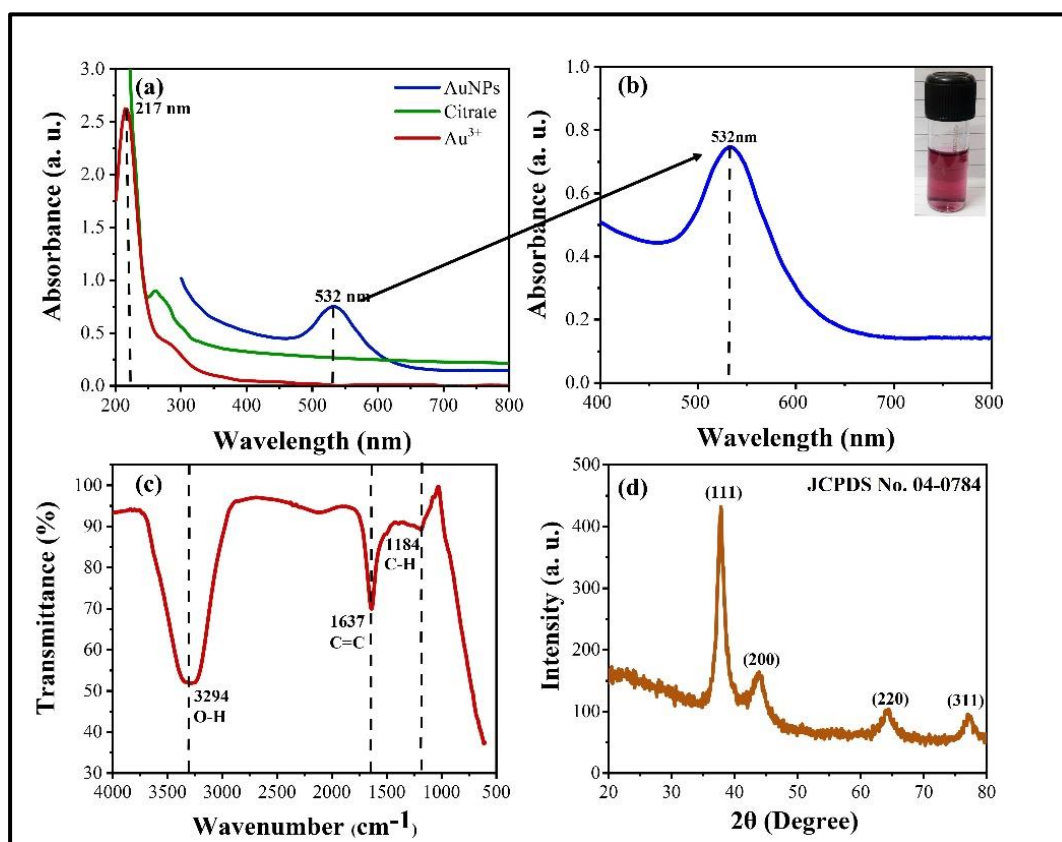
Figure 3.3: Characterization of gold nanoparticles (AuNPs), (a-b) UV-Vis spectroscopy of AuNPs, citrate, and Au precursor; inset photograph of synthesized AuNPs, (c) FTIR spectrum, and (d) XRD

- **FTIR analysis:**

FTIR spectra was used to detect the functional groups which are primarily involved in the production and stabilization of nanoparticles. According to FTIR

analysis, functional groups of trisodium citrate have a role in reducing metal ions into nanoparticles and enhancing colloidal stability [22]. The IR spectra of AuNPs, shown in **figure 3.3(c)**, reveal the presence of various functional groups. The spectrum exhibits an O-H vibrational stretching at a wavenumber of 3294 cm⁻¹ along with C=C stretching at 1637 cm⁻¹, and a C-H bending at 1184 cm⁻¹ for the AuNPs. This investigation found that stabilization of synthesized AuNPs as well as reduction was facilitated by the O-H functional group present in citrate.

- **XRD analysis:**

The XRD examination, a crucial characteristic method used to ascertain the crystalline structure of nanoparticles. **Figure 3.3(d)** shows XRD examination of AuNPs that revealed four distinct peaks with 2θ degree of 37.92, 44.14, 64.37, and 77.41 corresponding to the planes of (111), (200), (220), and (311), respectively. The (111) plane is a primary growth orientation plane among the four peaks. In addition to the typical JCPDS file number 04-0784 [23], these acquired values were corelated to the previously reported data for the synthesis of AuNPs [24].

The crystalline size of AuNPs was determined by Scherrer formula **equation 2.2.** The average crystalline size of AuNPs for (111) plane is 24.11 nm. The sharp and intense diffraction peaks presented in XRD analysis indicated the highly crystalline nature of AuNPs. Furthermore, the absence of any other additional peaks proved the purity of the synthesized AuNPs.

- **TEM analysis:**

Transmission electron microscopy (TEM) was used to examine the size, shape, and morphological properties of AuNPs. The AuNPs, observed at various scales (500, 100, 50, 20, 10, and 5 nm), are spherical in shape, as shown in **figure 3.4(a-f)**. The TEM images were studied through ImageJ application for analysis of size. The inset image displays the size distribution histogram of the AuNPs in the range of 20 to 30 nm. The TEM micrograph revealed that the AuNPs were 19.1 nm in size on average.
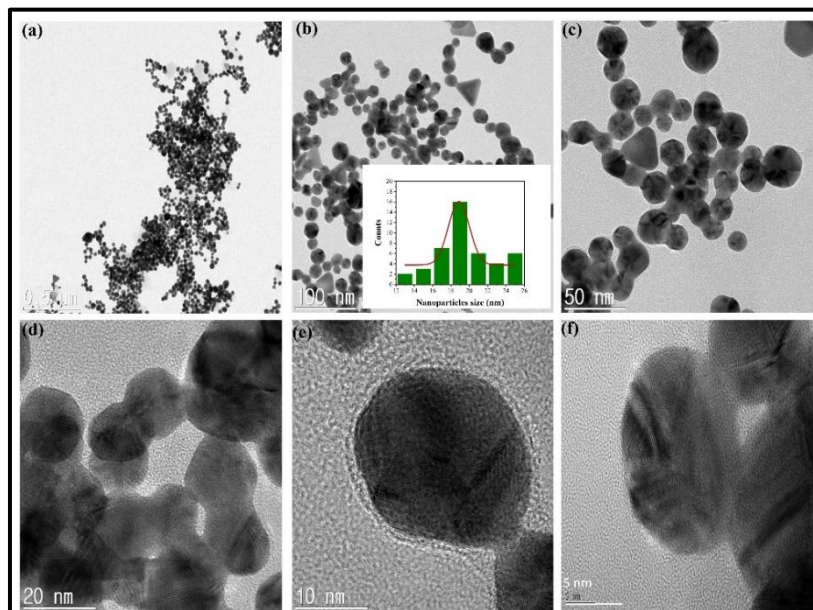
Figure 3.4: TEM images of gold nanoparticles (AuNPs) at scales (a) 500 nm, (b) 100 nm, (c) 50 nm, (d) 20 nm, (e) 10 nm, and (f) 5 nm. The inset image show size distribution histogram of AuNPs at the magnifications of 8KX, 50KX, 100KX, 200KX, 400KX, and 800KX, respectively

- **Zeta (ζ) potential:**

    The average ζ potential of AuNPs is determined from **figure 3.5(a)** to be -25.17±0.30 mV, indicating the stability of the synthesized AuNPs. The acquired ζ potential was comparable to previously reported AuNPs [26]. This negative value represents the vital role of the trisodium citrate in reduction of gold salt. Negative ζ potential indicates the stability of AuNPs, whereas the surface negative charge of AuNPs is frequently linked to the existence of a stabilizing agent generated during AuNPs synthesis. As previously mentioned, the potential of colloidal nanoparticles ranged from -30.0 to +30.0 mV and indicated the stability of the particles [25]. Thus, the negative ζ potential value of synthesized AuNPs (-25.17±0.30 mV) indicates stability of AuNPs.

- **DLS analysis:**

    Dynamic Light Scattering (DLS) is the most extensively used method for particle size measurement analysis in the nanoscale range. Hydrodynamic size refers

to the particle size and it is determined by DLS analysis. The DLS gives the information of hydrodynamic diameter of the material while TEM provides the projected area diameter of the particles. Here, the average hydrodynamic size of AuNPs is found to be 159.6 nm as presented in **figure 3.5(b).**
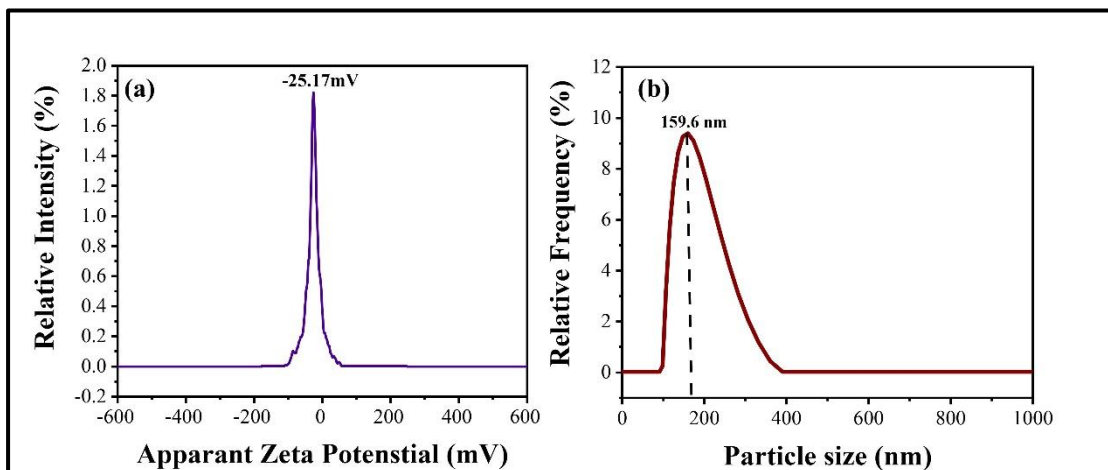
Figure 3.5: Surface charge and hydrodynamic size of gold nanoparticles (AuNPs) studied by (a) Zeta potential and (b) DLS, respectively

3.3.2   Optimization of PLL functionalized gold nanoparticles (PLL-AuNPs) synthesis:

Gold nanoparticles (AuNPs) were traditionally synthesized by reduction method and then different materials are used as capping agents for stabilization purpose [10]. In this study, AuNPs were synthesized by one-pot or single step synthesis method where the gold precursor was reduced by Poly-L-Lysine (PLL) solution. Here, the Poly-L-Lysine was playing role of both reducing as well as functionalizing agent. PLL is a biopolymer that contains high positive charge and made up of cationic amino acid, Lysine. PLL serves as reducing agent as it contains hydroxyl and amino group in its structure as a functional group [20]. **Figure 3.2** represents the reaction mechanism for synthesis of PLL-AuNPs which indicates reduction of gold salt (Au^{3+}) to gold (Au^0) by PLL at 80°C. The inclusion of an amine (-NH_2) group in PLL structure may be the reason of the reduction of the gold salt. Further, in same synthesis condition PLL was responsible for stabilization of gold nanoparticles with surface positive charge. The synthesis proceeds with color change

from light yellow to wine-red that indicates formation of gold nanoparticles. Formation of PLL-AuNPs was first visibly confirmed by observing color change from pale yellow to dark wine-red indicating the synthesis of PLL-AuNPs due to reduction of Au^{3+} to Au^0. The optimization of several parameters was required to study the effect on size and shape of nanoparticles [26]. Therefore, in this study, next optimization of PLL-AuNPs synthesis was studied by varying the different reaction parameters of synthesis.

- **Effect of precursor concentration on synthesis of PLL-AuNPs:**

To study the effect of variation in precursor concentration $HAuCl_4$ on PLL-AuNPs synthesis, the different concentrations were used as 0.5-4 mM and taking other parameters constant (pH 6, reaction time 6, and temperature 80ºC) **(figure 3.6a).** The precursor concentrations 0.5 and 4 mM were turned into wine-red color but absolute synthesis is not done as no sharp SPR peaks are observed. However, at the concentration of 1 mM $HAuCl_4$ color change is observed that shows SPR peak at 524 nm indicating reduction of Au^{3+} to Au^0. In case of increasing concentration of $HAuCl_4$ as 2-3 mM the SPR peaks are broadened and slightly red shifted to 530 and 536 nm, respectively. This result indicates that 1 mM concentration of precursor is optimized precursor concentration for synthesis of PLL-AuNPs.

- **Effect of pH on synthesis of PLL-AuNPs:**

The pH of the synthesis reaction plays vital role in reduction and stabilization of nanoparticles. It is reported that increase in pH helps in efficient capping and supports the formation of smaller nanoparticles [27]. In this study, the effect of variation of pH in the range of 2-10 on synthesis was studied by taking other parameters constant (temperature 80ºC, reaction time 6, and percussor concentration 1 mM) **(figure 3.7b).** Synthesis occurs at high acidic pH values of 2 and 4, where the reaction mixture turns purple in color, but no strong SPR peaks are observed. In this study at pH 6, an intense and sharp SPR peak is appeared at 524 nm, clearly validating the formation of PLL-AuNPs. However, further increases in pH to 8 and 10 led to the formation of clumps that settled at the bottom, resulting in the absence of a

characteristic SPR peak, as shown in **figure 3.6(b)**. This study concludes that a pH value of 6 is optimal for the synthesis of PLL-AuNPs.

- **Effect of temperature synthesis of PLL-AuNPs:**

Along with pH and precursor concentration, the reaction temperature is also an important factor in synthesis of nanoparticles which affects rate of reaction, growth, and other properties of AuNPs [28]. Rate of reaction increases with increase in temperature due to kinetic energy while, at low temperature the synthesis requires more time [29]. In account to this, the temperature effect was studied by variation the temperature in a range of 50-80°C and taking other parameters constant (pH 6, reaction time 6, and percussor concentration 1 mM) for optimization of synthesis **(figure 3.6c).** The characteristic peaks were not observed when the reaction was incubated at 50-70°C temperature. This indicated that, at 50-70°C temperature slow reduction of Au^{3+} is observed. However, incubating the reaction at 80°C shows typical SPR peak at 524 nm suggesting the optimum reduction of Au^{3+} to AuNPs as shown in **figure 3.6(c).** Therefore, this study indicated the 80°C temperature is optimum for PLL-AuNPs synthesis.

- **Effect of incubation time on synthesis of PLL-AuNPs:**

The effect of incubation time on the synthesis of PLL-AuNPs is represented in **figure 3.6(d)** where, reaction time is varied from 1-10 min and other parameters keep constant as, pH 6, temperature 80°C, and precursor concentration 1 mM. The reaction mixture appeared light yellow after 1 minute, with no distinct SPR peak, suggesting that the PLL and precursor were interacting at a slow rate. As reaction proceeds from 1 to 2 min, the formation of PLL-AuNPs takes place by reduction of Au^{3+}. Further continuation of reaction from 2 to 6 min the SPR peak intensity is increased and the sharp SPR peaks at 544 nm and 524 nm are observed for 4 min and 6 min incubation time, respectively as shown in **figure 3.6(d)**. Though the sharp peak is observed at 4 min incubation time, the peak (544 nm) is showing red shift as compared to 6 min incubation time peak at 524 nm. The absorption spectrum of AuNPs is a size and shape dependent property of AuNPs. Absorption spectra are associated with particular size of AuNPs [30]. Thus, the 6 min incubation time is selected as optimum for the

synthesis of PLL-AuNPs. When reaction is further increased from 7-10 min, the SPR peaks are broaden and shifted to higher wavelength with lower intensities. Thus, this study indicates that the reaction requires 6 min incubation for synthesis of PLL-AuNPs.
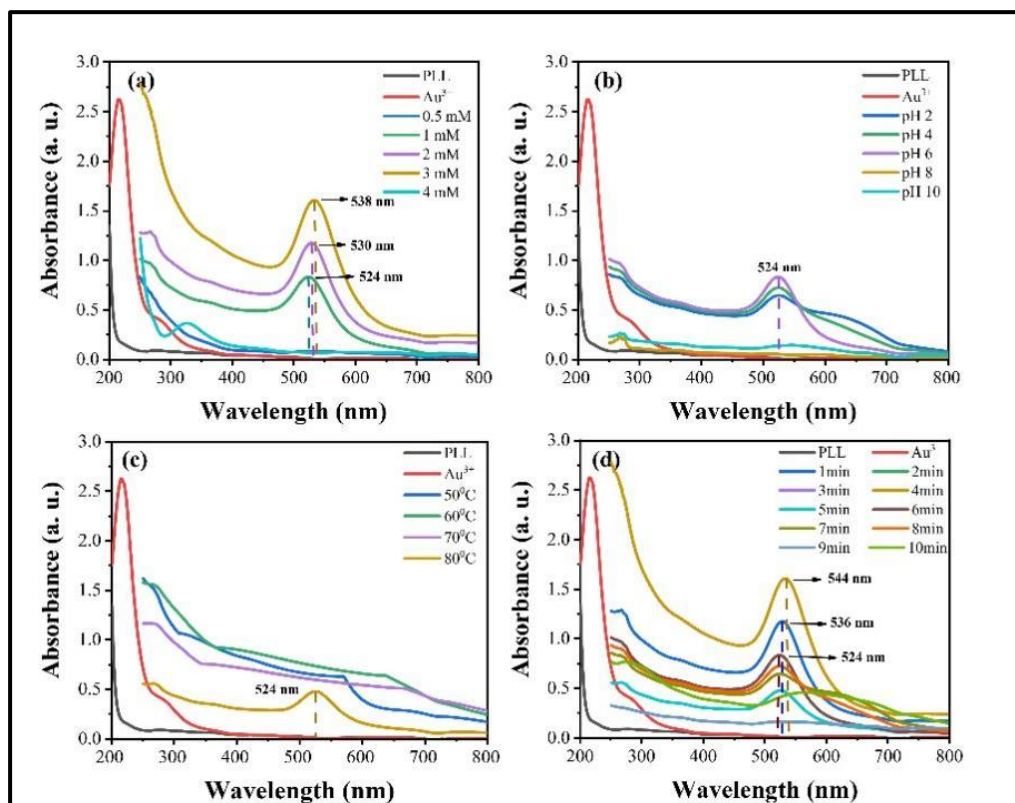
Figure 3.6: Optimization of synthesis parameters for PLL-AuNPs, (a) Precursor concentration, (b) pH, (c) Temperature, and (d) Reaction time

3.3.3   Characterization of PLL functionalized gold nanoparticles (PLL-AuNPs):

- **UV-Vis spectroscopy:**

The alteration of color from pale yellow to wine-red confirms the formation of PLL-AuNPs using PLL as both reducing and stabilizing agent. Then, the UV-Vis spectroscopy was used for initial characterization of synthesized PLL-AuNPs depending on Surface Plasmon Resonance (SPR) phenomenon. The synthesized PLL-AuNPs shows UV-Vis absorbance peak at 524 nm while, Au^{3+} solution shows peak 217 nm as represented in **figure 3.7(a)** indicating successful synthesis of PLL-AuNPs. The obtained result was compared with previously reported data, where cationic

AuNPs were synthesized by PLL and cysteamine that showed UV-Vis absorbance peak at 530 and 542 nm, respectively [12, 13].
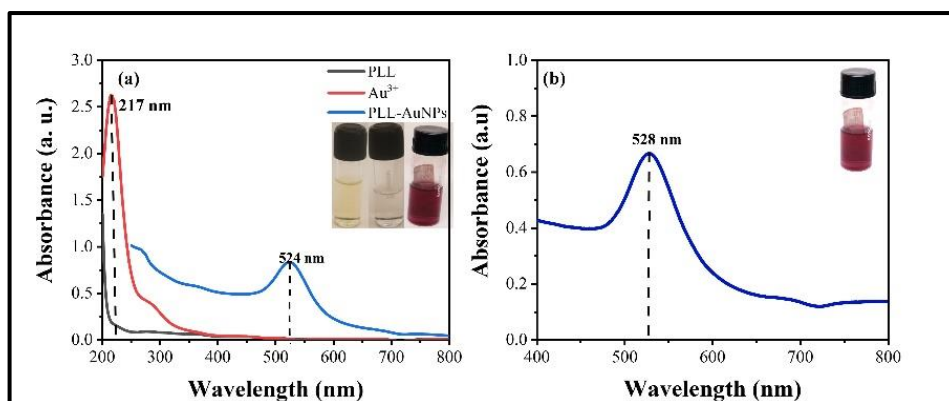
Figure 3.7: (a) UV-Vis absorption spectra of Poly-L-Lysine (PLL), Au precursor and PLL functionalized gold nanoparticles (PLL-AuNPs) after synthesis (524 nm). Inset image shows photographs of PLL, Au precursor, and synthesized PLL-AuNPs, and (b) UV-Vis absorbance spectrum of PLL-AuNPs after two months of synthesis (528 nm). Inset image shows photograph of PLL-AuNPs after two months

The stability of the synthesized PLL-AuNPs was assessed over a longer period by storing them in a refrigerator. The AuNPs remained stable for up to 2 months when stored at 4ºC in the dark. When PLL-AuNPs stored at 4ºC, they remain stable for longer period of time as compared to storing at 28ºC or above temperature condition. The PLL-AuNPs stored at 28ºC leads to increase in size of nanoparticles as 28ºC temperature provides sufficient kinetic energy responsible for aggregation of PLL-AuNPs [31]. The UV-Vis absorbance peak of PLL-AuNPs after 2 months of synthesis is presented in **figure 3.7(b)** showing absorbance peak at 528 nm representing the stability of synthesized PLL-AuNPs. Amino group ($-NH_2$) and hydroxyl group ($-OH$) of PLL acts as electron donor for reduction of gold salt (Au^{3+}) and a functionalizing agent that improve stability of PLL-AuNPs.

- **XRD analysis:**

The XRD measurement confirms the crystalline structure of PLL-AuNPs. The XRD examination of PLL-AuNPs reveal distinct peak with 2θ degrees of 37.92. According to **figure 3.8(a)**, this peak associated with the plane of (111) of Au. The

(111) plane is a primary growth orientation plane. In addition to the standard JCPDS file number 04-0784, these obtained values were equivalent to previously published data for the synthesis of AuNPs [32]. The crystalline size of PLL-AuNPs was determined by Scherrer formula by **equation 2.2**. The average crystalline size of PLL-AuNPs is 22.5 nm. Furthermore, the absence of any other additional peaks proved the purity of the synthesized PLL-AuNPs.

- **FTIR analysis:**

The functional groups that are principally responsible for the synthesis and stabilization of nanoparticles are identified by FTIR spectra. FTIR analysis shown that, functional groups of PLL involved in reduction of metal ions into nanoparticles and in promoting the colloidal stability. **Figure 3.8(b)** illustrates several IR spectra that correspond to various functional groups present in PLL. The O–H vibrational stretching for PLL-AuNPs is observed at a wavenumber of 3312.79 cm^{-1}, as shown in the **figure 3.8(b)**. The N-H stretching is observed at 1637.19 cm^{-1}. Additionally, the C-H bending for PLL-AuNPs is at wavenumber 700.1 cm^{-1}. The research also reveals C=C stretching at wavenumber 2122.32 cm^{-1}. According to the results of this investigation, PLL-AuNPs were reduced as well as stabilized by the O-H and N-H functional groups found in PLL.
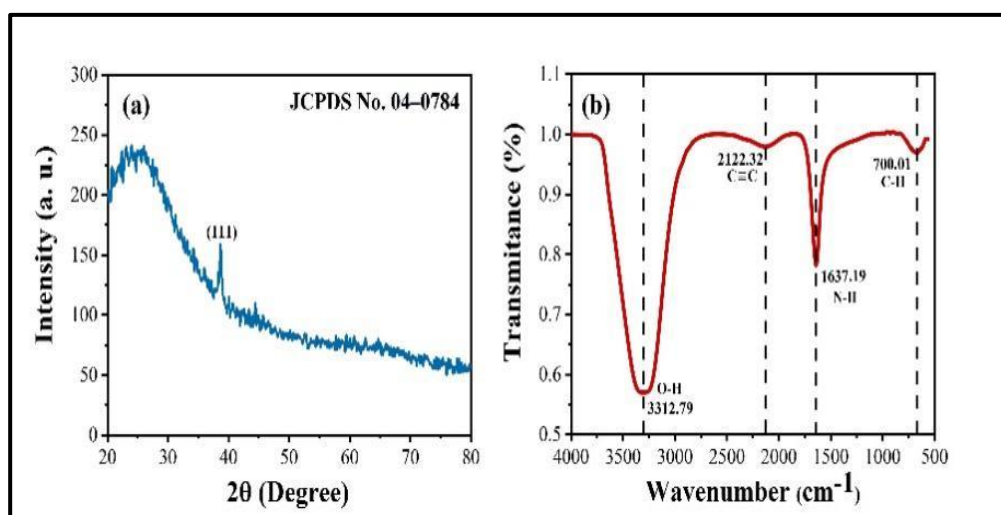
Figure 3.8: Characterization of PLL-AuNPs (a) XRD for crystalline nature and (b) FTIR analysis for functional group

- **EDAX analysis:**

Energy Dispersive X-Ray Analysis (EDAX) was used to confirm the elemental composition of PLL-AuNPs. EDAX data of PLL-AuNPs shows strong peaks of Au^0 at 2.2, 1.8, 8.5 and 9.7 keV as shown in **figure 3.9**. EDAX analysis shows atomic % of carbon, nitrogen, oxygen, and gold as 66.94, 2.40, 21.38, and 9.29%, respectively. The presence of carbon, nitrogen and oxygen is a result of PLL solution. This study shows the reduction ability of PLL for synthesis of PLL-AuNPs.
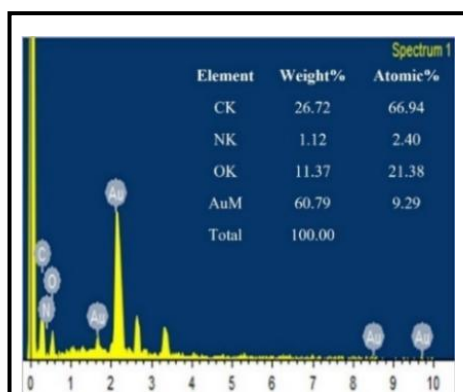
Figure 3.9: Elemental analysis of PLL-AuNPs by EDAX
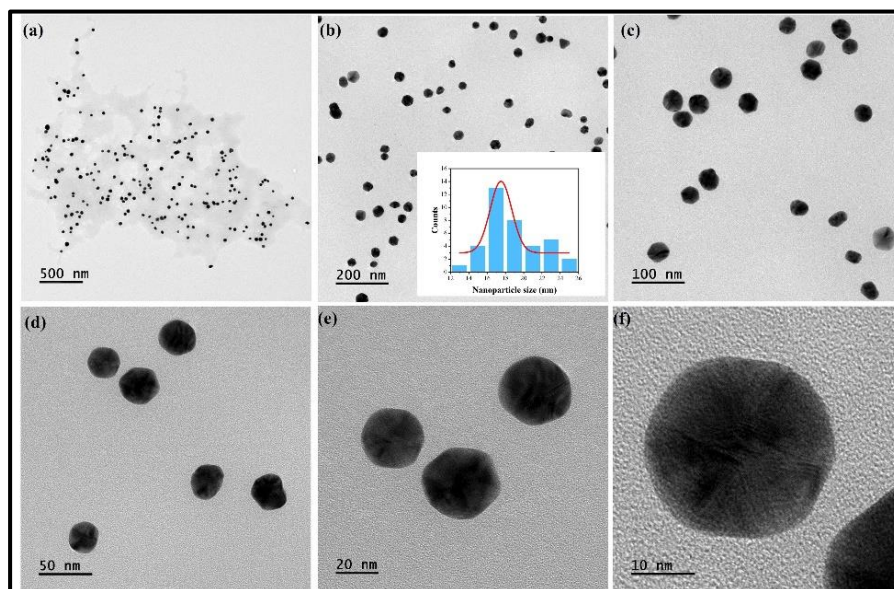
Figure 3.10: TEM images of PLL-AuNPs at scales (a) 500 nm, (b) 200 nm, (c) 100 nm, (d) 50 nm, (e) 20 nm, and (f) 10 nm. Inset image show size distribution histogram of PLL-AuNPs at the magnifications of 8KX, 25KX, 50KX, 100KX, 200KX, and 400KX, respectively

- **TEM analysis:**

Transmission electron microscopy (TEM) was used to examine the morphological properties of PLL-AuNPs, including their size and shape. The PLL-AuNPs exhibit a spherical shape, as shown in **figure 3.10(a-f)**, and are observed at various scales, including 500, 200, 100, 50, 20, and 10 nms. The size of nanoparticles was analyzed through TEM images by ImageJ applications. Inset image shows size distribution histogram of PLL-AuNPs showing size in the range of 10-25 nm with average size 17 nm.

- **Zeta (ζ) potential:**

The average potential of PLL-AuNPs is obtained from **figure 3.11(a)**, and it is +27.0±0.30 mV, indicating that the synthesized PLL-AuNPs are stable. The acquired cationic potential was comparable to that of PLL-AuNPs synthesis that had previously been reported [33]. This positive value denoted the important role of the PLL in reduction of gold salt. Positive potential of PLL-AuNPs suggests the stability of PLL-AuNPs, whereas positive surface charges of PLL-AuNPs are commonly associated with the presence of stabilizing chemicals produced during PLL-AuNPs formation. The positive ζ potential value of synthesized PLL-AuNPs (+27.0±0.30 mV) indicates stability of AuNPs.
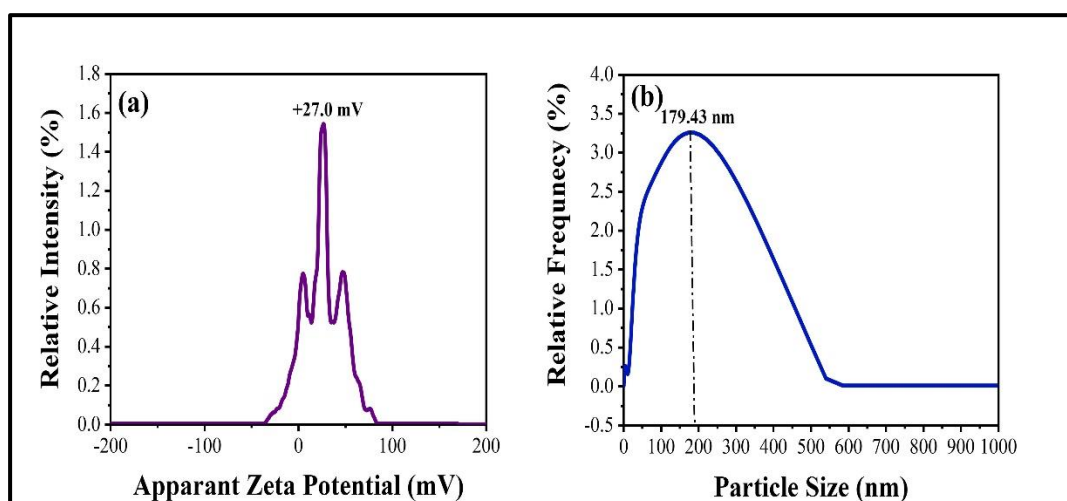
Figure 3.11: Surface charge and hydrodynamic size of PLL-AuNPs studied by (a) Zeta potential and (b) DLS, respectively

- **DLS analysis:**

The DLS provides information about the hydrodynamic radius of the material, while TEM offers the projected area diameter of the particles. The hydrodynamic diameter reveals details about the composition of the coating material and inorganic core. In this case, the hydrodynamic size of the synthesized PLL-AuNPs is found to be 179.43 nm, as shown in **figure 3.11(b).**

3.3.4   Comparison between characterization of AuNPs and PLL-AuNPs:

Both AuNPs and PLL-AuNPs were synthesized by the single step (one pot) synthesis method by using citrate and PLL as a reducing agent, respectively. The stabilization in AuNPs also required the addition of another stabilizing agent, but in the case of PLL-AuNPs, PLL alone serves as both a reducing and a stabilizing agent. As a result, it eliminates the need for additional functionalizing agents. The stability of AuNPs was lower than that of PLL-AuNPs, which was found to be stable for up to two months. Both AuNPs and PLL-AuNPs were appeared in wine-red color with SPR peaks at 532 nm and 524 nm, respectively. According to TEM pictures, the morphology of both AuNPs is spherical, but their diameters are different, being 19.1 nm for AuNPs and 17 nm for PLL-AuNPs. Due to the cationic nature of PLL, PLL-AuNPs have a positive charge on their surface (+27.0±0.30 mV), whereas citrate gives AuNPs a negative charge (-25.17±0.30 mV). AuNPs were reported to have a hydrodynamic size of 159.6 nm, while PLL-AuNPs had a size of 179.43 nm. The EDAX analysis revealed the presence of N in the case of PLL-AuNPs which is a result of PLL functionalization. Previously reported study showed that cationic AuNPs were suitable candidate for different biomedical applications such as, gene delivery, drug delivery, antibacterial applications, and biosensing. Thus, this study focuses on synthesis of cationic PLL-AuNPs and their interactions with nucleic acid for various biomedical applications.

3.4   Conclusions:

This chapter concludes that, PLL-AuNPs are synthesized by one pot synthesis method by using gold precursor and PLL as reducing agent. AuNPs has negative

surface charge whereas, the PLL functionalization influences the surface charge of AuNPs by providing cationic charge on its surface. The PLL-AuNPs were synthesized using 1 mM precursor concentration at pH 6 with approximately 6 min reaction time at 80ºC. The present strategy provides the easy and one pot synthesis approach for preparation of cationic AuNPs. The use of PLL reduced the need of any other functionalizing agent as PLL itself act as reducing and stabilizing agent. The synthesized AuNPs and PLL-AuNPs were of 19.1 nm and 17 nm in size showing UV-Vis absorbance at 532 nm and 524 nm, respectively. PLL-AuNPs were found to be stable upto two months in comparison to AuNPs. Thus, PLL-AuNPs were continued for further study for its biological applications. Cationic surface charge was responsible for repulsion of two particles that results in dispersion of PLL-AuNPs. The one pot synthesis method was useful to prepare the positively charged AuNPs in easy way that further used for various biomedical applications.

3.5   References:

[1]   Patil T, Gambhir R, Vibhute A, Tiwari AP. Gold nanoparticles: Synthesis methods, functionalization and biological applications. Journal of Cluster Science. 2023;34(2):705-25.

[2]   Ferreira-Gonçalves T, Ferreira D, Ferreira HA, Reis CP. Nanogold-based materials in medicine: From their origins to their future. Nanomedicine. 2021;16(30):2695-723.

[3]   Herizchi R, Abbasi E, Milani M, Akbarzadeh A. Current methods for synthesis of gold nanoparticles. Artificial cells, nanomedicine, and biotechnology. 2016;44(2):596-602.

[4]   Bansal SA, Kumar V, Karimi J, Singh AP, Kumar S. Role of gold nanoparticles in advanced biomedical applications. Nanoscale Advances. 2020;2(9):3764-87.

[5]   Shah M, Badwaik V, Kherde Y, Waghwani HK, Modi T, Aguilar ZP, Rodgers H, Hamilton W, Marutharaj T, Webb C, Lawrenz MB. Gold nanoparticles: various methods of synthesis and antibacterial applications. Front. Biosci. 2014;19(8):1320-44.

[6]   Turkevich J, Stevenson PC, Hillier J. A study of the nucleation and growth processes in the synthesis of colloidal gold. Discussions of the Faraday Society. 1951;11(1):55-75.

[7]   Frens G. Controlled nucleation for the regulation of the particle size in monodisperse gold suspensions. Nature physical science. 1973;241(105):20-22.

[8]   Dong J, Carpinone PL, Pyrgiotakis G, Demokritou P, Moudgil BM. Synthesis of precision gold nanoparticles using Turkevich method. KONA Powder and Particle Journal. 2020;37(1):224-32.

[9]   Gao Y, Torrente-Murciano L. Mechanistic insights of the reduction of gold salts in the Turkevich protocol. Nanoscale. 2020;12(4):2740-51.

[10]   Oliveira AE, Pereira AC, Resende MA, Ferreira LF. Gold Nanoparticles: a didactic step-by-step of the synthesis using the turkevich method, mechanisms, and characterizations. Analytica. 2023;4(2):250-63.

[11]   Moitra P, Alafeef M, Dighe K, Frieman MB, Pan D. Selective naked-eye detection of SARS-CoV-2 mediated by N gene targeted antisense oligonucleotide capped plasmonic nanoparticles. ACS nano. 2020;14(6):7617-27.

[12]   Jamaluddin ND, Ibrahim N, Yusof NY, Goh CT, Tan LL. Optical reflectometric measurement of SARS-CoV-2 (COVID-19) RNA based on cationic cysteamine-capped gold nanoparticles. Optics & Laser Technology. 2023;157(1):108763-72.

[13]   Yan X, Blacklock J, Li J, Möhwald H. One-pot synthesis of polypeptide–gold nanoconjugates for in vitro gene transfection. Acs Nano. 2012;6(1):111-17.

[14]   Bu T, Jia P, Liu J, Liu Y, Sun X, Zhang M, Tian Y, Zhang D, Wang J. Wang L.

Diversely positive-charged gold nanoparticles based biosensor: A label-free and sensitive tool for foodborne pathogen detection. Food chemistry: X. 2019;3(1):100052-60.

[15] De Souza CD, Nogueira BR, Rostelato ME. Review of the methodologies used in the synthesis gold nanoparticles by chemical reduction. Journal of Alloys and Compounds. 2019;798(1):714-40.

[16] Wuithschick M, Birnbaum A, Witte S, Sztucki M, Vainio U, Pinna N, Rademann K, Emmerling F, Kraehnert R, Polte J. Turkevich in new robes: key questions answered for the most common gold nanoparticle synthesis. ACS nano. 2015;9(7):7052-71.

[17] Li C, Li D, Wan G, Xu J, Hou W. Facile synthesis of concentrated gold nanoparticles with low size-distribution in water: temperature and pH controls. Nanoscale research letters. 2011;6(1):1-10.

[18] Han G, Wu S, Wang J, Geng X, Liu G. Poly-L-lysine mediated synthesis of gold nanoparticles and biological effects. Journal of Nanoscience and Nanotechnology. 2015;15(9):6503-08.

[19] Boldeiu A, Simion M, Mihalache I, Radoi A, Banu M, Varasteanu P, Nadejde P, Vasile E, Acasandrei A, Popescu RC, Savu D. Comparative analysis of honey and citrate stabilized gold nanoparticles: In vitro interaction with proteins and toxicity studies. Journal of Photochemistry and Photobiology B: Biology. 2019;197(1):111519-29.

[20] Sekar V, Al-Ansari MM, Narenkumar J, Al-Humaid L, Arunkumar P, Santhanam A. Synthesis of gold nanoparticles (AuNPs) with improved anti-diabetic, antioxidant and anti-microbial activity from Physalis minima. Journal of King Saud University-Science. 2022;34(6):102197-205.

[21] Patil TP, Vibhute AA, Patil SL, Dongale TD, Tiwari AP. Green synthesis of gold nanoparticles via Capsicum annum fruit extract: Characterization, antiangiogenic, antioxidant and anti-inflammatory activities. Applied Surface Science Advances. 2023;13(1):100372-82.

[22] Tirkey A, Babu PJ. Synthesis and characterization of citrate-capped gold nanoparticles and their application in selective detection of creatinine (A kidney biomarker). Sensors International. 2024;5(1):100252-60.

[23] Hosny M. and Fawzy M. Instantaneous phytosynthesis of gold nanoparticles via Persicaria salicifolia leaf extract, and their medical applications. Advanced Powder Technology. 2021;32(8):2891-904

[24] Ali Dheyab M, Abdul Aziz A, Jameel MS, Moradi Khaniabadi P, Oglat AA. Rapid sonochemically-assisted synthesis of highly stable gold nanoparticles as computed tomography contrast agents. Applied Sciences. 2020;10(20):7020-34.

[25] Qais FA, Ahmad I, Altaf M, Alotaibi SH. Biofabrication of gold nanoparticles using

Capsicum annuum extract and its antiquorum sensing and antibiofilm activity against bacterial pathogens. ACS omega. 2021;6(25):16670-82.

[26] Kumari M, Mishra A, Pandey S, Singh SP, Chaudhry V, Mudiam MK, Shukla S, Kakkar P, Nautiyal CS. Physico-chemical condition optimization during biosynthesis lead to development of improved and catalytically efficient gold nano particles. Scientific reports. 2016;6(1):27575-89.

[27] Khan S, Bakht J, Syed F. Green synthesis of gold nanoparticles using Acer pentapomicum leaves extract its characterization, antibacterial, antifungal and antioxidant bioassay. Dig. J. Nanomater. Biostruct. 2018;13(2):579-89.

[28] Katas H, Moden NZ, Lim CS, Celesistinus T, Chan JY, Ganasan P, Suleman Ismail Abdalla S. Biosynthesis and potential applications of silver and gold nanoparticles and their chitosan-based nanocomposites in nanomedicine. Journal of Nanotechnology. 2018;2018(1):1-3.

[29] Mountrichas G, Pispas S, Kamitsos EI. Effect of temperature on the direct synthesis of gold nanoparticles mediated by poly (dimethylaminoethyl methacrylate) homopolymer. The Journal of Physical Chemistry C. 2014;118(39):22754-59.

[30] Ngumbi PK, Mugo SW, Ngaruiya JM. Determination of gold nanoparticles sizes via surface plasmon resonance. IOSR Journal of Applied Chemistry (IOSR-JAC). 2018;11(7):25-9.

[31] Balasubramanian SK, Yang L, Yung LY, Ong CN, Ong WY, Liya EY. Characterization, purification, and stability of gold nanoparticles. Biomaterials. 2010;31(34):9023-30.

[32] Mubeen B, Rasool MG, Ullah I, Rasool R, Imam SS, Alshehri S, Ghoneim MM, Alzarea SI, Nadeem MS, Kazmi I. Phytochemicals mediated synthesis of AuNPs from citrullus colocynthis and their characterization. Molecules. 2022;27(4):1300-13.

[33] Manisekaran R, Jiménez-Cervantes Amieva E, Valdemar-Aguilar CM, López-Marín LM. Novel synthesis of polycationic gold nanoparticles and their potential for microbial optical sensing. Gold Bulletin. 2020;53(3-4):135-40.

Chapter IV

Optimization of parameters of nucleic acid (DNA) binding with Poly-L-Lysine functionalized gold nanoparticles (PLL-AuNPs)

4.1   Introduction:

Nucleic acids are macromolecules that hold great potential as therapeutic tools for diseases, including cancer and genetic disorders, as well as in diagnostic applications. [1]. Single stranded deoxyribonucleic acid (ssDNA), plasmids are used for gene delivery application in different diseases [2, 3]. Nucleic acids are small molecules that require delivery vehicle for protection against nucleases and other external agents to facilitate its entry inside cells. There are two types of delivery vehicles: biological and synthetic vectors. The biological vectors include use of viruses whereas, synthetic vectors include polymers, lipids, and dendrimers [4-6]. Although, these vehicles provide transfection efficacy but, has some limitations such as, low stability, limited *In-vivo* trafficking, immunogenicity and carcinogenicity with limited targeting efficacy [6, 7].

Metal nanoparticles have been used as non-viral or synthetic vectors for gene and drug delivery [8]. Amongst different metal nanoparticles, gold nanoparticles (AuNPs) have attracted researchers. AuNPs are employed various biomedical applications like, biosensors, drug delivery, gene delivery, diagnostic applications, and gene detection [9]. Among these applications, the transfection and biosensing are the most promising applications that involves use of DNA molecule. The conventional methods used for these applications are encountered with many difficulties such as, tedious, costly, time consuming, and require specific instrumentation facilities. Therefore, there is need to find alternative for conventional methods used for transfection and biosensing applications [10].

More studies are being conducted to gain a fundamental understanding of how interactions between AuNPs and DNA may change the molecular structure of the DNA and their biological activity. AuNPs interacts with nucleic acid molecule with either covalent or non-covalent interactions. The DNA molecule can be covalently attached to AuNPs through different groups like, thiol (-SH), hydroxyl (-OH), amine (-NH$_2$) or carboxyl (-COOH). These covalent interactions are responsible to generate specific binding of DNA to gold nanoparticles which are applicable in detection of target sequences. The non-specific interactions are achieved by non-covalent

interactions through simple adsorption of DNA on surface of gold nanoparticles. The non-covalent interactions include electrostatic interactions that depends on charge present on surface of AuNPs and nucleic acid without any surface modification (thiol). Non-covalent interactions are generally used for controlled release of DNA for gene therapy application. Therefore, it is essential to understand the molecular binding reaction of DNA and gold nanoparticles for describing the structural and functional basis of mechanisms. The functionalization of AuNPs is achieved through the use of thiolated oligonucleotides [1, 11].

Due to the fundamental properties of DNA bonding, specifically Watson-Crick base pairing, DNA strands can act as ligand molecules to combining with nanoparticles. Additionally, colloidal AuNPs are stable and durable in a variety of aqueous conditions due to the negative electrostatic nature of DNA backbones. Therefore, DNA conjugation to AuNPs surfaces is a crucial step for stabilizing, managing, and using DNA conjugated AuNPs, and the successful conjugation method should be used and executed for a particular application [12]. Mirkin *et. al.* [13] first time reported the interactions of DNA with gold nanoparticles where, AuNPs were covalently attached to thiol modified oligonucleotide and used this conjugate for siRNA-based gene silencing applications. Thiol modification of oligonucleotide makes disulphides (HS-SH) bond with AuNPs surface that provide specific interactions between DNA and AuNPs [14].

The DNA adsorption on surface of AuNPs can be influenced by various factors such as, pH and salt concentration that affects the charge present on DNA and AuNPs and weakens the non-specific interactions. The concentration, nature and length of DNA also influence the interactions between DNA and AuNPs. Thus, study of these parameters is required to evaluate the stability of AuNPs-DNA conjugate. The negatively charged (citrate) AuNPs interacts with thiol modified DNA by covalent interactions; that are utilized for various biomedical applications such as, biosensing, gene transfection, and delivery [15, 16].

The chapter includes, optimization of synthesis parameters of gold nanoparticles and nucleic acid conjugate and their characterization study. The surface

functionalized gold nanoparticles were conjugated with standard DNA (Calf thymus DNA) by optimizing the synthesis parameters such as, standard DNA concentration, pH, reaction time and salinity. The prepared conjugates were then characterized by UV-Vis spectroscopy, zeta potential, dynamic light scattering (DLS) and transmission electron microscopy (TEM). The conjugate preparation was finally confirmed by observing their electroneutrality using band shift assay or gel retardation assay.

4.2   Experimental details:

4.2.1   Materials:

The reagents employed in this investigation were all of analytical quality and utilized without further purification. The chemicals, gold tetrachloroaurate solution (Sigma Aldrich, Saint Louis, MO), 0.01% Poly-L-Lysine (Sigma), and Calf thymus DNA (Sigma) were purchased and used as per the requirement. Hydrochloric acid (HCl) and sodium hydroxide (NaOH) were obtained from Himedia and used for pH study. Agarose, DNA ladder, ethidium bromide, and gel loading dye were purchased from Himedia (India) and Thermofisher (India). The UV illuminator was used for observing gel bands.

4.2.2   Synthesis of PLL functionalized gold nanoparticles-nucleic acid (PLL-AuNPs-NA) conjugate:

The PLL-AuNPs were synthesized using PLL as reducing and stabilizing agent as described in **chapter 3**. After PLL-AuNPs synthesis, the PLL-AuNPs-NA conjugate were prepared by incubating the nanoparticles with NA concentration at 28°C for particular time period. The color of solution changes from wine-red to violet that indicates formation of conjugate. For this, 100 µL of PLL-AuNPs were incubated with 100 µg concentration of calf thymus DNA (standard DNA) at 28°C for 15 min with continuous stirring. The conjugate formation was then confirmed by observing change in UV-Vis absorption spectrum. PLL-AuNPs-NA conjugate were successfully synthesised and effect of parameters such as, standard DNA concentration, incubation time, pH, and salt concentration in the ranges of 5-200 µg/mL, 0-35 min, 2–12, and 0.1-0.5 M, respectively was studied. All optimization experiments were monitored

using UV-Vis spectroscopy in the range of 200–800 nm, with absorbance measured at 660 nm. PLL-AuNPs-NA conjugate were then synthesized for further experiments by using the optimized conditions. The prepared nanoparticles conjugates were washed twice with distilled water by centrifugation at 10000 rpm for 15 min at room temperature. The obtained nanoparticles were suspended in distilled water and stored at 4°C for further use.

4.2.3 Mechanism of synthesis of PLL functionalized gold nanoparticles-nucleic acid (PLL-AuNPs-NA) conjugate:

Mirkin *et. al.* [13] introduces AuNPs-NA hybrid that comprises use of citrate AuNPs and thiol modified oligonucleotides. Thiol modification of oligonucleotides helps in formation of covalent interactions between citrate AuNPs (negatively charged) surface and oligonucleotides. In this study, positively charged AuNPs were used for NA interactions. Here, unmodified oligonucleotides were used for interactions with AuNPs. The conjugates preparation is based on electrostatic interactions instead of covalent interactions thus, minimizes the need of thiol modification. PLL provides surface positive charge to synthesized AuNPs as PLL is a highly cationic biopolymer. These synthesized cationic gold nanoparticles are responsible to minimize the need of oligonucleotide modification by interacting with nucleic acid via electrostatic interactions. Nucleic acid contains phosphate residue in their backbone structure thus appears negatively charged molecule. Positively charged PLL-AuNPs interacts with negatively charged nucleic acid through electrostatic interactions thus, it reduces the need of surface modification of AuNPs or thiol modification of oligonucleotides for conjugate formation.

4.2.4 Characterization of PLL functionalized gold nanoparticles-nucleic acid (PLL-AuNPs-NA) conjugate:

Color change from wine-red to violet indicates formation of PLL-AuNPs-NA conjugate. The formation was further confirmed by observing change in UV-Vis spectroscopy result. The synthesized PLL-AuNPs-NA conjugate were then characterized by characterization techniques such as, TEM, Zeta potential, and DLS.

4.2.5 Band shift assay:

Preparation of PLL-AuNPs-NA conjugate was examined by assessing the electrophoretic mobility of prepared conjugate with comparison to PLL-NA conjugate. This was achieved by band shift assay method. For this study, the PLL-AuNPs-NA and PLL-NA conjugates were prepared by using different concentrations of PLL-AuNPs and PLL such as, 25, 50, and 100% with 100 µg/mL standard DNA concentration at 28°C and at pH 6. After incubation at 28°C for 15 min, the prepared conjugates were subjected to electrophoresis on 0.8% agarose gel containing ethidium bromide (1 µg/mL). After loading of samples to gel, the electrophoresis was performed at 35 V for one and half hour to allow 80% of gel run. After the gel run, power supply was turned off and the gel was carefully removed from the gel box. The interactions between PLL and PLL-AuNPs with standard DNA were analyzed, and images were captured under UV light by exposing the gel for 2-3 s [17].

4.3 Results and discussion:

4.3.1 Optimization of PLL functionalized gold nanoparticles-nucleic acid (PLL-AuNPs-NA) conjugate synthesis:

In this study, the conjugates were synthesized using cationic AuNPs functionalized with PLL biopolymer and unmodified (without thiol modification) nucleic acid. As PLL is a cationic biopolymer, it provides surface positive charge to synthesized AuNPs. This surface positive charge interacts with negatively charged nucleic acid molecule via electrostatic interactions. These electrostatic interactions result in reduction of surface positive charge. The formation of conjugate results in increasing the size of nanostructures leading to color change from wine-red to violet. Previously, PLL-AuNPs are repelling each other due to surface positive charge. After addition of negatively charged nucleic acid, the electrostatic attraction takes place between positively charged AuNPs and negatively charged nucleic acid to make the charge neutral. In this study, PLL-AuNPs and standard DNA were used to study the interactions between gold nanoparticles and nucleic acid. For this, PLL-AuNPs were incubated with standard DNA (calf thymus DNA) at 28°C by following the 15 min incubation time that results in uniformed size conjugate formation. The color change

from wine-red to violet confirms the formation of conjugate due to electrostatic interactions of PLL-AuNPs and nucleic acid. The PLL-AuNPs-NA conjugate shows broad SPR spectrum as compared to PLL-AuNPs alone. Different parameters of conjugate synthesis are needed to study to achieve successful synthesis of AuNPs-NA conjugate. Thus, in this chapter next study includes optimization of synthesis by varying the different reaction parameters.
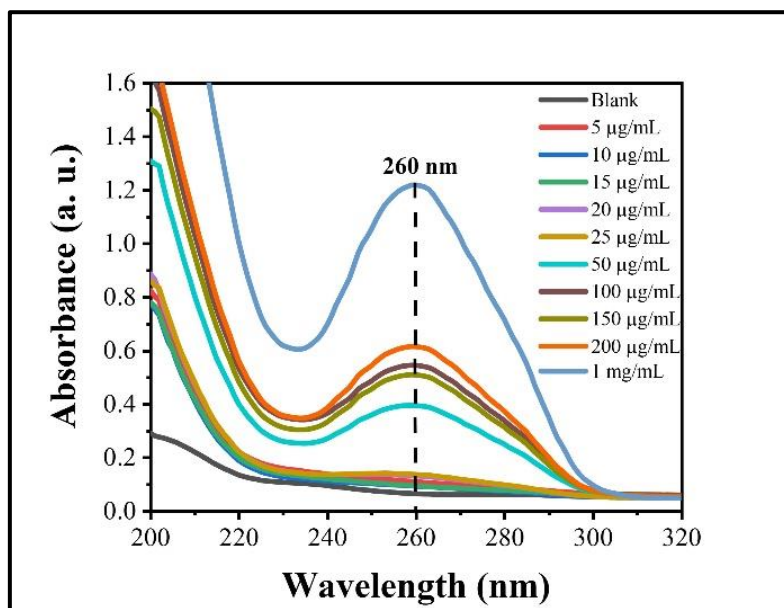
Figure 4.1: Purity check of various concentrations of standard DNA from 5-200 µg/mL and 1 mg/mL

The purity of standard DNA for 5-200 µg/mL concentration was checked by taking the A_{260}/A_{280} ratio and observing the peak at 260 nm as shown in **figure 4.1.** The pure DNA has maximum absorbance at 260 nm due to the aromatic structures present in nitrogenous bases of DNA (purine and pyrimidine). The DNA also shows A_{260}/A_{280} ratio at 1.8 whereas, good quality of DNA is considered to be obtained at ratio 1.7-2.0 [18, 19]. In **figure 4.1,** 5-25 µg/mL concentration of standard DNA did not show any absorbance peak at 260 nm as the nanodrop instrument (Multiscan sky) used for the study only show sensitivity above 50 µg/mL concentration of DNA. The concentrations from 50-200 µg/mL and 1 mg/mL shows absorbance at 260 nm representing the purity of standard DNA.

- **Effect of standard DNA concentration on synthesis of PLL-AuNPs-NA conjugate:**

    The effect of standard DNA concentration on synthesis of PLL-AuNPs-NA conjugate was studied by using different concentration of standard DNA as 5-200 µg/mL. The SPR peak at 534 nm is observed at 100 µg/mL concentration as presented in **figure 4.2** in comparison to other concentrations of standard DNA and PLL-AuNPs shows SPR peak at 524 nm. The small DNA purity peak at 260 nm is also observed for 100 µg/mL concentration that indicate the involvement of DNA in conjugate preparation. This result for standard DNA concentration effect indicates that 100 µg/mL concentration is optimized for the preparation of PLL-AuNPs-NA conjugate.
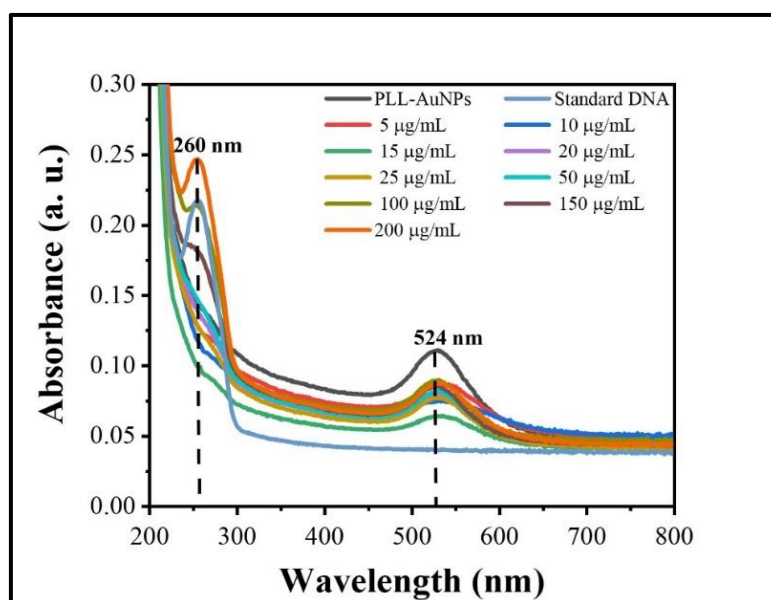
Figure 4.2: Change in UV-Vis absorbance spectra of PLL-AuNPs-NA conjugate at different concentrations of standard DNA (5-200 µg/mL)

- **Effect of pH on synthesis of PLL-AuNPs-NA conjugate:**

    The reaction pH plays a crucial role in the synthesis and stabilization of the PLL-AuNPs-NA conjugate. In this study, the effect of pH in the range of 2 to 12 on conjugate synthesis was examined. As shown in **figure 4.3**, no sharp SPR peaks are observed at pH 2 and 4. At pH 6, a strong SPR peak appears at 534 nm with slight red

shift compared to the PLL-AuNPs. Further increase in pH (8, 10, 12) results in a lower absorbance peak compared to pH 6. Thus, this study indicates that pH 6 is optimal for the synthesis of PLL-AuNPs-NA conjugate.
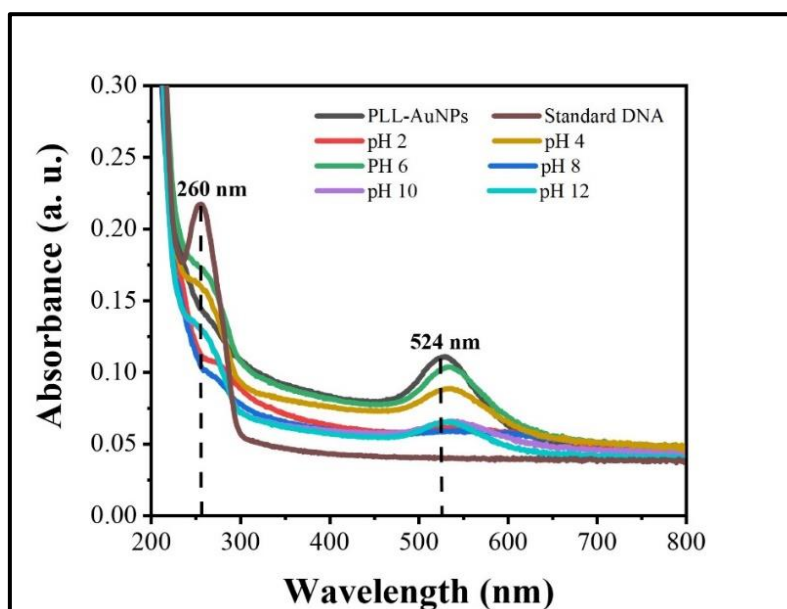
Figure 4.3: Change in UV-Vis absorbance spectra of PLL-AuNPs-NA conjugate at different pH (2, 4, 6, 8, 10, and 12)

- **Effect of reaction time on synthesis of PLL-AuNPs-NA conjugate:**

Reaction or incubation time affects the synthesis of PLL-AuNPs-NA conjugate depending on interactions of standard DNA and nanoparticles. This effect of reaction time on synthesis of conjugate is represented in **figure 4.4**. The effect is studied by observing change in absorbance spectra **(figure 4.4)**. At 0 min, the reaction mixture appears wine-red color indicating that the PLL-AuNPs have not participated in conjugate formation. All absorbance peaks at 260 nm further confirms the presence of unconjugated DNA in solution. As reaction proceeds from 0-10 min the initial wine-red color changes to light violet color and the standard DNA peak at 260 nm starts to disappear. At 15 minutes of reaction time, the standard DNA peak at 260 nm disappears completely, indicating full interaction of the standard DNA with PLL-AuNPs. At 15 to 35 minutes, the standard DNA peak reappears, suggesting an excess of standard DNA in the reaction mixture. These findings suggest that 15 minutes of reaction time is sufficient for the formation of the PLL-AuNPs-NA conjugate.
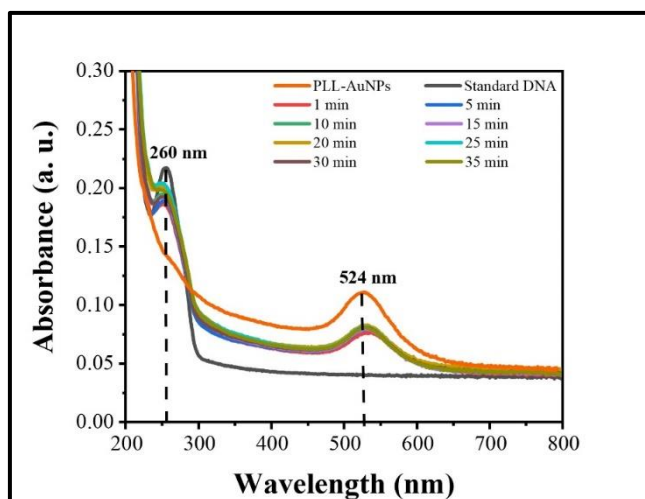
Figure 4.4: Change in UV-Vis absorbance spectra of PLL-AuNPs-NA conjugate at different reaction time (0-35 min)
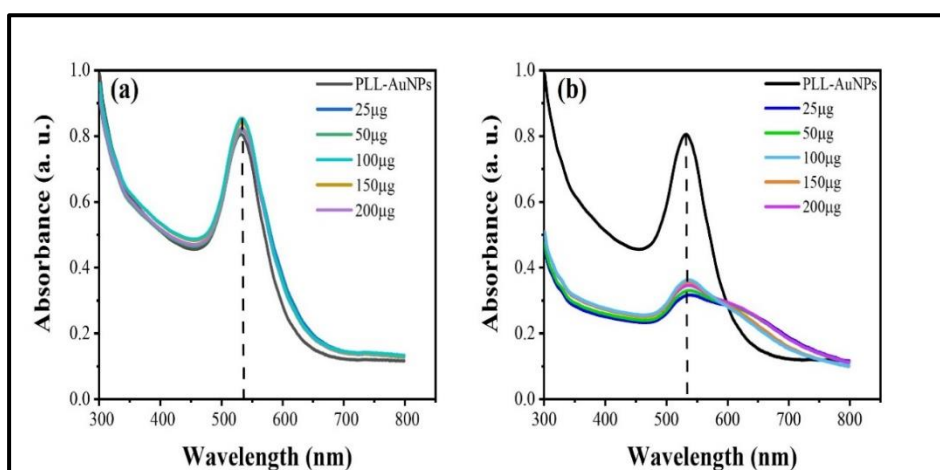
Figure 4.5: Change in Surface Plasmon resonance (SPR) spectra of PLL-AuNPs with different concentrations of standard DNA (25-200 µg/mL) at (a) 0 min and (b) 15 min of incubation

Further, this study validates the change in UV-Vis absorption spectrum of PLL-AuNPs after incubation of 15 min with different concentrations of standard DNA as shown in **figure 4.5.** Initially, after addition of standard DNA into PLL-AuNPs, there is no change in UV-Vis absorption spectrum as it appear similar to PLL-AuNPs as shown in **figure 4.5(a)**. Whereas, after 15 min of incubation the UV-Vis absorption spectrum changes for all concentrations of standard DNA as shown in **figure 4.5(b)**; it is result of electrostatic interactions of standard DNA and PLL-

AuNPs. This data clearly shows the difference between UV-Vis absorption spectrum of PLL-AuNPs before and after incubation with standard DNA indicating the successful formation of PLL-AuNPs-NA conjugate.

- **Effect of NaCl concentration on synthesis of PLL-AuNPs-NA conjugate:**

Stability of conjugate in presence of NaCl is another important parameter of conjugate synthesis. The effect of different concentrations of NaCl on synthesis of PLL-AuNPs-NA conjugate is presented in **figure 4.6**. To study this effect, different concentrations of NaCl were used such as, 0.1-0.5 M. **Figure 4.6** shows the change in SPR absorption spectrum of conjugate in case of different NaCl concentrations. 0.3 M NaCl concentration shows higher absorption peak at 533 nm as compared to other NaCl concentrations. Therefore, this study indicates that PLL-AuNPs-NA conjugate is stable at 0.3 M NaCl concentration.
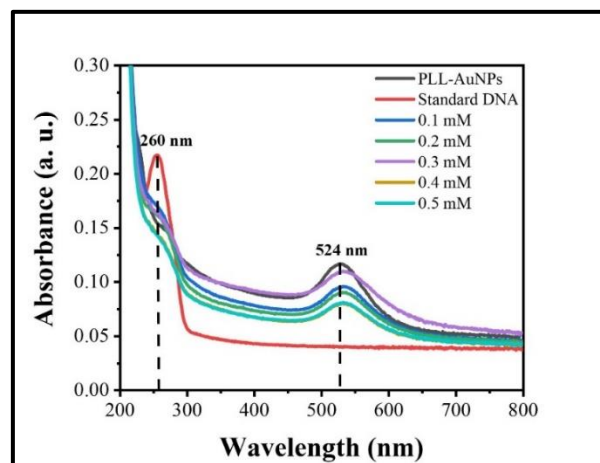
Figure 4.6: Change in UV-Vis absorbance spectra of PLL-AuNPs-NA conjugate at different concentrations of NaCl (0.1-0.5M)

4.3.2   Characterization of PLL functionalized gold nanoparticles-nucleic acid (PLL-AuNPs-NA) conjugate:

- **UV-Vis absorption Spectroscopy:**

The color shift from wine-red to violet served as the first visual indicator of the successful conjugation of standard DNA with PLL-AuNPs. After this visible confirmation, the conjugates were primarily characterized with UV-Vis spectroscopy

by Surface Plasmon Resonance (SPR) Phenomenon. The change in color is result of electrostatic interactions between negatively charged standard DNA and positively charged PLL-AuNPs. The prepared PLL-AuNPs-NA conjugate shows absorption peak at 534 nm whereas, PLL-AuNPs shows peak at 524 nm as shown in **figure 4.7** indicating successful synthesis of PLL-AuNPs-NA conjugate. The addition of standard DNA to PLL-AuNPs results in red shift and decrease in SPR absorption peak with comparison to PLL-AuNPs that ensures the interactions of standard DNA with PLL-AuNPs. Obtained data is associated with previously reported data that showed red shift after conjugation of chitosan AuNPs and standard DNA where the chitosan AuNPs has absorption peak at 560 nm [20]. The prepared conjugates were stored in the refrigerator for long-term use, but it was observed that the synthesized conjugates were not stable over extended periods. Hence, freshly prepared conjugate solutions were used for all the experiments.
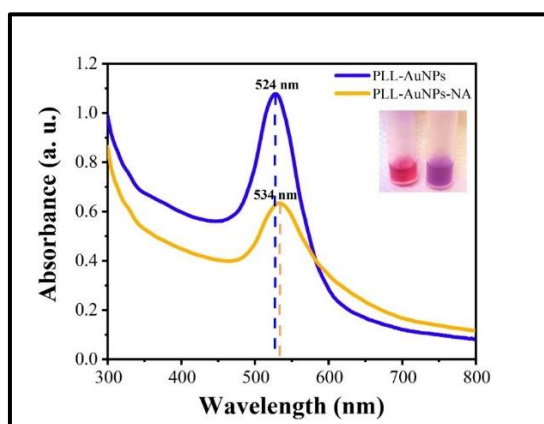
Figure 4.7: UV-Vis absorption spectra of PLL-AuNPs-NA conjugate showing red shift with absorption peak at 534 nm in comparison to PLL-AuNPs having absorption peak at 524 nm. Inset image of PLL-AuNPs (wine-red) and PLL-AuNPs-NA conjugate (violet)

- **Zeta (ζ) potential analysis:**

Zeta (ζ) potential is used to analyze the surface charge present on nanoparticles that indicates the stability of nanoparticles. **Figure 4.8** represents the surface charge of PLL-AuNPs-NA conjugate **(figure 4.8a)** and PLL-AuNPs **(figure 4.8b)**. The ζ potential of PLL-AuNPs-NA conjugate is obtained as $+0.10\pm0.02$ mV,

that indicated the conjugate formation. The obtained ζ potential is compared with the ζ potential of PLL-AuNPs and it is observed that the positive charge of PLL-AuNPs (+27.0±0.30 mV) decreases after conjugation of standard DNA. This decrease in positive charge of PLL-AuNPs is result of the conjugation of negatively charged standard DNA and positively charged PLL-AuNPs by electrostatic interactions.
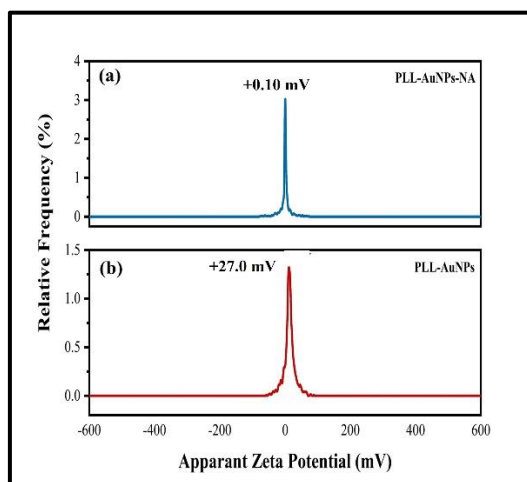
Figure 4.8: Apparent zeta (ζ) potential of (a) PLL-AuNPs-NA conjugate (+0.10±0.02 mV) in comparison to (b) PLL-AuNPs (+27.0±0.30 mV)

Also, **table 4.1** shows the comparison of ζ potential of citrate AuNPs, PLL-AuNPs, and PLL-AuNPs-NA conjugate. The citrate AuNPs has negative surface charge (-25.17±0.30 mV), PLL-AuNPs has positive surface charge (+27.0±0.30 mV) while PLL-AuNPs-NA conjugate show lower surface positive charge as +0.10±0.02 mV. As mentioned in characterization section of **chapter 3**, the -30.0 to +30.0 mV ζ potential of colloidal nanoparticles are considered to be stable. Thus, the obtained ζ potential value confirms the formation of conjugate and also indicates the stability of conjugate.

Table 4.1: Comparison of zeta (ζ) potential between AuNPs, PLL-AuNPs and PLL-AuNPs-NA conjugate

Sr. No.	Name of Nanostructures	Zeta (ζ) Potential (mV)
1.	AuNPs	-25.17±0.30
2.	PLL-AuNPs	+27.0±0.30
3.	PLL-AuNPs-NA	+0.10±0.02

- **DLS analysis:**

The hydrodynamic radius of the nanoparticles was analyzed using DLS. **Figure 4.9** shows the hydrodynamic sizes of (a) PLL-AuNPs and (b) PLL-AuNPs-NA conjugate, measuring 179.43 nm and 304.14 nm, respectively. This indicates that conjugation of standard DNA with PLL-AuNPs results in an increase in the hydrodynamic size. The increase in hydrodynamic size of nanostructure confirms the conjugation of standard DNA and PLL-AuNPs.
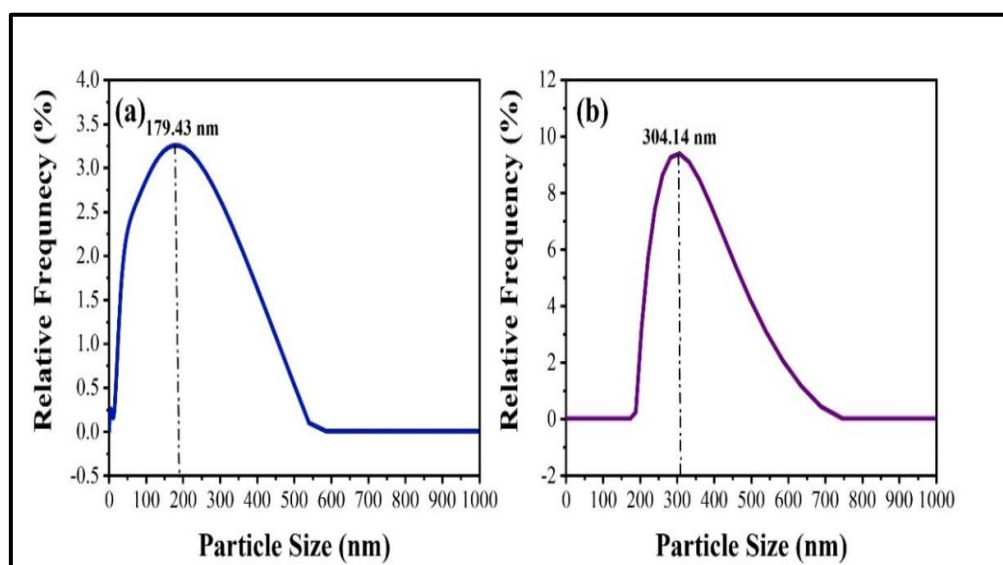
Figure 4.9: Hydrodynamic size of (a) PLL-AuNPs and (b) PLL-AuNPs-NA conjugate

- **TEM analysis:**

Transmission electron microscopy (TEM) was used to examine the size, shape, and morphological properties of AuNPs. The AuNPs were observed to be spherical in shape, as shown in **figure 4.10(a-b),** with scales of 100 and 50 nm, respectively. These obtained TEM images were examined by ImageJ software to define the particle size. Inset image shows size distribution histogram of the PLL-AuNPs-NA conjugate. The TEM micrograph displays AuNPs with sizes ranging from 30 to 60 nm with 38.3 nm average size.
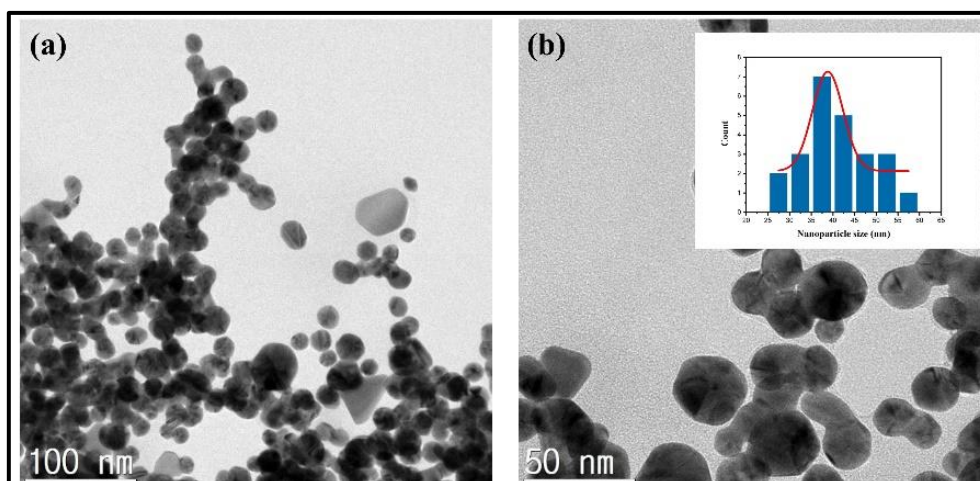
Figure 4.10: TEM images of PLL-AuNPs-NA conjugate at various scales (a) 100 nm and (b) 50 nm at the magnifications of 50KX and 100KX, respectively. Inset image shows size distribution histogram of PLL-AuNPs-NA conjugate

4.3.3   Band shift assay:

Band shift assay is also referred as mobility shift electrophoresis, an electrophoretic mobility shift assay (EMSA), gel mobility shift assay, gel shift assay, or gel retardation assay. It is a powerful technique that commonly used to study Protein-DNA interactions. The technique is based on separating free DNA from DNA-protein complexes using variations in charge, size, and structure [21, 22].

Figure 4.11 shows the band shift assay for PLL-NA and PLL-AuNPs-NA conjugate prepared by using different concentrations of PLL and PLL-AuNPs. The complexes in lanes 2-4 were prepared using different concentrations of PLL as 0.0001%, 0.001%, and 0.01%, combined with 100 µg/mL standard DNA. For lanes 5-7, the PLL-AuNPs-DNA conjugates were formulated with 25%, 50%, and 100% PLL-AuNPs, each containing 100 µg/mL standard DNA. In **figure 4.11,** the electroneutrality point indicates red color number (lane 6 and 7) and white arrows which represents the conjugation of anionic standard DNA and cationic PLL-AuNPs resulting in formation of an electroneutral conjugate. The conjugation of standard DNA and PLL-AuNPs shows strong effect on electrophoretic mobility of DNA within the gel. Surface positive charge of PLL-AuNPs is responsible for complete binding of negatively charged standard DNA on its surface. The PLL-AuNPs-NA conjugate

prepared by using of 50% (lane 6) and 100% (lane 7) concentration of PLL-AuNPs shows complete retardation that represents binding of standard DNA to nanoparticles, as shown in **figure 4.11**. The complete retardation is observed for the conjugate prepared by 100% PLL-AuNPs as compared to 50% PLL-AuNPs. Strong retardation was not observed in case of PLL-NA conjugate (lane 2-4) and PLL-AuNPs-NA conjugate prepared by 25% of PLL-AuNPs (lane 5). The electrostatic interactions between the positively charged PLL-AuNPs and negatively charged standard DNA result in the formation of an electroneutral complex, which is retained in the lane, demonstrating complete retardation of the PLL-AuNPs-DNA conjugate.
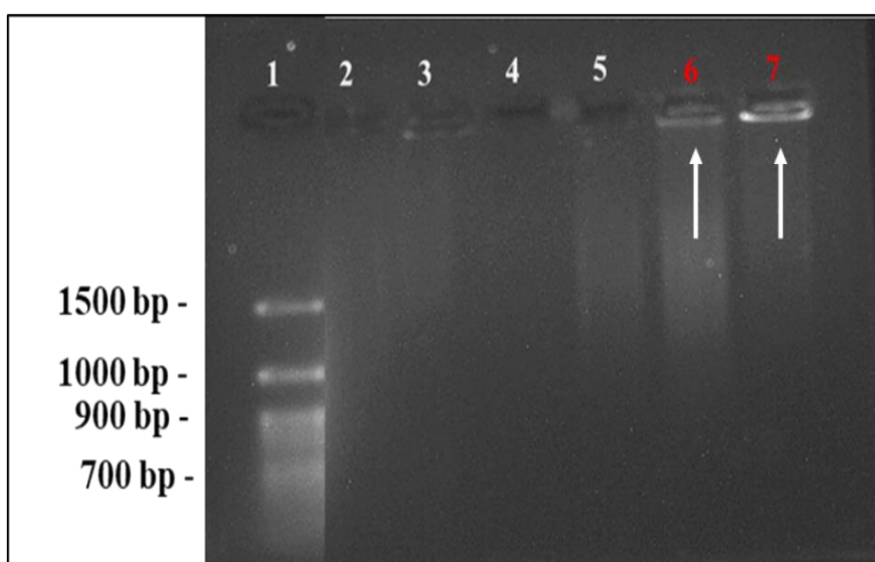
Figure 4.11: Band shift assay of prepared conjugates. Standard DNA concentration was kept constant as 100 µg/mL. Lane 1: DNA ladder, Lane 2-4: PLL-NA conjugate, and Lane 5-7: PLL-AuNPs-NA conjugate prepared by using 25, 50, and 100% concentration of PLL and PLL-AuNPs, respectively. The lane number showing electroneutrality point are indicated in red color and white arrows.

4.4   Conclusions:

The PLL-AuNPs-NA conjugate was synthesized by using 100 µg/mL concentration of standard DNA at 28°C with 15 min incubation time. The conjugates were stable at 0.3 M NaCl concentration. The conjugate preparation was first visibly confirmed by observing the color change from wine-red to violet. Furthermore, the

UV-Vis absorption spectrum exhibited a red shift, with the SPR peak shifting to 534 nm, compared to the PLL-AuNPs peak at 524 nm. The conjugate formation was confirmed by observing the change in ζ potential showing decreased positive charge as +0.10±0.02 mV from +27.0±0.30 mV. Increase in morphological size studied by TEM and the hydrodynamic size of conjugate indicated the binding of standard DNA to PLL-AuNPs. The band shift assay represented the electroneutrality of PLL-AuNPs-NA conjugate prepared by using 100% PLL-AuNPs by showing the retardation of conjugate into the well. Thus, this study indicated the electrostatic interactions of the positively charged PLL-AuNPs and negatively charged standard DNA for PLL-AuNPs-NA conjugate preparation. This strategy of PLL-AuNPs-NA conjugate preparation was further utilized to study biomedical applications such as, optical, electrochemical, and UV-Vis spectroscopy based biosensing of pathogenic (viral/bacterial) nucleic acid.

4.5 References:

[1]   Ding Y, Jiang Z, Saha K, Kim CS, Kim ST, Landis RF, Rotello VM. Gold nanoparticles for nucleic acid delivery. Molecular therapy. 2014;22(6):1075-83.

[2]   Martínez-Puente DH, Pérez-Trujillo JJ, Zavala-Flores LM, García-García A, Villanueva-Olivo A, Rodríguez-Rocha H, Valdés J, Saucedo-Cárdenas O, Montes de Oca-Luna R, Loera-Arias MD. Plasmid DNA for therapeutic applications in cancer. Pharmaceutics. 2022;14(9):1861-88.

[3]   Daniels AN, Singh M. Sterically stabilized siRNA: gold nanocomplexes enhance c-MYC silencing in a breast cancer cell model. Nanomedicine. 2019;14(11):1387-401.

[4]   Ramamoorth M, Narvekar A. Non viral vectors in gene therapy-an overview. Journal of clinical and diagnostic research: JCDR. 2015;9(1):GE01-GE06.

[5]   Yin, Hao, Rosemary L. Kanasty, Ahmed A. Eltoukhy, Arturo J. Vegas, J. Robert Dorkin, and Daniel G. Anderson. Non-viral vectors for gene-based therapy. Nat Rev Genet. 2014;15(8):541–554.

[6]   Wang C, Pan C, Yong H, Wang F, Bo T, Zhao Y, Ma B, He W, Li M. Emerging non-viral vectors for gene delivery. Journal of Nanobiotechnology. 2023;21(1):272-90.

[7]   Zu H, Gao D. Non-viral vectors in gene therapy: recent development, challenges, and prospects. The AAPS journal. 2021;23(4):78-90.

[8]   Dizaj SM, Jafari S, Khosroushahi AY. A sight on the current nanoparticle-based gene delivery vectors. Nanoscale research letters. 2014;9(1):1-9.

[9]   Patil T, Gambhir R, Vibhute A, Tiwari AP. Gold nanoparticles: Synthesis methods, functionalization and biological applications. Journal of Cluster Science. 2023;34(2):705-24.

[10] Chinchulkar SA, Patra P, Dehariya D, Appidi T, Rengan AK. Gold nanoparticle–based biosensing applications and fundamentals of sensor technology: principles and novel designs. InFundamentals of Sensor Technology. 1st edition, Woodhead publishing, 2023;669-723.

[11] Carnerero JM, Jimenez-Ruiz A, Castillo PM, Prado-Gotor R. Covalent and Non-Covalent DNA–Gold-Nanoparticle Interactions: New Avenues of Research. ChemPhysChem. 2017;18(1):17-33.

[12] Epanchintseva A, Dolodoev A, Grigor'eva A, Chelobanov B, Pyshnyi D, Ryabchikova E, Pyshnaya I. Non-covalent binding of nucleic acids with gold nanoparticles provides their stability and effective desorption in environment mimicking biological media. Nanotechnology. 2018;29(35):5601-21.

[13]   Mirkin CA, Letsinger RL, Mucic RC, Storhoff JJ. A DNA-based method for rationally assembling nanoparticles into macroscopic materials. InSpherical Nucleic Acids. 1st edition, Jenny Stanford publishing, 2020;3-11.

[14]   Nejati K, Dadashpour M, Gharibi T, Mellatyar H, Akbarzadeh A. Biomedical applications of functionalized gold nanoparticles: a review. Journal of Cluster Science. 2021;33(1):1-16.

[15]   Massich MD, Giljohann DA, Schmucker AL, Patel PC, Mirkin CA. Cellular Response of Polyvalent Oligonucleotide—Gold Nanoparticle Conjugates. InSpherical Nucleic Acids. 1st edition, Jenny Stanford publishing, 2020;437-450.

[16]   Graczyk A, Pawlowska R, Jedrzejczyk D, Chworos A. Gold nanoparticles in conjunction with nucleic acids as a modern molecular system for cellular delivery. Molecules. 2020;25(1):204-30.

[17]   Lazarus GG, Singh M. In vitro cytotoxic activity and transfection efficiency of polyethyleneimine functionalized gold nanoparticles. Colloids and Surfaces B: Biointerfaces. 2016;145(1):906-11.

[18]   https://assets.thermofisher.com/TFS-Assets/CAD/Product-Bulletins/T123-NanoDrop-Lite-Interpretation-of-Nucleic-Acid-260-280-Ratios.pdf

[19]   https://www.promega.in/resources/pubhub/enotes/how-do-i-determine-the-concentration-yield-and-purity-of-a-dna-sample/

[20]   Kukreti S, Kaushik M. Exploring the DNA damaging potential of chitosan and citrate-reduced gold nanoparticles: physicochemical approach. International journal of biological macromolecules. 2018;115(1):801-10.

[21]   Fillebeen C, Wilkinson N, Pantopoulos K. Electrophoretic mobility shift assay (EMSA) for the study of RNA-protein interactions: the IRE/IRP example. JoVE (Journal of Visualized Experiments). 2014;94(1):e52230-39.

[22]   Stowell JA, Tang TT, Seidel M, Passmore LA. Gel-Based Analysis of Protein–Nucleic Acid Interactions. Protein-Ligand Interactions: Methods and Applications. 2021;2263(1):321-39.

Chapter V

Poly-L-Lysine functionalized gold nanoparticle–nucleic acid conjugate for optical biosensing of viral RNA (SARS-CoV-2 RNA)

5.1   Introduction:

Severe acute respiratory syndrome corona virus 2 (SARS-CoV-2) has been responsible for outbreak of corona virus disease 2019 (COVID-19) which collapsed many health care systems and resulted in declination in economies [1]. The SARS-CoV-2 infection spreads through air and appears as asymptomatic infection that causes mild upper respiratory tract illness, severe viral pneumonia with respiratory failure and causes death [2]. The SARS-CoV-2 virus is a spherical, enveloped virus of 125 nm diameter that contains positive-sense single-stranded RNA as genetic material [3].

Conventional methods used for COVID-19 detection includes quantitative reverse transcription polymerase chain reaction (qRT-PCR) for gene detection, immunoassays for viral antigen and antibodies detection. RT-PCR method is considered as standard method for detection due to its sensitivity, specificity and ability to detect multiple pathogens in single test [4]. RT-PCR detects SARS-CoV-2 RNA by specific regions of genes that act as target [5]. These targets involve genes such as, RNA-dependent RNA polymerase gene (RdRp), Envelope Protein gene (E) or Nucleo-capsid gene (N) [6]. The immunoassays examine presence of IgG and IgM against SARS-CoV-2 during infection. The production of antibodies after infection is detected after five days of infection as well as the IgG production is detected after 14 days of infection [7]. Thus, the infection is difficult to detect at initial stages by using immunoassays. The alternative techniques are also developing such as, rapid antigen detection system [8], and direct fluorescent antibody testing (DFA) that are easy, inexpensive with speedy detection within 15-30 min [9]. The RT-PCR and immunoassays has several disadvantages such as, need of expensive instruments and chemicals, tedious steps, time consuming methods, and needs skilled technicians for handling [10]. Therefore, to overcome the limitations of existing techniques which are tedious and difficult to handle there is crucial need to develop simple, rapid, cost-effective and sensitive detection method for SARS-CoV-2 detection which can provide precise and fast results within short period of time [11].

Nanotechnology received attention of researchers for colorimetric biosensing which are convenient and suitable for biosensing due to their simple nature, visual appearance and no requirement of complex instrumentation [12]. Gold nanoparticles (AuNPs) show application of colorimetric biosensing due to their desirable optical characteristics such as, Surface Plasmon Resonance (SPR), high extinction coefficient, and photostability [13]. AuNPs are used in different colorimetric biosensing applications to detect metal ions, heavy metals, biological entities such as, microorganisms, nucleic acid, and proteins where AuNPs changes its color according to specific reactivity of nanoparticles with detectable material [14]. AuNPs are widely used for fabrication of biosensor to detect pathogens in the field of clinical diagnosis [15], biology, water bodies, and food contamination [16].

Nucleic acid biosensors are employed for detection of pathogen due to their sensitivity and specificity [17]. The conjugation of nucleic acids with gold nanoparticles for optical biosensing has gained significant attention from researchers due to the unique properties of gold nanoparticles. Gold nanoparticles based colorimetric bioassays are developed for DNA/RNA detection by combining the AuNPs with thiol modified DNA probe via disulphide (covalent) bonding [18]. This was first reported by Mirkin *et. al.* [19] where sulphur gold interaction specificity was widely exploited to mediate DNA-AuNPs assembly. Depending upon this concept nucleic acids conjugated gold nanoparticles were utilized for biosensing applications. For example, citrate capped AuNPs in conjugation with thiol modified nucleic acid were used for detection of *Klebsiella pneumoniae* [20], SARS-CoV-2 RNA [21], and *Mycobacterium avium* subspecies *paratuberculosis* DNA [22]. The use of positively charged gold nanoparticles minimizes the need of thiol modification of DNA. Such platforms were used to detect various analytes like antibiotics, microorganisms, nucleic acids of pathogens, and heavy metals [23].

The present chapter demonstrates optical biosensing assay of cationic PLL-AuNPs conjugated with nucleic acid for detection of target SARS-CoV-2 RNA. This detection is based on electrostatic interactions between unmodified anionic oligonucleotides (ASO) and cationic PLL-AuNPs. Here, Poly-L-Lysine polymer acts as both reducing and functionalizing agent that provide amino group which permits

binding of AuNPs to nucleic acid. Antisense oligonucleotides (ASO) are the single stranded DNA sequence which is complementary to RNA sequence of SARS-CoV-2. These ASOs were adsorbed on surface of PLL-AuNPs to make PLL-AuNPs-ASO conjugate. Concentration of ASO, reaction time, and temperature influence the formation of PLL-AuNPs-ASO conjugate. The immobilized oligonucleotide probe (ASO) binds to complementary SARS-CoV-2 RNA due to higher affinity of oligonucleotide probe towards SARS-CoV-2 RNA as compare to PLL-AuNPs. This interaction between probe and target RNA releases PLL-AuNPs which get aggregated in presence of sodium chloride (NaCl). The aggregation was visible by naked eyes and was confirmed by UV-Vis absorption at 660 nm. The working principle of this optical biosensing system is presented schematically in **figure 5.1**, which shows formation of PLL-AuNPs-ASO conjugate that is used for detection of SARS-CoV-2 RNA by forming DNA-RNA hybrid that leads to aggregation of PLL-AuNPs.
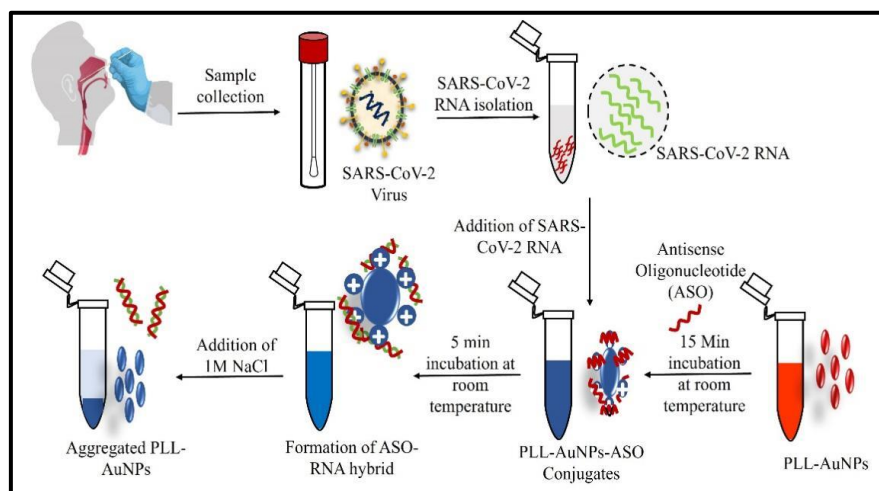
Figure 5.1: Schematic presentation of optical biosensing of SARS-CoV-2 RNA by PLL-AuNPs-ASO conjugate

5.2.   Experimental details:

5.2.1   Material:

All the reagents used in this study were of analytical grade obtained from commercial vendors and used without any purification step. Gold tetrachloroaurate (HAuCl₄) solution, 0.01% Poly-L-Lysine (PLL) solution were purchased from Sigma

(Maharashtra, India) and NaCl from Himedia (Maharashtra, India). Deionized water was used for preparation of all the respective solutions. The antisense oligonucleotide (ASO) sequence and target SARS-CoV-2 RNA sequence were purchased from Krumak Traders, Pune (Maharashtra, India) and stored at -20°C for further use. ASO solution was prepared in 1X TAE buffer. The sequences used in the study with their purity ratio are presented in **table 5.1**.

Table 5.1: The anti-sense oligonucleotide (ASO) and target sequences used in study

Sr. No.	Oligonucleotide	Base sequence (5'-3')	Purity ratio	Ref
1.	Anti-sense oligonucleotide (ASO)	CCAATGTGATCTTTTGGTGT	1.9	[24]
2.	Target sequence	ACACCAAAAGAUCACAUUGG	1.86	

5.2.2 Clinical samples:

Clinical samples of COVID-19 positive individual were collected by nasopharyngeal swab. SARS-CoV-2 RNA is crucial for detection of SARS-CoV-2 infection thus it should be extracted from the nasopharyngeal swab collected from SARS-CoV-2 infected person. The SARS-CoV-2 RNA was extracted using the RNA extraction kit (Viral RNA miniprep kit, Sigma). All the processes from collection to extraction of SARS-CoV-2 RNA were conducted by experts in biosafety laboratory-2 (BSL-2) in National Accreditation Board for Hospitals & Healthcare Providers (NABH) recognized molecular biology laboratory of Dr. D. Y. Patil Hospital, Kolhapur, India. These samples were verified for the presence of SARS-CoV-2 RNA using the qRT-PCR technique with Ct values (27.05, 30.27, and 33.42 for P1, P2, and P3 respectively).

  a) Ct value ≤ 25   :   high viral load.
  b) Ct value (26 to 36)   :   low viral load.
  c) Ct value (37 to 40)   :   not detected.

5.2.3 Synthesis of PLL-AuNPs and PLL-AuNPs-ASO conjugate:

The synthesis of PLL-AuNPs was achieved by one-step synthesis method where Poly-L-Lysine (PLL) itself acts as a reducing as well as stabilizing agent. The synthesis method for PLL-AuNPs is described in **chapter 3** of this thesis. In short, the synthesis was achieved by heating $HAuCl_4$ solution of 1 mM concentration on

magnetic stirrer at 80°C and rapid addition of 0.01% Poly-L-Lysine solution. The stirring was continued to obtain color change from pale yellow to wine-red which indicated formation of gold nanoparticles. Further, this mixture was cooled down at room temperature and prepared nanoparticles were washed thrice with distilled water by centrifugation at 13000 rpm for 15 min at room temperature. The obtained nanoparticles were suspended in distilled water and stored at 4°C for further use.

The PLL-AuNPs-ASO conjugate was prepared by incubating the synthesized PLL-AuNPs with antisense oligonucleotides (ASO). To achieve successful synthesis of PLL-AuNPs-ASO conjugate for detection of SARS-CoV-2 RNA, different reaction parameters were studied such as various concentrations of ASO (0.5-2 µM), reaction time (0-25 min), and temperature (28, 37 to 65ºC). The prepared conjugate (PLL-AuNPs-ASO) was then centrifuged at 10000 rpm at room temperature for 10 min. The pellet of PLL-AuNPs-ASO conjugate was then resuspended in equal volume of distilled water and stored at 4°C for further use.

5.2.4   Characterization of PLL-AuNPs and PLL-AuNPs-ASO Conjugate:

The change in color of gold precursor solution from pale yellow to wine-red during synthesis step indicates successful formation of PLL-AuNPs. The color of solution changed from wine-red to violet after addition of ASO. This formation of PLL-AuNPs and PLL-AuNPs-ASO conjugate was further confirmed by UV-Vis spectroscopy. The Surface Plasmon Resonance (SPR) of nanoparticles and their conjugates were analyzed in the UV-Vis range of 300-800 nm to study the change in absorption due to change in size and particle distribution. The PLL-AuNPs and PLL-AuNPs-ASO conjugate were then characterized with different characterization techniques such as, zeta (ζ) potential, dynamic light scattering (DLS), and transmission electron microscopy (TEM). The change in ζ potential and hydrodynamic diameters of the PLL-AuNPs, the PLL-AuNPs-ASO conjugate were analyzed by using BM10, Litesizer 500 with dynamic light scattering (DLS) analysis. The morphological shape and size of synthesized nanoparticles and their ASO conjugate were studied by transmission electron microscope (TEM) performed on

JEM-2100F, JEOL, Japan. For this analysis, a 10 µL PLL-AuNPs-ASO conjugate sample was air dried on copper grid for TEM analysis.

5.2.5 Optical biosensing experiment:

For the optical biosensing of SARS-CoV 2, the synthesized bioconjugate was incubated with SARS-CoV-2 RNA sequence that complementary to ASO sequence. The 100 µL conjugate solution was incubated with 1 ng/µL RNA sample at 28°C for 5 min. In above mixture, 40 µL of 1M NaCl solution was added. The range of detection was studied by taking different concentrations of SARS-CoV-2 RNA (0.1-3 ng/µL) incubated with PLL-AuNPs-ASO conjugate. Concentration of ASO was kept constant at 1 µM for formation of PLL-AuNPs-ASO conjugate. The detection was analyzed by observing change in UV-Vis spectrum and UV-Vis absorbance at 660 nm. The sensitivity of the conjugate was assessed by measuring the UV-Vis absorbance at 660 nm at various time intervals (0-60 min), using a standard 1 ng/µL concentration of target SARS-CoV-2 RNA. This was done in reference to a previous publication involving the AuNPs-ASO conjugate [24]. The selectivity of the conjugate was evaluated by using non-target RNA such as, Influenza A RNA. The UV-Vis spectrum and absorbance at 660 nm was then compared with the readings of target RNA.

5.2.6 Detection of SARS-CoV-2 RNA by PLL-AuNPs-ASO conjugate from clinical samples:

SARS-CoV 2 RNA was isolated from the nasopharyngeal swab taken from the COVID-19 positive individual. The three RNA samples named as, P1, P2 and P3 were obtained from the Dr. D. Y. Patil Hospital, Kolhapur, India. Isolation process was carried out in biosafety laboratory-2 (BSL-2) in National Accreditation Board for Hospitals & Healthcare Providers (NABH) recognized molecular biology laboratory of Dr. D. Y. Patil Hospital, Kolhapur, India. The total concentration of RNA was determined by Nanodrop (MultiSky Scan). These positive control samples were used for detection of SARS-CoV-2 RNA using prepared PLL-AuNPs-ASO conjugate. In detail, positive control RNA was incubated with PLL-AuNPs-ASO conjugate for 5 min at 28°C and the aggregation was observed in presence of 1M NaCl solution. The

results were compared with qRT-PCR analysis used for detection of SARS-CoV-2 RNA.

5.2.7 UV-Visible absorption spectra:

Nanodrop (Multisky Scan) was used for UV-Vis absorption spectrum analysis of PLL-AuNPs and their ASO conjugates in absence and presence of SARS-CoV-2 RNA. The Surface Plasmon Resonance (SPR) of nanoparticles and their conjugates were analyzed in the UV-Vis range of 300-800 nm to study the change in absorption due to change in size and particle distribution.

5.2.8 Hydrodynamic diameter analysis:

The change in ζ potential and hydrodynamic diameters of the PLL-AuNPs and PLL-AuNPs-ASO conjugate were analyzed by using BM10, Litesizer 500. The hydrodynamic diameter of the conjugate in the presence of a SARS-CoV-2 RNA sample at a 1 ng/μL concentration was also measured using the same method. For this analysis, the prepared nanoparticle and conjugate samples were diluted in distilled water, and the diluted samples were then injected into the machine to determine the hydrodynamic size.

5.2.9 Transmission electron microscopy (TEM):

The morphological shape and size of synthesized nanoparticles and their ASO conjugate in absence and presence of SARS-CoV-2 RNA sample were studied by transmission electron microscope (TEM) performed on JEM-2100F, JEOL, Japan. A 10 μL sample was air dried on copper grid for TEM analysis.

5.3 Results and discussion:

5.3.1 Optimization of PLL-AuNPs-ASO conjugates for SARS-CoV-2 detection:

Gold nanoparticles synthesized through citrate reduction method possesses negative charge on its surface that have interacted with -SH group of modified oligonucleotides with covalent interactions [25]. In this study, the modification of oligonucleotide was avoided by using positively charged PLL-AuNPs. Here, the

preparation of conjugate was based on electrostatic interactions between PLL-AuNPs and ASO. The reaction was occurred in single tube and did not require any complex reaction.

PLL functionalization provides surface positive charge on gold nanoparticles as it is a cationic biopolymer. These positively charged PLL-AuNPs were combined with negatively charged ASO by electrostatic attraction force. The reduction of the gold salt could be caused by the presence of an amine ($-NH_2$) group in the PLL structure [26]. The PLL-AuNPs-ASO conjugates were prepared by incubating the 1 µM concentration of ASO with PLL-AuNPs at 28°C for 15 min. The formation of conjugate was first visibly confirmed by observing color change from wine-red to violet indicating the conjugation of PLL-AuNPs and ASO due to electrostatic interactions. This conjugate formation was further confirmed by observing the change in UV-Vis absorption Spectrum. The optimization of reaction parameters was required to observe the effect on detection of SARS-CoV-2 RNA. Thus, different reaction parameters such as, reaction time, ASO concentration, and temperature were studied for synthesis of PLL-AuNPs-ASO conjugate.

- **Effect of reaction time on synthesis of PLL-AuNPs-ASO conjugate:**

To study the effect of reaction time for synthesis of PLL-AuNPs-ASO conjugate, three different concentrations of ASO (0.5, 1, and 2 µM) were incubated with PLL-AuNPs for different time period (0-25 min) at room temperature (28ºC). The use of 28ºC temperature is due to several reasons as, first it is a biologically relevant temperature as the interactions between DNA and AuNPs was studied at this temperature. It will reduce unnecessary thermal stress to the DNA molecule and gold nanoparticles. The room temperature (28ºC) is easy and convenient to maintain in laboratory conditions. The binding of DNA probe to PLL-AuNPs is due to positive surface charge of PLL-AuNPs and the efficiency of the interactions is optimal at 28ºC. The room temperature around 28ºC provides practical stability to DNA and gold nanoparticles. Thus, 28ºC temperature is used for experiment to synthesize DNA probe (ASO) conjugated PLL-AuNPs. The absorbance at 660 nm increases with increase in time from 0-15 min for all concentrations whereas, the absorbance

decreases after 15 min of reaction time. The maximum absorbance is observed when PLL-AuNPs were incubated with ASO of 1 µM concentration for 15 min of time period as shown in **figure 5.2(a)**. This suggests that 15 min of reaction time is optimum for synthesis of PLL-AuNPs-ASO concentration.
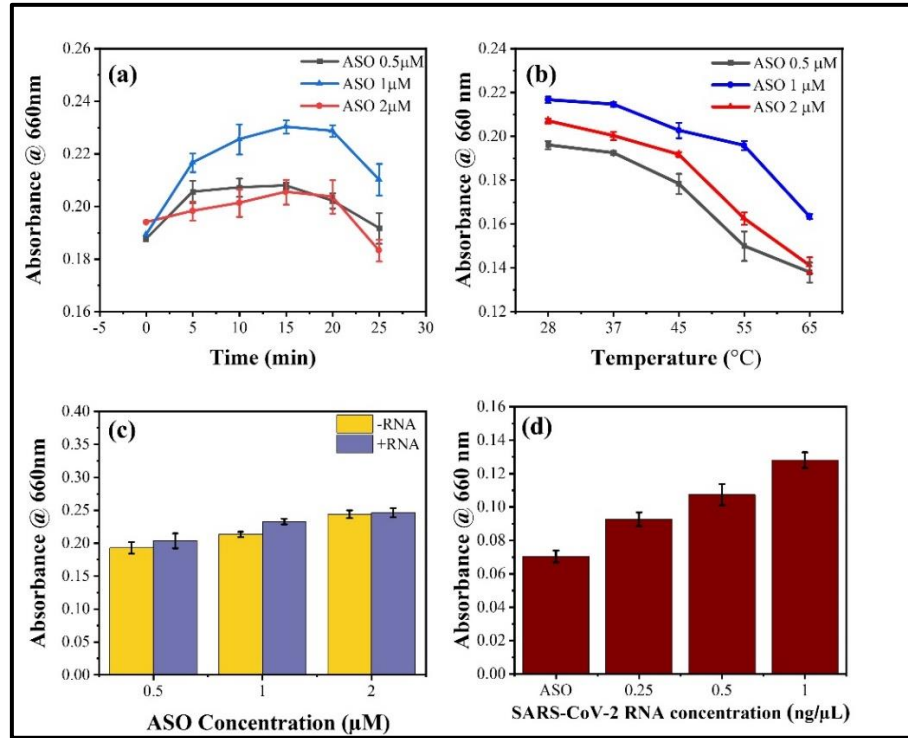
Figure 5.2: Optimization of (a) reaction time and (b) temperature for formation of PLL-AuNPs-ASO conjugate using different concentrations of ASO such as, 0.5, 1 and 2 µM, (c) Optimization of ASO concentrations for sensitive detection SARS-CoV-2 RNA using 1 ng/µL concentration of SARS-CoV-2 RNA, and (d) optimization of SARS-CoV-2 RNA for analysis of developed biosensor. The error bars in the diagram display the standard deviation of the readings derived from the three measurements

- **Effect of temperature on synthesis of PLL-AuNPs-ASO conjugate:**

In addition to reaction time, reaction temperature has a significant impact on the rate of reaction as well as other features of nanoconjugates during the synthesis process. To study this, the reaction was carried out at different time intervals such as, 28, 37, 45, 55, and 65ºC. The maximum absorbance at 660 nm is observed when the reaction is carried out at 28°C whereas, the absorbance is decreased with increase in

temperature as shown in **figure 5.2(b)**. Here, 1 µM concentration of ASO shows maximum absorption at 28°C as compared to other ASO concentrations. This is observed due to sensitivity of oligonucleotides towards temperature increase. The nucleic acid undergoes denaturation with an increase in reaction temperature; therefore, the immobilization of oligonucleotides onto PLL-AuNPs was carried out at 28°C. Increased temperature leads to denaturation of ASO thus there is no immobilization of ASO on PLL-AuNPs. At temperature below 28°C the kinetic energy of molecule is reduced which is responsible to reduce interactions between DNA molecule and PLL-AuNPs. DNA probe may not conjugate with AuNPs at lower temperatures that potentially decreasing surface coverage of nanoparticles. At lower temperatures, the mobility of ions and molecules may decrease, potentially weakening the electrostatic interactions between DNA and the nanoparticles. Therefore, the absorbance intensity will decrease with decrease in temperature. Thus, throughout the study synthesis of PLL-AuNPs-ASO conjugate was carried out at 28°C.

- **Effect of ASO concentration on synthesis of PLL-AuNPs-ASO conjugate:**

The impact of varying ASO concentrations, ranging from 0.5 to 2 µM, on the production of the PLL-AuNPs-ASO conjugate was examined **(figure 5.2c)**. The PLL-AuNPs-ASO conjugate prepared by 1 µM ASO concentration shows maximum absorbance at 660 nm in presence of 1 ng/µL concentration of SARS-CoV-2 RNA as compared PLL-AuNPs-ASO conjugate prepared by 0.5 and 2 µM ASO concentration. The 1 ng/µL concentration of SARS-CoV-2 RNA is optimum for detection of SARS-CoV-2 RNA as it shows maximum absorption at 660 nm as compared to 0.25 and 0.5 ng/µL concentration **(figure 5.2d).** The 1 µM ASO concentration is shown to be the most sensitive for detecting SARS-CoV-2 RNA out of the three tested ASO concentrations. It is observed that the concentration of ASO used for conjugate preparation played important role in sensitive detection of SARS-CoV-2 RNA.

By observing the results from **figure 5.2(a-c)**, 1 µM ASO concentration is found to be optimum for preparation of PLL-AuNPs-ASO conjugates. Therefore, for further study PLL-AuNPs-ASO conjugates were prepared by incubating 1 µM ASO concentration with PLL-AuNPs.
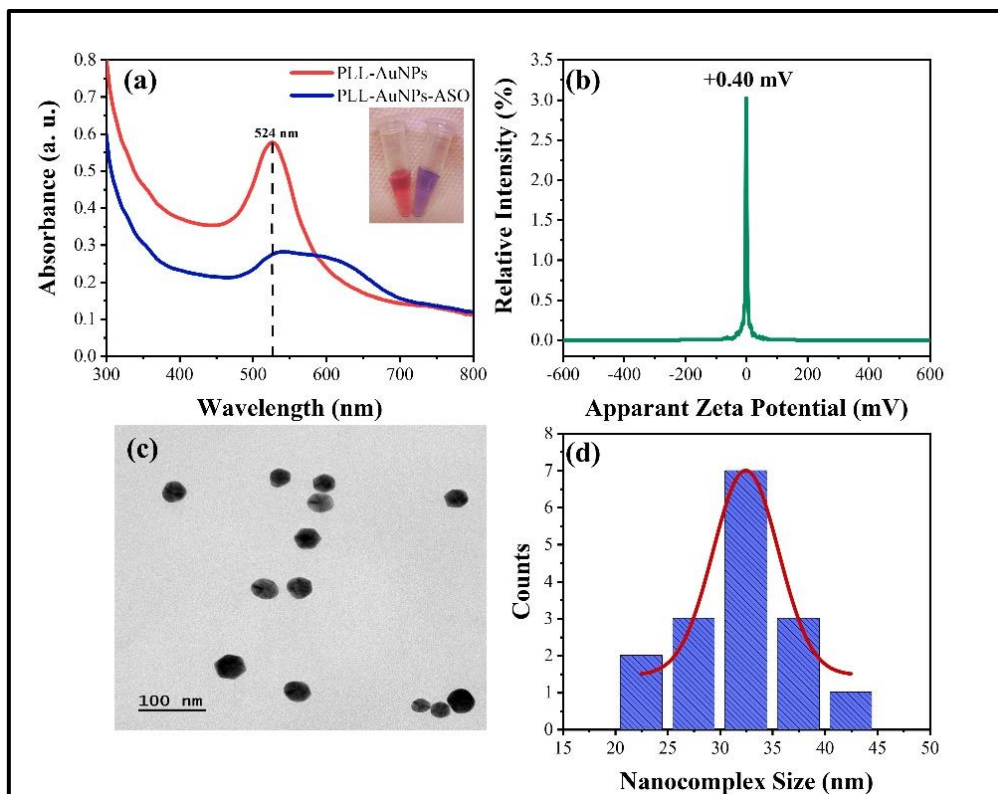
Figure 5.3: Characterization of PLL-AuNPs-ASO conjugate by (a) UV-Vis spectroscopy in comparison to PLL-AuNPs. Inset image shows color change of PLL-AuNPs (wine-red) after conjugation with ASO (violet). (b) ζ potential, (c) TEM image at 100 nm and at magnification of 50KX, and (d) size distribution histogram of PLL-AuNPs-ASO conjugate

5.3.2 Characterization of PLL-AuNPs-ASO conjugate:

The formation of PLL-AuNPs-ASO conjugate was first visibly confirmed by observing the color change from wine-red to violet. Upon conjugation, the sharp peak of PLL-AuNPs (524 nm) is replaced with broad absorption spectrum as shown in **figure 5.3(a).** The inset image of **figure 5.3(a)** shows color change where wine-red color of PLL-AuNPs changed to violet color after conjugation with ASO. Due to the interaction of cationic PLL-AuNPs and anionic ASO, the conjugate exhibited broad absorption spectrum. The formation of PLL-AuNPs-ASO conjugate is also confirmed by observing change in zeta potential. The positive surface charge of PLL-AuNPs ($+27.0\pm0.30$ mV) decreases to $+0.40\pm0.02$ mV after ASO conjugation with PLL-AuNPs as shown in **figure 5.3(b)**. This change in Zeta potential indicated the

electrostatic interactions between positively charged PLL-AuNPs and negatively charged ASO. Transmission electron microscopy (TEM) was used to examine the morphological properties of PLL-AuNPs, including their size, shape, and morphological aspects. **Figure 5.3(c)** shows TEM images of PLL-AuNPs-ASO conjugate, which demonstrate well-dispersed PLL-AuNPs-ASO conjugate without any aggregation. The TEM image represents spherical morphology for PLL-AuNPs-ASO conjugate as shown in **figure 5.3(c).** From the TEM micrograph PLL-AuNPs-ASO conjugate, the size distribution histogram is drawn with the help of ImageJ application **(figure 5.3d)**. The PLL-AuNPs-ASO conjugate display size between 20-45 nm whereas, the average size of PLL-AuNPs-ASO is 33.3 nm.

5.3.3   Principle of PLL-AuNPs based optical biosensing of SARS-CoV 2 RNA:

The synthesized PLL-AuNPs display a strong absorption peak at 524 nm, revealing small size gold nanoparticles. Due to the surface positive charge, two AuNPs are repelled from one another by electrostatic forces, resulting in a monodispersed solution of colloidal AuNPs. Due to the electrostatic interaction between the negatively charged ASO and the positively charged PLL-AuNPs, the initial wine-red PLL-AuNPs solution changes to violet when conjugated with the unmodified ASO solution. This conjugation approach was achieved without the need for salt ageing, which is often necessary for citrate stabilized AuNPs since they have ionic susceptibility and produce unstable colloidal solutions [27]. The coupling of cationic PLL-AuNPs with anionic ASO resulted in a remarkable modification in UV-Vis absorption. It was found that the PLL-AuNPs-ASO conjugate was responsible, as it maintained its violet color, unlike the wine-red PLL-AuNPs, and caused a significant shift from a sharp absorption peak to a broad-spectrum absorption.

In presence of target (SARS-CoV-2) RNA, the DNA-RNA hybrid structure is formed between immobilized ASO and target RNA that cause PLL-AuNPs to segregate everywhere. Monodispersed nanoparticles again aggregate at higher salt concentration due to ionic interactions. The affinity of immobilized ASO towards its complementary target RNA is more as compare to the positively charged PLL-AuNPs [23]. The formation of hybrid structure of ASO (DNA) and target RNA results in

neutralizing the electrostatic interactions between negatively charged ASO and positively charged PLL-AuNPs that leads to free AuNPs and get aggregated in presence of salt which was observed by naked eyes. However, in case of detection, the enhancement of UV-Vis absorption at 660 nm was based on concentration of loading RNA. The slight increase in UV-Vis absorption, compared to ASO alone, was attributed to a small amount of anionic ASO being released from the conjugate to react with the target RNA, while the majority remained bound to the cationic PLL-AuNPs. Addition of high concentration of RNA to PLL-AuNPs-ASO conjugate solution shows maximum UV-Vis absorption at 660 nm and proper visible aggregation that indicated maximum detachment of ASO from PLL-AuNPs due to competitive binding of ASO between PLL-AuNPs and complementary target RNA. The specific complementary interactions of ASO and target RNA annulled the electrostatic interactions between anionic ASO and cationic PLL-AuNPs. The redispersed PLL-AuNPs are aggregated in presence of NaCl solution.

5.3.4   Detection of SARS-CoV-2 RNA:

The total duration of the analysis for SARS-CoV-2 RNA detection is determined by the sensitivity or response time of the assay. After ASO conjugation, the original wine-red color of PLL-AuNPs turned to violet due to electrostatic attraction-induced aggregation, which display a broad UV-Vis spectrum as shown in **figure 5.3(a)**. After introduction of target RNA, the gold nanoparticles get aggregated in presence of NaCl concentration due to formation of DNA-RNA hybrid which releases ASO from surface of PLL-AuNPs. The sensitivity of PLL-AuNPs-ASO conjugate towards target RNA was further validated by observing change in UV-Vis absorption spectrum within the range 300-800 nm and % change in absorbance at 660 nm. The significant change in absorption is observed in absence and presence of SARS-CoV-2 RNA. As presented in **figure 5.4(a)**, the PLL-AuNPs-ASO conjugate shows broad range spectrum with maximum absorbance at 660 nm in presence of target RNA and increased absorbance at 660 nm as compared to only PLL-AuNPs-ASO conjugate and PLL-AuNPs **(figure 5.4b)**.
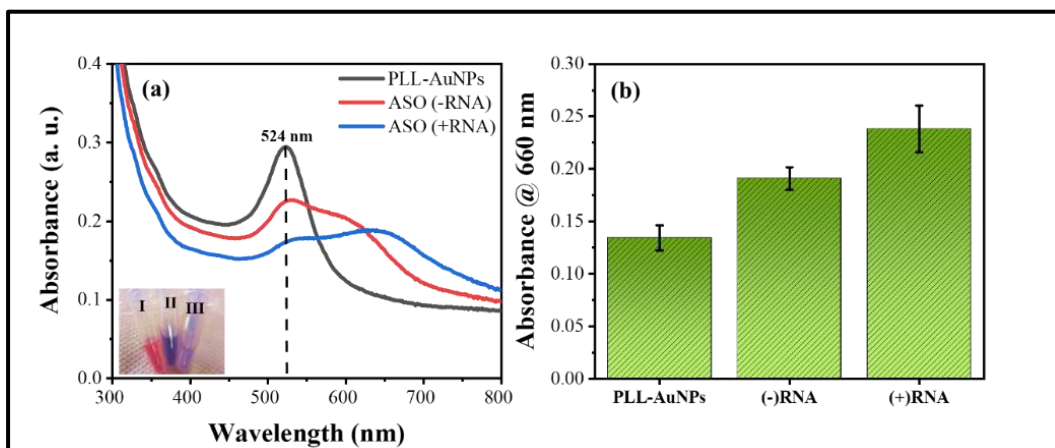
Figure 5.4: Change in (a) UV-Vis absorption spectra (300-800 nm) and (b) absorbance at 660 nm of PLL-AuNPs and PLL-AuNPs-ASO in absence (-RNA) and presence (+RNA) of viral SARS-CoV-2 RNA. Inset image shows color difference between PLL-AuNPs (I), PLL-AuNPs-ASO in absence (II) and in presence (III) of SARS-CoV-2 RNA. The error bars in the diagram display the standard deviation of the readings derived from the three measurements

The sensitivity of the assay with respect to response time was further validated by calculating % change in UV-Vis absorption at 660 nm. For this, the % change in absorbance for PLL-AuNPs-ASO conjugate in absence and presence of target RNA was calculated by taking absorbance at 660 nm for different time points from 0 to 60 min. The sensitivity of PLL-AuNPs-ASO conjugate is found within 5 min of incubation at 28°C in presence of definite concentration of SARS-CoV-2 RNA (1 ng/μL) as shown in **figure 5.5(a)**. The absorbance decreases due to formation of stable DNA-RNA hybrid and aggregation of gold nanoparticles. The hydrodynamic size of the conjugate increases in presence of SARS-CoV-2 RNA showing 586 nm with comparison to PLL-AuNPs-ASO conjugate that is 487 nm **(figure 5.5b)**. This indicates the formation of DNA-RNA hybrid that increases the hydrodynamic size of conjugate.

This sensitivity response of PLL-AuNPs-ASO conjugate for SARS-CoV-2 detection was further confirmed by TEM analysis. The TEM images represent aggregated gold nanoparticles in presence of target RNA and NaCl as shown in **figure 5.5(c-e)**. Single stranded RNA structure is unstable at 28°C and highly sensitive to

RNase. Though, the RNA was when bounds to conjugated oligonucleotides, it forms a stable DNA-RNA hybrid structure within 5 min of incubation time. The ASO has high affinity towards complementary RNA as compare to cationic PLL-AuNPs and the nanoparticles gets aggregated in presence of NaCl concentration. Since, in absence of target RNA, the conjugated ASO protects the gold nanoparticles from aggregation by shielding the surface of gold nanoparticles by electrostatic interactions. This proposed optical biosensing system exhibited diagnostic potential for detection of pathogenic nucleic acid.
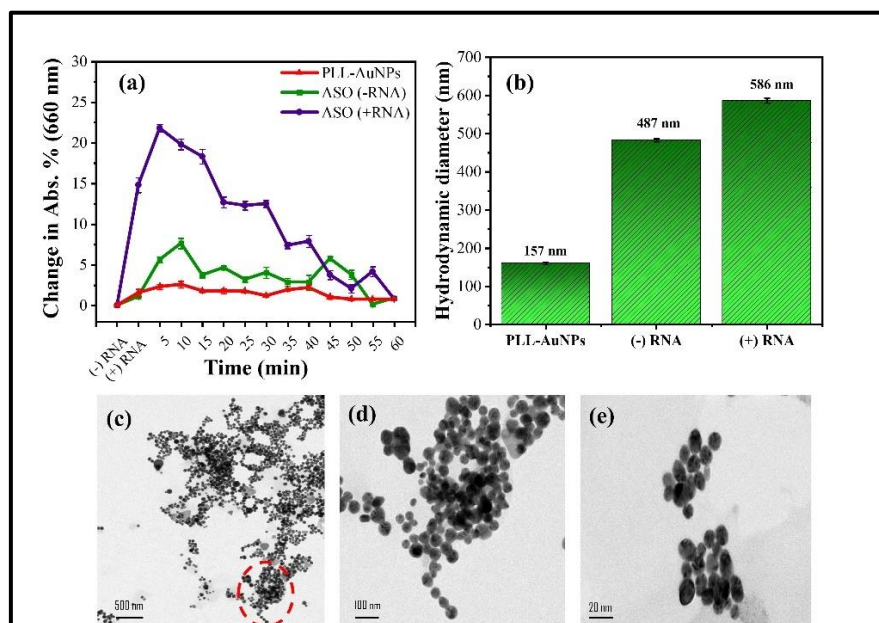
Figure 5.5: (a) The % change in UV-Vis absorption at 660 nm of PLL-AuNPs-ASO conjugate and (b) the change in hydrodynamic diameter of PLL-AuNPs-ASO conjugate in absence and presence of 1 ng/µL concentration of SARS-CoV-2 RNA, and (c-e) TEM images showing aggregation of PLL-AuNPs after addition of target SARS-CoV-2 RNA. The error bars in the diagram display the standard deviation of the readings derived from the three measurements

Interestingly, as per the hypothesis, the PLL-AuNPs-ASO conjugates were formed due to electrostatic interactions and primarily dispersed in solution in absence of SARS-CoV-2 RNA whereas, in presence of target viral RNA the DNA-RNA hybrid was formed and the PLL-AuNPs get aggregated forming clusters. A significant red shift is observed when PLL-AuNPs-ASO conjugates were treated with SARS-

CoV-2 RNA as shown in **figure 5.4(a)**. The **table 5.2** shows the change in ζ potential of PLL-AuNPs and PLL-AuNPs-ASO conjugate that represents the decrease in surface positive charge of PLL-AuNPs upon conjugation with ASO.

Table 5.2: Change in Zeta (ζ) potential of PLL-AuNPs before and after ASO conjugation

Sr. No.	Material	Zeta (ζ) potential
1.	PLL-AuNPs	$+27\pm0.30$ mV
2.	PLL-AuNPs-ASO	$+0.4\pm0.02$ mV

The analytical performance of developed biosensing method was analyzed at optimized conditions. The performance was validated by observing the change in absorbance at 660 nm for different concentrations of SARS-CoV-2 RNA. The linear increase in absorbance is observed with increasing concentration of SARS-CoV-2 RNA (0.1-3 ng/µL) as shown in **figure 5.6.** The presented result shows linear relationship between the absorbance at 660 nm with concentration of target RNA where, the linear relationship ($R^2 = 0.97773$) means the sensitivity of technique. The limit of detection was found to be 0.52 ng/µL with respect to the tested RNA range 0.1-3 ng/µL.
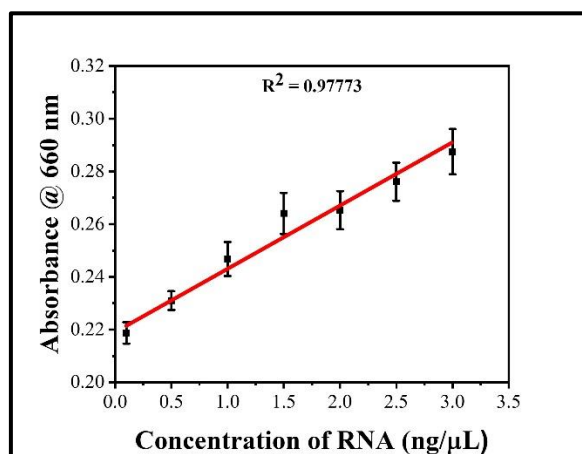
Figure 5.6: Linear regression of corresponding absorbance at 660 nm of PLL-AuNPs-ASO conjugate in presence of different concentrations of target SARS-CoV-2 RNA. The error bars in the diagram display the standard deviation of the readings derived from the three measurements

5.3.5 Selectivity of PLL-AuNPs-ASO conjugate for SARS-CoV-2 RNA detection:

Another important parameter for any biosensor is the selectivity of the biosensor toward its target. The selectivity of presented optical biosensing assay was examined by using different RNA sequences including the perfectly complementary positive control (SARS-CoV-2 RNA) and non-complementary negative control (Influenza A RNA). The response of PLL-AuNPs-ASO conjugate in presence of positive and negative control was recorded in terms of change in UV-Vis absorbance spectrum in the range of 300-800 nm and absorbance at 660 nm as presented in **figure 5.7(a)**. The PLL-AuNPs-ASO conjugate in presence of positive control shows the red shift broad spectrum absorbance with two peaks showing high peak at 660 nm (**figure 5.7a**). Also, the conjugate in presence of positive control shows maximum absorbance at 660 nm in comparison to negative control as shown in **figure 5.7(b)**. In presence of positive control SARS-CoV-2 RNA, the naked eye aggregation is observed whereas, no visible aggregation is observed in negative control tube as presented in **figure 5.7(a) (inset image)**. This affirms that redispersion of PLL-AuNPs and its aggregation in presence of NaCl is only occurred in presence of complementary SARS-CoV-2 RNA containing viral N gene. Whereas, in presence of non-complementary RNA (Influenza A RNA) no visible aggregation is seen because, ASO protects the PLL-AuNPs from aggregation. Thus, the developed optical biosensing system using PLL-AuNPs-ASO conjugate shows excellent selectivity towards SARS-CoV-2 RNA detection.

The molecular detection analysis for SARS-CoV-2 mainly depends on the highly conserved sequences such as, RNA-dependent RNA polymerase gene (RdRP gene), nucleocapsid protein gene (N gene) and envelope protein gene (E gene) [5, 28]. Among these genes, as per the reports, the N gene, which produces the N protein, is the most sensitive target for detecting SARS-CoV-2 [29]. In comparison to other structural proteins such as, spike (S), envelope (E) and membrane (M) the N gene contains large amount viral RNA genome [23, 30]. Recent data using nanopore-based transcriptome analysis showed that, the N gene RNA is the most frequently expressed transcript in SARS-CoV-2 infected cells [31].
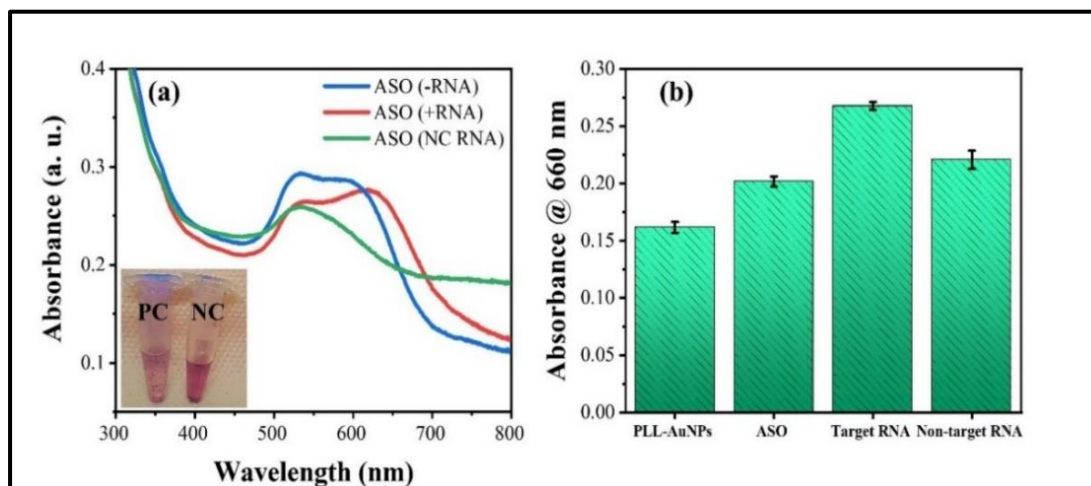
Figure 5.7: Change in (a) UV-Vis absorption spectra and (b) absorbance at 660 nm of the PLL-AuNPs-ASO conjugate in presence of positive control/target RNA (SARS-CoV-2 RNA) and negative control/Non-target RNA (Influenza A RNA). The inset image shows visual naked-eye detection of SARS-CoV-2 after addition of SARS-CoV-2 RNA (PC) into PLL-AuNPs-ASO conjugate solution in presence of 1-2 M NaCl solution in comparison to Influenza A RNA (NC). The error bars in the diagram display the standard deviation of the readings derived from the three measurements

5.3.6 Detection of SARS-CoV-2 RNA by PLL-AuNPs-ASO conjugate from clinical sample:

The practical application of PLL-AuNPs-ASO conjugate was investigated for nucleic acid detection from nasopharyngeal swab taken from COVID-19 positive individuals. The RNA was isolated from these samples using RNA extraction kit and quantify by Nanodrop (Multisky Scan). The RNA quantification of these three samples is presented in **table 5.3** with their purity ratio (A_{260}/A_{280}). Purity ratio for pure RNA is ~2.0 that usually used to asses any protein contamination presents in RNA solution. The three RNA samples are labelled as P1, P2 and P3. For direct comparison between optical biosensing assay and RT-PCR, the UV-Vis absorbance at 660 nm was taken in presence of SARS-CoV-2 RNA in target sample and non-target sample. Also, the visible aggregation in presence of target RNA from positive samples is observed.

Table 5.3: RNA quantification and purity ratio of RNA samples collected from COVID-19 individuals and healthy individual

Sr. No.	RNA Samples	Concentration (µg/mL)	Purity Ratio (260/280)
1.	P1	28.52	1.91
2.	P2	21.37	1.97
3.	P3	15.53	2.05
4.	Control	25.39	2.01

According to the results presented in **table 5.4**, the positive samples (P1, P2, and P3) exhibit visible aggregation, whereas the non-target RNA shows no visible aggregation. The observation and status obtained with RNA biosensor based on PLL-AuNPs-ASO conjugate are reliable with the results produced by RT-PCR analysis of the COVID-19 target samples and non-target sample.

Table 5.4: Comparison between the detection results of PLL-AuNPs-ASO conjugate with qRT-PCR for SARS-CoV-2 RNA detection isolated from oropharyngeal sample taken from three COVID-19 positive individuals (P1, P2, P3) and control RNA taken from healthy individual

Sr. No.	RNA Samples	qRT-PCR detection	Detection by PLL-AuNPs-ASO conjugate
1.	P1	Detected (27.05[b])	Detected
2.	P2	Detected (30.27[b])	Detected
3.	P3	Detected (33.42[b])	Detected
4.	Control	Not Detected (38.36[c])	Not Detected

a) Ct value ≤ 25   : high viral load.
b) Ct value (26 to 36) : low viral load.
c) Ct value (37 to 40) : not detected.

This suggests that the results obtained from PLL-AuNPs-ASO conjugate are agreeable to RT-PCR method for SARS-CoV-2 RNA detection. The commercial RT-PCR method provides specificity and sensitivity for detection of SARS-CoV-2 RNA but, requires specific instrumentation and sophisticated laboratory. Nanoparticles based biosensing approach like, AuNPs-nucleic acid conjugate would be useful for applications in point of care device for diagnosis of pathogenic nucleic acid that permits convenient acquisition of information about viral presence in less time and without use of any sophisticated instrument facility [32].

5.4   Conclusions:

This study presents the use of cationic Poly-L-Lysine conjugated with antisense oligonucleotides (ASO) for SARS-CoV-2 RNA detection. The conjugates were prepared using 1 µM concentration of ASO with 15 min incubation time at 28°C. The optical biosensing of pathogenic nucleic acid based on cationic PLL-AuNPs with antisense oligonucleotide conjugation demonstrated good potential as biosensor with high sensitivity and specificity as well as rapid detection within 5 min at the level of 0.52 ng/µL concentration. The formation of PLL-AuNPs-ASO conjugate was based on electrostatic interactions between cationic PLL-AuNPs and anionic nucleic acid (ASO) which, act as favorable sensor for detection of pathogenic nucleic acid without any need of sophisticated instrumentation. The PLL-AuNPs-ASO based detection assay shows visible aggregation in presence of complementary target RNA and NaCl which can be visualized by naked eyes, and UV absorbance at 660 nm was taken for the interpretation of results. The developed method was utilized successfully to detect SARS-CoV-2 RNA from clinical samples as well. The detection method is carried out in single tube with minimum steps and the synthesis of nanoparticles is also based on one pot synthesis method; therefore, offers simplicity. The method also offers rapidity and specificity as the detection occurred within 5 min and specifically detect SARS-CoV-2 over other RNA viruses (Influenza A RNA). Therefore, the proposed PLL-AuNPs-ASO conjugate based biosensing would serve as a promising platform in future for rapid and easy diagnosis of viral infections.

5.5   References:

[1]   Ciotti M, Ciccozzi M, Terrinoni A, Jiang WC, Wang CB, Bernardini S. The COVID-19 pandemic. Critical reviews in clinical laboratory sciences. 2020;57(6):365-88.

[2]   Han D, Li R, Han Y, Zhang R, Li J. COVID-19: Insight into the asymptomatic SARS-COV-2 infection and transmission. International Journal of Biological Sciences. 2020;16(15):2803-11.

[3]   Malik YA. Properties of coronavirus and SARS-CoV-2. The Malaysian journal of pathology. 2020;42(1):3-11.

[4]   Daniel SK, Pai PS, Sabbella HR, Singh K, Rangaiah A, Basawarajappa SG, Thakur CS. Handheld, low-cost, aptamer-based sensing device for rapid SARS-CoV-2 RNA detection using novelly synthesized gold nanoparticles. IEEE Sensors Journal. 2022;22(19):18437-45.

[5]   Eftekhari A, Alipour M, Chodari L, Maleki Dizaj S, Ardalan M, Samiei M, Sharifi S, Zununi Vahed S, Huseynova I, Khalilov R, Ahmadian E. A comprehensive review of detection methods for SARS-CoV-2. Microorganisms. 2021;9(2):232-51.

[6]   Udugama B, Kadhiresan P, Kozlowski HN, Malekjahani A, Osborne M, Li VY, Chen H, Mubareka S, Gubbay JB, Chan WC. Diagnosing COVID-19: the disease and tools for detection. ACS nano. 2020;14(4):3822-35.

[7]   Guo L, Ren L, Yang S, Xiao M, Chang D, Yang F, Dela Cruz CS, Wang Y, Wu C, Xiao Y, Zhang L. Profiling early humoral response to diagnose novel coronavirus disease (COVID-19). Clinical infectious diseases. 2020;71(15):778-85.

[8]   Strömer A, Rose R, Schäfer M, Schön F, Vollersen A, Lorentz T, Fickenscher H, Krumbholz A. Performance of a point-of-care test for the rapid detection of SARS-CoV-2 antigen. Microorganisms. 2020;9(1): 58-69.

[9]   Filik H, Avan AA. Nanotechnology-based colorimetric approaches for pathogenic virus sensing: A review. Current Medicinal Chemistry. 2022;29(15):2691-718.

[10]   Younes N, Al-Sadeq DW, Al-Jighefee H, Younes S, Al-Jamal O, Daas HI, Yassine HM, Nasrallah GK. Challenges in laboratory diagnosis of the novel coronavirus SARS-CoV-2. Viruses. 2020;12(6):582-609.

[11]   Eshghifar N, Busheri A, Shrestha R, Beqaj S. Evaluation of analytical performance of seven rapid antigen detection kits for detection of SARS-CoV-2 virus. International journal of general medicine. 2021;14(1):435-40.

[12]   Pinsky BA, Hayden RT. Cost-effective respiratory virus testing. Journal of Clinical Microbiology. 2019;57(9):10-128.

[13]   Patil T, Gambhir R, Vibhute A, Tiwari AP. Gold nanoparticles: Synthesis methods,

functionalization and biological applications. Journal of Cluster Science. 2023;34(2):705-25.

[14] Cui M, Liu Z, Tang Y. Application of visual biosensors based on gold nanoparticles for detection of target molecules. InInternational Conference on Optoelectronic Materials and Devices (ICOMD 2021) 2022;12164(1):136-42.

[15] Zheng L, Cai G, Wang S, Liao M, Li Y, Lin J. A microfluidic colorimetric biosensor for rapid detection of Escherichia coli O157: H7 using gold nanoparticle aggregation and smart phone imaging. Biosensors and Bioelectronics. 2019;124(1):143-49.

[16] Marin M, Nikolic MV, Vidic J. Rapid point-of-need detection of bacteria and their toxins in food using gold nanoparticles. Comprehensive Reviews in Food Science and Food Safety. 2021;20(6):5880-900.

[17] Du Y, Dong S. Nucleic acid biosensors: recent advances and perspectives. Analytical chemistry. 2017;89(1):189-215.

[18] Nooranian S, Mohammadinejad A, Mohajeri T, Aleyaghoob G, Kazemi Oskuee R. Biosensors based on aptamer-conjugated gold nanoparticles: a review. Biotechnology and Applied Biochemistry. 2022;69(4):1517-34.

[19] Mirkin CA, Letsinger RL, Mucic RC, Storhoff JJ. A DNA-based method for rationally assembling nanoparticles into macroscopic materials. InSpherical Nucleic Acids. 1st edition, Jenny Stanford publishing, 2020;3-11.

[20] Ahmadi S, Kamaladini H, Haddadi F, Sharifmoghadam MR. Thiol-capped gold nanoparticle biosensors for rapid and sensitive visual colorimetric detection of Klebsiella pneumoniae. Journal of Fluorescence. 2018;28(1):987-98.

[21] Daniel SK, Pai PS, Sabbella HR, Singh K, Rangaiah A, Basawarajappa SG, Thakur CS. Handheld, low-cost, aptamer-based sensing device for rapid SARS-CoV-2 RNA detection using novelly synthesized gold nanoparticles. IEEE Sensors Journal. 2022;22(19):18437-45.

[22] Ganareal TA, Balbin MM, Monserate JJ, Salazar JR, Mingala CN. Gold nanoparticle-based probes for the colorimetric detection of Mycobacterium avium subspecies paratuberculosis DNA. Biochemical and Biophysical Research Communications. 2018;496(3):988-97.

[23] Jamaluddin ND, Ibrahim N, Yusof NY, Goh CT, Tan LL. Optical reflectometric measurement of SARS-CoV-2 (COVID-19) RNA based on cationic cysteamine-capped gold nanoparticles. Optics & Laser Technology. 2023;157(1):8763-72.

[24] Moitra P, Alafeef M, Dighe K, Frieman MB, Pan D. Selective naked-eye detection of SARS-CoV-2 mediated by N gene targeted antisense oligonucleotide capped plasmonic nanoparticles. ACS nano. 2020;14(6):7617-27.

[25] Carnerero JM, Jimenez-Ruiz A, Castillo PM, Prado-Gotor R. Covalent and Non-Covalent DNA–Gold-Nanoparticle Interactions: New Avenues of Research. ChemPhysChem. 2017;18(1):17-33.

[26] Han G, Wu S, Wang J, Geng X, Liu G. Poly-L-lysine mediated synthesis of gold nanoparticles and biological effects. Journal of Nanoscience and Nanotechnology. 2015;15(9):6503-8.

[27] Wai JL, New SY. Cysteamine-coated gold nanoparticles for bimodal colorimetric detection with inverse sensitivity: a proof-of-concept with lysozyme. RSC advances. 2020;10(2):1088-94.

[28] Wu A, Peng Y, Huang B, Ding X, Wang X, Niu P, Meng J, Zhu Z, Zhang Z, Wang J, Sheng J. Genome composition and divergence of the novel coronavirus (2019-nCoV) originating in China. Cell host & microbe. 2020;27(3):325-38.

[29] Zhang X, Li M, Zhang B, Chen T, Lv D, Xia P, Sun Z, Shentu X, Chen H, Li L, Qian W. The N gene of SARS-CoV-2 was the main positive component in repositive samples from a cohort of COVID-19 patients in Wuhan, China. Clinica chimica acta. 2020;511(1):291-97.

[30] Wu F, Zhao S, Yu B, Chen YM, Wang W, Song ZG, Hu Y, Tao ZW, Tian JH, Pei YY, Yuan ML. A new coronavirus associated with human respiratory disease in China. Nature. 2020;579(7798):265-69.

[31] Kim D, Lee JY, Yang JS, Kim JW, Kim VN, Chang H. The architecture of SARS-CoV-2 transcriptome. Cell. 2020;181(4):914-21.

[32] Wang J, Drelich AJ, Hopkins CM, Mecozzi S, Li L, Kwon G, Hong S. Gold nanoparticles in virus detection: Recent advances and potential considerations for SARS-CoV-2 testing development. Wiley Interdisciplinary Reviews: Nanomedicine and Nanobiotechnology. 2022;14(1):e1754-84.

Chapter VI

Poly-L-Lysine functionalized gold nanoparticle–nucleic acid conjugate for electrochemical biosensing of viral RNA (SARS-CoV-2 RNA)

6.1   Introduction:

The outbreak of corona virus disease 2019 (COVID-19) was caused by severe acute respiratory syndrome corona virus 2 (SARS-CoV-2) which has collapsed the economy as well as global health [1]. The critical point in control of COVID-19 spread is the rapid and sensitive detection of SARS-CoV-2 infection. Primarily, quantitative Reverse Transcription Polymerase Chain Reaction (qRT-PCR) or immunogen assays are used as conventional methods for the detection of SARS-CoV-2 RNA or protein from clinical samples [2]. The gold standard diagnostic technique for identification of SARS-CoV-2 is qRT-PCR. But this tool requires sophisticated instrumentation, skilled technicians and is time consuming [3]. Point-of-care testing also has limited efficacy when the viral load is low, despite being quick, easy to operate, and under low equipped settings. To overcome these issues, varieties of virus detection methods are being developed. Specific biosensor systems for the detection of virus that may be an intriguing alternative in this regard as, they offer easy handling, cost-effective, highly sensitive way of detection.

Sequence specific nucleic acid detection is gaining attention of researchers due to their wide range of applications in detection of genetic disorders, viruses, bacteria, food borne pathogens as well as, drug screening and environmental monitoring [4]. These nucleic acid biosensors are emerging as an alternative strategy for the sensitive detection of the pathogen as it is equally sensitive to qRT-PCR and equally rapid as antigen point of care tests. These nucleic acid biosensors are based on the hybridization of complementary DNA to RNA sequences [5]. Another important aspect of these biosensors is transduction techniques and signal amplification such as, optical (fluorescence, colorimetric) and electrochemical (amperometric or potentiometric) detection [6]. Among these, electrochemical detection is reported for the diagnosis of SARS-CoV-2 RNA due to their rapid, sensitive, and easy to handle aspect in point of care devices [7]. These biosensors have analytical characteristics such as, duration of response ranges from 3 to 1 h and detection ranges from 10 nM to 3 aM [8-10]. Electrochemical detection of nucleic acid provides high specificity and sensitivity for rapid detection of nucleic acid. In recent years, nanomaterials with distinctive

electrocatalytic capabilities, great adsorption capacities, smallest sizes, large surface to volume ratio, and easy surface modification have proven to be suitable for biosensing applications [11]. Biosensors are analytical tools that translate biological data into a measurably strong signal. Electrochemical biosensors are the type of biosensors utilized to detect biological entity such as, enzymes, ligands, nucleic acids and pathogens. These are made up of five main components such as, a bioreceptor, an interface, a transducer element, computer software, and a user interface. The bioreceptor selectively binds to desirable analyte causing biochemical reaction to occur at an interface, electrochemical transducer for conversion of transducing signal into electronic signal that gets converted into meaningful interpretation by computer software. This interpretation then presented to operator through user interface [12]. The three-electrode system is used for electrochemical biosensing that contain, i) working, ii) counter and iii) reference electrode. These three electrodes are connected to potentiostat to record the signal.

Nanobiosensors are biosensors that make use of nanostructures and have great efficiency and sensitivity due to their extensive level of sample stabilization. Nanostructures are responsible for enhancement of the effectiveness, sensitivity, and reaction times of the sensors. Electrochemical techniques are based on electron transfer mechanism. Use of metal nanoparticles enhances electron transfer due to their electro catalytic effect. This enhancement results in reduction of response time, thus increases efficiency of biosensor. Also, metal nanostructures increase the sensitivity of the sensor by increasing the surface area of receptor. Therefore, use of nanostructure in electrochemical biosensor can detect smallest concentration of about femtomolar and also detect single molecule of analyte [13].

Among different nanostructures, gold nanoparticles have more attention due to their unique characteristics such as, large surface area, excellent biocompatibility, high electrical conductivity, and easy preparation methods [14]. The use of AuNPs in biosensor development was previously reported by many researchers for the detection of various pathogens. For example, Pan *et. al.* [15] reported the electrochemical detection of *Klebsiella pneumoniae* carbapenemase, Hajihosseini *et. al.* [16] reported the determination of *Helicobacter pylori* by AuNPs and graphene oxide whereas, Cano *et. al.* [17] reported gold nanotriangles for successful detection of SARS-CoV-2 RNA

from a clinical sample. In particular, these AuNPs required modified oligonucleotide for immobilization purposes either thiol or dithiol modification. The use of cationic AuNPs minimizes the need for thiol modification as it is conjugated with oligonucleotide by electrostatic interactions; where positively charged AuNPs interact with negatively charged oligonucleotide molecules [18]. Further, the hybridization of target nucleic acid and oligonucleotide takes place due to complementary interactions that can be detected electrochemically by using an electrochemical indicator.

In this chapter, the hybridization of target RNA to complementary ASO sequence was carried out for specific detection of SARS-CoV-2 RNA by conjugation of unmodified ASO to cationic PLL-AuNPs through electrostatic interactions. Here, methylene blue was used as an electrochemical indicator for hybridization events. The biosensor efficiency was studied by differential pulse voltammetry (DPV), square wave voltammetry (SWV), and electrochemical impedance spectroscopy (EIS). The developed biosensor provided specificity and sensitivity for the detection of SARS-CoV-2 RNA from clinical samples collected from nasopharyngeal samples of COVID-19 individuals.

6.2   Experimental details:

6.2.1   Materials:

Gold tetrachloroaurate ($HAuCl_4$) solution, 0.01% Poly-L-Lysine solution, and methylene blue were purchased from Sigma (Maharashtra, India). Tris Acetate EDTA (TAE) buffer, phosphate buffer saline (PBS), and methylene blue were purchased from Himedia (Maharashtra, India). The 0.1 M concentration of phosphate buffer saline was prepared by dissolving 0.858 g of PBS powder into 1000 mL of distilled water. The antisense oligonucleotide (ASO) sequence and target sequence were purchased from Krumak Traders, Pune (Maharashtra, India), and stored at -20ºC for further use. Stock solutions of ASO and target sequences were prepared in 1X TAE solutions. All the chemicals were of analytical grade and used without any purification step. Deionized water was used for the preparation of all the respective solutions used in this study. The purity of the studied sequence was analysed using nanodrop (Multiscan skyhigh microplate reader) by checking the purity ratio (above A_{260}/A_{280}). The ASO sequence

used in this study was previously reported for naked eye detection of SARS-CoV-2 RNA using AuNPs [19]. The sequence employed in this study and its purity ratio are mentioned in **table 5.1** of **chapter 5.**

6.2.2 Clinical samples:

Clinical samples of COVID-19 positive individuals were collected by nasopharyngeal swab. The SARS-CoV-2 RNA was extracted using the RNA extraction kit (Viral RNA miniprep kit, Sigma). All the processes from collection to extraction of SARS-CoV-2 RNA were conducted by experts in biosafety laboratory-2 (BSL-2) in National Accreditation Board for Hospitals & Healthcare Providers (NABH) recognized molecular biology laboratory of Dr. D. Y. Patil Hospital, Kolhapur, India. These samples were verified for the presence of SARS-CoV-2 RNA using the qRT-PCR technique with cycle threshold (C_t) values (26.05, 30.27, and 33.42 for P1, P2, and P3 respectively). The purity ratio and concentrations of collected RNA samples are given in **table 5.3 of chapter 5**.

a) C_t value ≤ 25 :   high viral load.
b) C_t value (26 to 36) :   low viral load.
c) C_t value (37 to 40) :   not detected.

6.2.3 Apparatus:

The cyclic voltammetry (CV), differential pulse voltammetry (DPV), and electrochemical impedance spectroscopy (EIS) were performed by using Biologic Electrochemical Workstation (VSP). The electrochemical detection was performed by using three-electrode system consisting of (i) Reference electrode (Ag/AgCl), (ii) Counter electrode (helical platinum wire), and (iii) Working electrode [Glassy Carbon Electrode (GCE) with 0.05 cm^2 surface area].

6.2.4 Synthesis of PLL-AuNPs:

The synthesis of PLL-AuNPs was previously explained in **chapter 3** of the thesis. The PLL-AuNPs were synthesised by one-step synthesis method using PLL as reducing and stabilizing agent. For PLL-AuNPs synthesis, the PLL was added into

1 mM HAuCl₄ solution and stirred on magnetic stirrer until color change from pale yellow to wine-red. The prepared nanoparticles were washed thrice with distilled water by repeating the step of centrifugation at 13000 rpm for 15 min.

6.2.5 GCE preparation:

Prior to the modification of GCE with PLL-AuNPs, the bare GCE was polished to get a mirror-like surface using 0.05 µm alumina powder on a circular micro cloth pad. Polished bare GCE was then rinsed with distilled water, ethanol, and acetone for 2-4 min. This polished bare GCE was used for further experiments.

6.2.6 GCE modification by PLL-AuNPs:

The polished GCE was modified with synthesized PLL-AuNPs (PLL-AuNPs/GCE) by drop cast method with the help of a micropipette. The drop was allowed to dry using a hot air oven heated up to 70ºC for 1 to 2 minutes. After drying, the PLL-AuNPs/GCE was scanned for CV twice to check its stability and deposition from -1 to 1 V with a 20 mV scan rate using 0.1 mM PBS buffer.

6.2.7 Biosensor development and characterization:

ASOs are single-stranded DNA sequences that are complementary to target sequences (SARS-CoV-2 RNA). The ASO immobilization on PLL-AuNPs/GCE was explained as follows: 10 µL of 1 µM ASO concentration was deposited on the PLL-AuNPs/GCE surface by drop cast method and allowed to dry at 28ºC. Finally, it was rinsed with distilled water to remove unbound ASO and named this modified electrode as ASO/PLL-AuNPs/GCE. The bare GCE electrode and the modified electrodes (PLL-AuNPs/GCE and ASO/PLL-AuNPs/GCE) were characterized by CV from -1 to 1 V with a 20 mV scan rate using 0.1 mM PBS buffer.

6.2.8 Hybridization with target RNA and electrochemical detection:

The modified ASO/PLL-AuNPs/GCE electrode was allowed to hybridize with target SARS-CoV-2 RNA in 0.1 mM PBS containing 10 µL of target RNA of 10 nM concentration. This electrode was denoted as RNA/ASO/PLL-AuNPs/GCE. The

electrochemical detection of ASO-RNA hybridization was achieved by immersing the ASO/PLL-AuNPs/GCE and RNA/ASO/PLL-AuNPs/GCE electrode into 0.1 mM PBS containing methylene blue of 2×10^{-5} mol/L concentration as an electrochemical indicator for 15 min. These modified electrodes were then scanned for DPV, SWV, and EIS in 0.1 mM PBS using the electrochemical indicator methylene blue. The change in peak current due to the oxidation of methylene blue was observed for the response of biosensors.

6.2.9 Electrochemical detection of SARS-CoV-2 RNA from clinical sample:

The isolated SARS-CoV-2 RNA samples were quantified using nanodrop (Multiscan skyhigh microplate reader). For electrochemical detection, 4-5 μL of SARS CoV-2 RNA sample of 10 nM concentration was deposited on modified ASO/PLL-AuNPs/GCE for hybridization at 28ºC. Afterward, the electrode was immersed in 0.1 mM PBS containing methylene blue, and the DPV, SWV, and EIS were recorded at a scan rate of 20 mV from -1 to 1 V with compared to biosensor ASO/PLL-AuNPs/GCE.

6.3 Results and discussion:

6.3.1 Deposition of PLL-AuNPs on GCE:

The primary step for the development of biosensor includes the deposition of PLL-AuNPs on the surface of polished GCE by drop cast method. The strategy used to deposit nanoparticles on GCE includes the use of the drop cast method and the application of heat. The bare GCE and PLL-AuNPs modified GCE that named as PLL-AuNPs/GCE are scanned for CV at scanning rate of 20 mV/s in 0.1 mM PBS as shown in **figure 6.1(a)**, the PLL-AuNPs/GCE shows increased peak current (at -0.3 V) than bare GCE. This indicates that the PLL-AuNPs are well deposited over GCE along with good electrical conductivity and catalysis activity. **Figure 6.1(b)** shows no significant change in 10 cycles of CV for PLL-AuNPs/GCE with 20 mV/s scan rate. this study represents the proper deposition of PLL-AuNPs on GCE surface.
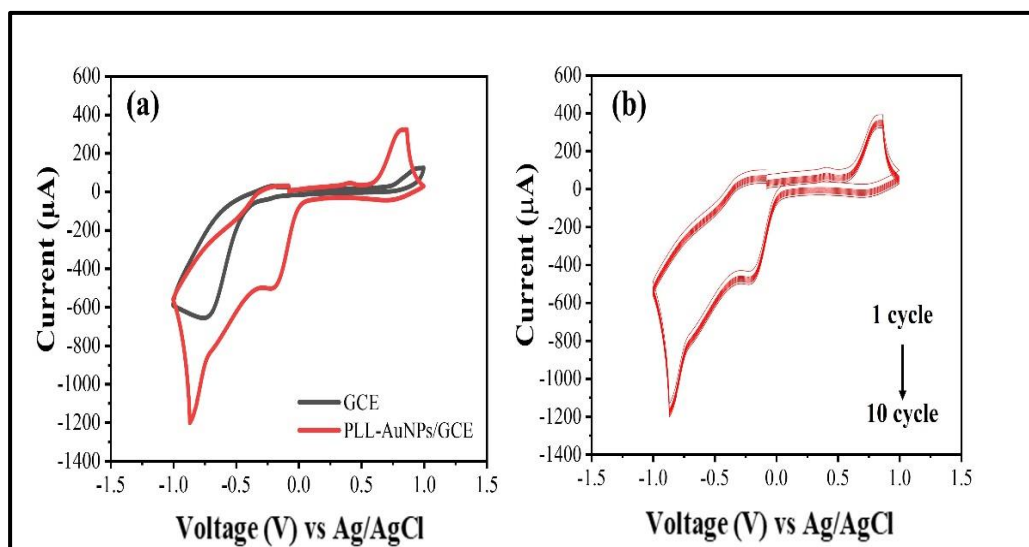
Figure 6.1: (a) Cyclic Voltammogram (CV) at scan rate of 20 mV/s of GCE with compare to PLL-AuNPs/GCE, and (b) 10 cycles of cyclic Voltammogram (CV) at scan rate of 20 mV/s for PLL-AuNPs/GCE

6.3.2 Biosensor development and characterization:

PLL-AuNPs were deposited on polished GCE surface by drop cast method in primary step of biosensor development. After the deposition of nanoparticles, the ASO sequence, which is complementary to the target RNA was added to the PLL-AuNPs/GCE electrode. The positively charged PLL-AuNPs interact with negatively charged ASO through electrostatic interactions. To analyze the change in peak current with modification step, the ASO was added separately after deposition of PLL-AuNPs on GCE as shown in **figure 6.2**. The addition of ASO also increases the surface area of reaction during the electrochemical sensing. After the formation of PLL-AuNPs and ASO conjugate, the hybridization of target RNA and conjugate was allowed to be done on a biosensor surface. Methylene blue (MB) was employed as an electrochemical indicator for the hybridization event that accumulated on the ASO-RNA hybrid produced due to hybridization. The biosensor was then characterized with cyclic voltammetry (CV) with a 20 mV/s scan rate in 0.1 mM PBS as shown in **figure 6.2**, the PLL-AuNPs/GCE shows increased peak current (at -0.3 V) than bare GCE. This indicates, the PLL-AuNPs were well deposited over GCE along with good electrical conductivity and catalysis activity. In case of ASO/PLL-AuNPs/GCE, the

peak current goes on decreasing compared to PLL-AuNPs/GCE electrode due to interaction occurring between cationic PLL-AuNPs and anionic ASO that reduces the electron transfer **(figure 6.2)**.
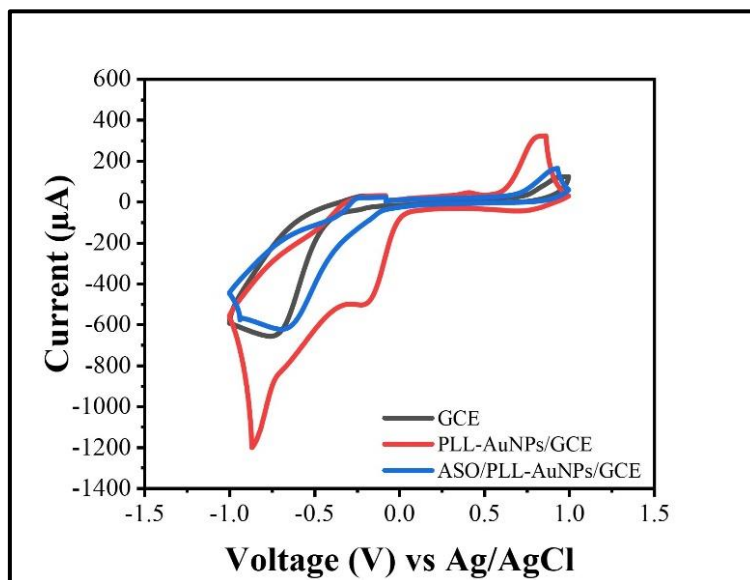
Figure 6.2: Cyclic Voltammogram (CV) at scan rate of 20 mV/s of GCE, PLL-AuNPs/GCE, and ASO/PLL-AuNPs/GCE electrode in 0.1 mM PBS

6.3.3 The working principle of developed electrochemical biosensor:

Figure 6.3 represents the working principle of developed electrochemical biosensor of SARS-CoV-2 RNA using modified GCE. This study explains the development of a simple and sensitive electrochemical sensing method, depending on cationic gold nanoparticles and ASO deposition on the GCE surface. As presented in **figure 6.3**, the first step of GCE modification includes the deposition of PLL-AuNPs on the surface of GCE by drop cast method following the deposition of ASO to make a PLL-AuNPs-ASO conjugate by electrochemical interactions between cationic PLL-AuNPs and anionic ASO. Next, the target RNA and ASO hybridization were carried out for specific and sensitive SARS-CoV-2 RNA detection. Then, the detection of target RNA and ASO hybridization was detected by measuring DPV, SWV, and EIS with the help of methylene blue as a redox indicator.
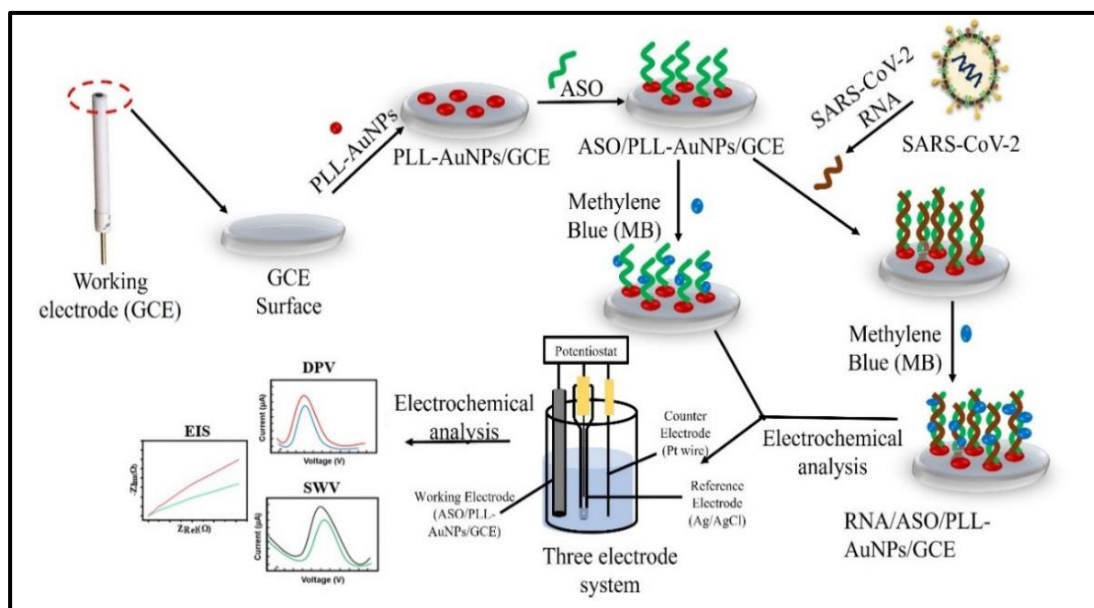
Figure 6.3: Schematic representation of biosensor development and electrochemical investigations of SARS-CoV-2 RNA detection

6.3.4   Detection of SARS-CoV-2 RNA:

Cyclic voltammetry technique is not able to significantly distinguish the interactions of ASO/PLL-AuNPs and target RNA. Differential Pulse Voltammetry (DPV), Square Wave Voltammetry (SWV), and Electrochemical Impedance Spectroscopy (EIS) techniques were employed for the detection of pathogens from test samples due to their high sensitivity. The analytical ability of biosensor for viral RNA detection was investigated by using different concentrations of target RNA. The electrochemical response of developed biosensor was recorded using electrochemical indicator, methylene blue. The MB can intercalate into the helical structure of an immobilized double-stranded DNA-RNA hybrid structure. As shown in **figure 6.4**, more concentration of MB interacts with DNA-RNA hybrid structure through major and minor groove as compare to ssDNA probe. The variation in MB binding results into increased current response for DNA-RNA hybrid than ssDNA probe.

The SARS-CoV-2 RNA concentration was optimized for biosensing by taking three different concentrations of SARS-CoV-2 RNA such as 1, 10, and 100 nM. The response current was measured using DPV by adding three different concentrations of

SARS-CoV-2 RNA (1, 10, and 100 nM) to the developed biosensor ASO/PLL-AuNPs/GCE. The current response for 10 nM and 100 nM is higher as compared to 1 nM concentration of SARS-CoV-2 RNA as shown in **figure 6.5**. Though 100 nM concentration shows higher response current, it cannot be further used because of a requirement of very high concentration of RNA. The 10 nM concentration shows significant current change as compared to the biosensor ASO/PLL-AuNPs/GCE. Thus, for the further study 10 nM concentration of RNA is used as optimum concentration of SARS-CoV-2 RNA.
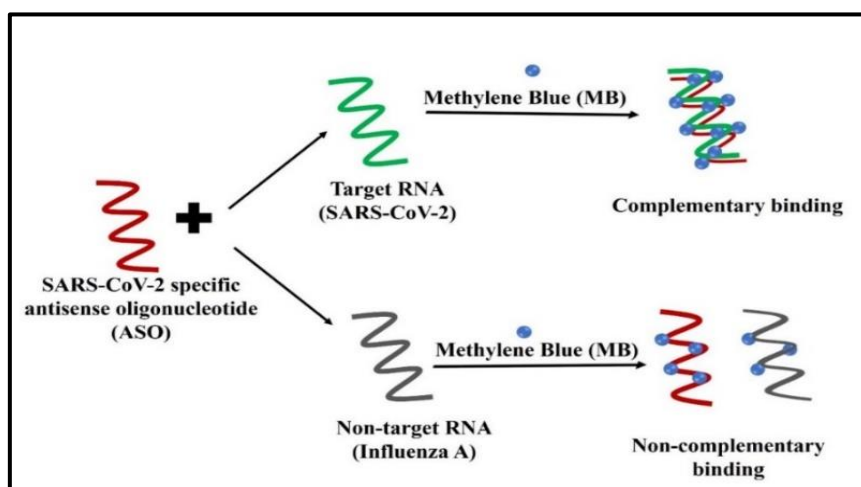
Figure 6.4: Mechanism of methylene blue interaction with DNA-RNA hybrid and ssDNA
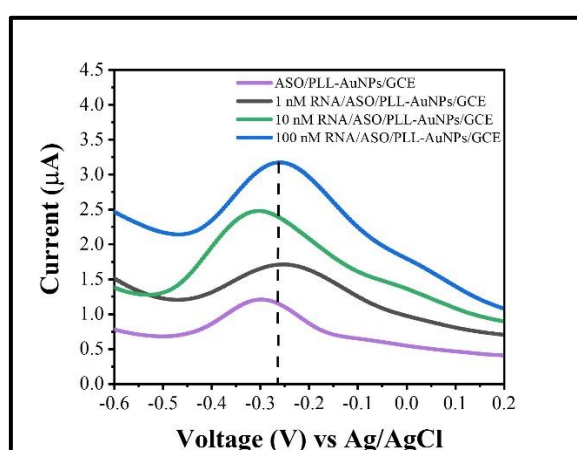
Figure 6.5: Differential Pulse Voltammogram (DPV) of ASO/PLL-AuNPs/GCE with varying concentration of SARS-CoV-2 RNA (1, 10, 100 nM).

The DPV, SWV, and EIS response of modified electrodes with and without target RNA using MB as an electrochemical indicator was recorded and shown in **figure 6.6(a), (b), and (d),** respectively. The DPV response for target RNA shows an increased current value as compared to the modified electrode in the absence of target RNA in MB. As shown in **figure 6.6(a)**, after the hybridization of target RNA with ASO, the redox signal (peak current) is higher (1.7 µA) as compared to the redox signal of ASO (1.2 µA). The increase in peak current with increased redox potential is a result of the intercalation of MB on the DNA-RNA hybrid structure. The obtained data demonstrated that methylene blue is accumulated on modified electrodes (PLL-AuNPs/GCE, ASO/PLL-AuNPs/GCE and RNA/ASO/PLL-AuNPs/GCE).

The accumulation of MB on RNA/ASO/PLL-AuNPs/GCE surface shows higher oxidoreductase signal that results in increased redox peak current. This result was similar to the previous report showing an increased current peak for dsDNA due to MB accumulation. This may be due to the high concentration of MB used in the study, resulting in the intercalation of MB on the double helix of dsDNA [20-22]. Furthermore, confirmation and understand the sensitivity of the current experiment, SWV was performed, and the results are shown in **figure 6.6(b)**. The results show the same trend as DPV, after hybridization of target RNA with ASO, the peak current (2.7 µA) goes on increasing as compared to the redox signal of ASO (2.5 µA). As shown in **figure 6.6(c)**, after deposition of PLL-AuNPs the current is increases as compere to bare GCE. Whereas, after hybridization of ASO and target SARS-CoV-2 RNA, DPV and SWV response is increased as compare to ASO.

Electrochemical impedance spectroscopy (EIS) is a potent method for analysing the interfacial characteristics of bio-recognition processes that takes place at the electrode surface such as, antibody-antigen recognition, substrate-enzyme interaction, whole cell interaction, and DNA. Also, it is an effective method for demonstrating the characteristics of modified electrodes. Hence for a detailed understanding of ASO/PLL-AuNPs and RNA/ASO/PLL-AuNPs interactions, electrodes were tested by EIS technique in the range of 200 KHz to 100 mHz. **Figure 6.6(d)** shows the EIS response of bare GCE, PLL-AuNPs/GCE, and ASO/PLL-AuNPs/GCE before and after the hybridization event with target RNA in the presence of MB, and the corresponding

equivalent circuit of EIS is depicted in the inset of **figure 6.6(d).** The equivalent circuit consists of solution resistance (Rs) in series with the parallel combination of constant phase element (Q2) and charge transfer resistance (Rct). In the Nyquist plot of **figure 6.6(d)** higher Rct values are denoted by the incomplete semicircle. This is probably due to the non-faradaic analysis [23].
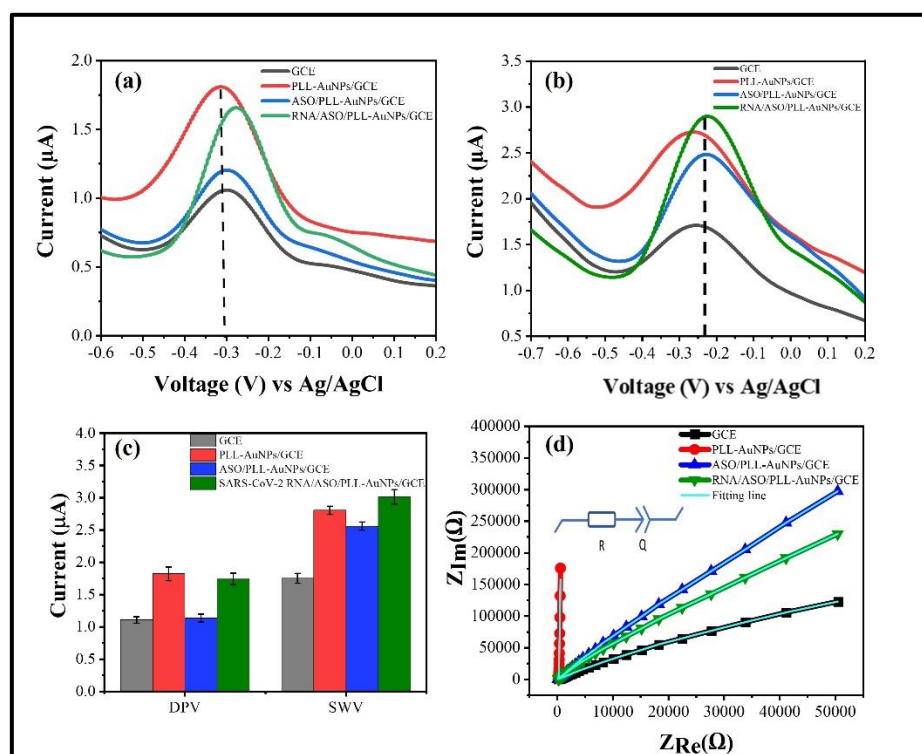
Figure 6.6: Electrochemical analysis of developed biosensor. (a) Differential Pulse Voltammogram (DPV), (b) Square Wave Voltammogram (SWV), (c) bar diagram of DPV and SWV, and (d) Nyquist plot of GCE, PLL-AuNPs/GCE, ASO/PLL-AuNPs/GCE, RNA/ASO/PLL-AuNPs/GCE electrode in 0.1 mM PBS. The error bars in the diagram display the standard deviation of the readings derived from the three measurements

The Nyquist plot shows reduction in radius of curvature of incomplete semi-circle which is associated with increase in MB accumulation on ASO-RNA hybridization as compared to ASO alone. The values of circuit elements for bare GCE, PLL-AuNPs/GCE, ASO/PLL-AuNPs/GCE, and RNA/ASO/PLL-AuNPs/GCE electrodes are mentioned in **table 6.1.** It is found that the solution resistance of RNA/ASO/PLL-AuNPs/GCE electrodes (605.7 Ω) is higher as compared to the

remaining electrodes which indicates the decrease in electroactive species in electrolyte due to the hybridization of probe (ASO) and target RNA. The value of α provided for constant phase element (CPE) exposes the capacitive behavior, which becomes 0 for pure resistive behavior and 1 for optimum capacitive behavior. The values of α were found to be > 0.7 for all electrodes, revealing non-ideal capacitive behavior of all electrodes.

Table 6.1: Equivalent circuit elements values of bare GCE, PLL-AuNPs/GCE, ASO/PLL-AuNPs/GCE, and RNA/ASO/PLL-AuNPs/GCE electrodes.

Sr. No	Electrode	Rs (Ω)	Q (Fs⁻¹)	α
1.	Bare GCE	183.9	9.828×10^{-6}	0.87
2.	PLL-AuNPs/GCE	166.6	6.796×10^{-6}	0.79
3.	ASO/PLL-AuNPs/GCE	155.6	4.652×10^{-6}	0.78
4.	RNA/ASO/PLL-AuNPs/GCE	605.7	5.62×10^{-6}	0.77

The analytical ability of biosensor for viral RNA detection was investigated by using different concentrations of SARS-CoV-2 RNA. **Figure 6.7(a)** shows the response of the biosensor towards increasing concentration of target RNA from 0 nM to 100 nM. The response increases with increasing concentration of SARS-CoV-2 RNA. The linear increase in peak current was observed for different (0 to 100 nM) concentrations with a slope (0.01431 ± 0.001125) and intercept (1.3315 ± 0.05344) and good fitting parameter ($r^2 = 0.98181$), as shown in **figure 6.7(b)**. In the present case, the limit of detection (LOD) is 30.2 nM. The LOD was calculated by the equation, D = 3.3(σ/s) where, the D is the limit of detection, σ is the standard deviation of the regression line, and s is the slope.

6.3.5 Selectivity of the biosensor:

For the development of a sensitive electrochemical biosensor, it is necessary to check its selectivity towards the target analyte. The activity of the biosensor is influenced by interference from many external substances, so a selectivity study of the

modified electrode is essential. Given this, the developed electrode was then analyzed for its selectivity through non-complementary RNA sequence (Influenza A RNA) as non-target. Influenza A viruses and SARS-CoV-2 viruses are single-stranded RNA viruses that are responsible to cause contagious respiratory illnesses. Thus, in this study, the Influenza A RNA was used to study the selectivity of biosensors. **Figures 6.8(a)** and **6.8(b)** shows the DPV and SWV results of 10 nM concentration of target (SARS-CoV-2) compared with 10 nM concentration of non-target (Influenza A) RNA.
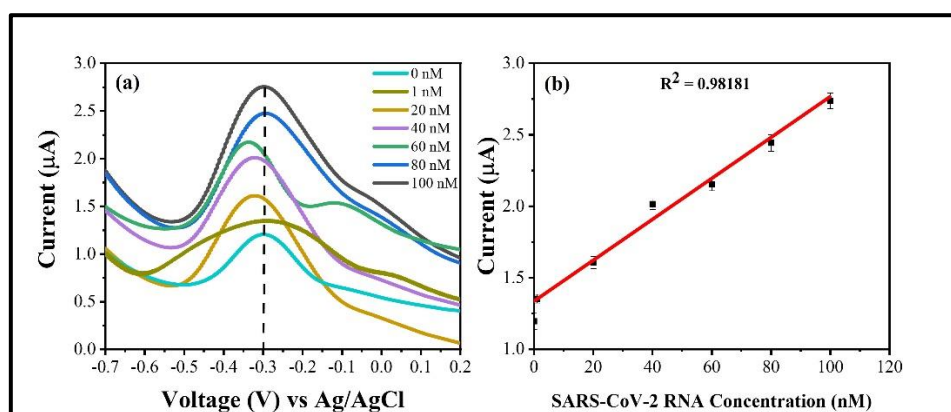
Figure 6.7: (a) DPV of MB accumulation on ASO/PLL-AuNPs/GCE after hybridization with different concentrations of target SARS-CoV-2 RNA (0-100 nM), and (b) Linear regression of corresponding DPV peak current for biosensor with different concentrations of target SARS-CoV-2 RNA. The error bars in the diagram display the standard deviation of the readings derived from the three measurements (0-100 nM)

The results show that after hybridization with the target (SARS-CoV-2 RNA), the current response increases in comparison to the ASO-modified electrode. **Figure 6.8(c)** shows the comparative difference between DPV and SWV current response after hybridization of target SARS-CoV-2 RNA and non-target Influenza A RNA. As shown in **figure 6.8(c)**, for 10 nM concentration of non-target sequence, the DPV and SWV response is lower than 10 nM concentration of target SARS-CoV-2 RNA. The data indicates that lower concentrations of target SARS-CoV-2 RNA can be detected by the biosensor in comparison to same concentration of non-target SARS-CoV-2 RNA. The minute increase in current response for non-target was possibly due to non-specific adsorption. The results suggest that the developed biosensor is selective towards

complementary target SARS-CoV-2 RNA sequences. **Figure 6.8(d)** represents the Nyquist plots of ASO/PLL-AuNPs/GCE, RNA/ASO/PLL-AuNPs/GCE, and Influenza A RNA/ASO/PLL-AuNPs/GCE electrodes in the range of 200 KHz to 100 mHz. The equivalent circuit element values are depicted in **table 6.2**. The capacitance values (CPE) for ASO/PLL-AuNPs/GCE and Influenza A RNA/ASO/PLL-AuNPs/GCE are comparatively low as compared to RNA/ASO/PLL-AuNPs/GCE, suggesting the accumulation of MB on RNA/ASO is more than Influenza A RNA/ASO. The overall results suggest that the developed biosensor has good selectivity towards SARS-CoV-2 RNA.
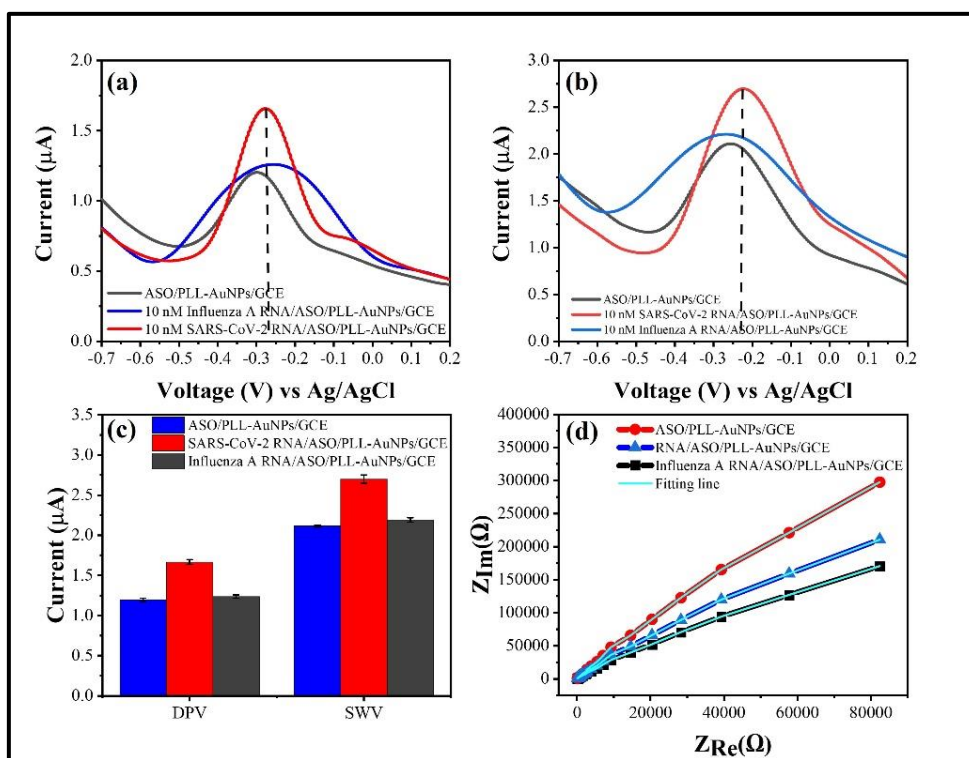
Figure 6.8: (a) DPV, (b) SWV, (c) bar diagram of DPV and SWV for MB accumulation on ASO/PLL-AuNPs/GCE before and after hybridization with the 10 nM concentration of target (SARS-CoV-2) with comparison to 10 nM concentration of non-target (Influenza A) RNA, and (d) EIS results of ASO/PLL-AuNPs/GCE, RNA/ASO/PLL-AuNPs/GCE, and Influenza A RNA/ASO/PLL-AuNPs/GCE electrodes. The error bars in the diagram display the standard deviation of the readings derived from the three measurements

Table 6.2: Equivalent circuit elements values of ASO/PLL-AuNPs/GCE and RNA/ASO/PLL-AuNPs/GCE and Influenza A RNA/ASO/PLL-AuNPs/GCE electrodes.

Sr. No	Electrode	Rs (Ω)	Q (Fs^{-1})	α
1.	ASO/PLL-AuNPs/GCE	155.6	4.6×10^{-6}	0.78
2.	RNA/ASO/PLL-AuNPs/GCE	605.7	4.5×10^{-6}	0.74
3.	Influenza A RNA/ASO/PLL-AuNPs/GCE	144.5	4.3×10^{-6}	0.73

6.3.6 Detection of SARS-CoV-2 RNA from clinical sample:

The development of rapid, easy, and specific detection methods for SARS-CoV-2 is required for early diagnosis of COVID-19. The gold standard technique, qRT-PCR though provides specificity and sensitivity but, requires sophisticated laboratory, amplification, and required a lot of time. The developed biosensor was used to detect SARS-CoV-2 RNA from clinical samples taken from COVID-19 individuals as nasopharyngeal swabs without the need for amplification and oligonucleotide modification. The developed biosensor was used to detect SARS-CoV-2 RNA from COVID-19 individuals by collecting their nasopharyngeal swabs. The collected samples were already analyzed through qRT-PCR and then used to validate the developed biosensor. In this study, three samples were collected from COVID-19 individuals named P1, P2, and P3 with C_t values 26.05, 30.27, and 33.42, respectively. The nasopharyngeal sample from a healthy individual was considered a control.

The P1 sample with high viral load shows increased response as compared to P2 and P3 with lower viral load; whereas, the control shows a small increase in DPV and SWV current response **(figure 6.9a and b)**. **Figure 6.9(c)** shows a comparative increase in DPV and SWV pick current after hybridization with different RNA samples taken from COVID-19 individuals compared to RNA taken from healthy individual (control RNA). The results show that the developed biosensor can differentiate between infected and non-infected individuals along with various viral loads. Furthermore, EIS results of the P1, P2, and P3 samples with C_t values 26.05, 30.27, and 33.42,

respectively, and control RNA are shown in **figure 6.9(d).** The corresponding equivalent circuit was shown in the inset. The circuit fitting parameters as summarized in **table 6.3**. These results justify solution resistance is higher for the P1 sample and the low for the P3 sample which is directly related to the concentration of viral RNA. The diffusion coefficient value that appeared for the P1 sample is lower than P2 and P3 represents the higher diffusion rate of MB at the RNA/ASO surface, which indirectly suggest the higher concentration of SARS-CoV-2 RNA. The obtained biosensor results are correlated with the qRT-PCR results as shown in **figure 6.10**, representing the potential of the proposed method. The developed biosensor exhibits robust responsiveness for the samples with different viral loads without any amplification step.
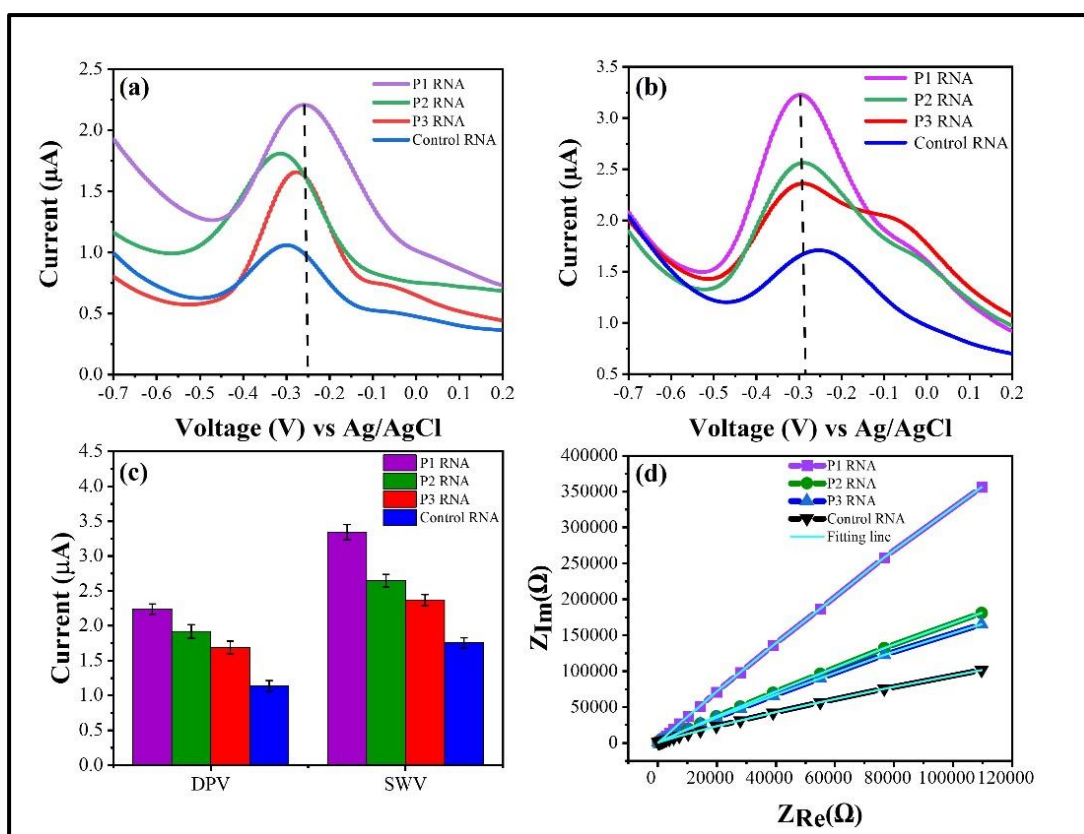
Figure 6.9: (a) DPV, (b) SWV, (c) bar diagram for comparison of DPV with SWV, and (d) Nyquist plot of methylene blue accumulated on ASO before and after hybridization with target RNA from clinical samples P1, P2, P3, and RNA from healthy individual taken as control. The error bars in the diagram display the standard deviation of the readings derived from the three measurements

Table 6.3: Equivalent circuit elements values of control RNA/ASO/PLL-AuNPs/GCE, P1-RNA/ASO/PLL-AuNPs/GCE, P2-RNA/ASO/PLL-AuNPs/GCE, and P3-RNA/ASO/PLL-Au NPs/GCE electrodes.

Sr. No	Electrode	Rs (Ω)	Q (Fs^{-1})	α
1.	Control RNA/ASO/PLL-AuNPs/GCE	189.7	6.11×10^{-6}	0.73
2.	P1 RNA/ASO/PLL-AuNPs/GCE	270.4	0.8×10^{-6}	0.81
3.	P2 RNA/ASO/PLL-AuNPs/GCE	254.2	4.05×10^{-6}	0.80
4.	P3 RNA/ASO/PLL-AuNPs/GCE	240.4	4.39×10^{-6}	0.74
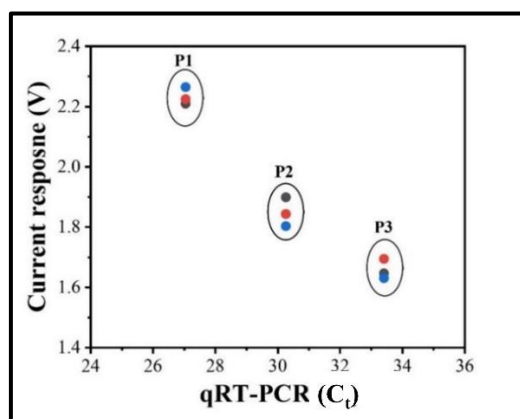
Figure 6.10: Correlation between the current response of biosensor (Y-axis) and C_t values of qRT-PCR (X-axis) of the COVID-19 positive nasopharyngeal samples P1 (26.05), P2 (30.27), and P3 (33.42).

6.3.7 Reproducibility and stability of developed biosensor:

An important feature of the developed biosensor is the reproducibility of the response and reproducibility of the biosensor preparation. The electrochemical detection of SARS-CoV-2 RNA was performed five times by using the modified electrode under the same experimental conditions as per the procedure explained above. The DPV and SWV **(figures 6.11a and 6.11b)** were recorded to study the reproducibility of biosensor. The relative standard deviation (RSD) is found to be 3.99%, which indicated the excellent reproducibility of the developed DNA biosensor.
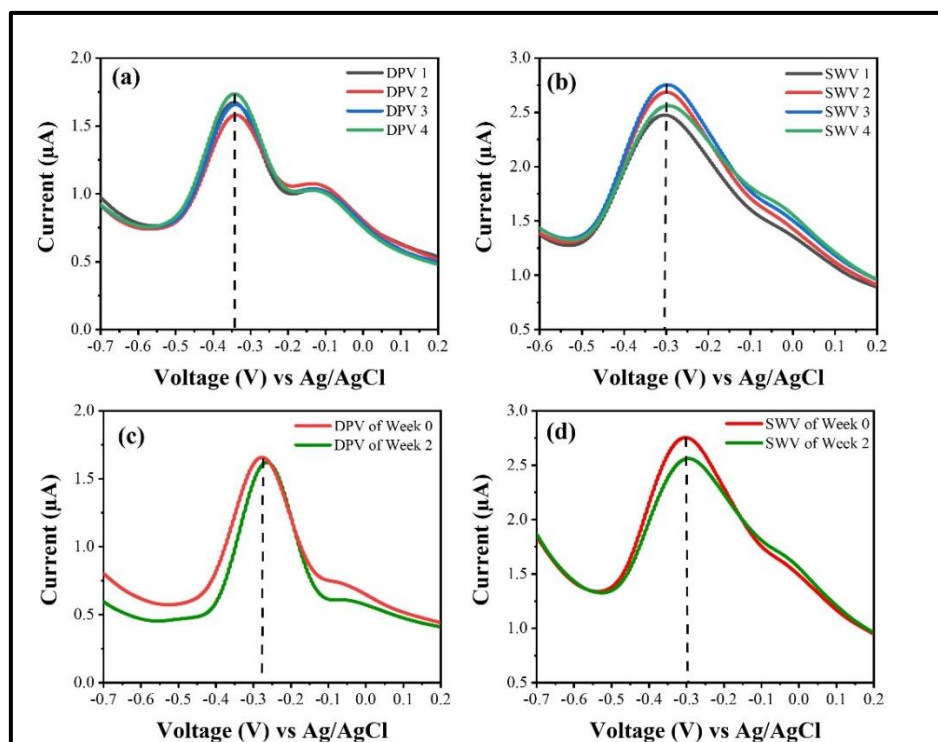
Figure 6.11: (a-b) Reproducibility and (c-d) stability of developed biosensor studied by DPV and SWV techniques after accumulation of MB in the presence of target SARS-CoV-2 RNA.

Apart from the reproducibility, the stability of the biosensor is another important parameter to assess the quality of biosensor. For this study, the modified electrode (ASO/PLL-Au NPs/GCE) was stored at 4ºC in a refrigerator for two weeks and then used for the detection of target RNA by hybridization through DPV and SWV techniques **(figure 6.11c and 6.11d)**. The stability investigation revealed that following electrode storage, the analytical accuracy of biosensor is unaffected, and the resulting RSD value is found to be 2.16 %. These results asserted that the present biosensor has good reproducibility and stability.

6.3.8 Comparison between various electrochemical biosensors for nucleic acid detection:

Available reports on electrochemical biosensing have shown its great potential for nucleic acid detection. Nowadays, viral or bacterial nucleic acid detection is gaining attention of researcher due to specificity and sensitivity. C. Hwang *et. al.* [8] reported

detection of SARS-CoV-2 RNA using electrochemical method by capacitance measurement with 10 nM limit of detection. However, the amino group functionalized DNA probe is required for biosensor preparation with Interdigitated platinum/titanium electrodes. The analysis time for SARS-CoV-2 detection is about 2 h. The detection of bacterial nucleic acids (*Klebsiella pneumoniae* carbapenemase and *Helicobacter pylori*) using AuNPs/GCE via electrochemical biosensing was performed by Pan *et. al.* [15] and Hajihosseini *et. al.* [16], using methylene blue and oracet blue as hybridization indicators, respectively. The detection is based on DPV analysis with lower limit of detection. Anyhow, the thiol modified DNA probes are required for biosensor development along with high analysis time as 1.5 h and 3.41 h for detection of *Klebsiella pneumoniae* carbapenemase and *Helicobacter pylori,* respectively. Likewise, SARS-CoV-2 RNA detection by electrochemical biosensing with lower detection limit was reported in various studies. However, the detection required 10 min to 1.5 h analysis time with DPV and EIS methods [17, 24-26]. The formation of the biosensor required either a thiol-modified DNA probe or a probe with a length of 51 nucleotides. Also, the study was completed with different electrodes such as, GCE, SCPE, and gold screen printed electrode. The electrochemical indicator used in these studies are azure A and methylene blue functionalized carbon dots that accumulated on DNA-RNA hybrid within specific time of incubation.

The proposed electrochemical biosensing method, utilizing cationic AuNPs and unmodified probes, offers an alternative approach for the detection of SARS-CoV-2 RNA. This method is simple, efficient, and allows for the specific detection of SARS-CoV-2 RNA in a short time frame. The cationic PLL-AuNPs are synthesized using a straightforward one-pot method, with PLL acting as both the reducing and functionalizing agent. The adsorption of the ASO onto these PLL-AuNPs relies on electrostatic interactions, eliminating the need for thiol modifications commonly required by other biosensing techniques. Electrochemical detection is performed using DPV, SWV, and EIS methods, all within short period of time (15 minutes). The fabricated electrode demonstrates excellent analytical performance, with a low limit of detection (30.2 nM), good reproducibility (3.99%), and stability (2.16%), outperforming other reported biosensors. The developed biosensor needs to be carried forward for study related to stability and specificity. The principle of biosensor is based

on electrostatic interactions, which are non-covalent in nature and are affected by small changes in pH and temperature. Therefore, the biosensor was developed at constant pH and temperature. The method offers a quick, specific and sensitive alternative to detection over conventional gold standard methods like PCR which have complicated processing steps, require more time for reporting and cannot be performed in underequipped laboratory settings.

6.4 Conclusions:

The study presents a successful development of an electrochemical biosensor for the sensitive detection of SARS-CoV-2 RNA. A cationic gold nanoparticle (PLL-AuNPs) biosensor has been developed, significantly reducing the need for surface modification of oligonucleotides. The cationic PLL-AuNPs were conjugated with an unmodified anionic antisense oligonucleotide (ASO) through electrostatic interactions. An immobilized ASO serves as the capture probe, enabling specific recognition of viral SARS-CoV-2 RNA. Methylene blue (MB) is used as an electrochemical indicator to monitor the hybridization event between the capture probe (ASO) and the target SARS-CoV-2 RNA. The analytical performance of the biosensor is assessed through various electrochemical techniques, including Differential Pulse Voltammetry (DPV), Square Wave Voltammetry (SWV), and Electrochemical Impedance Spectroscopy (EIS). Notably, the biosensor demonstrates sensitive and specific detection of SARS-CoV-2 RNA with approximately 30.2 nM limit of detection. Furthermore, the developed ASO/PLL-AuNPs/GCE biosensor shows reproducibility and stability with low RSD values of 3.99 and 2.16%, respectively indicating consistent and reliable performance. The biosensor can detect a 10 nM concentration of SARS-CoV-2 RNA in comparison to same concentration of Influenza A RNA. This ability of the biosensor to discriminate between complementary (SARS-CoV-2 RNA) and non-complementary RNA sequences (Influenza A RNA) confirms the specificity of the proposed biosensor. The study concludes by suggesting potential future applications of the present biosensor in the sensitive detection of viral RNA, underscoring its versatility and promising attributes for broader use in viral RNA detection.

6.5 References:

[1]   Ciotti M, Ciccozzi M, Terrinoni A, Jiang WC, Wang CB, Bernardini S. The COVID-19 pandemic. Critical reviews in clinical laboratory sciences. 2020;57(6):365-88.

[2]   Eftekhari A, Alipour M, Chodari L, Maleki Dizaj S, Ardalan M, Samiei M, Sharifi S, Zununi Vahed S, Huseynova I, Khalilov R, Ahmadian E. A comprehensive review of detection methods for SARS-CoV-2. Microorganisms. 2021;9(2):232-51.

[3]   Younes N, Al-Sadeq DW, Al-Jighefee H, Younes S, Al-Jamal O, Daas HI, Yassine HM, Nasrallah GK. Challenges in laboratory diagnosis of the novel coronavirus SARS-CoV-2. Viruses. 2020;12(6):582-609.

[4]   Wang J, Zhou H, Liu J, He J, Liu J, Yang W. Electrochemical detection of DNA by formation of efficient electron transfer pathways through adsorbing gold nanoparticles to DNA modified electrodes. Microchemical Journal. 2021;169(1):581-89.

[5]   Du Y, Dong S. Nucleic acid biosensors: recent advances and perspectives. Analytical chemistry. 2017;89(1):189-215.

[6]   Drobysh M, Ramanaviciene A, Viter R, Chen CF, Samukaite-Bubniene U, Ratautaite V, Ramanavicius A. Biosensors for the determination of SARS-CoV-2 virus and diagnosis of COVID-19 infection. International journal of molecular sciences. 2022;23(2):666-91.

[7]   Kim HE, Schuck A, Lee SH, Lee Y, Kang M, Kim YS. Sensitive electrochemical biosensor combined with isothermal amplification for point-of-care COVID-19 tests. Biosensors and Bioelectronics. 2021;182(1):168-74.

[8]   Hwang C, Park N, Kim ES, Kim M, Kim SD, Park S, Kim NY, Kim JH. Ultra-fast and recyclable DNA biosensor for point-of-care detection of SARS-CoV-2 (COVID-19). Biosensors and Bioelectronics. 2021;185(1):177-83.

[9]   Peng Y, Pan Y, Sun Z, Li J, Yi Y, Yang J, Li G. An electrochemical biosensor for sensitive analysis of the SARS-CoV-2 RNA. Biosensors and Bioelectronics. 2021;186(1):309-15.

[10]   Zhao H, Liu F, Xie W, Zhou TC, OuYang J, Jin L, Li H, Zhao CY, Zhang L, Wei J, Zhang YP. Ultrasensitive supersandwich-type electrochemical sensor for SARS-CoV-2 from the infected COVID-19 individuals using a smartphone. Sensors and Actuators B: Chemical. 2021;327(1):899-908.

[11]   Liu X, Huang L, Qian K. Nanomaterial-Based Electrochemical Sensors: Mechanism, Preparation, and Application in Biomedicine. Advanced NanoBiomed Research. 2021;1(6):104-16.

[12]   https://www.news-medical.net/life-sciences/What-are-Electrochemical Biosensors.aspx

[13] Huang X, Zhu Y, Kianfar E. Nano biosensors: properties, applications and electrochemical techniques. Journal of Materials Research and Technology. 2021;12(1):1649-72.

[14] Patil T, Gambhir R, Vibhute A, Tiwari AP. Gold nanoparticles: Synthesis methods, functionalization and biological applications. Journal of Cluster Science. 2023;34(2):705-25.

[15] Pan HZ, Yu HW, Wang N, Zhang Z, Wan GC, Liu H, Guan X, Chang D. Electrochemical DNA biosensor based on a glassy carbon electrode modified with gold nanoparticles and graphene for sensitive determination of Klebsiella pneumoniae carbapenemase. Journal of biotechnology. 2015;214(1):133-38.

[16] Hajihosseini S, Nasirizadeh N, Hejazi MS, Yaghmaei P. A sensitive DNA biosensor fabricated from gold nanoparticles and graphene oxide on a glassy carbon electrode. Materials Science and Engineering: C. 2016;61(1):506-15.

[17] Del Caño R, García-Mendiola T, García-Nieto D, Álvaro R, Luna M, Iniesta HA, Coloma R, Diaz CR, Milán-Rois P, Castellanos M, Abreu M. Amplification-free detection of SARS-CoV-2 using gold nanotriangles functionalized with oligonucleotides. Microchimica Acta. 2022;189(4):171-83.

[18] Jamaluddin ND, Ibrahim N, Yusof NY, Goh CT, Tan LL. Optical reflectometric measurement of SARS-CoV-2 (COVID-19) RNA based on cationic cysteamine-capped gold nanoparticles. Optics & Laser Technology. 2023;157(1):763-72.

[19] Moitra P, Alafeef M, Dighe K, Frieman MB, Pan D. Selective naked-eye detection of SARS-CoV-2 mediated by N gene targeted antisense oligonucleotide capped plasmonic nanoparticles. ACS nano. 2020;14(6):7617-26.

[20] Raju VM, Bhavana V, Gayathri GK, Suryan S, Reddy R, Reddy N, Ravikumar CR, Santosh MS. A novel disposable electrochemical DNA biosensor for the rapid detection of Bacillus thuringiensis. Microchemical Journal. 2020;159(1):105434-42.

[21] Pothipor C, Aroonyadet N, Bamrungsap S, Jakmunee J, Ounnunkad K. A highly sensitive electrochemical microRNA-21 biosensor based on intercalating methylene blue signal amplification and a highly dispersed gold nanoparticles/graphene/polypyrrole composite. Analyst. 2021;146(8):2679-88.

[22] Low SS, Loh HS, Boey JS, Khiew PS, Chiu WS, Tan MT. Sensitivity enhancement of graphene/zinc oxide nanocomposite-based electrochemical impedance genosensor for single stranded RNA detection. Biosensors and Bioelectronics. 2017;94(1):365-73.

[23] Dhamu VN, Poudyal DC, Telang CM, Paul A, Muthukumar S, Prasad S. Electrochemically mediated multi-modal detection strategy-driven sensor platform to detect and quantify pesticides. Electrochemical Science Advances. 2022;2(6):e2100128-42.

[24]   Silva LR, Stefano JS, Orzari LO, Brazaca LC, Carrilho E, Marcolino-Junior LH, Bergamini MF, Munoz RA, Janegitz BC. Electrochemical biosensor for SARS-CoV-2 cDNA detection using AuPs-modified 3D-printed graphene electrodes. Biosensors. 2022;12(8):622-42.

[25]   Pina-Coronado C, Martínez-Sobrino Á, Gutiérrez-Gálvez L, Del Caño R, Martínez-Periñán E, García-Nieto D, Rodríguez-Peña M, Luna M, Milán-Rois P, Castellanos M, Abreu M. Methylene Blue functionalized carbon nanodots combined with different shape gold nanostructures for sensitive and selective SARS-CoV-2 sensing. Sensors and Actuators B: Chemical. 2022;369(1):217-29.

[26]   Hussein HA, Hanora A, Solyman SM, Hassan RY. Designing and fabrication of electrochemical nano-biosensor for the fast detection of SARS-CoV-2-RNA. Scientific Reports. 2023;13(1):5139-50.

Chapter VII

Poly-L-Lysine functionalized gold nanoparticle–nucleic acid conjugate for detection of bacterial DNA (*Klebsiella pneumoniae* DNA)

7.1 Introduction:

Klebsiella pneumoniae (*K. pneumoniae*) is a Gram negative, rod shaped, non-motile, encapsulated bacterium that belongs to Enterobacteriaceae family. It is an opportunistic pathogen commonly found in intestine and feces. The organism becomes pathogenic when spread to other body parts such as, lungs and urinary tract. *K. pneumoniae* is reported to cause variety of infections such as, pneumonia, urinary tract infection (UTI), skin or soft tissue infection, meningitis, endophthalmitis, and bacteremia [1]. In recent years, *Klebsiella* spp. gaining attention of researcher due to its resistant nature towards different antibiotics and its disease severity [2]. The development of resistance is due to overuse of antibiotic and drugs for the treatment of infection. The bacteria have ability to develop resistance against antibiotics through variety of methods including efflux pump system and formation of biofilm [3]. *K. pneumoniae* is capable of producing capsular polysaccharides (CPS), that encourage anti-phagocytosis and resistance nature. The CPS production of *K. pneumoniae* is identified by using K2 associated protein A *(K2A)* gene [4]. Capsular nature of *K. pneumoniae* help to escape them from the host immune system [5]. *Klebsiella* infection generally caused due to direct entry of organism into host body via person to person contact or infected hospital equipment [1].

The *Klebsiella* infection is identified by conventional diagnostic methods as well as molecular based detection system. The conventional diagnostic methods including immunoassay such as, immunodiffusion assay, capsular swelling technique, enzyme linked immuno sorbent assay (ELISA), and immunoblot assay whereas; molecular based detection system includes southern blot and PCR based methods [6, 7]. Biochemical tests have various limitations, such as being time-consuming, costly, and exhibiting lower specificity and sensitivity [8]. Similarly, molecular-based methods like PCR offering improved specificity and sensitivity, also come with challenges. These include the need for advanced laboratory equipment, skilled technicians and are being time-consuming and expensive [7].

Recently the researchers have developed different types of biosensors for sensitive and rapid detection of pathogens and pathogenic products. Simple, sensitive, and trustworthy nucleic acid detection has become increasingly important with the advancement of molecular biology in numerous applications, including disease prevention, diagnosis, controlling food quality, and detection of environmental pollutants. Nanoparticles based biosensor development is gaining attention of researchers due to unique features of nanoparticles. Among different metal nanoparticles, gold nanoparticles (AuNPs) attract researchers due to their extensive characterization such as, easy synthesis methods, biomolecule functionalization, stabilization, less toxicity, and biocompatible nature [9]. AuNPs are widely used nanoparticles for biosensor development due to their optical properties [10]. AuNPs are functionalized with different biomolecules including nucleic acid and proteins for detection of pathogenic DNA, various antigens, and cancer biomarkers [11]. The AuNPs are functionalized with nucleic acid either by thiol modification or electrostatic interactions. AuNPs are utilized for colorimetric detection of pathogens by combining them with DNA probe. The drawbacks of using citrate capped AuNPs for DNA functionalization are explained in introduction section of **chapter 4**. In short, they need thiol modification and salt aging process for stabilization whereas, cationic AuNPs minimize the requirement of thiol modification and salt aging procedure. The cationic AuNPs are functionalized with DNA probe by electrostatic interactions and then be used for detection of interested analyte.

In this chapter, the Exonuclease III and cationic AuNPs based detection method is used for detection of bacterial DNA. Exonuclease III (Exo III) is an enzyme from exonuclease family that specifically degrade double stranded DNA [12]. The cationic AuNPs were synthesized by one pot synthesis method using Poly-L-Lysine (PLL) as reducing and functionalizing agent. The DNA probes specific to *K. pneumoniae* were conjugated with PLL functionalized AuNPs (PLL-AuNPs) by electrostatic interactions that protects the PLL-AuNPs from aggregation. After introduction of target DNA of *K. pneumoniae,* double stranded DNA structure is formed with complementary probe sequences. Exo III addition leads to degradation of this double stranded DNA that decreases the UV absorption at 660 nm. In absence of

target DNA there is no degradation by Exo III thus, the UV absorbance remains unchanged. The developed detection system can specifically detect target DNA in small period of time. s

7.2 Experimental details:

7.2.1 Materials:

All the reagents used in this study were of analytical grade obtained from commercial vendors and used without any purification step. Gold tetrachloroaurate ($HAuCl_4$) solution, 0.01% Poly-L-Lysine (PLL) solution were purchased from Sigma (Maharashtra, India) and Exonuclease III from ThermoFisher Scientific (Maharashtra, India). Deionized water was used for preparation of all the respective solutions. The ssDNA probe sequences and target sequence were purchased from Krumak Traders, Pune (Maharashtra, India) and stored at -20ºC for further use. Probe and target DNA solution were prepared in 1X TAE buffer. The sequences were presented in **table 7.1**.

Table 7.1: The DNA probes and target DNA sequences used in this study

Sr. No.	Oligonucleotide	Base sequence (5'-3')	Ref
1.	DNA Probe 1	CCTTCCGTTGCAAGTAAAATC	
2.	DNA probe 2	CCGTTCTAGGTTGAGAGAAAT	[13]
3.	Target sequence	TTCATTTTAGGGCAAGATCC	

7.2.2 Synthesis of PLL-AuNPs and PLL-AuNPs-DNA conjugate:

The synthesis of PLL-AuNPs was carried out using a one-step method. The details of this synthesis process are outlined in **chapter 3** of this thesis. In short, the synthesis was achieved by heating the $HAuCl_4$ solution of 1 mM concentration on magnetic stirrer at 80°C and rapid addition of 0.01% Poly-L-Lysine solution. The stirring was continued to obtained color change from pale yellow to wine-red which indicated formation of gold nanoparticles. Further, this mixture was cooled down at room temperature and prepared nanoparticles were washed thrice with distilled water

by centrifugation at 13000 rpm for 15 min at room temperature. The obtained nanoparticles were suspended in distilled water and stored at 4°C for further use.

The PLL-AuNPs-DNA conjugate was prepared by incubating the synthesized PLL-AuNPs with DNA probes mixture. The successful synthesis of the PLL-AuNPs-DNA conjugate for detecting K. pneumoniae DNA was achieved by applying the optimization parameters detailed in Chapter 5 for its synthesis. In short, 0.5 µM concentration of each DNA probe (probe 1 and probe 2) was incubated with synthesized PLL-AuNPs at 28ºC for 15 min reaction time. The purification step was carried out by repeating the step of centrifugation at 10000 rpm for 10 min. The pellet was resuspended in distilled water for further use.

7.2.3   Characterization PLL-AuNPs-DNA conjugate:

Synthesized PLL-AuNPs were characterized by UV-Vis spectroscopy, XRD, FTIR, EDAX, and TEM. The results were explained in **chapter 3**. In short, the PLL-AuNPs shows spherical morphology with UV-Vis absorption at 524 nm. The initial wine-red color of PLL-AuNPs changed to violet color due to DNA probe addition. The formation of PLL-AuNPs-DNA conjugate was further confirmed by UV-Vis absorption spectroscopy in range of 300-800 nm. These conjugates were then characterized by zeta (ζ) potential, dynamic light scattering (DLS), and transmission electron microscopy (TEM). The change in ζ potential and hydrodynamic diameters of PLL-AuNPs-DNA conjugate were analyzed by using BM10, Litesizer 500 with dynamic light scattering (DLS) analysis. The morphological shape and size of synthesized nanoparticles and their DNA conjugate were studied by transmission electron microscope (TEM) performed on JEM-2100F, JEOL, Japan. For this analysis, a 10 µL sample was air dried on copper grid for TEM analysis.

7.2.4   Detection of *K. pneumoniae* DNA by PLL-AuNPs-DNA conjugate:

For the UV-Vis spectroscopy-based detection of *K. pneumoniae,* the synthesized PLL-AuNPs-DNA conjugate was treated with target DNA sequence that complementary to the DNA probe sequence. Basically, the 100 µL PLL-AuNPs-DNA conjugate solution was incubated with 1 ng/µL concentration of target DNA at 28ºC

for 4-6 min. After incubation, the different concentrations of Exonuclease III enzyme (10-100 U) were added and incubated at 28ºC for further 4-5 min time period for optimization of enzyme concentration. After this Exonuclease III treatment, the mixture was examined to observe change in UV-Vis absorption spectroscopy and UV-Vis absorption at 660 nm.

The range of detection was studied by utilizing the different concentration of target DNA as (0.2-2.0 ng/µL) which were incubated with PLL-AuNPs-DNA conjugate and further treated with 50 U concentration of Exonuclease III enzyme. The detection was analyzed by observing change in UV-Vis spectrum and UV-Vis absorbance at 660 nm. The selectivity of the prepared conjugate was studied by using other different non-target bacterial DNA such as, *E. coli* and *S. aureus* with compare to target *K. pneumoniae* DNA.

7.2.5   UV-Visible absorption spectra:

Nanodrop (Multiscan skyhigh microplate reader) was used for UV-Vis absorption spectrum analysis of PLL-AuNPs and PLL-AuNPs-DNA conjugate in absence and presence of *K. pneumoniae* DNA. The Surface Plasmon Resonance (SPR) of nanoparticles and their conjugates were analyzed in the UV-Vis range of 300-800 nm to study the change in absorption due to change in size and particle distribution.

7.3   Results and discussion:

7.3.1   Synthesis and characterization of PLL-AuNPs-DNA conjugates:

Thiol-modified oligonucleotides were used for conjugation with gold nanoparticles in the nucleic acid-based pathogen detection assay. The thiol (-SH) group is added to the 5' or 3' end of the oligonucleotide sequence, which then covalently bonds with the nanoparticles [13]. Use of cationic PLL-AuNPs reduces the need of thiol modification where, the nucleic acid interacts with PLL-AuNPs through electrostatic interactions. The conjugation reaction was carried out in single tube that did not require any complex reaction steps.

Synthesis and characterization of PLL-AuNPs were described in **chapter 3**. Positive charge of PLL involved in electrostatic interactions with nucleic acid. The color shift from wine-red to violet served as the first visual indication that the PLL-AuNPs-DNA conjugate had formed. The PLL-AuNPs-DNA conjugate formation was further confirmed by observing the change in UV-Vis absorption spectrum in the range of 300-800 nm. Due to DNA conjugation the initial sharp peak of PLL-AuNPs is replaced with broad range of absorption spectrum as presented in **figure 7.1(a)**. The inset image of **figure 7.1(a)** shows wine-red to violet color change after DNA conjugation.
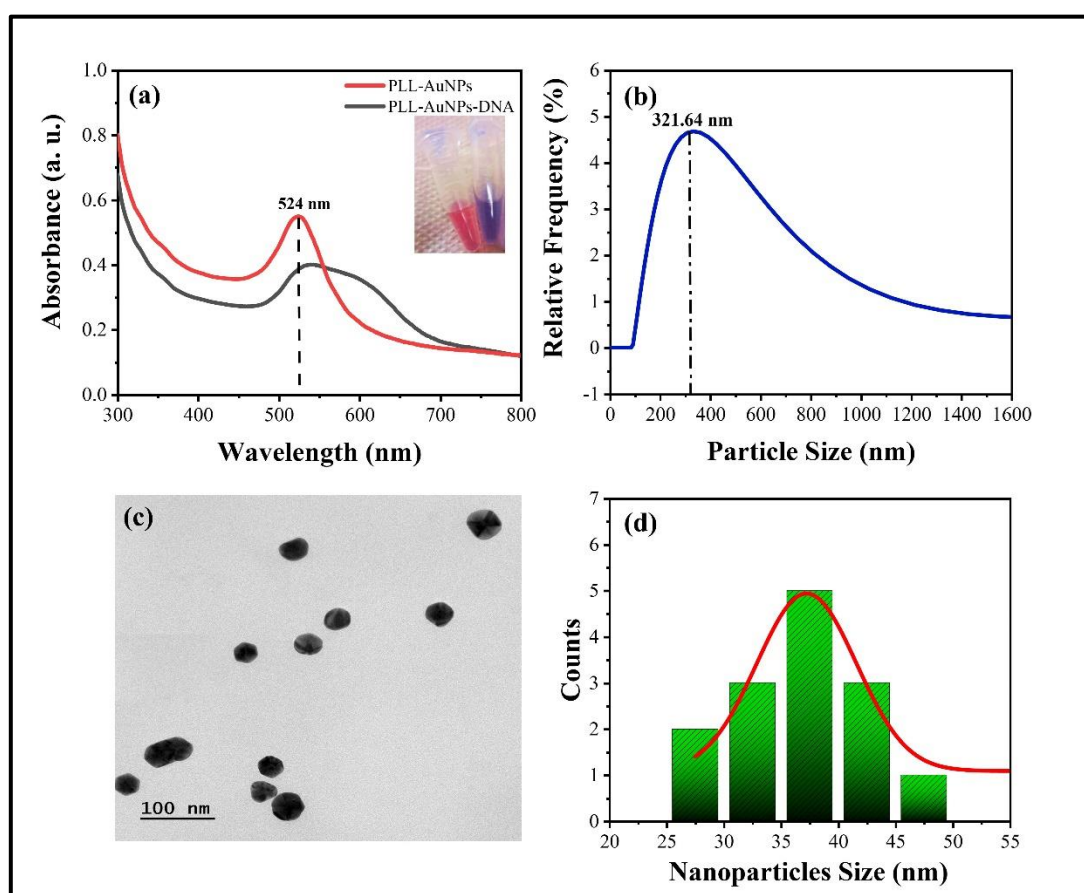
Figure 7.1: Characterization of PLL-AuNPs-DNA conjugate by (a) UV-Vis spectroscopy in comparison to PLL-AuNPs. Inset image shows color change of PLL-AuNPs (wine-red) after conjugation with DNA probes (violet), (b) hydrodynamic diameter, (c) TEM image at magnification of 50KX, and (f) Histogram of size distribution depending on TEM

The conjugate formation also shows change in zeta (ζ) potential **(table 7.2)**, where the surface positive charge of PLL-AuNPs decreases after DNA conjugation. PLL-AuNPs initially had +27.0±0.30 mV surface charge that get decreased to +0.50±0.07 mV due to conjugation of DNA probes. The change in ζ potential indicated the electrostatic interactions between PLL-AuNPs and DNA probes. The hydrodynamic size of PLL-AuNPs-DNA conjugate also increases as compare to PLL-AuNPs. As shown in **figure 7.1(b)**, the hydrodynamic size of PLL-AuNPs-DNA conjugate is 321.64 nm. The conjugation of DNA to PLL-AuNPs is evidenced by the increase in hydrodynamic size.

The **figure 7.1(c)** shows TEM micrograph of PLL-AuNPs-DNA conjugate that demonstrating spherical shaped well dispersed PLL-AuNPs-DNA conjugate. The size distribution histogram was drawn from the TEM micrograph by ImageJ application as presented in **figure 7.1(d)**. According to measurements, the PLL-AuNPs-DNA conjugates size ranges between 25-40 nm with average size of 37.02 nm.

Table 7.2: Change in zeta potential of PLL-AuNPs before and after DNA conjugation

Sr. No.	Material	Zeta potential
1.	PLL-AuNPs	+27.0±0.30 mV
2.	PLL-AuNPs-DNA	+0.50±0.07 mV

7.3.2   Principle of UV-Vis based biosensing of *K. Pneumoniae* DNA using PLL-AuNPs-DNA conjugate:

The synthesized PLL-AuNPs possesses surface positive charge obtained from cationic biopolymer PLL. Thus, two positively charged PLL-AuNPs repel each other and generate monodispersed solution of colloidal AuNPs. The initial wine-red color of PLL-AuNPs changed to violet color due to electrostatic interaction between cationic PLL-AuNPs and anionic probe DNA. Though the interactions are based on electrostatic force there is no need of thiol modification of probe DNA and surface modification of AuNPs. Thus, unmodified DNA probes are used for conjugation. The DNA probe conjugation with PLL-AuNPs shows observable change in UV-Vis absorption spectrum as the initial sharp peak of PLL-AuNPs changes to broad

spectrum range. After addition of target *K. pneumoniae* DNA to conjugate solution, there is formation of dsDNA structure between target *K. pneumoniae* DNA and DNA probe. This formed dsDNA structure is degraded by Exonuclease III enzyme as it specifically degrades dsDNA structure. The detection is based on change in UV-Vis absorption at 660 nm. The absorbance increases after addition of target *K. pneumoniae* DNA with increasing concentration of target *K. pneumoniae* DNA. Further, the absorption decreases due to degradation of dsDNA by Exonuclease III enzyme which is similar to absorbance of PLL-AuNPs. In the presence of non-complementary DNA, no dsDNA formation occurs, and as a result, no degradation by the Exonuclease III enzyme takes place. Thus, the DNA probe remains attached to PLL-AuNPs showing increased UV-Vis absorbance at 660 nm.
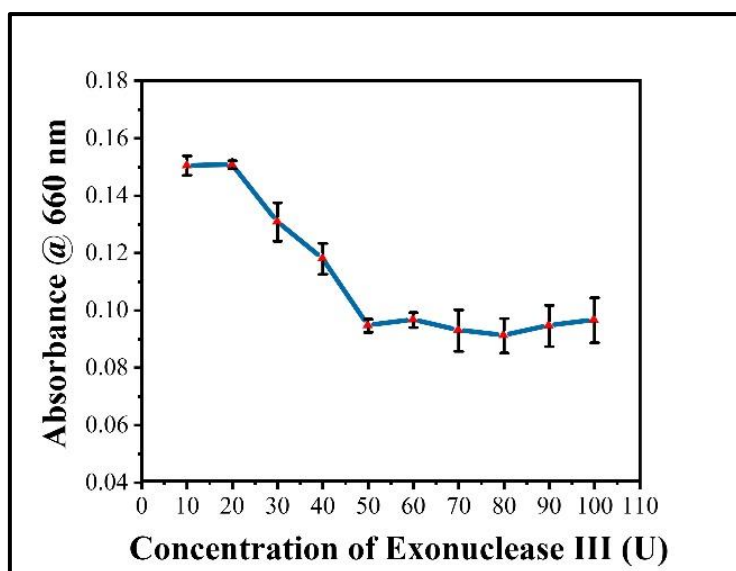
Figure 7.2: Change in absorbance at 660 nm of PLL-AuNPs-DNA conjugate in presence of target *K. pneumoniae* DNA for different concentrations of Exonuclease III (10-100 U). The error bars in the diagram display the standard deviation of the readings derived from the three measurements

7.3.3 Optimization of Exonuclease III for *K. pneumoniae* DNA detection:

The dsDNA structure was formed after addition of target *K. pneumoniae* DNA due to complementary sequence. This dsDNA sequence was then degraded with Exonuclease III as it specifically degrade dsDNA structure. To study the effect of

different concentration of Exonucease III for *K. pneumoniae* DNA detection, different concentration of Exonuclease III as 10-100 U were added to detection mixture and incubated at 28ºC for 4-5 min. The absorbance was then taken at 660 nm. As shown in **figure 7.2**, the absorbance at 660 nm decreases with increaeing concentration of Exonuclease III upto 50 U concentration and then shows slight decrese in absorption from 60-100 U of concentrations. The major decrease in absorbance is observed at 50 U concnetration of Exonuclease III enzyme. This study suggested that 50 U concentration of Exonuclease III enzyme was optimum for detection of *K. pneumoniae* DNA.

7.3.4   Detection of *K. pneumoniae* DNA:

The sensitivity or response time of the assay determines the overall length of the analysis for *K. pneumoniae* DNA detection. After addition of target *K. pneumoniae* DNA, there is formation of dsDNA which is degraded by introduction of Exonuclease III enzyme. The sensitivity of prepared PLL-AuNPs-DNA conjugate was evaluated by observing the change in UV-Vis absorption spectrum in the 300-800 nm range as well as change in UV-Vis absorption at 660 nm. As shown in **figure 7.3(a)**, the PLL-AuNPs-DNA conjugate shows broad range spectrum in presence of target *K. pneumoniae* DNA with increased absorbance at 660 nm as compared to PLL-AuNPs and PLL-AuNPs-DNA conjugate. The absorbance at 660 nm is eventually decreased after Exonuclease III treatment as a result of dsDNA degradation as shown in **figure 7.3(b)**. The sensitivity of the PLL-AuNPs-DNA conjugate is discovered after only 10-12 min including the Exonuclease III treatment in the presence of *K. pneumoniae* DNA.

The analytical performance of the bioconjugate was determined in optimized conditions. **Figure 7.4** shows the linear increase in absorbance for increasing concentrations of target *K. pneumoniae* DNA. The presented data demonstrated the linear relationship between absorbance of bioconjugate at 660 nm with concentration of target *K. pneumoniae* DNA with a slope (0.08507±0.00494) and intercept (0.11709±0.00475). A good fitting parameter or a linear relationship ($r^2 = 0.097369$)

shows the sensitivity of the biosensor. In this case, the limit of detection was 0.78 ng/µL.
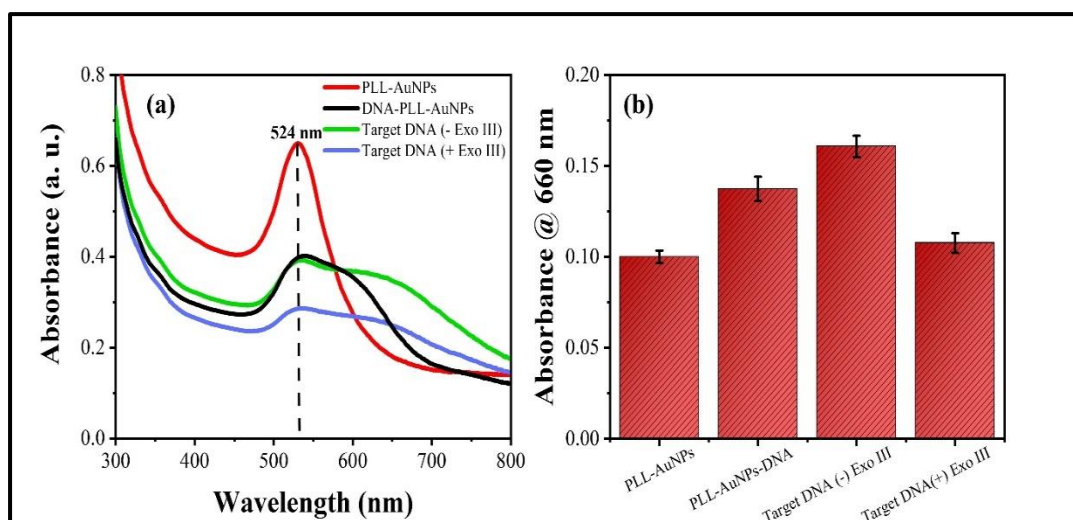
Figure 7.3: Change in (a) UV-Vis absorption spectra (300-800 nm) and (b) absorbance at 660 nm of PLL-AuNPs and PLL-AuNPs-DNA in absence and presence target *K. pneumoniae* DNA with and without treatment of Exonuclease III. The error bars in the diagram display the standard deviation of the readings derived from the three measurements
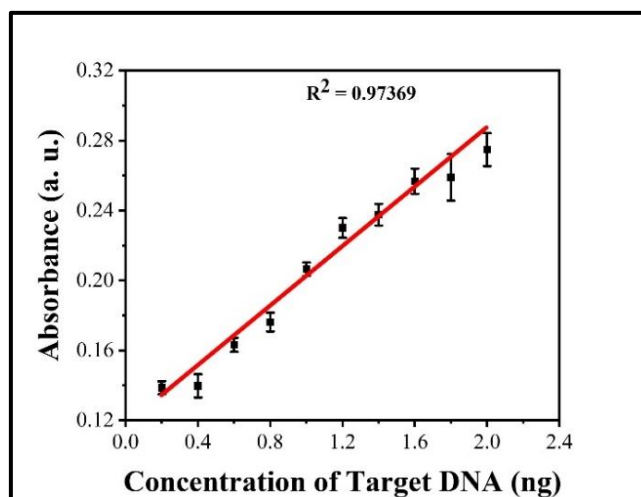
Figure 7.4: Linear regression of corresponding absorbance at 660 nm of bioconjugate in presence of different concentrations of target *K. pneumoniae* DNA. The error bars in the diagram display the standard deviation of the readings derived from the three measurements

Intriguingly, according to the hypothesis, in the absence of target *K. pneumoniae* DNA, PLL-AuNPs-DNA conjugates were predominantly distributed in solution due to electrostatic interactions, however in the presence of target viral RNA, the dsDNA structure was generated which get degraded by Exonuclease III. The UV-Vis absorbance of the PLL-AuNPs-DNA conjugate was decreased after enzyme treatment in presence of target *K. pneumoniae* DNA whereas, in absence of target *K. pneumoniae* DNA the absorbance was similar to the absorbance of PLL-AuNPs-DNA conjugate.

7.3.5 Selectivity of PLL-AuNPs-DNA conjugate for *K. pneumoniae* DNA detection:

The selectivity of the biosensor towards its target is another crucial factor for every biosensor. The selectivity of the biosensor was evaluated by examining the detection using different DNA of different pathogens as, *E. coli* and *S. aureus*. The conjugate shows maximum absorbance at 660 nm in presence of target *K. pneumoniae* DNA with comparison to non-target one **(figure 7.5)**. It was found that, after the Exonuclease III treatment the absorbance at 660 nm of conjugate was decreased in case of target *K. pneumoniae* DNA whereas, there was no decrease in absorbance for non-complementary DNA as shown in **figure 7.5**. This change confirms that a decrease in absorbance at 660 nm after Exonuclease III treatment occurs only in the presence of target *K. pneumoniae* DNA containing the K. pneumoniae K2A gene. In contrast, no decrease in absorbance is observed when non-target DNA is present after Exonuclease III treatment. The *K2A* gene of *K. pneumoniae* involved in formation of biofilm that responsible for pathogenesis. *K2A* gene is harboring the carbapenemase gene that hydrolyze the β lactamase present in antibiotics. Thus, the *K2A* gene is responsible to develop resistance against many β lactam antibiotics [13, 14].

AuNPs conjugated with thiol modified oligonucleotide were reported for detection of various pathogens by optical, electrochemical, and spectrometric method. AuNPs based colorimetric and spectrometric detection of pathogen have been reported for their specificity and sensitivity with compare to other conventional

methods [15, 16]. Oligonucleotide conjugated AuNPs were utilized for detection of many bacteria such as, *Brucella* spp. [17] *Mycobacterium tuberculosis* [18], *Escherichia coli* [19], *Pseudomonas aeruginosa* [20], *Klebsiella pneumoniae* [21], and *Listeria monocytogenes* [22] with considerable specificity and sensitivity. Very few studies are available on utilization of cationic AuNPs with unmodified nucleic acid conjugation for detection of pathogens such as, cysteamine capped AuNPs conjugated with nucleic acid that utilized for SARS-CoV-2 RNA detection [23]. The present study provides the use of cationic PLL-AuNPs conjugated with unmodified nucleic acid through electrostatic interactions for detection of *K. pneumoniae* DNA. The proposed study does not require any sophisticated laboratory facilities for detection purpose without PCR amplification. The method is easy to handle and dependent on UV-Vis absorption at 660 nm after Exonuclease III treatment. The use of cationic AuNPs and unmodified nucleic acid probe for detection of *K. pneumoniae* DNA is the new aspect of this study.
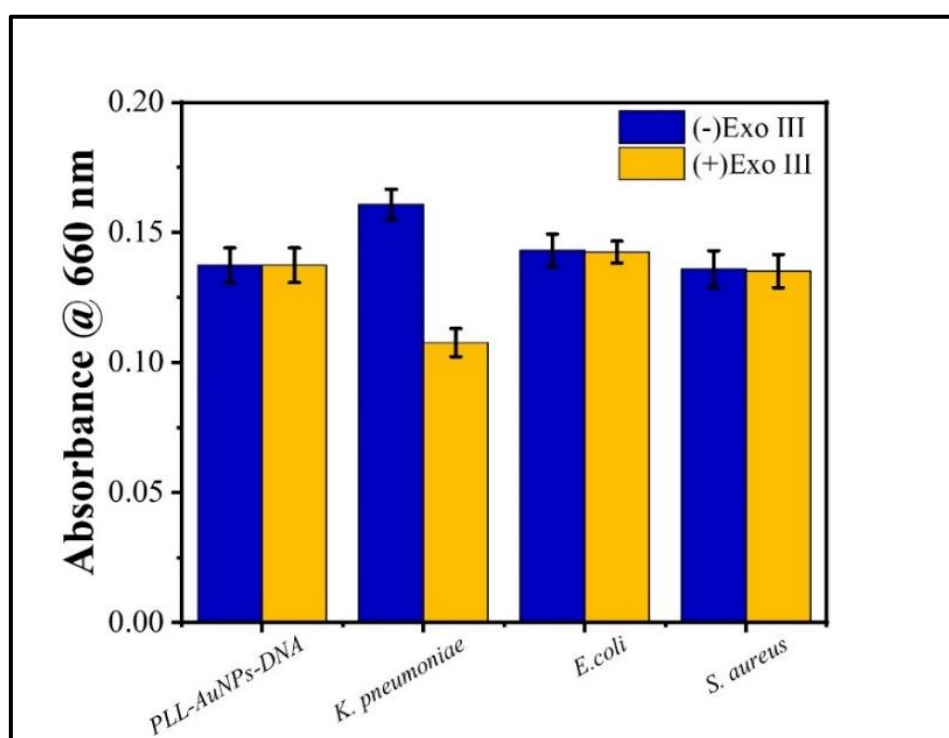
Figure 7.5: Change in absorbance at 660 nm of PLL-AuNPs-DNA conjugate in presence target DNA (*K. pneumoniae*) and Non-target DNA (*E. coli, S. aureus*) with and without Exonuclease III treatment

7.4   Conclusions:

The current study presents the application of cationic PLL-AuNPs conjugated with probe DNA for *K. pneumoniae* DNA specific for *K2A* gene. The PLL-AuNPs-DNA conjugate was prepared by using 1 µM concentration of probe DNA (0.5 µM of each probe) simply incubating with PLL-AuNPs at 28ºC for 15 min. The UV-Vis based detection of bacterial nucleic acid using cationic PLL-AuNPs and Exonuclease III treatment shows considerable potential as a biosensor with a high degree of specificity and sensitivity, as well as quick detection within 10-12 minutes at the level of 0.78 ng/µL concentration. The PLL-AuNPs-DNA conjugate was utilized for detection of bacterial nucleic acid without a need of any complex instrumentation. The PLL-AuNPs-DNA based bacterial nucleic acid with Exonuclease III treatment showed decreased UV-Vis absorbance at 660 nm in presence of target *K. pneumoniae* DNA. The detection procedure was carried out in a single tube with simple and minimum steps thus, offers simplicity. This method also offers rapidity as it completed within 10-12 min including Exonuclease III treatment. It also provides specificity as the method specifically detects *K. pneumoniae* DNA over other non-target bacterial DNA (*E. coli* and *S. aureus*). Use of Exonuclease III enzymes confirm the formation of dsDNA due to presence of target complementary DNA that, get degraded and results in decreased absorption at 660 nm. Therefore, the PLL-AuNPs-DNA conjugate with Exonuclease III treatment based biosensing method would might offer a viable platform for quick and simple detection of *K. pneumoniae* DNA.

7.5   References:

[1]   https://www.healthline.com/health/klebsiella-pneumonia#risk-factors

[2]   Ranjbar R, Fatahian Kelishadrokhi A, Chehelgerdi M. Molecular characterization, serotypes and phenotypic and genotypic evaluation of antibiotic resistance of the *Klebsiella pneumoniae* strains isolated from different types of hospital-acquired infections. Infection and drug resistance. 2019;12(1):603-11.

[3]   Mirzaie A, Ranjbar R. Antibiotic resistance, virulence-associated genes analysis and molecular typing of *Klebsiella pneumoniae* strains recovered from clinical samples. AMB Express. 2021;11(1):1-11.

[4]   Jun JB. *Klebsiella pneumoniae* liver abscess. Infection & chemotherapy. 2018;50(3):210-17.

[5]   Paczosa MK, Mecsas J. *Klebsiella pneumoniae*: going on the offense with a strong defense. Microbiology and molecular biology reviews. 2016;80(3):629-61.

[6]   https://www.healthline.com/health/klebsiella-pneumonia#risk-factors

[7]   Feng J, Cui X, Du B, Zhao H, Feng Y, Cui J, Yan C, Gan L, Fan Z, Fu T, Xu Z. Detection and Quantification of *Klebsiella pneumoniae* in Fecal Samples Using Digital Droplet PCR in Comparison with Real-Time PCR. Microbiology Spectrum. 2023;11(4):4249-59.

[8]   Osman EA, El-Amin N, Adrees EA, Al-Hassan L, Mukhtar M. Comparing conventional, biochemical and genotypic methods for accurate identification of *Klebsiella pneumoniae* in Sudan. Access microbiology. 2020;2(3):96-100.

[9]   Nooranian S, Mohammadinejad A, Mohajeri T, Aleyaghoob G, Kazemi Oskuee R. Biosensors based on aptamer-conjugated gold nanoparticles: a review. Biotechnology and Applied Biochemistry. 2022;69(4):1517-34.

[10]   Patil T, Gambhir R, Vibhute A, Tiwari AP. Gold nanoparticles: Synthesis methods, functionalization and biological applications. Journal of Cluster Science. 2023;34(2):705-25.

[11]   Si P, Razmi N, Nur O, Solanki S, Pandey CM, Gupta RK, Malhotra BD, Willander M, de la Zerda A. Gold nanomaterials for optical biosensing and bioimaging. Nanoscale Advances. 2021;3(10):2679-97.

[12]   https://en.wikipedia.org/wiki/Exonuclease

[13]   Ahmadi S, Kamaladini H, Haddadi F, Sharifmoghadam MR. Thiol-capped gold nanoparticle biosensors for rapid and sensitive visual colorimetric detection of *Klebsiella pneumoniae*. Journal of Fluorescence. 2018;28(1):987-97.

[14]   Carnerero JM, Jimenez-Ruiz A, Castillo PM, Prado-Gotor R. Covalent and Non-Covalent DNA–Gold-Nanoparticle Interactions: New Avenues of Research. ChemPhysChem. 2017;18(1):17-33.

[15]   Remya P, Shanthi M, Sekar U. Occurrence and characterization of hyperviscous K1 and K2 serotype in *Klebsiella pneumoniae*. Journal of laboratory physicians. 2018;10(3):283-87.

[16]   Bansal SA, Kumar V, Karimi J, Singh AP, Kumar S. Role of gold nanoparticles in advanced biomedical applications. Nanoscale Advances. 2020;2(9):3764-87.

[17]   Sattarahmady N, Tondro GH, Gholchin M, Heli H. Gold nanoparticles biosensor of *Brucella* spp. genomic DNA: Visual and spectrophotometric detections. Biochemical engineering journal. 2015;97(1):1-7.

[18]   Zhang X, Feng Y, Duan S, Su L, Zhang J, He F. Mycobacterium tuberculosis strain H37Rv electrochemical sensor mediated by aptamer and AuNPs–DNA. ACS sensors. 2019;4(4):849-55.

[19]   Xie Y, Huang Y, Wu J. A trigger-based aggregation of aptamer-functionalized gold nanoparticles for colorimetry: An example on detection of *Escherichia coli* O157:H7. Sensors and Actuators B: Chemical. 2021;339(1):865-77.

[20]   Schmitz FR, Cesca K, Valério A, de Oliveira D, Hotza D. Colorimetric detection of *Pseudomonas aeruginosa* by aptamer-functionalized gold nanoparticles. Applied Microbiology and Biotechnology. 2023;107(1):71-80.

[21]   Deb A, Gogoi M, Mandal TK, Sinha S, Pattader PS. Specific Instantaneous Detection of *Klebsiella pneumoniae* for UTI Diagnosis with a Plasmonic Gold Nanoparticle Conjugated Aptasensor. ACS Applied Bio Materials. 2023;6(8):3309-17.

[22]   Fu Z, Zhou X, Xing D. Sensitive colorimetric detection of *Listeria monocytogenes* based on isothermal gene amplification and unmodified gold nanoparticles. Methods. 2013;64(3):260-66.

[23]   Jamaluddin ND, Ibrahim N, Yusof NY, Goh CT, Tan LL. Optical reflectometric measurement of SARS-CoV-2 (COVID-19) RNA based on cationic cysteamine-capped gold nanoparticles. Optics & Laser Technology. 2023;157(1):763-72.

Chapter VIII

Summary and conclusions

Summary and conclusions

Modern nanotechnology methods have been successfully replacing conventional medical diagnosis and treatments due to their higher sensitivity, rapidity and efficiency. The conventional biosensing methods such as, immunological assays and RT-PCR for pathogen detection are tedious and time consuming. Though they provide specificity and sensitivity these methods have some drawbacks like, need of sophisticated laboratory, skilled technician, and expensive chemicals. Therefore, there is need to develop rapid, sensitive, and easy to handle biosensing methods for pathogen detection. Nucleic acid is considered as promising therapeutic tool for the treatment of many genetic disorders, diabetes, and for diagnosis applications. Nucleic acid-based biosensors are now emerged for rapid and sensitive detection of pathogens. Nucleic acids are highly sensitive to nuclease degradation thus, needed delivery vehicle for stabilization and protection.

Nanoparticles based biosensors are gaining attention of researchers for their unique characterization. Among them, gold nanoparticles (AuNPs) are widely applied in field of biomedical due to their desirable physico-chemical characterization. AuNPs are used in various biomedical applications including biosensing, gene delivery, drug delivery, and bioimaging. Easy surface functionalization of AuNPs with biomolecules makes them suitable candidate for various biomedical applications.

The conjugation of gold nanoparticles with nucleic acids, such as DNA or RNA, enhances the sensitivity and specificity of biosensors by enabling easy detection of target molecules. The surface plasmon resonance (SPR) effect of AuNPs amplifies the signal, allowing for the detection of very low concentrations of target analytes. These conjugates are widely used in various biosensing techniques, including nucleic acid hybridization, enzyme-linked assays, and pathogen detection, offering advantages such as rapid response times, cost-effectiveness, and high sensitivity. This study focuses on synthesis of cationic gold nanoparticles-nucleic acid conjugate for biosensing applications. The schematics of the present work is presented as follows:

Schematics of the present work

Synthesis of AuNPs and PLL-AuNPs

↓

Characterization of AuNPs and PLL-AuNPs (UV-Vis Spectroscopy, FTIR, TEM, Zeta potential, and DLS)

↓

Optimization of PLL-AuNPs-nucleic acid conjugate (Reaction time, Concentration of standard DNA, pH, and salinity) and their characterization (UV-Vis Spectroscopy, TEM, zeta Potential, and band shift assay)

↓

Biomedical applications of PLL-AuNPs-nucleic acid conjugate

Optical biosensing of Viral RNA (SARS-CoV-2 RNA)	Electrochemical biosensing of Viral RNA (SARS-CoV-2 RNA)	Biosensing of bacterial DNA (*Klebsiella pneumoniae* DNA)

Chapter I provides an introduction of the presented thesis work. The chapter deals with a general introduction of various biomedical applications of gold nanoparticle. It displays various synthesis methods of AuNPs including chemical, physical, and biological methods. This clarifies the easy and less expensive synthesis method for AuNPs. The chapter also explain surface functionalization strategies for AuNPs with different chemicals and biomolecules. It clarifies the easy surface modification of AuNPs that used for various biomedical applications. The chapter further discuss about the covalent and non-covalent interactions of AuNPs with nucleic acid. The different biomedical applications of AuNPs and their nucleic acid conjugates are discussed along with references including biosensing and gene delivery applications. The drawbacks of conventional biosensing methods and the need of AuNPs based biosensor development is highlighted in this chapter. The advantages of using cationic AuNPs for nucleic acid conjugation are explained. The electrostatic interactions between cationic AuNPs and anionic nucleic acid are discussed. The objective of the research work is synthesis of surface functionalized AuNPs-nucleic acid conjugate for various biomedical applications such as, optical and electrochemical biosensing.

Negatively charged AuNPs are widely reported for biosensing applications with thiol modified nucleic acid conjugation. The chapter discusses that very few data is reported for cationic AuNPs for biosensing applications without the need of thiol modification. Nucleic acid conjugated AuNPs are reported for gene delivery, optical, and electrochemical biosensing applications. The reported data showed AuNPs based biosensors are able to detect pathogens at very low concentrations such as, nM to pM.

Chapter II deals with the instrumentation that were used in this study for characterization purpose. It discusses the detailed information of instruments used for characterization such as, UV-Vis spectroscopy, X-ray Diffraction (XRD) analysis, Fourier Transform Infrared spectroscopy (FTIR), Energy Dispersive X-ray (EDAX) analysis, transmission electron microscopy (TEM), Zeta potential, and Dynamic Light Scattering (DLS) analysis. The chapter presents the working principle and specifications employed for study of nanoparticles.

Chapter III presents the synthesis and characterization of citrate capped AuNPs (AuNPs) and Poly-L-Lysine functionalized AuNPs (PLL-AuNPs). The PLL is a cationic biopolymer made up of Lysine residue that were used for the synthesis of cationic AuNPs. The chapter gives detail about the synthesis method, its mechanism, and physicochemical characterization of AuNPs and PLL-AuNPs.

The synthesis of AuNPs is based on chemical reduction of gold precursor where, sodium citrate was used as reducing agent. The formation of AuNPs was confirmed by observing color change from pale yellow to wine-red and then further confirmed by UV-Vis absorption spectroscopy by obtaining absorption peak at 532 nm. The XRD analysis represented the crystalline nature of AuNPs that showed four distinguishable peaks at 2θ degree value as 37.92, 44.14, 64.37, and 77.41° corresponding to the planes of (111), (200), (220), and (311), respectively. FTIR data showed presence of O-H functional group of citrate involved in synthesis of AuNPs. The TEM study shows spherical morphology of AuNPs within 20-30 nm size range with average size 19.1 nm. Zeta potential analysis confirmed the negative surface charge present on surface of AuNPs.

The chapter further presented the one pot synthesis method for PLL-AuNPs. Here, the PLL itself acted as reducing as well as functionalizing agent. The synthesis was carried out using 1 mM concentration of $HAuCl_4$ by 0.01% PLL solution at 80ºC with pH 6 within 6 min of reaction time. The color changed from pale yellow to wine-red indicates formation of PLL-AuNPs which was further validated by UV-Vis absorption spectroscopy. PLL-AuNPs showed UV-Vis absorption spectrum at 524 nm. The synthesized PLL-AuNPs was further evaluated by XRD, FTIR, EDAX, TEM, and DLS. FTIR study showed the presence of amine and O-H functional group of PLL that involved in synthesis. The synthesized PLL-AuNPs showed spherical morphology with average size of 17 nm. The cationic nature of PLL-AuNPs was analyzed by zeta potential showing positive surface charge (+27.0±0.30 mV). Later in the chapter, a comparison was made between characterization of AuNPs and PLL-AuNPs.

In **chapter IV** synthesis of PLL-AuNPs-NA conjugate by optimizing the synthesis parameters such as, nucleic acid concentration, reaction time, pH, and NaCl

concentration has been studied. The PLL-AuNPs-NA conjugate was synthesized using 100 µg concentration of calf thymus DNA at 28ºC, at pH 6 with 15 min incubation time and 0.3 mM NaCl concentration. The chapter further present different characterization of synthesized PLL-AuNPs-NA conjugate. Initial wine-red color of PLL-AuNPs changed to violet after conjugation of nucleic acid. The prepared PLL-AuNPs-NA conjugate was further characterized by UV-Vis spectroscopy that showed change in absorption spectrum as compare to PLL-AuNPs. The surface positive charge of PLL-AuNPs decreased due to negatively charged nucleic acid conjugation which was analysed by zeta potential analysis. Also, the TEM result showed increased size of conjugate in comparison to PLL-AuNPs. The conjugate formation was finally confirmed by band shift or electrophoretic mobility shift assay. It confirmed electroneutrality of PLL-AuNPs-NA conjugate by stacking of band into the well due to electrostatic interactions between positively charged PLL-AuNPs and negatively charged nucleic acid.

Chapter V presented the application of PLL-AuNPs-NA conjugate for optical biosensing of viral (SARS-CoV-2 N gene) nucleic acid. The antisense oligonucleotide (ASO) is a single stranded DNA sequence which was conjugated to cationic PLL-AuNPs through electrostatic interactions. Here, the unmodified ASO sequence was used for conjugation. The PLL-AuNPs-ASO conjugate was prepared by optimizing the synthesis parameters such as, concentration of ASO, incubation time, and temperature. 1 µM concentration of ASO was incubated with PLL-AuNPs at 28ºC for 15 min to get PLL-AuNPs-ASO conjugate. The conjugate formation was first visibly confirmed by observing color change from wine-red to violet. Then it was further characterized by UV-Vis spectroscopy to observe change in UV-Vis absorption spectrum. Initial sharp peak of PLL-AuNPs was replaced with broad range of spectrum after ASO conjugation. TEM microscopic study showed increased size of particles that confirmed the formation of conjugate. The initial positive surface charge of PLL-AuNPs (+27.0±0.3 mV) decreased (+0.40±0.02 mV) after ASO conjugation.

The optical biosensing of SARS-CoV-2 RNA was studied by PLL-AuNPs-ASO conjugate. The target SARS-CoV-2 RNA of N gene was added to PLL-AuNPs-ASO conjugate where; target RNA combined with complementary ASO sequence that

released PLL-AuNPs. After addition of NaCl, PLL-AuNPs gets aggregated which was observed by naked eyes. The target SARS-CoV-2 RNA was detected within 4-5 min of incubation time by naked eyes. The detection was also confirmed by observing change in UV-Vis absorption spectrum as well as change in absorption at 660 nm. The TEM microscopic images clarify the aggregate formation. The specificity of the biosensing was analysed against other viral RNA, Influenza A. There was no aggregation in presence of Influenza A RNA as compare to SARS-CoV-2 RNA. The developed biosensing assay was able to detect RNA of 0.52 ng/µL concentration. Finally, the PLL-AuNPs-ASO conjugate was utilized to detect SARS-CoV-2 RNA from clinical samples. It was found that the synthesized conjugate can successfully detect the SARS-CoV-2 RNA from COVID-19 positive samples of individuals.

Chapter VI presented the electrochemical biosensing of SARS-CoV-2 RNA by using PLL-AuNPs-NA conjugate. Glassy carbon electrode (GCE) was used as working electrode and methylene blue was used as electrochemical indicator. The biosensor was developed by modifying the GCE with PLL-AuNPs and ASO. The polished GCE was modified with PLL-AuNPs via drop cast method while, ASO was adsorbed on PLL-AuNPs through electrostatic interactions between them. After modification the modified GCE was characterized with Cyclic Voltammetry (CV) with 20 mV scan rate. Increased current after addition of PLL-AuNPs indicated the modification of GCE with PLL-AuNPs. The change in current with addition of ASO and then target RNA characterized the modified GCE for successful formation of electrochemical biosensing.

The electrochemical detection of SARS-CoV-2 RNA was studied by modified GCE (ASO/PLL-AuNPs/GCE). The analytical performance of the developed electrochemical biosensor was studied by DPV, EIS, and SWV. Methylene blue was used as electrochemical indicator that separately binds with ASO and dsDNA or DNA-RNA hybrid. The electrochemical biosensor was specific for SARS-CoV-2 RNA detection with 30.2 nM detection limit. The reproducibility and stability were studied by DPV and SWV. The Biosensor showed reproducibility and stability with 3.99 and 2.16% RSD values, respectively. It was found that, the developed biosensor

was able to differentiate between complementary (SARS-CoV-2 RNA) and non-complementary (Influenza A RNA) RNA sequences.

Chapter VII presented the UV-Vis based bacterial nucleic acid (*K. pneumoniae* K2A gene) biosensing application of PLL-AuNPs-NA conjugate in presence of Exonuclease III enzyme. The 0.5 µM concentration of each DNA probe that was complementary to bacterial DNA was conjugated to PLL-AuNPs by incubation at 28˚C for 15 min. After visible confirmation, these conjugates were characterized by UV-Vis spectroscopy, TEM, and zeta potential showing broad UV-Vis absorption, increased TEM size and decreased surface positive charge with comparison to PLL-AuNPs.

Then the target *K. pneumoniae* DNA was added to conjugate where dsDNA structure was formed between target DNA and probe DNA. The 50 U concentration of Exonuclease III was added that specifically degraded the dsDNA structure. The UV-Vis absorbance of mixture was taken at 660 nm to observe the change in absorbance within 4-6 min of Exonuclease III treatment. The developed biosensing method was able to detect 0.78 ng/µL concentration of DNA within 10-12 min of time period including Exonuclease III treatment. The specificity of the biosensing was evaluated by using different non-complementary bacterial DNA such as, *E. coli* and *S. aureus*.

Major Conclusions of the study:

1. Cationic AuNPs are synthesized in single step using Poly-L-Lysine (PLL) as reducing as well as stabilizing agent.
2. The synthesis of PLL-AuNPs is achieved by adding PLL solution in 1 mM gold precursor ($HAuCl_4$) solution at 80ºC, at pH 6 within 5-6 min of reaction time.
3. The PLL-AuNPs shows wine-red color with 524 nm UV-Vis absorption, surface positive charge (+27.0±0.30 mV), and spherical morphology with 17 nm average size.
4. The cationic PLL-AuNPs are conjugated with unmodified anionic nucleic acid through electrostatic interactions. Therefore, minimizing the need of thiol modification of nucleic acid.

5. The nucleic acid is incubated with PLL-AuNPs at 28˚C and at pH 6 for 15-20 min to form a PLL-AuNPs-NA conjugate.

6. The PLL-AuNPs-NA conjugates are utilized for viral and bacterial nucleic acid detection by optical and electrochemical biosensing method.

7. The PLL-AuNPs are conjugated with 1 µM concentration of antisense oligonucleotide (ASO) and are utilized for optical biosensing of SARS-CoV-2 RNA with 0.52 ng/µL detection limit. The detection is confirmed by observing the change in UV-Vis absorption spectrum and UV-Vis absorption at 660 nm.

8. This optical biosensing approach is used to detect SARS-CoV-2 RNA from clinical samples of COVID-19 patients.

9. The PLL-AuNPs-ASO conjugate is also used for electrochemical biosensing of SARS-CoV-2 RNA using glassy GCE. The analytical performance of electrochemical biosensor is studied by DPV, EIS, and SWV with 30.2 nM detection limit. The biosensor showed reproducibility and stability with 3.99 and 2.16% RSD values, respectively.

10. The PLL-AuNPs are conjugated with DNA probe that complementary to *K. pneumoniae* DNA for UV-Vis based detection of *K. pneumoniae* DNA in presence of Exonuclease III enzyme with 0.78 ng detection limit.
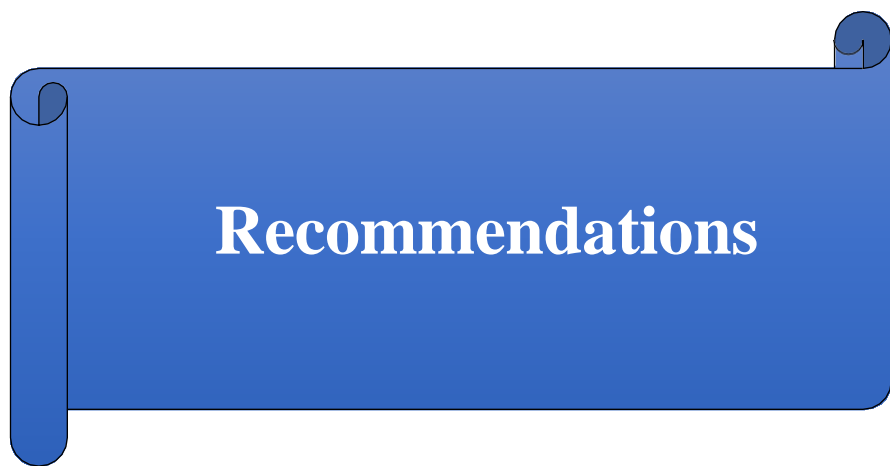
Recommendations

Recommendations

9.1   Recommendations:

The present study on gold nanoparticles and their interactions with nucleic acid opens new promising approach in nanobiotechnology. Gold nanoparticles have attracted interest of researchers due to their desirable characteristics such as, size tunability, easy synthesis and surface modification, biocompatible nature, and large surface to volume ratio. However, nucleic acids are the biomolecules that acts as promising therapeutic tool in diagnosis and therapy. Study of gold nanoparticles-nucleic acid conjugate has potential implications in various biomedical applications including biosensing and gene delivery.

It is recommended that in the present study, Poly-L-Lysine functionalized gold nanoparticles (PLL-AuNPs) are synthesized by one pot or single step synthesis method. The synthesized PLL-AuNPs possesses surface positive charge due to cationic biopolymer PLL. Interactions of AuNPs with nucleic acid require thiol modification and other surface modifying chemicals. Use of cationic AuNPs minimizes the need of thiol modification as they interact with anionic nucleic acid through electrostatic interactions. hence, role of other cationic polymers can be explored for preparation of AuNPs as reducing agent.

In this study, the mechanism of positively charged PLL functionalized AuNPs (PLL-AuNPs) is described. The amine (-NH$_2$) group of PLL may be responsible for reduction of gold precursor to generate PLL-AuNPs. Detailed study about the mechanism of PLL-AuNPs synthesis is needed to give exact reaction occurred between PLL and gold precursor. The use of PLL introduces positive surface charge to AuNPs that enhances nucleic acid binding to AuNPs. Instead of PLL, other cationic polymers such as, cysteine, polyethyleneimine (PEI) can be used for synthesis of cationic AuNPs.

The synthesized cationic PLL-AuNPs were conjugated with anionic nucleic acid by electrostatic interactions. The synthesis was carried out by optimizing the

synthesis parameters like, nucleic acid concentration, reaction time, pH, and salinity. The conjugate formation was confirmed by gel retardation assay by observing the electroneutrality point. The conjugate formation further needs to be studied for nuclease protection assay and ethidium bromide intercalation assay to check whether the PLL-AuNPs could provide adequate protection to nucleic acid from nucleases or not. Also, to understand the interactions between nucleic acid and AuNPs, more are needed regarding their characterization and stability.

The synthesized PLL functionalized gold nanoparticles-nucleic acid (PLL-AuNPs-NA) conjugate was then utilized for optical and electrochemical detection of viral/bacterial nucleic acid. The specificity of conjugate is further improved by comparing it with different viral/bacterial nucleic acid samples other than target. The specificity is also need to check in presence of body fluids like, saliva, serum and urine. More clinical samples should be tested for analysing the efficacy of developed PLL-AuNPs-NA conjugate to be used for industrial applications.

The proposed PLL-AuNPs-NA conjugate-based detection method is simple, easy to handle, and do not need any sophisticated laboratory facilities. The studied applications can be potentially used for clinical diagnosis at industrial level with minimum modifications. In addition to biosensing applications, the PLL-AuNPs-NA conjugate can also be utilized in gene delivery application.

Annexure

PATIENT CONSENT FORM

D Y Patil Education society (Deemed to be University) Department of Medical Biotechnology and Stem cell & Regenerative Medicine, Center for Interdisciplinary Research, Kolhapur

I Miss. Tejaswini Pruthviraj Patil Ph.D. student working under guidance of Dr. Arpita Pandey Tiwari (Associate Professor), department of Medical Biotechnology and Stem Cell & Regenerative Medicine, Center for Interdisciplinary Research, has prepared the following consent form to be filled by patient, at the time of sample collection needed for my research work entitled "Study of biomedical applications of surface functionalized gold nanoparticles - nucleic acid conjugate".

I, Mr/Mrs/Ms ………….. Gender ………… Age: …………………
Residing at...

Do hereby confirm that:

(i) I have been asked by the Ph.D. student whether I wish to participate in a study under the aegis of D Y Patil Education society (Deemed to be University) Department of Medical Biotechnology and Stem cell & Regenerative Medicine, Center for Interdisciplinary Research.

(ii) The nature of the study being undertaken by the student as well as the extent of my participation in it, have been duly explained to me in a language that I understand.

(iii) The potential risks and consequences associated with this study have also been duly explained to me in a language that I understand.

(iv) I also understand that my participation in this study is only for the benefit of advancement in the field of research and that at no point in time is my participation being solicited for any pecuniary gain by the student.

(v) I have also been explained that I am in no way obliged to participate in the study and that, once I have agreed to participate in the study, I am still free to withdraw from participation in the study at any point in time upon notifying the Ph.D. student in writing in the prescribed form without assigning any reason.

(vi)There will be no financial transaction between myself and Ph.D. student for my participation in that study;

(vii) I have been explained that any data collected out of my participation in the study will only be used for research work.

(viii) I have also been reassured that any publication of the data collected during the course of the study or any publication of its conclusions, shall be done on a 'no names' basis and shall under no circumstances reveal my personal identity. Any personal details likely to reveal my personal identity shall at all times remain confidential;

PATIENT CONSENT FORM

D Y Patil Education society (Deemed to be University) Department of Medical Biotechnology and Stem cell & Regenerative Medicine, Center for Interdisciplinary Research, Kolhapur

(ix) The contents and effect of this consent form have also been duly explained to me in a language that I understand.

By affixing my signature/thumb print hereto, I am therefore freely and voluntarily signifying my consent, intent and willingness to participate in the study of the student researcher for the purposes of the research work. I also certify that my right to privacy has not been infringed in any manner.

[SIGNATURE/THUMB PRINT OF PARTICIPANT]

DATE:

WITNESSED BY:

(1) NAME:

TITLE/CAPACITY:

SIGNATURE:

(2) NAME:

TITLE/CAPACITY:

SIGNATURE:

D. Y. PATIL MEDICAL COLLEGE KOLHAPUR

Constiuent Unit of D. Y. Patil Education Society (Deemed to be University), Kolhapur.
Re-accredited by NAAC with 'A' Grade

Dr. Rakesh Kumar Sharma	Padmashree Dr. D. Y. Patil	Dr. Sanjay D. Patil
Dean & Professor (Obst. & Gyn)	Founder president	President

No. DYPMCK/....427..../2021/IEC

Date: 2 4 MAR 2021

INSTITUTIONAL ETHICS COMMITTEE, D. Y. PATIL MEDICAL COLLEGE, KOLHAPUR.

This is to certify that the research project titled,

"Study of Biomedical Applications of Surface Functionalized Gold Nanoparticles - Nucleic Acid Conjugate."

Submitted by : **Ms. Tejaswini Pruthviraj Patil**

Under the supervision of appointed Guide (if any): **Dr. Arpita Pandey Tiwari**

Has been studied by the Institutional Ethics Committee (IEC) at its meeting held on **24/03/2021** and granted approval for the study with due effect with the following caveats:

1. If you desire any change in the protocol or standard recording document at any time, please submit the same to the IEC for information and approval before the change is implemented.
2. As per recommendations of ICMR, you must register your study with the Central Trials Registry- India (CTRI), hosted at the ICMR's National Institute of Medical Statistics (http://icmr-nir.s nic.in). The registration details as provided by the website are to be submitted to the Institutional Ethics Committee within a period of 3 months from issue of this letter.
3. All serious and/or unexpected adverse events due to the drug/procedures tested in the study must be informed to the IEC within 24 hours and steps for appropriate treatment must be immediately instituted.
4. In case of injury/disability/death of any participant attributable to the drug/procedure under study, all compensation is to be made by the sponsor of the study.
5. The Chief investigator/Researcher must inform the IEC immediately if the study is terminated earlier than planned with the reasons for the same.
6. The final results of the study must be communicated to the IEC within 3 months of the completion of data collection.
7. The researcher must take all precautions to safeguard the rights, safety, dignity and wellbeing of the participants in the study.
8. The researcher must be up to date about all information regarding the risk/benefit ratio of any drug/procedure being used and any new information must be conveyed to the IEC immediately. The IEC reserves the right to change a decision on the project in the light of any new knowledge.
9. Before publishing the results of the study, the researcher must take permission from the Dean of the Institution.
10. Annual progress report should be submitted for all sponsored projects to the committee.
11. Unethical conduct of research in non-sponsored projects will result in withdrawal of the ethics approval and negation of all data collected till that date.

Prof. C. D. Lokhande
(Act. Member Secretary, IEC)

Publications

Office of the Controller General of Patents, Designs & Trade Marks
Department of Industrial Policy & Promotion,
Ministry of Commerce & Industry,
Government of India

(http://ipindia.nic.in/index.htm)

INTELLECTUAL
PROPERTY **INDIA**
PATENTS I DESIGNS I TRADE MARKS
GEOGRAPHICAL INDICATIONS

(http://ipindia.nic.in/index.htm)

Application Details

APPLICATION NUMBER	202321003114
APPLICATION TYPE	ORDINARY APPLICATION
DATE OF FILING	16/01/2023
APPLICANT NAME	D.Y.PATIL EDUCATION SOCIETY (DEEMED TO BE UNIVERSITY)
TITLE OF INVENTION	"A METHOD FOR DETECTION OF VIRAL/BACTERIAL NUCLEIC ACID USING GOLD NANOPARTICLES".
FIELD OF INVENTION	BIOTECHNOLOGY
E-MAIL (As Per Record)	
ADDITIONAL-EMAIL (As Per Record)	info@dypatilkolhapur.org
E-MAIL (UPDATED Online)	
PRIORITY DATE	
REQUEST FOR EXAMINATION DATE	16/02/2023
PUBLICATION DATE (U/S 11A)	03/03/2023

Application Status

APPLICATION STATUS	Application Awaiting Examination

			View Documents

INTELLECTUAL PROPERTY INDIA
PATENTS | DESIGNS | TRADE MARKS
GEOGRAPHICAL INDICATIONS

दिनांक/Dated:26/02/2024

1.	पंजीकरण संख्या/Registration Number	:	**L-144215/2024**
2.	आवेदक का नाम, पता तथा राष्ट्रीयता Name, address and nationality of the applicant	:	THE REGISTRAR , D. Y. PATIL EDUCATION SOCIETY, DEEMED TO BE UNIVERSITY, KASABA BAWADA, KOLHAPUR-416006 INDIAN
3.	कृति के प्रतिलिप्यधिकार में आवेदक के हित की प्रकृति Nature of the applicant's interest in the copyright of the work	:	PUBLISHER
4.	कृति का वर्ग और वर्णन Class and description of the work	:	LITERARY/ DRAMATIC WORK
5.	कृति का शीर्षक Title of the work	:	COLORIMETRIC DETECTION OF NUCLEIC ACID BY GOLD NANOPARTICLES (AUNPS)
6.	कृति की भाषा Language of the work	:	ENGLISH
7.	रचयिता का नाम, पता और राष्ट्रीयता तथा यदि रचयिता की मृत्यु हो गई है, तो मृत्यु की तिथि Name, address and nationality of the author and if the author is deceased, date of his decease	:	DR. ARPITA PANDEY TIWARI, ASSOCIATE PROFESSOR , DEPARTMENT OF STEM CELL AND REGENERATIVE MEDICINE, CENTRE FOR INTERDISCIPLINARY RESEARCH, D. Y. PATIL EDUCATION SOCIETY, DEEMED TO BE UNIVERSITY, KASABA BAWADA, KOLHAPUR-416006 INDIAN MS. TEJASWINI PRUTHVIRAJ PATIL, PH. D. SCHOLAR , DEPARTMENT OF STEM CELL AND REGENERATIVE MEDICINE, CENTRE FOR INTERDISCIPLINARY RESEARCH, D. Y. PATIL EDUCATION SOCIETY, DEEMED TO BE UNIVERSITY, KASABA BAWADA, KOLHAPUR-416006 INDIAN
8.	कृति प्रकाशित है या अप्रकाशित Whether the work is published or unpublished	:	PUBLISHED
9.	प्रथम प्रकाशन का वर्ष और देश तथा प्रकाशक का नाम, पता और राष्ट्रीयता Year and country of first publication and name, address and nationality of the publisher	:	2023 INDIA THE REGISTRAR , D. Y. PATIL EDUCATION SOCIETY, DEEMED TO BE UNIVERSITY, KASABA BAWADA, KOLHAPUR-416006 INDIAN
10.	बाद के प्रकाशनों के वर्ष और देश, यदि कोई हों, और प्रकाशकों के नाम, पते और राष्ट्रीयताएँ Years and countries of subsequent publications, if any, and names, addresses and nationalities of the publishers	:	N.A.
11.	कृति में प्रतिलिप्यधिकार सहित विभिन्न अधिकारों के स्वामियों के नाम, पते और राष्ट्रीयताएं और समनुदेशन और अनुज्ञप्तियों के विवरण के साथ प्रत्येक के अधिकार का विस्तार, यदि कोई हो। Names, addresses and nationalities of the owners of various rights comprising the copyright in the work and the extent of rights held by each, together with particulars of assignments and licences, if any	:	THE REGISTRAR , D. Y. PATIL EDUCATION SOCIETY, DEEMED TO BE UNIVERSITY, KASABA BAWADA, KOLHAPUR-416006 INDIAN
12.	अन्य व्यक्तियों के नाम, पते और राष्ट्रीयताएं, यदि कोई हों, जो प्रतिलिप्यधिकार वाले अधिकारों को समनुदेशित करने या अनुज्ञप्ति देने के लिए अधिकृत हों Names, addresses and nationalities of other persons, if any, authorised to assign or licence of rights comprising the copyright	:	N.A.
13.	यदि कृति एक 'कलात्मक कृति' है, तो कृति पर अधिकार रखने वाले व्यक्ति का नाम, पता और राष्ट्रीयता सहित मूल कृति का स्थान। (एक वास्तुशिल्प कृति के मामले में पूरी होने का वर्ष भी दिखाया जाना चाहिए) If the work is an 'Artistic work', the location of the original work, including name, address and nationality of the person in possession of the work. (In the case of an architectural work, the year of completion of the work should also be shown).	:	N.A.
14.	यदि कृति एक 'कलात्मक कृति' है जो किसी भी माल या सेवाओं के संबंध में उपयोग की जाती है या उपयोग किए जाने में सक्षम है, तो आवेदन में प्रतिलिप्यधिकार अधिनियम, 1957 की धारा 45 की उप–धारा (i) के प्रावधान के अनुसार व्यापार चिह्न रजिस्ट्रार से प्रमाणन शामिल होना चाहिए If the work is an 'Artistic work' which is used or capable of being used in relation to any goods or services, the application should include a certification from the Registrar of Trade Marks in terms of the provision to Sub-Section (i) of Section 45 of the Copyright Act, 1957.	:	N.A.
15.	यदि कृति एक 'कलात्मक कृति' है, तो क्या यह डिजाइन अधिनियम 2000 के अंतर्गत पंजीकृत है? यदि हां, तो विवरण दें। If the work is an 'Artistic work', whether it is registered under the Designs Act 2000, if yes give details.	:	N.A.
16.	यदि कृति एक 'कलात्मक कृति' है, जो डिजाइन अधिनियम 2000 के तहत एक डिजाइन के रूप में पंजीकृत होने में सक्षम है, तो क्या यह औद्योगिक प्रक्रिया के माध्यम से किसी वस्तु पर प्रयुक्त की गई है और यदि हाँ, तो इसे कितनी बार पुनरुत्पादित किया गया है? If the work is an 'Artistic work', capable of being registered as a design under the Designs Act 2000.whether it has been applied to an article though an industrial process and ,if yes ,the number of times it is reproduced.	:	N.A.
17.	टिप्पणी, यदि कोई हो/Remarks, if any		

डायरी संख्या/Diary Number: 639/2024-CO/L

आवेदन की तिथि/Date of Application: 05/01/2024

Registrar of Copyrights

Extracts from the
Register of
Copyrights

प्रतिलिप्यधिकार कार्यालय, भारत सरकार | Copyright Office, Government Of India

दिनांक/Dated:09/05/2024

1.	पंजीकरण संख्या/Registration Number	:	**L-147677/2024**
2.	आवेदक का नाम, पता तथा राष्ट्रीयता Name, address and nationality of the applicant	:	THE REGISTRAR , D. Y. PATIL EDUCATION SOCIETY, DEEMED TO BE UNIVERSITY, KASABA BAWADA, KOLHAPUR-416006 INDIAN
3.	कृति के प्रतिलिप्यधिकार में आवेदक के हित की प्रकृति Nature of the applicant's interest in the copyright of the work	:	PUBLISHER
4.	कृति का वर्ग और वर्णन Class and description of the work	:	LITERARY/ DRAMATIC WORK
5.	कृति का शीर्षक Title of the work	:	COVALENT INTERACTIONS BETWEEN GOLD NANOPARTICLES (AUNPS) AND NUCLEIC ACID
6.	कृति की भाषा Language of the work	:	ENGLISH
7.	रचयिता का नाम, पता और राष्ट्रीयता तथा यदि रचयिता की मृत्यु हो गई है, तो मृत्यु की तिथि Name, address and nationality of the author and if the author is deceased, date of his decease	:	DR. ARPITA PANDEY TIWARI, ASSOCIATE PROFESSOR , DEPARTMENT OF STEM CELL AND REGENERATIVE MEDICINE, CENTRE FOR INTERDISCIPLINARY RESEARCH, D. Y. PATIL EDUCATION SOCIETY, DEEMED TO BE UNIVERSITY, KOLHAPUR-416006 INDIAN MS. TEJASWINI PRUTHVIRAJ PATIL, PH. D. SCHOLAR , DEPARTMENT OF STEM CELL AND REGENERATIVE MEDICINE, CENTRE FOR INTERDISCIPLINARY RESEARCH, D. Y. PATIL EDUCATION SOCIETY, DEEMED TO BE UNIVERSITY, KOLHAPUR-416006 INDIAN
8.	कृति प्रकाशित है या अप्रकाशित Whether the work is published or unpublished	:	PUBLISHED
9.	प्रथम प्रकाशन का वर्ष और देश तथा प्रकाशक का नाम, पता और राष्ट्रीयता Year and country of first publication and name, address and nationality of the publisher	:	2023 INDIA THE REGISTRAR , D. Y. PATIL EDUCATION SOCIETY, DEEMED TO BE UNIVERSITY, KASABA BAWADA, KOLHAPUR-416006 INDIAN
10.	बाद के प्रकाशनों के वर्ष और देश, यदि कोई हों, और प्रकाशकों के नाम, पते और राष्ट्रीयताएँ Years and countries of subsequent publications, if any, and names, addresses and nationalities of the publishers	:	N.A.
11.	कृति में प्रतिलिप्यधिकार सहित विभिन्न अधिकारों के स्वामियों के नाम, पते और राष्ट्रीयताएं और समनुदेशन और अनुज्ञप्तियों के विवरण के साथ प्रत्येक के अधिकार का विस्तार, यदि कोई हो। Names, addresses and nationalities of the owners of various rights comprising the copyright in the work and the extent of rights held by each, together with particulars of assignments and licences, if any	:	THE REGISTRAR , D. Y. PATIL EDUCATION SOCIETY, DEEMED TO BE UNIVERSITY, KASABA BAWADA, KOLHAPUR-416006 INDIAN
12.	अन्य व्यक्तियों के नाम, पते और राष्ट्रीयताएं, यदि कोई हों, जो प्रतिलिप्यधिकार वाले अधिकारों को समनुदेशित करने या अनुज्ञप्ति देने के लिए अधिकृत हों Names, addresses and nationalities of other persons, if any, authorised to assign or licence of rights comprising the copyright	:	N.A.
13.	यदि कृति एक 'कलात्मक कृति' है, तो कृति पर अधिकार रखने वाले व्यक्ति का नाम, पता और राष्ट्रीयता सहित मूल कृति का स्थान। (एक वास्तुशिल्प कृति के मामले में कृति पूरी होने का वर्ष भी दिखाया जाना चाहिए) If the work is an 'Artistic work', the location of the original work, including name, address and nationality of the person in possession of the work. (In the case of an architectural work, the year of completion of the work should also be shown).	:	N.A.
14.	यदि कृति एक 'कलात्मक कृति' है जो किसी भी माल या सेवाओं के संबंध में उपयोग की जाती है या उपयोग किए जाने में सक्षम है, तो आवेदन में प्रतिलिप्यधिकार अधिनियम, 1957 की धारा 45 की उप–धारा (i) के प्रावधान के अनुसार व्यापार चिह्न रजिस्ट्रार से प्रमाणन शामिल होना चाहिए। If the work is an 'Artistic work' which is used or capable of being used in relation to any goods or services, the application should include a certification from the Registrar of Trade Marks in terms of the provision to Sub-Section (i) of Section 45 of the Copyright Act, 1957.	:	N.A.
15.	यदि कृति एक 'कलात्मक कृति' है, तो क्या यह डिजाइन अधिनियम 2000 के अंतर्गत पंजीकृत है? यदि हां, तो विवरण दें। If the work is an 'Artistic work', whether it is registered under the Designs Act 2000, if yes give details.	:	N.A.
16.	यदि कृति एक 'कलात्मक कृति' है, जो डिजाइन अधिनियम 2000 के तहत एक डिजाइन के रूप में पंजीकृत होने में सक्षम है, तो क्या यह औद्योगिक प्रक्रिया के माध्यम से किसी वस्तु पर प्रयुक्त की गई है और यदि हाँ, तो इसे कितनी बार पुनरुत्पादित किया गया है? If the work is an 'Artistic work', capable of being registered as design under the Designs Act 2000,whether it has been applied to an article though an industrial process and ,if yes ,the number of times it is reproduced.	:	N.A.
17.	टिप्पणी, यदि कोई हो/Remarks, if any	:	

डायरी संख्या/Diary Number: 6796/2024-CO/L

आवेदन की तिथि/Date of Application: 02/03/2024

Registrar of Copyrights

प्रतिलिप्यधिकार कार्यालय, भारत सरकार | **Copyright Office, Government Of India**

दिनांक/Dated:26/11/2024

1.	पंजीकरण संख्या/Registration Number		**L-157364/2024**
2.	आवेदक का नाम, पता तथा राष्ट्रीयता Name, address and nationality of the applicant	:	THE REGISTRAR , D. Y. PATIL EDUCATION SOCIETY, DEEMED TO BE UNIVERSITY, KASABA BAWADA, KOLHAPUR-416006 INDIAN
3.	कृति के प्रतिलिप्यधिकार में आवेदक के हित की प्रकृति Nature of the applicant's interest in the copyright of the work	:	PUBLISHER
4.	कृति का वर्ग और वर्णन Class and description of the work	:	LITERARY/ DRAMATIC WORK
5.	कृति का शीर्षक Title of the work	:	ELECTROCHEMICAL DETECTION OF SARS-COV-2 RNA BY POLY-L-LYSINE FUNCTIONALIZED GOLD NANOPARTICLES (PLL-AUNPS)
6.	कृति की भाषा Language of the work	:	ENGLISH
7.	रचयिता का नाम, पता और राष्ट्रीयता तथा यदि रचयिता की मृत्यु हो गई है, तो मृत्यु की तिथि Name, address and nationality of the author and if the author is deceased, date of his decease	:	DR. ARPITA PANDEY TIWARI, ASSOCIATE PROFESSOR , DEPARTMENT OF STEM CELL AND REGENERATIVE MEDICINE, CENTRE FOR INTERDISCIPLINARY RESEARCH, D. Y. PATIL EDUCATION SOCIETY, DEEMED TO BE UNIVERSITY, KOLHAPUR-416006 INDIAN MS. TEJASWINI PRUTHVIRAJ PATIL, PH. D. SCHOLAR , DEPARTMENT OF STEM CELL AND REGENERATIVE MEDICINE, CENTRE FOR INTERDISCIPLINARY RESEARCH, D. Y. PATIL EDUCATION SOCIETY, DEEMED TO BE UNIVERSITY, KOLHAPUR-416006 INDIAN
8.	कृति प्रकाशित है या अप्रकाशित Whether the work is published or unpublished	:	PUBLISHED
9.	प्रथम प्रकाशन का वर्ष और देश तथा प्रकाशक का नाम, पता और राष्ट्रीयता Year and country of first publication and name, address and nationality of the publisher	:	2023 INDIA THE REGISTRAR , D. Y. PATIL EDUCATION SOCIETY, DEEMED TO BE UNIVERSITY, KASABA BAWADA, KOLHAPUR-416006 INDIAN
10.	बाद के प्रकाशनों के वर्ष और देश, यदि कोई हों, और प्रकाशकों के नाम, पते और राष्ट्रीयताएँ Years and countries of subsequent publications, if any, and names, addresses and nationalities of the publishers	:	N.A.
11.	कृति में प्रतिलिप्यधिकार सहित विभिन्न अधिकारों के स्वामियों के नाम, पते और राष्ट्रीयताएं और समनुदेशन और अनुज्ञप्तियों के विवरण के साथ प्रत्येक के अधिकार का विस्तार, यदि कोई हो। Names, addresses and nationalities of the owners of various rights comprising the copyright in the work and the extent of rights held by each, together with particulars of assignments and licences, if any	:	THE REGISTRAR , D. Y. PATIL EDUCATION SOCIETY, DEEMED TO BE UNIVERSITY, KASABA BAWADA, KOLHAPUR-416006 INDIAN
12.	अन्य व्यक्तियों के नाम, पते और राष्ट्रीयताएं, यदि कोई हों, जो प्रतिलिप्यधिकार वाले अधिकारों को समनुदेशित करने या अनुज्ञप्ति देने के लिए अधिकृत हों Names, addresses and nationalities of other persons, if any, authorised to assign or licence of rights comprising the copyright	:	N.A.
13.	यदि कृति एक 'कलात्मक कृति' है, तो कृति पर अधिकार रखने वाले व्यक्ति का नाम, पता और राष्ट्रीयता तथा मूल कृति का स्थान। (एक वास्तुशिल्प कृति के मामले में कृति पूरी होने का वर्ष भी दिखाया जाना चाहिए) If the work is an 'Artistic work', the location of the original work, including name, address and nationality of the person in possession of the work. (In the case of an architectural work, the year of completion of the work should also be shown).	:	N.A.
14.	यदि कृति एक 'कलात्मक कृति' है जो किसी भी माल या सेवाओं के संबंध में उपयोग की जाती है या उपयोग किए जाने में सक्षम है, तो आवेदन में प्रतिलिप्यधिकार अधिनियम, 1957 की धारा 45 की उप-धारा (i) के प्रावधान के अनुसार व्यापार चिह्न रजिस्ट्रार से प्रमाणन शामिल होना चाहिए। If the work is an 'Artistic work' which is used or capable of being used in relation to any goods or services, the application should include a certification from the Registrar of Trade Marks in terms of the provision to Sub-Section (i) of Section 45 of the Copyright Act, 1957.	:	N.A.
15.	यदि कृति एक 'कलात्मक कृति' है, तो क्या यह डिजाइन अधिनियम 2000 के अंतर्गत पंजीकृत है? यदि हां, तो विवरण दें। If the work is an 'Artistic work', whether it is registered under the Designs Act 2000, if yes give details.	:	N.A.
16.	यदि कृति एक 'कलात्मक कृति' है, जो डिजाइन अधिनियम 2000 के तहत एक डिजाइन के रूप में पंजीकृत होने में सक्षम है, तो क्या यह औद्योगिक प्रक्रिया के माध्यम से किसी वस्तु पर प्रयुक्त की गई है और यदि हाँ, तो कितनी बार पुनरुत्पादित किया गया है? If the work is an 'Artistic work', capable of being registered as design under the Designs Act 2000.whether it has been applied article though an industrial process and ,if yes ,the number of time it is reproduced.	:	N.A.
17.	टिप्पणी, यदि कोई हो/Remarks, if any		

Registrar of Copyrights

डायरी संख्या/Diary Number: 6797/2024-CO/L

आवेदन की तिथि/Date of Application: 02/03/2024

REVIEW PAPER

Gold Nanoparticles: Synthesis Methods, Functionalization and Biological Applications

Tejaswini Patil[1] · Rutuja Gambhir[1] · Anuja Vibhute[1] · Arpita Pandey Tiwari[1]

Abstract

Nanotechnology has vast applications in medicine and biomedical engineering like tissue engineering, diagnosis, and therapy. Nowadays incorporation of functionalized nanostructures in various biomedical applications has generated considerable research interest. Gold nanoparticles (AuNPs) are one of the most stable metal nanoparticles with unique physicochemical properties and are reflected as a promising candidate for widespread biological applications. Among different synthesis methods, biological synthesis methods are advantageous as it reduces the need for toxic chemicals for reduction purpose. Surface functionalization provides colloidal stability to gold nanoparticles which are achieved by using various materials. This review mainly focuses on the biological applications of AuNPs such as bioimaging, biosensing, anticancer therapy, drug delivery, hyperthermia, and antimicrobial activity. The surface plasmon resonance (SPR) related optical properties are used for biosensing and bioimaging applications for diagnosis to detect pathogens as well as biomarkers. Biomolecules and drug functionalized AuNPs are effectively used to treat various cancer and other diseases. Thus, the study of gold nanoparticles opens a new percept in the biological field for varieties of applications.

Keywords Gold nanoparticles · Synthesis · Biological applications · Bioimaging · Anticancer · Antibacterial

Introduction

Nanoscale materials have begun to pervade the areas of biomedical applications. The large matter is reduced to get nanoscale size material with unique physicochemical properties which differ from the actual bulk component. The size, shape, and surrounding environment of nanoparticles influence the physical properties that govern the alteration for a range of applications in different fields [1]. In recent years, conventional biomedical methods have been successfully replaced with modern nanotechnology methods for considerable accuracy, sensitivity, efficiency, and high-speed measurement. Among different nanoparticles, the gold nanoparticles (AuNPs) are one of the most explored nanoparticles for biological applications due to their desirable physicochemical properties like easy synthesis, easy surface modification,

biocompatibility, non-toxicity, and large surface to volume ratio, and size tunability as shown in Fig. 1. The physical properties and color diversity of AuNPs depend on the size and shape whereas the bulk gold exhibit different properties as compared to nanoscale particles [2].

The colloidal gold suspension has a particle size in the range of 1–100 nm and its color change from wine red to purple depending on the particle size. The nanometer-sized gold exhibit different properties from bulk gold. Gold nanoparticles have optical and electrochemical properties which strongly depend on their size, shape, interparticle distance, and surface chemistry. Different synthesis methods were developed for various sized AuNPs preparation. The variation in particle size depends on the synthesis parameters like reaction temperature, pH, precursor concentration as well as the ratio of precursor to reducing agent. The various sizes of AuNPs influence the Surface Plasmon Resonance (SPR) frequency [3]. The AuNPs tend to precipitate in fluids due to the high surface energy of gold. This self-assembly is prevented by surface modification of AuNPs with the help of various functionalizing molecules such as polymers that decrease the surface energy of gold and stabilize the AuNPs. Surface chemistry of gold nanoparticles is crucial for their

✉ Arpita Pandey Tiwari
arpitaptiwari@gmail.com

1 Department of Stem Cell and Regenerative Medicine and Medical Biotechnology, Center for Interdisciplinary Research, D.Y. Patil Education Society, Institution Deemed to be University, Kolhapur, Maharashtra, India

ORIGINAL PAPER

Optical Biosensing of SARS-CoV-2 RNA Based on Positively Charged Poly-L-Lysine Functionalized Gold Nanoparticles

Tejaswini P. Patil[1] · Arun Kumar Parthasarathy[2] · Dhanaji Malavekar[3] · JinHyeok Kim[3] · Arpita P. Tiwari[1]

Abstract

The World Health Organization (WHO) announced corona virus disease 2019 (COVID-19) caused by severe acute respiratory syndrome corona virus 2 (SARS-CoV-2), a serious pandemic in March 2020. The situation demands, development of rapid, convenient and easy to handle detection system for SARS-CoV-2. In this regard, the optical biosensing assay was developed using antisense oligonucleotide (ASO) conjugated Poly-L-Lysine functionalized gold nanoparticles (PLL-AuNPs) for detection of SARS-CoV-2 RNA. The negatively charged ASOs were conjugated with positively charged PLL-AuNPs by electrostatic interactions which were characterized by UV–Vis spectroscopy and Transmission Electron Microscopy (TEM). ASO-PLL-AuNPs conjugate was used to detect target SARS-CoV-2 RNA within 5–6 min from COVID-19 positive samples. In presence of target SARS-CoV-2 RNA, the DNA-RNA (ASO-RNA) hybrid structure was formed that released PLL-AuNPs which was aggregated in presence of sodium chloride (NaCl). This has rendered observable red shift in Surface Plasmon Resonance (SPR) with maximum absorbance at 660 nm and visual aggregation of PLL-AuNPs. Selectivity of ASO-PLL-AuNPs conjugate was evaluated in presence of Influenza A RNA with limit of detection 0.52 ng/μL. The obtained results were compared with qRT-PCR results for nasopharyngeal samples collected from COVID-19 positive patients and were found in good agreement with qRT-PCR results. This study reports selective and sensitive optical biosensing assay for detection of SARS-CoV-2 RNA using ASO-PLL-AuNPs conjugate without utilization of any sophisticated instruments.

✉ Arpita P. Tiwari
  arpitaptiwari@gmail.com

[1] Department of Stem Cell & Regenerative Medicine and Medical Biotechnology, D. Y. Patil Education Society (Institution Deemed to be University), Kolhapur, Maharashtra 416006, India

[2] Dhanalakshmi Srinivasan Group of Institutions, Perambalur, Trichy, Chennai 621212, India

[3] Department of Materials Science and Engineering, Optoelectronic Convergence Research Center, Chonnam National University, Gwangju 61186, South Korea

Antisense oligonucleotide conjugated gold nanoconstructs-based electrochemical biosensor for detection of SARS-CoV-2

Tejaswini P. Patil [a], Vishakha S. Parkhe [a], Somnath S. Kundale [b], Rajanish K. Kamat [c,d], Tukaram D. Dongale [b], Rajendra S Patil [e], Arpita P. Tiwari [a,*]

[a] *Department of Medical Biotechnology and Stem Cell and Regenerative Medicine, Centre for Interdisciplinary Research, D. Y. Patil Education Society (Deemed to be University), Kolhapur-416006, Maharashtra, India*
[b] *Computational Electronics and Nanoscience Research Laboratory, School of Nanoscience and Biotechnology, Shivaji University, Kolhapur 416004, Maharashtra, India*
[c] *Department of Electronics, Shivaji University, Kolhapur 416004, Maharashtra, India*
[d] *Dr. Homi Bhabha State University, 15, Madam Cama Road, Mumbai 400032, Maharashtra, India*
[e] *Department of Pathology, D Y Patil Medical College, Kolhapur 416006, Maharashtra, India*

ARTICLE INFO

ABSTRACT

Nanoconstructs of gold nanoparticles (AuNPs) conjugated with SARS-CoV-2 specific antisense oligonucleotides (ASO) have been utilized to develop sensitive electrochemical nucleic acid biosensor for the detection of SARS-CoV-2 RNA. AuNPs were prepared through a one-pot synthesis method by utilizing Poly-L-Lysine (PLL) biopolymer and as synthesised AuNP were characterized by various analytical techniques such as UV–Vis spectroscopy, X-ray Diffraction (XRD) analysis, Fourier Transform Infra-Red spectroscopy (FT-IR), zeta potential, and Transmission Electron Microscopy (TEM). Poly-L-Lysine functionalized AuNPs (PLL-AuNPs) nanoconstructs platform was employed for immobilization of SARS-CoV-2 specific antisense oligonucleotides (ASO-conjugated PLL-AuNPs) via electrostatic interactions. The PLL-AuNPs were drop casted on glassy carbon electrode (GCE) following immobilization of ASO for fabrication of electrochemical biosensor. The ASO-conjugated PLL-AuNPs nanoconstructs were characterized by cyclic voltammetry (CV), differential pulse voltammetry (DPV), and electrochemical impedance spectroscopy (EIS) techniques. The responsiveness of ASO-conjugated PLL-AuNPs nanoconstructs in presence SARS-CoV-2 RNA was monitored using the DPV, SWV and EIS technique, where methylene blue was employed as an electrochemical indicator for DNA-RNA hybridization detection. The biosensor exhibits a detection range for SARS-CoV-2 RNA infection ranging from 0 to 100 nM, with a limit of detection at 30.2 nM. The electrode, modified with ASO-conjugated PLL-AuNPs, was employed for the detection of SARS-CoV-2 RNA from clinical samples collected from COVID-19-positive individuals.

1. Introduction

The emergence of the coronavirus disease 2019 (COVID-19), caused by severe acute respiratory syndrome coronavirus 2 (SARS-CoV-2), had profound impacts on both the economy and global health [1]. Rapid diagnosis and effective treatment of COVID-19 have posed significant challenges during the corona pandemic. Consequently, extensive research has been conducted on preventive measures, diagnostic techniques, and treatment modalities related to SARS-CoV-2. In addition to treatment, the prompt and accurate detection of SARS-CoV-2 infection is crucial for controlling the spread of COVID-19. Currently, conventional methods such as quantitative Reverse Transcription Polymerase Chain Reaction (qRT-PCR) or immunogen assays are primarily utilized for detecting SARS-CoV-2 RNA or protein from clinical samples [2,3]. The qRT-PCR method serves as the gold standard diagnostic method for identifying SARS-CoV-2. However, this technique necessitates sophisticated instrumentation, skilled technicians, and is time-consuming [4]. Continuing efforts are underway to develop alternative virus detection methods, with specific biosensor systems emerging as intriguing alternatives. Biosensors offer cost-effective, highly sensitive, and easy-to-handle detection methods, and are increasingly utilized for pathogen detection due to their specificity and simplicity. Biosensors

* Corresponding author at: Department of Medical Biotechnology and Stem Cell and Regenerative Medicine, Centre for Interdisciplinary Research, D. Y. Patil Education Society (Deemed to be University), Kolhapur-416006, Maharashtra, India.
E-mail address: arpitaptiwari@gmail.com (A.P. Tiwari).

Green synthesis of gold nanoparticles via *Capsicum annum* fruit extract: Characterization, antiangiogenic, antioxidant and anti-inflammatory activities

Tejaswini P. Patil [a], Anuja A. Vibhute [a], Snehal L. Patil [b], Tukaram D. Dongale [b], Arpita P. Tiwari [a],*

[a] *Department of Medical Biotechnology and Stem Cell & Regenerative Medicine, D.Y. Patil Education Society (Institution Deemed to be University), Kolhapur, Maharashtra 416006, India*
[b] *Computational Electronics and Nanoscience Research Laboratory, Shivaji University, Kolhapur, Maharashtra 416004, India*

ARTICLE INFO

ABSTRACT

Biological synthesis of gold nanoparticles (AuNPs) is gaining attention of researchers because of their varieties of biomedical applications. This study reported the novel, eco-friendly synthesis of AuNPs using dried fruit extract of *Capsicum annum* (*C. annum*). Biosynthesized gold nanoparticles (Ca-AuNPs) showed UV absorption peak at 540 nm and were found to be stable for up to three months. The nanoparticles were further characterized by Transmission Electron Microscopy (TEM), Fourier Transform Infrared (FT-IR), Energy Dispersive X-ray Analysis (EDAX) and X-ray diffraction (XRD) analysis. The nanoparticles were spherical in shape with size range of 20–30 nm and zeta potential study confirmed the surface charge of -26.5 mV. The Ca-AuNPs were tested for anti-angiogenic activity using Chorioallantoic membrane (CAM) assay that implied a significant anti-angiogenic efficiency of Ca-AuNPs at 100 μg/mL concentration. The antioxidant activity of Ca-AuNPs studied by 2,2- diphenyl-1-picrylhydrazyl (DPPH) assay was found to be significant with 86.0% radical scavenging activity. These nanoparticles also revealed anti-inflammatory activity at concentration range 100–1200 μg/mL with IC-50 value619.4 μg/mL. The present study includes synthesis of Ca-AuNPs by using phytoconstituents of plant material as reducing agents to efficiently exploit the biomedical applications of the nanoparticles.

1. Introduction

Nanoparticles have wide applicability in the field of biomedicine, drug delivery, material chemistry and pollution control [1,2]. The capping agents of nanoparticles such as, PEG, PVA, BSA and different plant extract also play important role in various biological applications [3]. Biosynthesized nanoparticles have reported to shown effective antibacterial and photocatalytic activity [4,5]. It has been reported that metal nanoparticles, such as iron oxide, zinc oxide, Cu_2Sn_3 (CTS), gold nanoparticles, and quantum dots, have been employed in a variety of applications, including optics, biosensing, catalysis, antibacterial activity, and therapy [6–9]. In recent years, gold nanoparticles (AuNPs) are gaining attention in research area due to their unique intrinsic features such as, size tunability, large surface to volume ratio, optical properties, excellent biocompatibility, low toxicity and easy surface modification [10,11]. Thus, they are widely used in medical research for diagnosis

[12] and therapies [13,14]. Gold nanoparticles are synthesized by various techniques like, chemical reduction method, lithography and physical methods [15]. Each method successfully synthesizes the metallic nanoparticles but has several disadvantages such as, requirement of toxic chemicals in synthesis method, high pressure and high processing cost, and may be toxic to environment [16]. Hence, it is necessary to develop novel, eco-friendly process for AuNPs synthesis. The biological synthesis of AuNPs using plants, algae, fungi and microorganisms minimizes the disadvantages of above methods as they are simple in nature, reduces the need of toxic chemicals, and are based on green chemistry approach [17]. Biosynthesis of AuNPs using plant is gaining interest of researchers as the phytoconstituents of plant extract are acting as both reducing and stabilizing agent which results in effective and rapid synthesis. Different plant extracts are reported to be rich in active phytoconstituents that promoted stable AuNPs synthesis methods for various applications like, drug delivery, antibacterial,

ORIGINAL ARTICLE

Single-step antibiotic-mediated synthesis of kanamycin-conjugated gold nanoparticles for broad-spectrum antibacterial applications

T. Patil[1], V. Khot[2] and A. Pandey-Tiwari[1] (iD)

1 Department of Medical Biotechnology, Center for Interdisciplinary Research, D.Y. Patil Education Society (Institution Deemed to be University), Kolhapur, Maharashtra, India
2 Department of Medical Physics, Center for Interdisciplinary Research, D.Y. Patil Education Society (Institution Deemed to be University), Kolhapur, Maharashtra, India

Significance and Impact of the Study: A low-cost single-step method of antibiotic-mediated synthesis of kanamycin-conjugated gold nanoparticles (Kan-AuNPs), eliminating the use of reducing agents and capping agents is proposed. Kan-AuNPs display broad-spectrum antibacterial activity against Gram-positive and Gram-negative bacteria pathogens. Kan-AuNPs show significant antibacterial activity against *Pseudomonas aeruginosa* and *Escherichia coli* strain isolated from patients suffering from urinary tract infections. The minimum inhibitory concentration of Kan-AuNPs for antibacterial activity is lower as compared to antibiotic kanamycin alone for all tested bacterial strains.

Abstract

Widespread and irrational use of antibiotics results in the development of antibiotic-resistant bacteria. Thus, there is a need to develop novel antibacterial agents in order to replace conventional antibiotics and to increase the efficacy of already existing antibiotics by combining them with other materials. Herein, a single-step antibiotic-mediated synthesis of antibiotic-conjugated gold nanoparticles is reported. In this single-step method antibiotic Kanamycin, an aminoglycoside itself plays the role of reducing as well as capping agent by reducing gold salt into gold nanoparticles. The kanamycin-conjugated gold nanoparticles (Kan-AuNPs) were confirmed by UV–Visible spectroscopy and further physico-chemically characterized by various instrumental techniques. Synthesized Kan-AuNPs showed broad-spectrum antibacterial activity against Gram-positive *Staphylococcus aureus* as well as Gram-negative *Escherichia coli* bacterial strains. They are also found to be effective against *Pseudomonas aeruginosa* and pathogenic *E. coli* isolated from urinary tract infections (UTIs) patients, which are responsible to cause hospital-acquired infections like nosocomial, burn wound and UTIs. The minimum inhibitory concentration (MIC) of Kan-AuNPs is 50 μg ml^{-1} for *S. aureus* and *E. coli*, 125 μg ml^{-1} for *P. aeruginosa* and 100 μg ml^{-1} for *E. coli* isolated from UTIs patients. It is also evident that the MIC of Kan-AuNPs for antibacterial activity is lower as compared to antibiotic kanamycin alone for all bacterial strains. Hence, the one-step strategy of synthesis for Kan-AuNPs is a suitable strategy for fighting infectious bacterial strains in hospitals, healthcare and the pharmaceutical industry.

Introduction

The irrational and widespread use of antibiotics leads to the development of resistant strains of bacteria. The emergence of multidrug-resistant bacteria (MDR) is increased which showed resistance to multiple antibiotics (Gupta *et al.* 2019). Hence, there is a need to develop novel strategies for new antibacterial agents, search for

AMITY
UNIVERSITY
— MUMBAI —

INTERNATIONAL WORKSHOP on
RECENT TRENDS IN FUNCTIONAL NANOMATERIALS
FOR TECHNOLOGICAL APPLICATIONS

August 2-3, 2022 (Virtual Mode)

CERTIFICATE OF APPRECIATION

This is to certify that Mr. / Ms. ___Tejaswini Pruthviraj Patil___ has Presented Poster in International Workshop
on Recent Trends in Functional Nanomaterials for Technological Applications which was held on the 2
& 3 of August 2022 organized by Center for Nanoscience and Nanotechnology,
Amity University, Mumbai and ICON Labs, Navi Mumbai, India.

Dattatray Late
Convenor

Co-convenor

D. Y. PATIL EDUCATION SOCIETY
(Deemed to be University), KOLHAPUR
NAAC 'A'' Grade in 3rd Cycle

Certificate

This is to certify that ~~Mr.~~ /Ms. **Patil Tejaswini Pruthviraj** of Centre for Interdisciplinary Research, DYPES, Kolhapur has delivered invited ~~talk~~/ chaired the ~~session~~/ presented oral/ ~~presented poster~~/ participated in the **International Conference on Nanotechnology Addressing the Convergence of Materials Science, Biotechnology and Medical Science (IC-NACMBM-2024)** held at the Centre for Interdisciplinary Research, D. Y. Patil Education Society (Deemed to be University), Kolhapur, Maharashtra, India during 12th to 14th February 2024. His/ Her contribution to the conference is highly appreciated.

Dr. Jayavant L. Gunjakar

Convener

Prof. Meghnad G. Joshi

Convener

Prof. Chandrakant D. Lokhande

Chairman

Savitribai Phule Pune University
Department of Biotechnology

75th Anniversary Celebration
सावित्रीबाई फुले पुणे विद्यापीठ
॥ य. क्रियावान् स पण्डितः ॥

International Conference on
Biology Beyond Boundaries
29th to 31st January 2024

Certificate of Presentation

MISS. TEJASWINI PATIL *from* **D. Y. PATIL EDUCATION SOCIETY (DEEMED TO BE UNIVERSITY), KOLHAPUR** *has presented a paper (Oral/Poster) in International Conference on Biology Beyond Boundaries: Mitochondrial Insights, Computational Breakthroughs, and Clinical Transformations organized by the Department of Biotechnology, Savitribai Phule Pune University, Pune during 29-31 January 2024.*

Prof. Rajesh N. Gacche
Convener

Prof. Dhyan Chandra
Convener

Prof. Raymond B. Birge
Convener

SAVITRIBAI PHULE PUNE UNIVERSITY

ROSWELL PARK.
COMPREHENSIVE CANCER CENTER

RUTGERS, USA